OCT 6 1949

THE PHYSICAL REVIEW

VOLUME 76 *Second Series* NUMBER 7

OCTOBER 1, 1949

Published for the

AMERICAN PHYSICAL SOCIETY

by the

AMERICAN INSTITUTE OF PHYSICS

Incorporated

LANCASTER, PA., AND NEW YORK, N. Y.

THE PHYSICAL REVIEW

A journal of experimental and theoretical physics established by E. L. Nichols in 1893

Published by the American Institute of Physics for the

AMERICAN PHYSICAL SOCIETY

Officers

President

F. W. Loomis
University of Illinois
Urbana, Illinois

Vice-President

I. I. Rabi
Columbia University
New York, New York

Secretary

K. K. Darrow
Bell Telephone Laboratories
Office:
Columbia University
New York 27, New York

Treasurer

G. B. Pegram
Columbia University
New York 27, New York

Local Secretary for the Pacific Coast

J. Kaplan
University of California at Los Angeles
Los Angeles, California

Managing Editor

John T. Tate
University of Minnesota
Minneapolis, Minnesota

BOARD OF EDITORS

Editor

John T. Tate

Assistant Editor

J. W. Buchta

Associate Editors

H. A. Bethe — S. A. Goudsmit — W. E. Lamb, Jr.
L. A. Ridenour — E. M. Purcell — R. G. Herb
W. H. Zachariasen — V. F. Weisskopf — J. Bardeen

Manuscripts for publication should be submitted to John T. Tate, University of Minnesota, Minneapolis, Minnesota. The authors' institutions are requested to pay a publication charge of $4 per page which, if honored, entitles them to 100 free reprints. Instructions will be sent with galley proofs.

Proof and all correspondence concerning papers in the process of publication should be addressed to the Publication Manager, American Institute of Physics, 57 East 55 Street, New York 22, New York.

Subscription Price

United States and Canada.....$25.00
Elsewhere.....$27.00

Back Numbers[1]

Yearly back number rate when complete year is available:
Prior to 1949: $20.00
Thereafter: $27.00
Single copies: $2.00 each, prior to July, 1929;
$1.00 each, July, 1929–December, 1941;
$2.00 each, January, 1942–December, 1946;
$1.00 each, January, 1947–December, 1948.
Current issues: $1.25 each.
General index, 1893–1920: $4.00.

Subscriptions and orders for back numbers should be addressed to Prince and Lemon Streets, Lancaster, Pennsylvania, or to the American Institute of Physics, 57 East 55 Street, New York 22, New York.

Changes of address in the case of members of the American Physical Society should be addressed to the Treasurer; in the case of other subscribers to the Business Manager, American Institute of Physics.

[1] For Series 1 inquire of Physics Department, Cornell University, Ithaca, New York.

The Physical Review is published semi-monthly at Prince and Lemon Streets, Lancaster, Pennsylvania.

Entered as second-class matter March 6, 1947, at the Post Office at Lancaster, Pennsylvania, under the Act of March 3, 1879.

Acceptance for mailing at special rate of postage provided for in paragraph 4, section 538, P. L. & R., authorized January 27, 1933.

THE
PHYSICAL REVIEW

A journal of experimental and theoretical physics established by E. L. Nichols in 1893

SECOND SERIES, VOL. 76, NO. 7 OCTOBER 1, 1949

A Determination of the Half-Life of Carbon 14

W. M. JONES
Los Alamos Scientific Laboratory of the University of California, Los Alamos, New Mexico
(Received June 6, 1949)

Experiments are described involving the counting of an analyzed and diluted sample of carbon dioxide containing C^{14} in a Geiger counter of known effective volume. The value of the half-life is found to be 5589 ± 75 years.

INTRODUCTION

A CONSIDERABLE number of investigators have reported measurements of the C^{14} half-life, but, even excluding the earliest estimates, the values range from 4700 to 7200 years. Factors contributing to the undertaking of this research were the availability of starting material rich in C^{14},[1] and so permitting more certainty in the number of active carbon atoms, availability of the counters used, and the possible importance of the half-life for the measurement of time.[2]

The method, in general, consisted of the mass spectrometric analysis of a sample of CO_2 rich in C^{14}, the dilution of a portion of this material in a known way, and the counting of a portion of the diluted material in a Geiger counter of known effective volume.

PREPARATION, ANALYSIS, AND DILUTION OF RADIOACTIVE CARBON DIOXIDE

The carbon dioxide containing C^{14} which was counted was obtained by dilution of some rich material with ordinary CO_2. The dilution can be performed more accurately than the mass spectrometric analysis of the original material, and it is therefore desirable that the starting material be rich in C^{14} in order to decrease uncertainty in the number of active carbon atoms. The very rich sample of $BaCO_3$ described by Norris and Snell[1] seemed ideal for this purpose, and a 39.4-mg sample of this material was made available by the Oak Ridge National Laboratory.

A small vacuum system was constructed for the conversion of small amounts of barium carbonate to carbon dioxide by means of concentrated and outgassed sulfuric acid. The gas generated was passed through a dry ice trap and was then passed several times over a tube of phosphorus pentoxide. Finally the gas was condensed into an accurately known volume of about 13 cc, one boundary of which was the mercury surface in one limb of a mercury manometer. Pressures were read with a cathetometer and temperatures were measured with a calibrated thermometer graduated in 0.02°C intervals. In computing the number of moles of gas formed, a small correction was made for the non-ideal character of the gas. No inert gas was found to be present in the material produced. Two trial runs with ordinary barium carbonate were made. The results of these determinations and of the conversion of the enriched material are given in Table I. It is apparent from the trial runs that quantitative conversions can be made, and it appears that the enriched material is 86.9 percent barium carbonate. The probable presence of impurities had previously been indicated.[1] The enriched carbon dioxide appears quite stable. Some of the material was kept frozen for three months and showed no evidence of decomposition. The enriched gas did not appear to produce material non-condensable in liquid nitrogen. This behavior is perhaps to be expected in view of the comparatively low radiation level (about 4 mc) and the known stability of carbon dioxide under irradiation.[3]

Prior to the analysis of the enriched material a series of tests was made with a 60° Nier-type mass spectrometer on the C^{12}/C^{13} ratio using tank carbon dioxide

[1] L. D. Norris and A. H. Snell, Phys. Rev. 73, 254 (1948); Phys. Rev. 74, 1240 (1949).
[2] Anderson, Libby, Weinhouse, Reid, and Grosse, Phys. Rev. 72, 931 (1947).
[3] S. C. Lind, *The Chemical Effects of Alpha Particles and Electrons* (The Chemical Catalog Company, Inc., New York, 1928), pp. 109, 155.

of coal origin. The value obtained for the ratio was in good agreement with the data of Nier and Gulbransen.[4] It was found that the conditions for optimum beam were the same for the 44 and 45 peaks, and that, with electrode voltages set for optimum beam, the 44/45 ratio did not change by more than 0.6 percent for an accelerating voltage change of 40 percent. Varying the magnetic field by 20 percent did not change the ratio by more than 0.5 percent. The theoretical treatment of Coggeshall[5] would predict considerable discrimination in the case of electrostatic scanning, but this treatment does not apply without modification to a Nier-type ion source, the focus and beam center electrodes of which should decrease the effect. Inghram[6] has found that large discrimination may occur with electrostatic scanning in this type of instrument if the ion source is in poor focus. In the analysis of the enriched material, magnetic scanning was employed, and the permanent magnet at the ion source was removed in order to eliminate possible discrimination effects.[6]

A portion of the gas was analyzed on the mass spectrometer. It was present at about 100 microns pressure in a large 6-liter bulb in the center of which was a leak of the type used in mass spectrometers of the Consolidated Engineering Corporation, and which was purchased from that concern. Three of the original five parallel leakage paths were eliminated. This arrangement made the correction for change of sample composition with time very small. Preliminary tests with ordinary CO_2 showed that this leak gave molecular flow into the mass spectrometer below 250 microns pressure. For a leak providing molecular flow, discrimination should not occur.[7]

Prior to introduction of the sample for analysis, the spectrometer tube was baked out thoroughly; background in the mass region of interest was less than about 1/20,000 of the subsequent mass 44 peak height. Flowing spectroscopic argon, contained in a bulb immersed in liquid nitrogen, into the spectrometer did not alter this situation.

Thirteen separate scans of the mass spectrum from mass 43 to mass 48 were made. No trend was noted in peak height ratios beyond that resulting from the small change in composition occurring with time in the sampling bulb.[7] A correction was made for this effect. Suitable corrections were made for the C^{13} isotope and for the O^{17} and O^{18} isotopes. The composition of the carbon isotopes in the sample is given in Table II. In the uncertainty estimates, allowance is made for a possible absolute error equal to the probable precision error of the measurements.

Since the 44 and 46 peaks are of approximately the same size, any non-ohmic character in the $4\times10^{10}\Omega$ IRC grid resistor of the FP-54 tube in the detector circuit should be insignificant. Inghram[6] has given detailed information on IRC resistors of the type used. The d.c. amplifier was calibrated with voltages from a Type K-2 Leeds & Northrup potentiometer just before the analysis.

It may be noted that some enriched material, presumably of the same composition as the starting material of this investigation, has been found by Jenkins[8] to be about 40 percent C^{14} by photographic photometry of band spectra of the isotopic C_2 molecules. The value previously obtained[1] for the C^{14} content by the counting of $BaCO_3$ from the same lot as that of the present research is raised from 32 percent to 37 percent by recognizing the existence of impurities. If a half-life of 5600 years instead of 5100 years, is used, the C^{14} content is raised to 40 percent.

In the dilution of the enriched material, a known portion of the latter, contained in a small volume which had been calibrated with mercury, was mixed with a known amount of pure ordinary carbon dioxide contained in a larger volume, also calibrated with mercury. The once-diluted material was again diluted in order to obtain a gas of suitable activity. The smaller volume consisted of the 8-mm bore of a stopcock, together with the sealed-off portion on one side of the stopcock. A ground joint was provided on the other side so that the smaller calibrated volume could be connected to the larger volume. The value of the smaller calibrated volume was 1.8994 ± 0.0003 cm^3 (25°C). An experimentally determined correction of about 0.06 percent was applied to this value for the alteration of volume due to the Apiezon N stopcock lubricant. The larger volume was of about $\frac{1}{2}$-liter capacity and was provided with a small leg for freezing-out purposes. The volumes were chosen so that no pressures measured in the dilution were below about 20 cm Hg. The manometer was constructed from selected 1-in. Trubore tubing. The cathetometer was graduated to 0.005 cm, but the mesicus positions were estimated to 0.001 cm. Temperatures were read with a thermometer graduated in

TABLE I. Conversion of $BaCO_3$ to CO_2.

Run	Moles $BaCO_3$ taken	Moles CO_2 found
Trial I	0.0_3 1242	0.0_3 1238
Trial II	0.0_3 4178	0.0_3 4178
C^{14} sample	0.0_3 1761*	0.0_3 1530

* This value is based on the weight of material, 34.9 mg, as supplied by the Oak Ridge National Laboratory, and a molecular weight of 198.2, involving a correction for the C^{14} content.

TABLE II. Isotopic carbon composition in C^{14} sample.

Percent C^{12}	Percent C^{13}	Percent C^{14}
59.93 ± 0.1	0.67 ± 0.01	39.4 ± 0.1

[4] A. O. Nier and E. A. Gulbransen, J. Am. Chem. Soc. **61**, 697 (1939).
[5] N. D. Coggeshall, J. Chem. Phys. **12**, 19 (1944).
[6] M. G. Inghram, Phys. Rev. **70**, 653 (1946).
[7] R. E. Honig, J. App. Phys. **16**, 646 (1945).
[8] F. A. Jenkins, Phys. Rev. **74**, 355 (1948).

0.02°C intervals and calibrated by the manufacturer against a standard resistance thermometer. The thermometers were taped to the calibrated volumes. These were surrounded by insulating material, and the whole covered with aluminum foil. In computing the amounts of gas used, a correction was made for gas imperfection.

Following exposure of the glass vacuum system to radioactive material in the dilution procedure, stopcocks were degreased and cleaned, and tank CO_2 was flowed through the system. Following evacuation of the line pure CO_2 was admitted and allowed to stand for several hours. A portion of this gas was then counted to test the efficiency of the decontamination. It was found that activity was not detectable after slowly flowing CO_2 through the system for a 24-hour period. Similar precautions were taken with the calibrated volumes.

The equilibration of the active and inert portions of gas in the dilution procedure was assisted by alternately freezing out and subliming the material, following which a period of about 18 hours was allowed for equilibrium to be established. Whenever material containing C^{14} was frozen before a critical step, several hours were allowed to elapse after sublimation in order to avoid any effects owing to small differences in vapor pressure. Similar precautions were observed in the mass spectrometric analysis.

The pure CO_2 gas used was prepared in a glass vacuum system from anhydrous sodium carbonate and outgassed concentrated sulphuric acid. The CO_2 was dried by several distillations from dry ice temperature and finally by slow passage several times over a 3-foot P_2O_5 tube. The CO_2 was freed from inert gas by cycles of freezing, pumping, and sublimation.

THE COUNTERS

A diagram of the counters used is given in Fig. 1. Close tolerances were held in the machining of the parts. The insulators, 2, were selected pieces of $\frac{1}{8}$-in. Trubore tubing into which the $\frac{1}{8}$-in. Kovar shields, 4, slipped. The holes in the end plugs, 3, were made so as to provide snug fits for the insulators. The relative positions of 2, 3, and 4 in assembly were attained by the use of jigs, and the seals between these parts were made with thinned Glyptal. Baking provided a strong enough seal so that parts did not move appreciably with respect to each other. Small corrections were made for such dimensional changes as did occur. From the dimensions and measurements on the volume of the pumping lead the volume available to gas was known. A central portion of the counter wall was turned down to about 0.010 in. so that counter behavior could be checked with strips of uranium foil. Resolving times were measured by the counting of two approximately equal foils, separately and together, at about the same counting rates encountered in the subsequent work.

Shown in Fig. 1 is a micarta cold reservoir, 8, which was made in two parts which could be clamped together around the counter. Liquid nitrogen in the reservoir provided a satisfactory means of transferring carbon dioxide into the counter quantitatively.

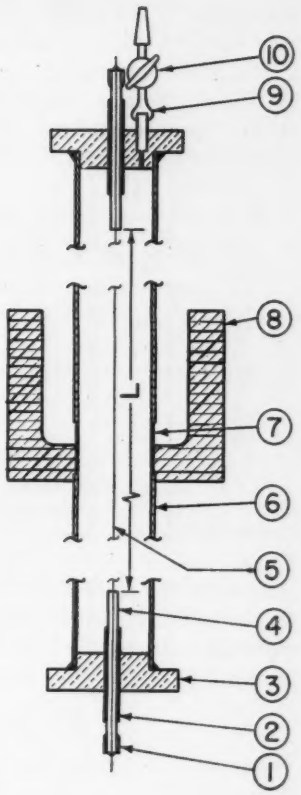

FIG. 1. Cross section of counter. 1—Brass cap. 2—$\frac{1}{8}$-in. Trubore Pyrex tubing insulator. 3—Brass end plug. 4—$\frac{1}{8}$-in. O.D. Kovar shield. 5—0.005-in. Kovar wire. 6—Brass shell, 1 in. O.D., 0.035-in. wall thickness. 7—Wall thickness 0.010 in. in this region. 8—Micarta refrigeration well. 9—Kovar to glass seal. 10—Stopcock and 10/30 standard taper ground glass joint.

The carbon dioxide was present in the counters at partial pressures in the approximate range 1–3 mm Hg. The pressure of the 94 percent argon–6 percent C_2H_5OH quencher gas was approximately 10 or more cm Hg as described later. Under these conditions a satisfactory plateau region is obtainable.

In making an absolute counting measurement on a gaseous radioactive material which is uniformly distributed throughout a counter, it is necessary to know the fraction of the disintegrations which produce counts. This fraction times the total volume available to the gas may be called the effective volume. The size of the effective volume depends on such factors as the distortion of the electric field in the region where the central wire emerges from its shield, the geometry of the end portion of the counter, the pressure, and the particle range. In correcting for the end effect, Libby and co-workers[2] have made use of counters which differ only in length. A similar technique has recently been described by a Canadian group.[9,10] In first approximation the effective volume may be regarded as bounded by the cylinder walls and by planes per-

[9] Hawkings, Hunter, Mann, and Stevens, Phys. Rev. **74**, 696 (1948).
[10] W. B. Mann and G. B. Parkinson, Rev. Sci. Inst. **20**, 41 (1949).

pendicular to the counter axis at the points where the wire emerges from its shields.

The bare wire length, L, should be replaced, however, by $L-\epsilon$, where ϵ will depend on the factors noted above. Suppose that one has counters of different unshielded wire lengths L (see Fig. 1), which have the

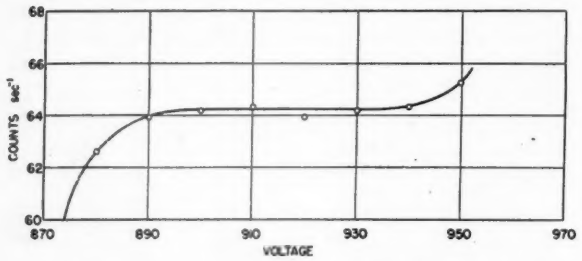

FIG. 2. Counting rate *versus* voltage characteristic for Geiger tube at CO_2 partial pressure of about 2 mm Hg and total pressure 10.0 cm Hg.

same effective cross sections A, and which are filled so as to have the same atomic density of radioactive material ρ. Then the counting rate, R_L, owing to the material of decay constant λ is given by

$$R_L = A\rho\lambda(L-\epsilon), \tag{1}$$

and ϵ can be determined by fitting the data to the linear relationship (1).

In one experiment, three counters, identical except for length, were filled simultaneously to a pressure of 10.0 cm Hg with a carbon dioxide-quencher gas mixture. The partial pressure of the carbon dioxide, which contained enough C^{14} to give convenient counting rates, was about 1.1 mm Hg. Small corrections for resolving time losses, previously determined for gas of this composition, were made. Background corrections were made by utilizing monitor counters with which the master counters had previously been intercompared within the lead shield used for background reduction. The results of this experiment, together with the value of ϵ found, are given in Table III. Column 4 is computed from the least squares line through the data, assuming only counting rates to be uncertain.

Like measurements were made at total pressures of 16.6 and 20.3 cm Hg with counters 1 and 2. The values of ϵ are 0.47 and 0.50 cm at these pressures, respectively. In subsequent counting experiments, only counter 3 was used. The effective volume for this counter is about 90 percent of the total volume available to gas.

It will be shown in the next section that the effective cross section A in Eq. (1) is equal to the geometric cross section of the counter within experimental error.

COUNTING MEASUREMENTS

A known portion of the diluted radioactive carbon dioxide gas was measured in the small calibrated volume referred to previously by making pressure, volume, and temperature measurements. A small correction was made for the non-ideal character of carbon dioxide gas. The pressures measured were in the neighborhood of 10 cm Hg. This material was then quantitatively transferred to the counter by condensing with liquid nitrogen. When the counter had reached room temperature, quencher gas was admitted to the counter to the desired total pressure. Since the quencher enters the counter through a section of capillary tubing, a negligible amount of carbon dioxide should be lost from the counter by back diffusion. This point was checked experimentally by counting the contents of the vacuum line after such a filling. In order to be sure that a uniform concentration of materials existed, the counter was allowed to stand overnight before counting was commenced. Previous experiments had shown that this was sufficient time to allow, since counting measurements over a subsequent 72-hour period showed no change. The background was measured with a monitor counter as above.

Counting data were then obtained as a function of overvoltage. Although the usable voltage range was not long, the counter showed a voltage range where the counting rate was satisfactorily independent of voltage. A plot of counting rate *versus* overvoltage is shown in Fig. 2 for a counter containing CO_2 at about 2 mm Hg partial pressure, the total pressure being 10.0 cm Hg. The material was then counted at the selected position on the plateau for a long enough time to give probable counting errors of about 0.2 percent or better. In most cases duplicate runs were made at a slightly different voltage. The results of the experiments are given in Table IV.

As mentioned, a set of preliminary measurements showed that the counting rate did not change beyond the experimental error over a 72-hour period. The absence of a trend in the counting rate makes it seem likely that no loss of active material was occurring by slow adsorbtion.

TABLE III. Effective length of counters at 10.0 cm Hg pressure.

Counter	L, cm	R_L observed counts/sec.$^{-1}$	R_L calculated counts/sec.$^{-1}$
1	8.674	14.56	14.56
2	21.466	37.13	37.13
3	34.287	59.76	59.76
	$\epsilon=0.42_8$ cm.		

TABLE IV. Counting measurements.

Experiment	Half-life, years	Comments
1	5539	CO_2 1.1 mm Hg, total pressure 10.0 cm Hg
2	5586	CO_2 2.3 mm Hg, total pressure 10.0 cm Hg
3	5613	CO_2 3.4 mm Hg, total pressure 10.0 cm Hg
4	5595	CO_2 2.3 mm Hg, total pressure 16.6 cm Hg
5	5613	CO_2 2.3 mm Hg, total pressure 20.3 cm Hg

Average 5589±41 years. The error quoted is the probable error from the above data.

In Experiment 1, no additional carbon dioxide was added to the counter beyond the diluted material containing the C^{14}. In Experiments 2 and 3, additional pure carbon dioxide was added. If active carbon dioxide were being adsorbed on the counter walls, the addition of carrier CO_2 might increase the counting rate. It must be admitted, however, that if the adsorbtion were small, the amounts of inert and radioactive carbon dioxide might be separately proportional to their pressures in the gas; the role of the appreciable amount of quencher gas is not easy to evaluate in this connection. In any case, no indication of a trend in counting rate was observed. In addition, Experiments 4 and 5, in which the total pressure is increased, do not give indication of adsorbtion. While the processes of mixed adsorbtion are complicated it does not seem likely that an appreciable loss in counting rate is occurring because of adsorbtion. Backgrounds of counters which were exposed to activity for considerably longer times than those of the experiments in Table IV did not show any increase in background on pumping out and refilling with quencher. Permanent increases of a few percent in background did occur over very long periods. This behavior may be owing to the deposition of nonvolatile radioactive material on counter walls. Preliminary calculations based on the known adsorbtion of carbon dioxide on zinc and copper oxides, and reasonable estimates of the amounts of such materials within the brass counter, had suggested that such absorbtion should be negligibly small.

Experiments 4 and 5, in which the quencher gas pressure was increased, were performed chiefly for the purpose of uncovering a wall effect. The number of β-particles, produced near the counter wall and, failing to produce a count because of too long a mean free path for ion pair formation, should decrease as the pressure is increased. Experiments 4 and 5 do not show such a trend. It seems likely that this observation is connected in part with the very efficient geometry which exists for the detection of backscattered particles. On the basis of these experiments, it is assumed that the effective and geometric counter cross sections are the same.

In the above experiments, account was taken of the slight decrease in effective length of the counters as the pressure increased. Small corrections were made, on the basis of a preliminary experiment, for the effect of CO_2 on the resolving time. Correction was also made for increase in resolving time with total pressure.[11] The total resolving time losses were about 1.3 percent of the observed counting rates.

TABLE V. Comparison of half-life values.

Observers	Half-life, years
Reid, Dunning, Weinhouse, and Grosse[a]	4700±5–10%
Norris and Inghram[b]	5100±200
Hawkings, Hunter, Mann, and Stevens[c]	6100±200
Yaffe and Grunlund[d]	7200±500
This research	5589±75

[a] Reid, Dunning, Weinhouse, and Grosse, Phys. Rev. **70**, 431 (1946).
[b] L. D. Norris and M. G. Inghram, Phys. Rev. **73**, 350 (1948).
[c] See reference 9.
[d] L. Yaffe and M. G. Inghram, Phys. Rev. **73**, 350 (1948).

DISCUSSION OF ERRORS AND COMPARISON WITH OTHER WORK

The probable error derived from the measurements of Table IV is 41 years. Other uncertainties exist, however. An uncertainty of 0.3 percent arises from the mass spectrometric analysis, the dilution factor may be in error by 0.05 percent, and an error of 0.05 percent may exist in the amount of material condensed into the counter. At the higher pressures, the effective counter lengths may be in error by 0.1 percent. Uncertainties of 0.1 percent may exist because of uncertainties in background and resolving time corrections. These known uncertainties raise the probable error in the half-life to 46 years. It seems safer to increase this estimate, however, and the half-life will be taken as 5589±75 years. In Table V the present value is compared with other values which have been obtained for the half-life. Detailed reports have not been given in all cases. Earlier and more uncertain estimates are omitted.*

I thank Arthur Murray for assistance in the preparation of the pure carbon dioxide used in the dilution measurements. I am indebted to the Oak Ridge National Laboratory for the C^{14} material.

This document is based on work performed at the Los Alamos Scientific Laboratory of the University of California under government contract W-7405-eng-36.

[11] L. Costrell, J. Research Nat. Bur. Stand. **42**, 241 (1949).

* After the present work was submitted for publication the results of a careful measurement of the C^{14} half-life were reported by Engelkemeier, Hamill, Inghram, and Libby, Phys. Rev. **75**, 1825 (1949). This group obtained a value of 5720 years. The uncertainty expressed as the standard deviation was stated to be 48 years, and the "safe" uncertainty was estimated as 100 years.

Proton Groups from the Bombardment of Argon by Deuterons

P. W. DAVISON,* J. O. BUCHANAN,** AND ERNEST POLLARD
*Sloane Physics Laboratory, Yale University,*** New Haven, Connecticut*
(Received June 29, 1949)

The deuteron bombardment of argon in both ordinary form and with a 26 percent concentration of A^{36} shows the presence of thirteen groups of protons. Correct assignment to isotope can be made for ten of these and probable assignment for the others. The Q-values for the reactions are: $A^{36}(dp)A^{37}$ 6.59; 5.06; 4.92; 4.32; 4.03; 3.13 and 1.58 and $A^{40}(dp)A^{41}$ 3.84; 3.18; 2.63; 2.50; 1.90; 1.57; 1.04; 0.55; 0.15; −0.17. The mass difference $A^{37}-A^{36}$ is 0.99951 and $A^{41}-A^{40}$ is 1.00247. Considering that the nuclei differ by four neutrons there is surprisingly little difference in general level structure. The first excited state of A^{37} is at an unusually high value.

INTRODUCTION

THE observation of proton groups produced in the bombardment of argon by deuterons can be made to give information on the energy levels of A^{41} and A^{37}. There is some interest in energy levels of two isotopes differing by four neutrons, especially as it is likely that a new neutron shell is being developed at about this mass number.

This method was employed by W. L. Davidson, Jr.[1] Davidson reported excited states at 1.36 and 2.14 Mev in A^{41}. The maximum nuclear energy change (Q-values) was given as 4.37 Mev. A repetition of this work using postwar counting methods was reported by two of the authors[2] in which Q-values were reported at 3.82, 3.19, 2.65, 1.97, 0.95 Mev. These confirm the two excited states found by Davidson but give a new value for the maximum Q.

Ordinary argon contains A^{40}, 99.63 percent; A^{38}, 0.061 percent; and A^{36}, 0.307 percent. It was thought likely that by a reasonable separation of A^{36}, new proton groups of sufficient intensity would be found and therefore energy levels in A^{37} could be discovered.

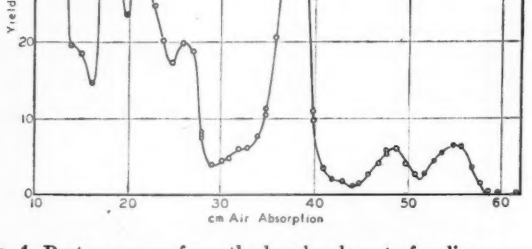

FIG. 1. Proton groups from the bombardment of ordinary argon by deuterons. All the groups are assigned to A^{41}.

The separation of argon isotopes was achieved by one of us (J. O. Buchanan) by means of thermal diffusion columns: the technique will be described in a separate paper. Mass spectrographic analysis showed that the separated gas sample contained 26.2 percent A^{36}, 1.6 percent A^{38}, 72.2 percent A^{40} and <0.2 percent N_2[28]. This was considered adequate for work and the results are herein described.

EXPERIMENTAL RESULTS

The gas was bombarded in a special bombardment chamber in which the beam was brought through an aluminum foil into a space with an exit port for observation of protons at 90° to the beam. The details of this bombardment chamber are described in a paper by one of us (P. W. Davison).[3] The thickness of the target can be varied by varying the gas pressure and it has been our experience that such targets can be made to give very precise evidence regarding group structure. Protons were observed with a proportional counter containing argon at 20 cm pressure. Bias was employed to ensure counting protons which are nearly stopped. Experimental results are given in Figs. 1, 2, and 3. Figure 1 shows the result of bombarding ordinary argon. The

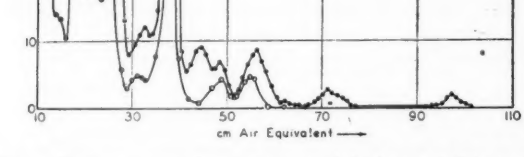

FIG. 2. Proton groups from argon enriched in A^{36} (black dots) together with normal argon (white rings) for comparison. The presence of longer range groups is clearly seen, also some change in the relative intensities indicating groups due to A^{36} at shorter range.

* Now at R.C.A. Laboratories.
** Now at University of West Virginia.
*** Assisted by the joint program of ONR and AEC.
[1] W. L. Davidson, Jr., Phys. Rev. **57**, 244 (1940).
[2] E. Pollard and P. W. Davison, Phys. Rev. **73**, 1241A (1948).
[3] P. W. Davison, Phys. Rev. **75**, 757 (1949).

group structure can be seen and has been analyzed into the Q-values listed in Table I.

The result of bombarding the sample enriched in A^{36} is shown in Fig. 2. The unenriched curve is shown for comparison. It can be seen that several groups are present at longer ranges than any previously observed and moreover, two groups at shorter ranges can be seen to be clearly enhanced in yield.

The detail of the long range groups is shown in Fig. 3. The width of the second group at range 76 cm is greater than that of a single group and we are confident that this group is double. A group of low yield appears just beyond the Q_0 group from $A^{40}(dp)^{41}$ and in addition there is clearly an increased width to the group ending

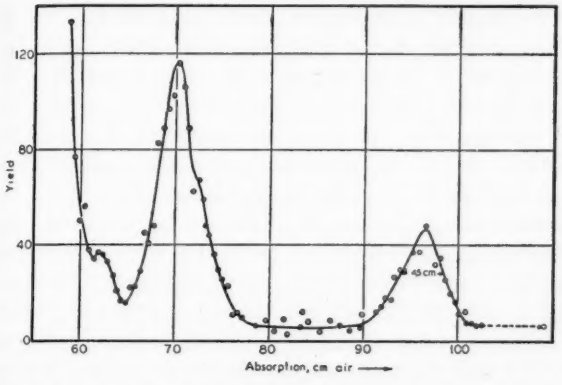

FIG. 3. Detail of the groups from A^{36} which have range beyond any due to A^{40}. The group with peak at 70 cm, is double. A total of five groups due to the light isotope can be recognized.

near 60 cm which is due to the superposition of the q_4 group from $A^{36}(dp)A^{37}$ on the Q_0 group from $A^{40}(dp)A^{41}$. It is thus possible to assign the ground state and four excited states to the A^{37} nucleus. Assignment within the group structure of A^{41} is difficult, but it can be seen from Fig. 3 where the curves for separated and unseparated targets are plotted for comparison, that groups at 47 cm and 28 cm and possibly 24 cm are due to A^{37} excited states. There is also a likelihood that the large yield group at 40 cm is wider for the separated sample. It is very likely that two or three groups from A^{36} are masked by abundant A^{40} groups.

The result of this analysis is given in Table I which lists the Q-values for the two reactions. Doubtful assignments are starred.

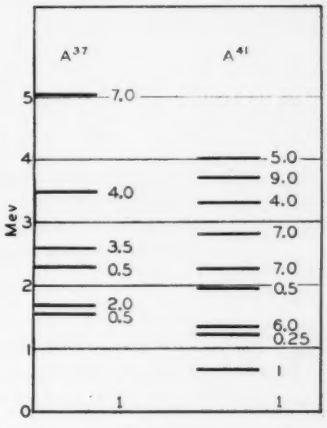

FIG. 4. Energy levels and relative abundances for A^{37} and A^{41}. The first excited state of A^{37} is unusually wide and the second unusually narrow. Gaps undoubtedly exist in the levels indicated for A^{37} above 2.6 Mev excitation owing to the masking of group structure by A^{41} groups. Below that, the structure should be complete.

TABLE I. Q-values for the two $A(dp)$ reactions.

	$A^{36}(dp)A^{37}$	Relative yield		$A^{40}(dp)A^{41}$	Relative yield
q_0	6.59±0.03	1	Q_0	3.84±0.03	1
q_1	5.06±0.03	0.5	Q_1	3.18±0.05	1
q_2	4.92±0.05	2.0	Q_2	2.63±0.04	0.25
q_3	4.32±0.05	0.5	Q_3	2.50±0.04	6.0
q_4	4.03±0.03	3.5	Q_4	1.90±0.04	0.5
q_5*	Probably masked		Q_5	1.57±0.05	7.0
q_6*	3.13	4.0	Q_6	1.04±0.05	7.0
q_7*	Probably masked		Q_7	0.55±0.03	4.0
q_8	1.58	7.0	Q_8	0.15±0.05	9.0
			Q_9	−0.17±0.05	5.0

DISCUSSION

The energy levels for A^{37} and A^{41} are shown in Fig. 4. The first excited state of A^{37} is wider than usual and appears to be double. The average spacing of the first four levels is only slightly greater than that of A^{41}. The difference of four neutrons appears therefore to produce no very dramatic effect.

We feel reasonably confident that the first four Q-values we list in each case are single and do not contain overlapping groups. The expected line width, in view of the known beam inhomogeneity and target thickness is about the experimentally found line width. At higher excitations this is not true and there may be an overlapping. It will be noticed that in any event there seem to be more protons in highly excited states than in the states of low excitation. This is generally observed in dp reactions.

Taking the values 1.00812 and 2.01471 for the mass of the proton and deuteron respectively the values of the mass differences $A^{37}-A^{36}$ and $A^{41}-A^{40}$ are 0.99951 and 1.00247±0.0001 in each case.

Classification of Nuclear Isomers

P. AXEL AND S. M. DANCOFF
University of Illinois, Urbana, Illinois
(Received June 16, 1949)

A classification is made on the basis of the forbiddenness of the transitions from the known nuclear isomeric states. The resultant grouping is shown to be in agreement with the Weizsäcker theory of isomerism and with internal conversion theory. The predictions of internal conversion theory are also compared with the experimental values that are available for the isomers considered.

A NUCLEAR isomeric state may be defined as an excited state of a nucleus which exists for a measurable length of time ($\tau \geq 10^{-9}$ second). Since most nuclear excited states decay with much shorter half-lives, isomeric states must be characterized by having only highly forbidden transitions. Weizsäcker[1] first explained this forbiddenness by postulating that each transition had a large angular momentum change associated with it and that, therefore, only quanta of high multipole order could be emitted.

The effect of this high multipole order can be exhibited by considering the analogous system of an oscillating distribution of charge in classical electrodynamics. The total radiation, R, from such a distribution is given by:

$$R=(R_{E1})+(R_{M1}+R_{E2})+(R_{M2}+R_{E3})+\cdots, \quad (1)$$

where R_{Ei} is the rate of electric 2^i pole radiation and R_{Mi} is the rate of magnetic 2^i pole radiation. In this expansion, individual contributions which are of the same order of magnitude are bracketed into terms. Successive terms decrease rapidly if the dimension of the oscillator is small compared to the radiated wavelength. Therefore, the first contributing term essentially determines the total probability of radiation and a high forbiddenness corresponds to the vanishing of the first group of terms. It is convenient to designate this forbiddenness by l, the number of the first contributing term. A given l value corresponds to either electric 2^l or magnetic 2^{l-1} pole radiation.

A semiquantitative theory for the decay of isomeric states can be developed by extending these electrodynamic considerations to a nucleus in an excited state. The mean life of the state (for gamma-ray emission only) can be shown to be:

$$\tau_\gamma=\frac{3(l!)^2}{\rho^{2l}}\left(\frac{137}{W}\right)^{2l+1}\frac{\hbar}{mc^2}, \quad (2)$$

where ρ=radius of the nucleus in units of e^2/mc^2, W=excitation energy in units of mc^2, and $\hbar/mc^2=1.31\times10^{-21}$ second. The derivation of this relation involves various approximations. The crudest of these is that the nuclear matrix element for the transition depends solely on the size of the nucleus. Thus, Eq. (2) could be expected to give only an average value for τ_γ. Fluctuations about this average by factors of 10 or 100 may be anticipated by considering the results of the analogous procedure applied to atomic transitions. The derivation of Eq. (2) is based on the model of a single charge executing oscillations whose amplitude is equal to the nuclear radius. Other models yield formulas agreeing as to the dependence of τ_γ on ρ and W but differing as to numerical factors.

A comparison can be made between the experimentally determined lifetimes and those predicted by Eq. (2). Figure 1 shows the experimental data for 56 isomers; each isomer is exhibited as a point on a graph of $\log\tau_{exp}$ as a function of $\log W$. Only those isomers that decay predominantly to another state in the same nucleus (i.e., generically related isomers) are included; of these, isomers living for less than 1 second are omitted since they are too few to define groups. (A plot of this type was first published by Wiedenbeck.[2]) While a grouping is in evidence, the dependence of the lifetime on energy is certainly not as is predicted by Eq. (2).

However, one would expect that the experimentally determined lifetime, τ_{exp}, would be less than the gamma-ray lifetime, τ_γ. This decrease in lifetime is caused by the competing process of internal conversion which tends to increase the total transition rate.[3] If this additional process is considered, the relation between the two lifetimes is given by

$$\tau_\gamma=\tau_{exp}\left(1+\frac{N_e}{N_\gamma}\right), \quad (3)$$

where N_e/N_γ is the total conversion coefficient. Since the internal conversion coefficient depends on the atomic number, Z, τ_{exp} cannot be expressed as a function of W alone. Therefore, for a quantitative comparison, it is necessary to convert τ_{exp} to τ_γ for each isomer. (Wiedenbeck[2] did not make this type of point-by-point correction.)

The values for τ_γ must be calculated by using theoretical conversion coefficients since the experimental internal conversion data are inadequate. The calculations can be made for each nucleus if the energy of the metastable state is known and if a tentative l value

[1] C. F. von Weizsäcker, Naturwiss. **24**, 813 (1936).

[2] M. L. Wiedenbeck, Phys. Rev. **69**, 567 (1946).

[3] H. M. Taylor and M. F. Mott, Proc. Roy. Soc. **A142**, 215 (1933).

assignment is made on the basis of Fig. 1. Because of the approximate nature of the formula for τ_γ, the difference between electric and magnetic conversion coefficients is not significant; for simplicity, only the electric conversion coefficients are used. The correction factors for the 56 isomers range from 1.04 at the highest energy to 7.8×10^{7} at the lowest energy. The values of τ_γ are plotted as a function of energy in Fig. 2. Not only is the resultant grouping much more definite, but also there is qualitative agreement with regard to the predicted energy dependence (i.e., $\tau_\gamma \propto W^{-(2l+1)}$).

A more quantitative check may be made on the absolute value of τ_γ by taking account of the value of ρ^{2l} for each isomer. Equation (2) indicates that the product $\tau_\gamma\rho^{2l}$ depends only on the transition energy. Except for the expected variation in nuclear matrix elements, this product is directly calculable from Eq. (2) without any adjustable parameters. Figure 3 shows the isomers on a plot of $\log\tau_\gamma\rho^{2l}$ as a function of $\log W$. (The value of the nuclear radius was taken as $r=1.5A^{\frac{1}{3}}\times10^{-13}$.) The unadjusted theoretical lines are drawn in for $l=3$, 4, 5, and 6. The agreement between the $l=4$ and $l=5$ lines and the experimental points is seen to be quite good; the experimental points all fall within the anticipated factor of 100 of the theoretical lines. Pb^{204}, which is the only even-even isomer on this graph, seems to fit the $l=6$ group. (The point that is shown for Pb^{204} was calculated by assuming $l=5$; for $l=6$, $\tau_\gamma\rho^{2l}$ would increase by a factor of 10.)

The existence of distinct groups corresponding to $l=4$ and $l=5$ is not shown by a superficial examination of Fig. 3, since the conversion correction which is based on an assumed l value tends to produce a grouping. (The conversion correction increases with l, especially at low energy.) However, the following three considerations tend to substantiate the existence of these groups: (a) Groups are already in evidence in Fig. 1, particularly in the significant region above 200 kev where internal conversion corrections are very small. (b) The grouping of Fig. 1 would be accentuated even if the same l value were used to calculate the conversion correction for all points. Therefore, the assumed l value is not responsible for artificially inducing a grouping. (c) The most striking evidence for the existence of two groups is the semiquantitative agreement which is exhibited in Fig. 3.

Once the existence of groups is established, the maintenance of these can be used as the criterion for assigning l values in the few questionable cases. For example, in the case of the most doubtful member of the $l=5$ group, Te^{131}, a reassignment to $l=4$ would shift the point down 0.76 unit on the logarithmic plot of Fig. 2. Similarly, reassignment of Tc^{99} and Cs^{134} to the $l=5$ group would shift these points up by 0.83 and 0.88. These changes would obviously not fit the above criterion since the isomers concerned would then be further separated from either group.

On the basis of the agreement achieved, it is possible

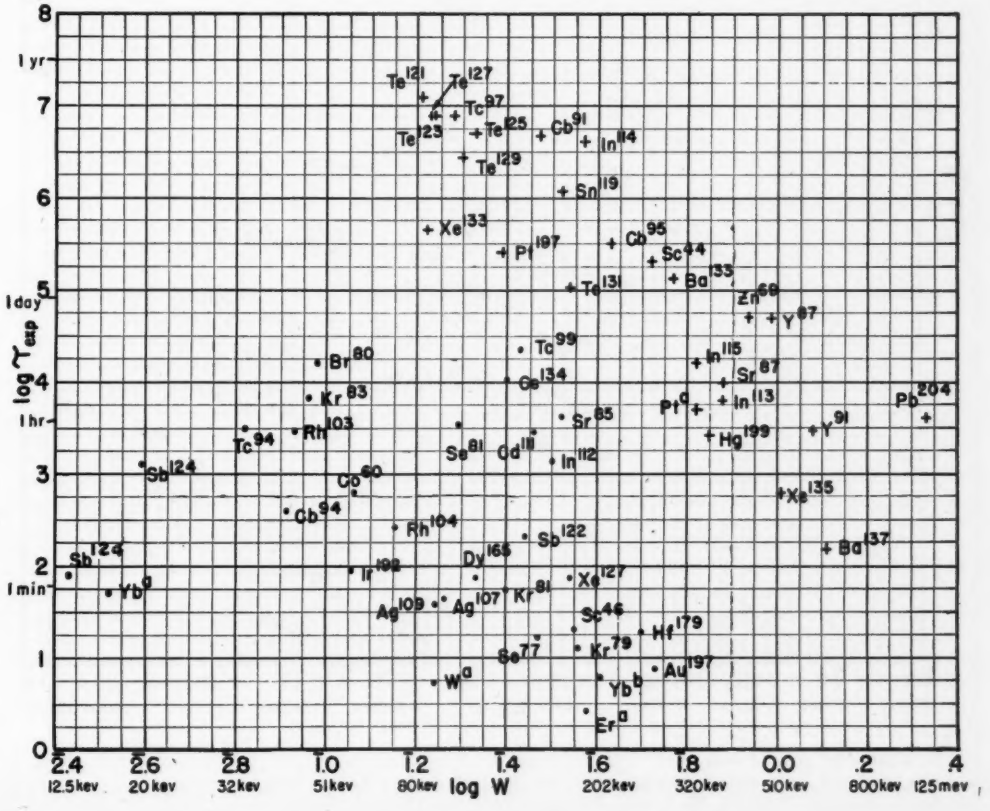

FIG. 1. Comparison between experimentally determined lifetimes of isomers and those predicted by Eq. (2).

to draw several conclusions. The existence of the $l=4$ and $l=5$ groups tends to substantiate Weizsäcker's explanation of the existence of isomeric states. The semiquantitative agreement shown in Fig. 3 further indicates the qualitative validity of internal conversion theory. Finally, the specific l value assignments seem valid and may be useful in the evaluation of the proposed "shell" models of nuclei which purport to describe the detailed nature of isomeric transitions.

Notes added in proof.—(1) Xe^{133} was erroneously listed as an isomer; it should be deleted from the three figures. (2) The energy of Hf^{179} has been redetermined so that log $W=\bar{1}.47$. This changes the ordinates on the three figures to 1.3, 2.62, and 6.45. (3) Four new isomers should be added to the 55 remaining in the three figures. The values for the abscissa and for the ordinates appropriate for the three figures for each of these isomers are, respectively: Co^{58} $\bar{2}.65$; 4.55, 9.8, and 12.35; Ta^{182} $\bar{1}.55$; 2.95, 3.95, and 7.8; Xe^{131} $\bar{1}.51$; 6.0, 7.8, and 12.2; and Ba^{135} $\bar{1}.75$; 5.0, 5.6, and 9.95.

INTERNAL CONVERSION DATA

In principle, it should be possible to provide a further check on the l value assignments by comparing experimental internal conversion data with the theoretical predictions. For this purpose, independent checks might be afforded by both the absolute value of the K conversion coefficient and the ratio of K conversion to L conversion. However, the present status of both experiment and theory makes such checks impractical.*

One limitation has been the lack of adequate theoretical calculations caused by the computational difficulties involved. Recently, Rose and his collaborators[4] have made some relativistic calculations using the Mark I Relay Calculator at Harvard. Thus far, these calculations are available only for K conversion (both electric and magnetic) and only in the energy range above 150 kev. It is, therefore, necessary to use calculations based

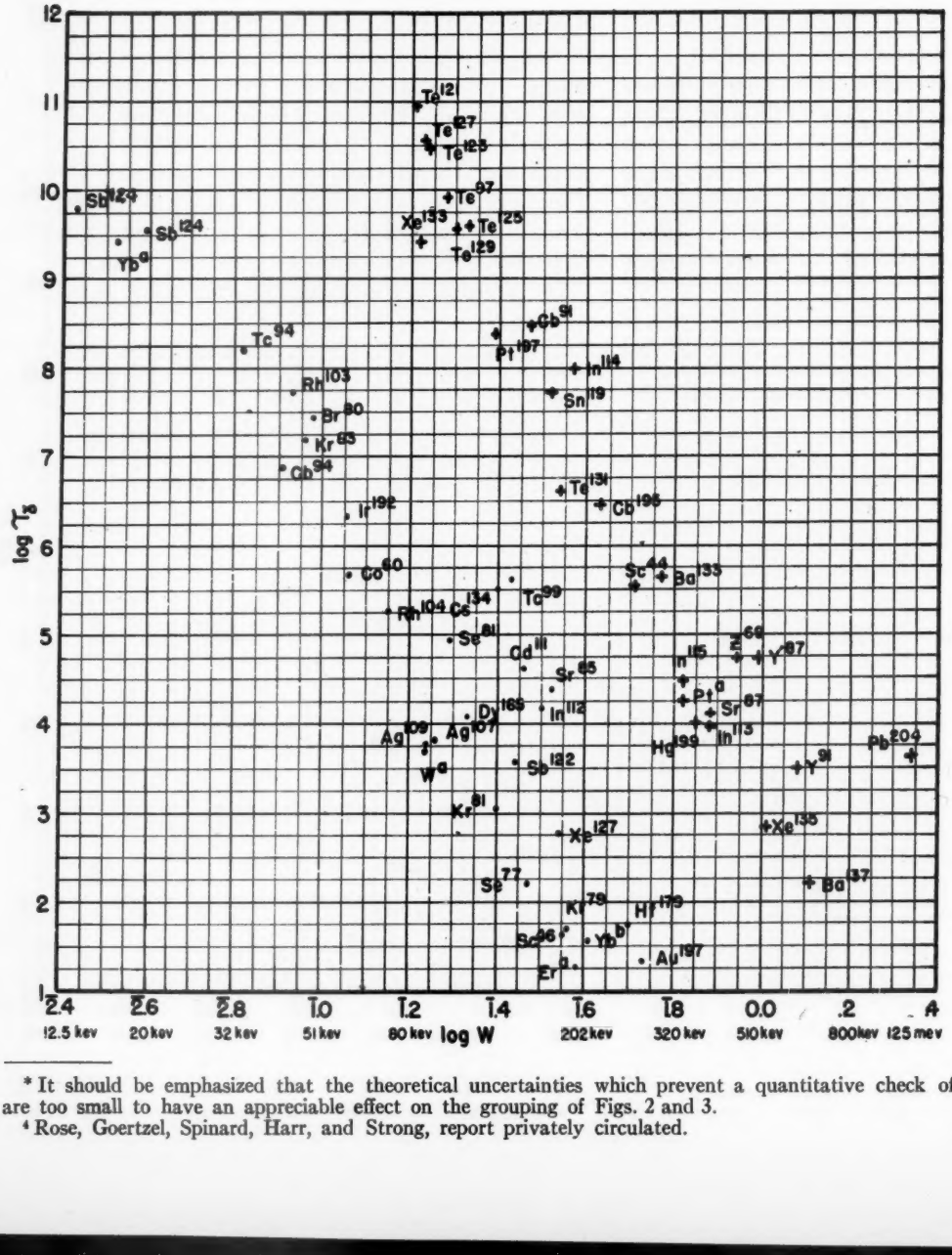

FIG. 2. Values of the calculated γ-ray lifetimes of isomers as a function of the energy.

* It should be emphasized that the theoretical uncertainties which prevent a quantitative check of internal conversion theory are too small to have an appreciable effect on the grouping of Figs. 2 and 3.

[4] Rose, Goertzel, Spinard, Harr, and Strong, report privately circulated.

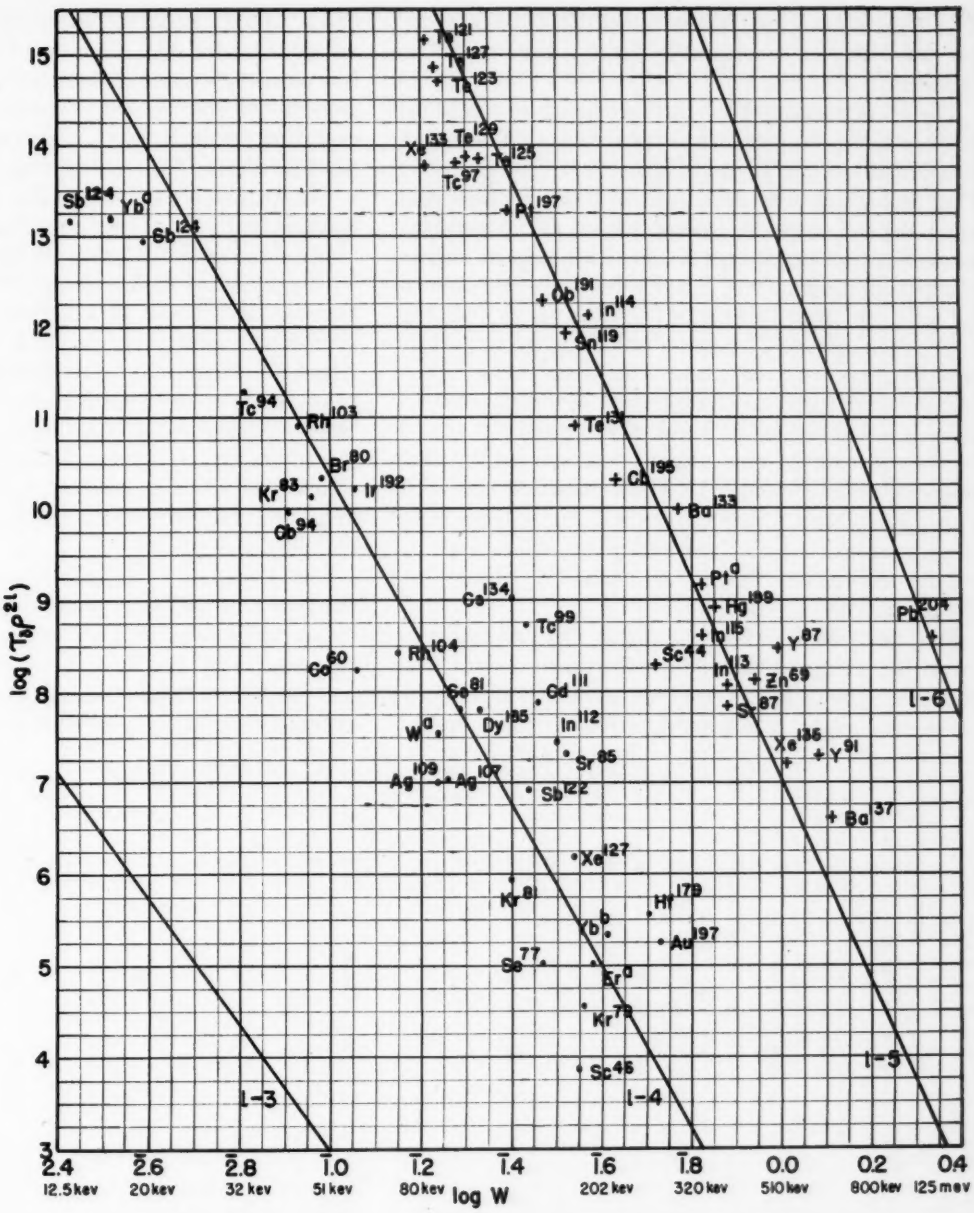

FIG. 3. Values of log $(\tau_\gamma \rho^{21})$ as a function of log$W$.

on simpler approximations when dealing with either K conversion coefficients for energies below 150 kev or any L conversion coefficients.

There are two sources for the approximate K conversion coefficients. A non-relativistic theory of electric K shell conversion was developed by Hebb and Uhlenbeck[5] and Dancoff and Morrison;[6] the calculations from this theory are available in the tabulation of Hebb and Nelson.[7] A comparison of these theoretical predictions with those of Rose (in the region above 150 kev) shows that the approximate results are always low and that they improve as the energy decreases. However, even at energies as low as 150 kev, errors as large as 70 percent exist. The magnetic K conversion coefficients can be estimated from Drell's calculations,[8] which give the ratio of the magnetic K to electric K conversion. Comparison with Rose's data shows that these approximate results are also in error; Drell's ratio is always low and may be in error by a factor as large as 3.

The approximate calculations for L shell conversion coefficients have been made by Hebb and Nelson[6] for the electric case and by Lowen and Tralli[9] and Drell[10] for the magnetic case. Although the calculations for the K and L shells are similar, the deviation of the derived

[5] M. H. Hebb and G. E. Uhlenbeck, Physica **5**, 605 (1938).
[6] S. M. Dancoff and P. Morrison, Phys. Rev. **55**, 122 (1939).
[7] M. H. Hebb and E. Nelson, Phys. Rev. **58**, 486 (1940).
[8] S. D. Drell, Phys. Rev. **75**, 132 (1949).
[9] I. S. Lowen and N. Tralli, Phys. Rev. **75**, 529 (1949).
[10] S. D. Drell, private communication.

K to L ratio from the true value is difficult to estimate; the possibility of considerable discrepancies cannot be excluded.

The l value assigned by the correlation of Fig. 3 can indicate either only electric 2^l pole radiation or a combination of electric 2^l and magnetic 2^{l-1} pole radiation. This ambiguity exists because of the selection rules which depend on parity considerations. If the transition occurs between two energy levels which have an angular momentum difference of S, then the multipole order of the radiation must be at least S. If the parity change is $(-)^S$, then electric 2^S pole radiation can occur and the forbiddenness, $l=S$. In this case the transition is termed parity allowed and the radiation is essentially electric in nature. On the other hand, if the parity change is $(-)^{S+1}$, electric 2^S pole radiation cannot occur. Both magnetic 2^S and electric 2^{S+1} pole radiation can occur with probabilities which are of the same order of magnitude and $l=S+1$. In these parity forbidden cases, the relative amounts of electric and magnetic radiation are not predictable.

Despite this uncertainty, it might still be possible to check the theory if adequate experimental data were available on both the internal conversion coefficient and the K to L ratio. The procedure for carrying out this check would consist of using the lifetime to fix the l value. It would then often be possible to use one of the two pieces of internal conversion data to fix the relative amounts of electric and magnetic radiation. The other experimental determination would then provide an independent check of these assignments.

Unfortunately, the available experimental data are inadequate for this type of analysis. There are very few internal conversion coefficients that have been measured with sufficient precision. In many cases, the gamma-rays have not even been observed; in the other cases, the precision is limited by the lack of information on the relative efficiencies for detecting gamma-rays and electrons. While many K to L ratios have been determined, most of these were investigated with early beta-ray spectrographs that were incapable of giving precise ratios. The broad line shapes, the weak sources and the unknown efficiency characteristics of the detectors all limited the precision.

The data that have been reported for the isomers in the $l=4$ and $l=5$ groups are collected in Table I. The theoretical values that are listed were calculated from the sources which have been discussed. The experimental K to L ratios marked with asterisks are crude estimates based on published spectrograms. Although

TABLE I. Data for the isomers in the $l=4$ and $l=5$ groups.

				K to L Ratio			Conversion coefficient		
					theoretical				
Z	Element	A	kev	experimental	Electric	Magnetic	Experimental	$\alpha_K+\alpha_L$	$\beta_K+\beta_L$
					$l=4$				
27	Co	60	59	4±0.5	2.6	7.0			
34	Se	81	99	4	2.6	7.2			
35	Br	80	49	2*	0.59	4.5			
36	Kr	79	187	10*	4.6	8.5			
36	Kr	81	127	4*	3.1	7.6			
36	Kr	83	46	1	0.43	4.0			
41	Cb	94	41.4	.31	0.11	2.8			
43	Tc	99	136	4*	1.8	6.8			
47	Ag	107	94	.92±.06; 1	0.58	4.7	99; 75^{+200}_{-45}	145	44
47	Ag	109	88	1.01±.06	0.49	4.4	19±3	214	37
48	Cd	111	148	10*	1.4	6.3			
54	Xe	127	175	5*	1.2	6.2			
55	Cs	134	150	.64	0.55	5.4			
66	Dy	165	109	0.08	0.10	2.8			
79	Au	197	273	3.4	0.51	4.8			
					$l=5$				
21	Sc	44	270	8±4	19.5	9.2	0.07±0.012; 0.5	0.72	0.15
30	Zn	69	440				0.01 to 0.1	0.091	0.056
38	Sr	87	386	6 to 7	5.6	8.3	0.15	0.32	0.58
43	Tc	97	97	2	0.45	4.0			
49	In	113	390	5.4	3.0	7.2	2.3±0.6	0.47	0.58
49	In	114	190	1.0±0.1	1.03	5.4	>9	23	14
49	In	115	340	5.0±0.5	2.64	6.8	1±0.3	0.88	0.97
52	Te	121	82	0.75	0.07	1.8			
52	Te	123	88.5	0.68	0.10	1.9			
52	Te	125	109	1.5	0.21	3.0			
52	Te	127	86	0.75±0.25	0.088	1.9			
52	Te	129	102	1.0	0.16	2.9			
52	Te	131	177	2	0.69	4.8			
54	Xe	135	520				0.2	0.15	0.24
56	Ba	133	300	3.18	1.33	6.1	2.4±0.6	2.25	2.8
56	Ba	137	663	4.8±0.3	3.9	7.9	0.12	0.068	0.11
78	Pt	197	126	$\ll 1$	0.01	1			
80	Hg	199	362	2.3*	0.41	4.4			

the accuracy of the experimental K to L ratios is often quite poor, it seems safe to assume that the listed values correctly indicate which component is larger. In the case of the reported internal conversion coefficients, the general accuracy claim is only one of order of magnitude.

A study of the data in Table I shows that the experimental results do not contradict the theory nor the l value assignments. In general, the theoretical values can be made to agree with the experimental values by assuming appropriate arbitrary quantities of electric 2^l and magnetic 2^{l-1} radiations. However, the significance of this agreement is very questionable since the lack of precision and the existence of the arbitrary adjustment make other l values equally acceptable.

The data in Table I do show one characteristic of isomers which may be significant. A large majority of the transitions have K to L ratios which indicate that magnetic radiation occurs (i.e., most of the transitions are parity forbidden). Because of the large difference between electric and magnetic K to L ratios, this conclusion seems relatively sound in spite of the possible uncertainties. This apparent predominance of parity forbidden transitions, if substantiated by future experiments and more trustworthy theoretical calculations, might further aid in evaluating the "shell" models of nuclei.

Note added in proof.—(4) Additional internal conversion data have appeared on Cd^{111}, Hf^{179}, Ta^{182}, Ba^{137}, Pt^{197}, Hg^{199}, and Pt^{a}. These new data are mostly values of the K to L ratio. With the exception of Ta^{182} and Cd^{111}, these isomers seem to have parity forbidden transitions.

The authors are indebted to Professor M. Goldhaber for his discussions on, and criticisms of the experimental data.

This work was assisted by the joint program of the ONR and AEC.

PHYSICAL REVIEW VOLUME 76, NUMBER 7 OCTOBER 1, 1949

Experiments on the Effect of Atomic Electrons on the Decay Constant of Be^7. II

R. F. LEININGER, E. SEGRÈ, AND C. WIEGAND
Radiation Laboratory, Department of Physics, University of California, Berkeley, California
(Received June 14, 1949)

A comparison of the decay constants of Be^7 in beryllium oxide and in beryllium fluoride has given $\lambda(BeO)-\lambda(BeF_2)=(+1.375\pm0.053)10^{-3}\lambda(BeO)$ thus showing a definite effect of the chemical binding on the radioactive decay constant.

IN previous papers on this subject[1] we pointed out the possibility of altering the half-life of Be^7 by chemical binding and we compared the decay constants of beryllium metal and beryllium oxide.[2] This experiment was not too conclusive because the effect $\lambda(BeO)-\lambda(Be)=(-3.0\pm1.8)10^{-4}\lambda(Be)$ was only about 1.7 times the standard deviation of the measurement and for this reason we decided to try another pair of compounds, and to use stronger samples. Our choice was beryllium fluoride and beryllium oxide and this time we have observed a definite effect, namely $\lambda(BeO)-\lambda(BeF_2)=(+1.375\pm0.053)10^{-3}\lambda(BeO)$.

The apparatus used was the same as that described in reference 2, the only change being that we enclosed the ionization chambers by a thermally insulating box. This provision kept the temperature of the two chambers equal to each other and effectively reduced the tendency of ambient temperature gradients to alter the relative sensitivity of the chambers. This effect of the temperature gradients was inconvenient, although it did not affect the results of the previous experiments because samples were interchanged between the chambers every 20 minutes. Also the positioning of the sample was carefully rechecked in order to have the sources in a position in which they would give a maximum of ionization. Small displacements from this position affect the sensitivity of the chamber only by a term quadratic in the displacement.

The Be^7 was obtained from a proton bombardment of lithium with the 60-inch Crocker cyclotron. The beryllium was purified as follows.

The bombarded lithium was dissolved in dilute hydrochloric acid containing approximately 20 milligrams of beryllium. Carriers of cadmium, cobalt, copper, nickel and zinc were added and the beryllium was precipitated by excess ammonium hydroxide from a hot solution. After cooling, the precipitate of beryllium hydroxide was washed two times by dilute ammonium hydroxide. The precipitate was redissolved in dilute nitric acid and precipitation by ammonium hydroxide after the addition of the carriers was repeated four times.

The last by-product of added carriers had a small amount of activity, but on adding to it normal beryllium and reseparating no activity was found in the fraction containing the carrier and all went with the inactive beryllium, showing that the activity was due to Be^7 and not to isotopes of the carrier. At this point an

[1] E. Segrè, Phys. Rev. **71**, 274 (1947).
[2] E Segrè and C. Wiegand, Phys. Rev. **75**, 39 (1949).

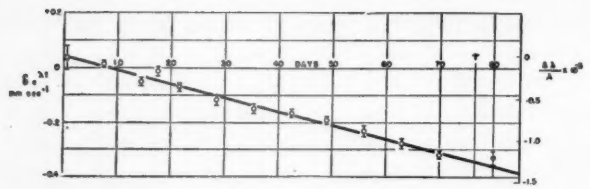

FIG. 1. Observed difference of activities of BeO and BeF_2 corrected for decay. $\delta e^{\lambda t}=\delta_0+A(\Delta\lambda/\lambda)(t/T)$ in mm sec.$^{-1}$. The initial difference of activity is 0.04 mm sec.$^{-1}$ and the initial activity A, 280 mm sec.$^{-1}$. The scale on the right hand side indicates the slope of the line for various values of $\Delta\lambda/\lambda$. The errors indicated are standard deviations.

aluminum absorption curve was run on the purified beryllium and failed to show the presence of any extraneous beta-ray activity.

The beryllium hydroxide was then converted to the basic beryllium acetate and dissolved in chloroform. The chloroform solution was washed by water two times to remove all water soluble impurities. The basic acetate-chloroform solution was evaporated to dryness and the residue dissolved in nitric acid.

To prepare beryllium fluoride, beryllium hydroxide was first precipitated and the washed precipitate dried at 110°C in a platinum boat. The platinum boat protected by a platinum shield was placed in a monel metal tube and the beryllium hydroxide converted to the fluoride by hydrofluorination with anhydrous hydrofluoric acid at 200°–220°C for two hours. The temperature was then increased to 500°C for five hours to sinter the product and to convert it to a definite crystalline form.

In the previous experiment there could be no doubt as to the compounds being measured since a button of the metal and the oxide were used. However, for the second experiment absolute evidence that the beryllium fluoride measured was actually the fluoride and not an oxyfluoride or oxide was considered necessary. X-ray diffraction studies were used as a method of analysis since the samples used are small and even radioactive preparations can be easily checked.

Crystallographic measurements were made for us by Dr. D. Templeton. The active beryllium fluoride had the same crystal structure as that which was observed for a previously submitted inactive sample. This structure is not the same as that usually reported for beryllium fluoride although chemical determination of the formula of this material gave BeF_2. The structure was hexagonal with constants of $A=4.72$A, $C=5.18$A in agreement with a beryllium fluoride structure observed by A. V. Novoselova *et al.*[3]

In order that the beryllium involved in the two compounds should have as nearly as possible the same treatment it was all converted to the fluoride and thereafter one half was dissolved in water and converted to the hydroxide and then to the oxide at 1000°C.

The samples were sealed in glass so that no moisture would affect them during the course of the measurements. Initially each sample gave in one of our chambers ionization equivalent to 317 micrograms of radium. This comparison was made by using the same ionization chambers and electrometer tube arrangement as was used in the differential measurements, but shunting the galvanometer and inserting a grid leak on the electrometer tube according to the intensity of radiation to be measured. With the grid leak we observed steady deflections of the galvanometer. We found that on the scale used in Fig. 1 the BeO sample gave initially a rate of drift of 280 mm sec.$^{-1}$. This was not, of course, measured directly, but by a ladder of successive comparisons of the strong beryllium oxide sample with a series of radium standards, the weakest of which could be measured using the same sensitivity as in the differential measurement. The same procedure had been used in the experiments referred in reference 2 but the shunt used then was different and for this reason 1 mm sec.$^{-1}$ in the two experiments corresponds to different activities.

In Fig. 1 we plot the difference of the activities of BeO and BeF_2 corrected for decay. This figure is analogous to Fig. 2 of our previous paper[2] and the slope of the line connecting the circles gives $\Delta\lambda/\lambda$. A least square reduction of the observed data gives

$$\lambda(\mathrm{BeO})-\lambda(\mathrm{BeF_2})=(1.375\pm0.053)10^{-3}\lambda(\mathrm{BeO}).$$

This datum combined with our previous one on $\lambda(\mathrm{BeO})-\lambda(\mathrm{Be})$ gives

$$\lambda(\mathrm{Be})-\lambda(\mathrm{BeF_2})=(1.675\pm0.19)10^{-3}\lambda(\mathrm{Be}).$$

Recently this quantity has also been measured by Bouchez, R. and P. Daudel, and Muxart[4] and they report a change in decay constant about 5 times larger than we observed.

This work was performed under the auspices of the AEC.

---

[3] Novoselava, Levina, Simanov, and Zhasmin, J. Gen. Chem. (U.S.S.R.) **14**, 385–402 (1944).

[4] Bouchez, Daudel, Daudel, and Muxart, Comptes Rendus **227**, 525 (1948). We thank these authors and Mr. A. Rogozinski for having also communicated to us a manuscript on the same subject submitted to the Journal de Physique et Radium.

Coincidence Experiments in Ni^{65}, Ni^{57}, Ag^{110} and In^{114}

FRED MAIENSCHEIN* AND J. LAWRENCE MEEM, JR.†
Department of Physics, Indiana University, Bloomington, Indiana
(Received June 20, 1949)

Absorption in aluminum of the beta-radiation from Ni^{57} gave a maximum beta-energy of 1.97 Mev. Beta-gamma-coincidence absorption indicated another beta-ray group at 0.46 Mev. Gamma-gamma-coincidences were obtained, and coincidence absorption of the Compton-recoil electrons gave gamma-rays of 1.64 and 0.3 Mev. The maximum energy of the positrons from Ni^{57} was found to be 0.72 Mev by absorption in aluminum. Beta-gamma-coincidences indicated the presence of only a single beta-ray group. Gamma-gamma-coincidences were obtained, and the energy of the most energetic gamma-ray was found to be 1.97 Mev. The beta-spectrum of Ag^{110} was shown to consist of beta-ray groups of 0.09, 0.55 Mev and a very high-energy component of low intensity. Beta-gamma-coincidences showed that the most energetic group leads to the ground state. A large gamma-gamma-coincidence rate was obtained, and the most energetic gamma-ray was found to have an energy of 1.48±0.1 Mev. In^{114} was found to emit a 0.196 Mev gamma-ray and a 2.05 Mev beta-ray as has been shown previously. In addition, gamma-rays of about 0.5, 0.7, and 1.3 Mev were found. Gamma-gamma-coincidences showed that two of these are in cascade and beta-gamma-coincidence absorption showed that they are not in coincidence with the 2.05 Mev beta-ray.

I. INTRODUCTION

COINCIDENCE and absorption measurements have been made on the radioactive isotopes Ni^{65}, Ni^{57}, Ag^{110}, and In^{114}. The G-M counters and coincidence amplifier used have been previously described.[1] The arrangement of the counters with respect to the source was that generally used for coincidence and absorption measurements.[2]

Earlier work on the two nickel isotopes, other than the mass assignments, has been performed by Livingood and Seaborg.[3] These investigators reported a half-life of 2.6±0.03 hours for Ni^{65} and a range for the most energetic beta-ray of 0.90±0.1 gm/cm² of aluminum. The gamma-ray half-value thickness was 10.8 gm/cm² of lead. Ni^{57} was found to be a positron-emitter with a half-life of 36±2 hours. The most energetic beta-radiation had a range of 0.25±0.05 gm/cm² of aluminum.

The radiations of Ag^{110} have been extensively studied on the beta-ray spectrometer.[4–7] The most recent of these investigations, that of Siegbahn,[7] indicated a complex beta-spectrum with groups at 0.087, 0.530, and 2.79 Mev. Ten gamma-rays were reported, with strong groups at 0.656, 0.885, and 1.389 Mev. A gamma-ray of 0.116 Mev was reported to be fairly highly converted and the most energetic gamma-radiation was given as 1.516 Mev. Cloud-chamber measurements have shown the presence of beta-ray groups of 0.09 and 0.59 Mev.[8]

In^{114} has been shown by Cork and co-workers to have an isomeric state which decays by a highly converted gamma-ray.[9] The gamma-ray energy was determined from the conversion lines in a magnetic spectrometer as 0.192 Mev and the half-life as 48 days. This level then was shown to decay by emission of a beta-ray of 1.98 Mev. The half-life of this transition was 72 sec. Absorption of the gamma-radiation in lead gave an energy of 0.81 Mev.[6]

All range-energy relations used in the following experiments were taken from the curves of Glendenin.[10]

II. NICKEL 65

Sources of radioactive Ni^{65} were prepared by bombarding pure (99.96 percent) nickel targets with slow neutrons from the Indiana University cyclotron. No chemical separation was necessary with these sources. The half-life of all samples was found to be 2.6±0.1 hours.

Absorption measurements of the beta-radiation were

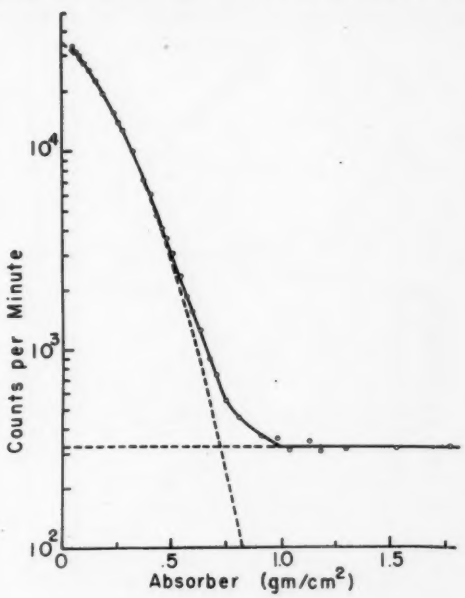

FIG. 1. Beta-ray absorption in Ni^{65}. The dotted curve has the gamma-ray background subtracted.

* Now at NEPA project, Oak Ridge, Tennessee.
† Now at NACA, Cleveland, Ohio.
[1] J. L. Meem, Jr. and F. Maienschein, Phys. Rev. **76**, 328 (1949).
[2] A. C. G. Mitchell, Rev. Mod. Phys. **20**, 246 (1948).
[3] J. J. Livingood and G. T. Seaborg, Phys. Rev. **53**, 765 (1938).
[4] W. Rall and R. Wilkinson, Phys. Rev. **71**, 321 (1947).
[5] M. Deutsch, Phys. Rev. **72**, 527 (1947).
[6] Cork, Shreffler, and Fowler, Phys. Rev. **74**, 1657 (1948).
[7] K. Siegbahn, Phys. Rev. **75**, 1278 (1949).
[8] W. S. Emmerich and J. O. Kurbatov, Phys. Rev. **75**, 1446 (1949).
[9] J. Lawson and J. Cork, Phys. Rev. **57**, 983 (1940).
[10] L. E. Glendenin, Nucleonics **2**, 12 (1948).

made with a cylindrical glass counter with relatively thick walls (about 45 mg/cm²). The geometry used corresponded closely to that of Bleuler and Zünti.[11] Figure 1 shows the counting rate *vs.* g/cm² of aluminum absorber. The dotted curve shows the beta-

FIG. 2. Beta-gamma coincidence absorption in Ni^{65}.

absorption with the gamma-ray background subtracted. An analysis of this curve by the method of Bleuler and Zünti gives an energy for the most energetic beta-ray of 1.97±0.13 Mev. Although no obvious break occurs in the absorption curve, this analysis requires the presence of another beta-ray of about 0.3 or 0.4 Mev. This lower energy group was seen more clearly by using a thin window counter (5.6 mg/cm²). However, the energy of this group may be best determined from absorption of beta-gamma-coincidences.

The geometry used for beta-gamma-coincidences consisted of a cylindrical lead cathode counter for counting gamma-rays and a thin window beta-counter. Figure 2 shows the beta-gamma-coincidence rate per recorded beta-ray plotted against the amount of aluminum absorber. This curve clearly shows the presence of a low energy beta-ray with an end point corresponding to 0.44±0.04 Mev. It also follows from Fig. 2 that a more energetic beta-ray is in coincidence with gamma-radiation. This is true since the ratio $N_{\beta\gamma}/N_\beta$ does not drop to zero at the lower beta-end point but continues to fall slowly with increasing absorber thickness. No measurements were made at the end point of this beta-ray group since the number of beta-rays was very small and the errors would be correspondingly large. However, Siegbahn[12] has found a beta-ray group of 1.01 Mev, in addition to the other two groups. This 1.01 Mev group, therefore, is presumably in coincidence with gamma-radiation, while the most energetic beta-ray leads to the ground state.

The gamma-ray spectrum was investigated by coincidence absorption of Compton recoil electrons using the counter arrangement previously described.[1] The Compton radiator used was the wall of the first counter, and the combined window thickness, through which the secondaries had to pass, was 11.2 mg/cm². Figure 3, showing the coincidence rate plotted against absorber, indicates a range in aluminum of 0.626±0.03 gm/cm². This is equivalent to an electron energy of 1.42±0.07 Mev. The corresponding gamma-ray energy, according to the Compton formula, is 1.64±0.08 Mev. Closer investigation of the low energy region, shown in the insert of Fig. 3, indicates a break in the curve at a gamma-ray energy of about 0.3 Mev. Gamma-gamma-coincidences were obtained, thus confirming the presence of more than one gamma-ray. The coincidence rate was rather small $(0.233\pm0.044)\times10^{-3}$, as would be expected if one gamma-ray is of low energy.

The results of these experiments are consistent with the disintegration scheme proposed by Siegbahn. The

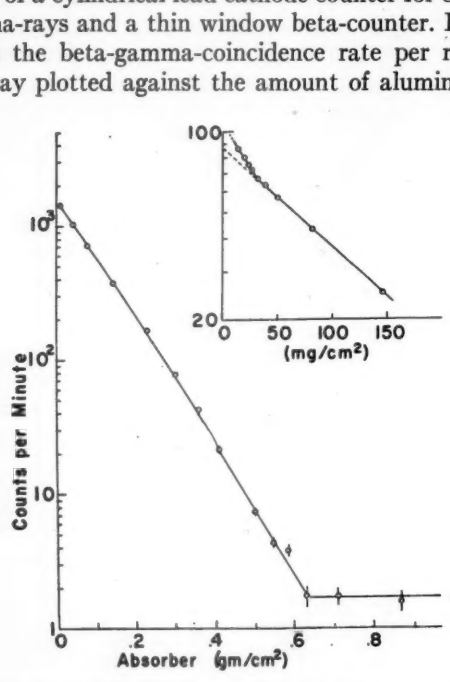

FIG. 3. Coincidence absorption of Compton-recoil electrons in Ni^{65}. The insert is an enlargement of the low-energy region.

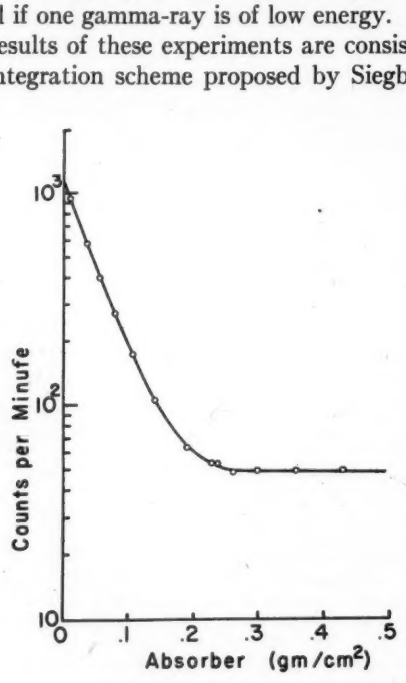

FIG. 4. Absorption of the beta-rays from Ni^{57}.

[11] E. Bleuler and W. Zünti, Helv. Phys. Acta **XIX**, 375 (1946).

[12] K. Siegbahn, private communication.

1.97 Mev beta-ray apparently leads to the ground state. The 0.44 Mev group is followed by both the 1.64 Mev gamma-ray group and two gamma-rays in cascade. One of these is the 0.3 Mev gamma-ray and the other was determined by Siegbahn as 1.12 Mev. This group would not appear on the Compton-recoil curve (Fig. 3) because its energy is so close to that of the most energetic group. The 1.01 Mev beta-group also leads to the 1.12 Mev gamma-ray.

III. NICKEL 57

The source of Ni^{57} used in these experiments was obtained by the (α, n) reaction on iron. Bombardment was by 23 Mev alpha-particles from the Indiana University cyclotron. The nickel activity was separated chemically as the dimethylglyoxime after removal of iron, cobalt, manganese, and copper. A determination of the half-life, which was followed for twelve days, gave a value of 35.7 ± 1 hours.

Absorption of the beta-radiation in aluminum with a 5.6 mg/cm² counter is shown in Fig. 4. The energy of the most energetic beta-ray is 0.725 ± 0.03 Mev. No break, corresponding to a lower energy group, is apparent from the absorption curve.

The energy of the gamma-radiation was investigated by absorbing the Compton-recoil electrons in the same geometry as was used for Ni^{65}. The maximum recoil-electron energy was found to be 1.75 ± 0.05 Mev (Fig. 5), which corresponds to a gamma-energy of 1.97 ± 0.06 Mev. There is a break in the absorption curve at an electron energy of 0.315 ± 0.04 Mev. Since this corresponds to a 0.48 ± 0.06 Mev gamma-energy, it is probably due to annihilation radiation.

Definite confirmation of the presence of annihilation radiation was obtained by measuring gamma-gamma-coincidences with counters at right angles and at 180° with respect to the source. Strong angular correlation is to be expected with annihilation radiation since the quanta are emitted in opposite directions. Measurements with a known positron emitter, Cu^{64}, gave coincidences with the counters at 180° but essentially none at 90°. With Ni^{57}, coincidences were observed in both positions, the values of $N_{\gamma\gamma}/N_{\gamma}$ being $(1.37\pm0.05)\times10^{-3}$ at 180° and $(0.59\pm0.03)\times10^{-3}$ at 90°. The much greater ratio at 180° shows that annihilation radiation is present.

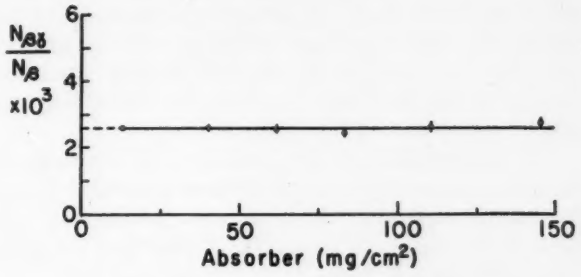

FIG. 6. Beta-gamma coincidences in Ni^{57}.

The presence of coincidences at 90° indicates that at least two nuclear gamma-rays are in cascade. It is true that with only one nuclear gamma-ray, annihilation-gamma-coincidences would be observed. However, from a knowledge of the solid angle and counter efficiencies, it may be shown that this rate would be less than 15 percent of that observed at 180°. Since gamma-gamma-coincidences are present, two gamma-ray groups should appear on the Compton curve. However, if the energy of the second gamma-ray were less than 0.5 Mev, it

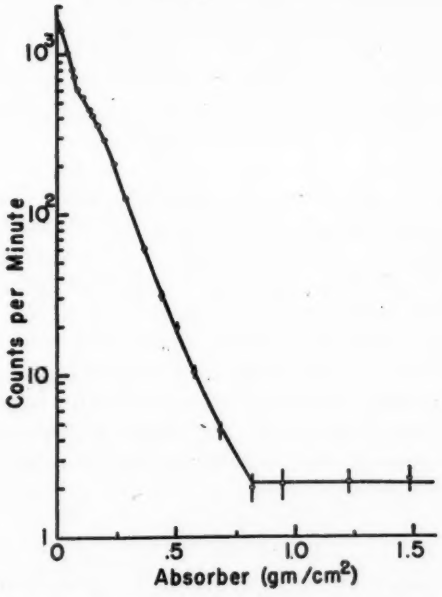

FIG. 5. Coincidence absorption of Compton-recoil electrons from Ni^{57}.

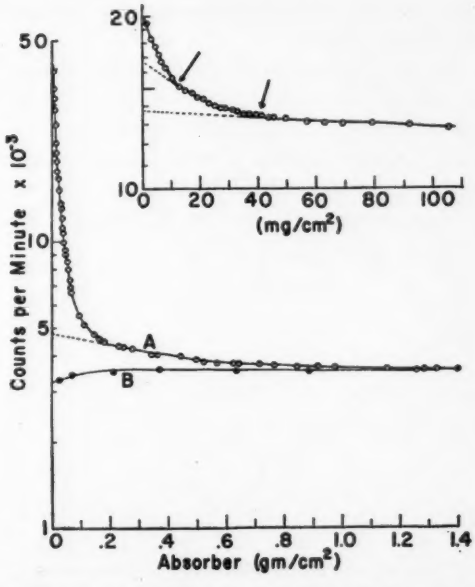

FIG. 7. Beta-ray absorption in Ag^{110}. Curve *B* shows the gamma-ray background. The insert is an enlargement of the low energy region.

would presumably be masked by the annihilation radiation.

A large beta-gamma-coincidence rate per recorded beta-ray was observed. Figure 6 shows that this ratio is independent of absorber thickness down to about 10 mg/cm². Such a straight line beta-gamma-curve indicates again that only one beta-ray is present. An attempt was made to measure coincidences between beta-rays and any possible internal conversion electrons. None were obtained with absorbers down to 20 mg/cm², which corresponds to 0.130 Mev.

The experiments on Ni^{57} indicate that the mode of disintegration consists of a 0.725 Mev positron followed by gamma-radiation. At least two gamma-rays are present in cascade. The energy of the most energetic gamma-ray is 1.97 Mev.

IV. SILVER 110

Slow neutron bombardment of silver nitrate by the Oak Ridge Pile was used to produce Ag^{110}. The silver was chemically separated as the chloride by the usual procedure after taking out mercury and lead.

Absorption of the beta-radiation of Ag^{110} in aluminum is shown in Fig. 7. Curve *A* is a composite curve taken with two different counters, one of which had a very thin window (0.8 mg/cm²). The end-point at 0.19 gm/cm² corresponds to a beta-ray group of 0.57±0.04 Mev. There is a higher energy group apparent with an energy of more than 2 Mev. The points of curve *B* were taken with a magnet arranged to deflect the beta-rays away from the counter and thus represent the gamma-ray background. It is interesting to note that this gamma-counting rate increases with small absorber thicknesses. This is probably due to the fact that the absorber acts as a radiator for producing secondary electrons and thus increases the counter efficiency for counting gamma-rays.

The low energy region of the beta-absorption curve shows a very steep rise as has been reported by Deutsch.[5] The insert in Fig. 7 which is an expanded curve of the low energy region, shows a break corresponding to a beta-ray group of 0.09±0.02 Mev, as has been reported. In addition, there appears to be another group at 0.19±0.05 Mev. These low energy groups appear to be at least as intense as the 0.57 Mev beta-ray while the very high energy group accounts for less than 5 percent of the total beta-ray transitions.

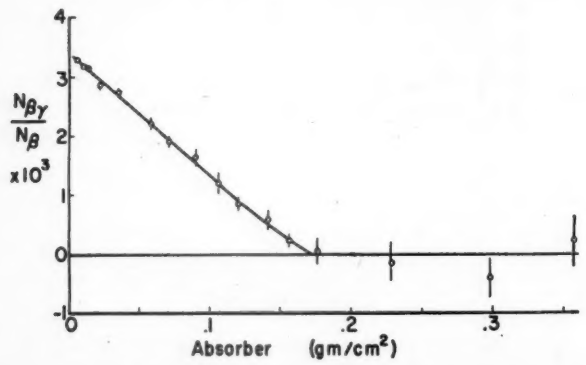

FIG. 8. Beta-gamma coincidence absorption in Ag^{110}.

Figure 8 shows the beta-gamma-coincidence rate per recorded beta-ray that was observed using a 5.6 mg/cm² beta-counter and a lead gamma-counter. The end-point obtained corresponds to 0.53±0.04 Mev. Therefore this beta-ray is in coincidence with gamma-radiation while the most energetic beta-ray leads to the ground state. The low energy region was again investigated with the 0.8 mg/cm² beta-counter and a lead gamma-counter. A larger ratio for $N_{\beta\gamma}/N_\beta$ was obtained below 10 mg/cm² showing that the 0.09 Mev beta-ray group is in coincidence with gamma-radiation. The gamma-gamma background was so large for the geometry used, however, that no end-point could be determined.

The energy of the most energetic gamma-ray was determined by absorption of Compton-recoil electrons in aluminum (Fig. 9). This maximum energy was found

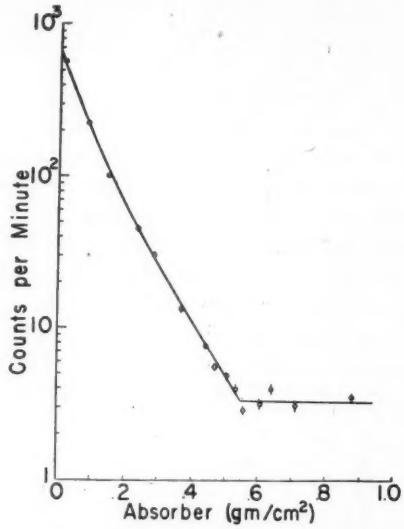

FIG. 9. Coincidence absorption of Compton-recoil electrons from Ag^{110}.

to be 1.48±0.1 Mev, in agreement with the results obtained by Siegbahn.[7] A very large, $(2.13\pm0.03)\times10^{-3}$, gamma-gamma-coincidence rate was obtained as would be expected from the large number of gamma-rays present. Coincidences were obtained between internal conversion electrons and beta-rays. The ratio of these coincidences to the number of recorded particles was $(0.058\pm0.027)\times10^{-3}$ at 50 mg/cm². The large errors, which were caused by the large beta-gamma and gamma-gamma backgrounds, made it impractical to obtain an absorption curve.

V. INDIUM 114

One source of In^{114} was prepared by deuteron bombardment of cadmium on the cyclotron. Another was made by exposing indium metal to slow neutrons from

the Oak Ridge pile. Both sources were separated chemically.

Absorption of the beta-radiation is shown in Fig. 10. An analysis of the high energy beta-ray group by the method of Bleuler and Zünti gave an energy of 2.05±0.10 Mev. A sharp rise, due to the conversion electrons from a low energy gamma-ray, appears in the low energy region. Closer investigation of this region with an 0.8 mg/cm² counter gave the results shown in the insert. The electron end point corresponds to a gamma-ray energy of 0.196±0.01 Mev. The total conversion coefficient for this gamma-ray, assuming that it leads to the 2.05 Mev beta-ray, is found from the absorption curve to be 90±5 percent. An absorption curve in lead of the gamma-radiation gives an energy of about 0.78 Mev, in agreement with Cork.[6] Also, a less

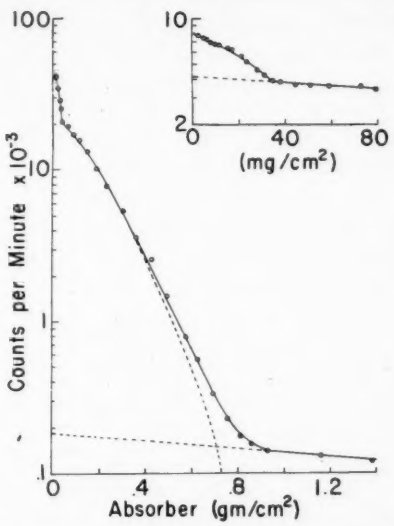

FIG. 10. Beta-ray absorption in In^{114}. The insert shows the low energy region.

energetic gamma-group of about 0.20 Mev is present. This value agrees closely with that found from the conversion electron absorption discussed above. Coincidence absorption of Compton-recoil electrons (Fig. 11) gives a maximum gamma-energy of 1.3±0.1 Mev with an indication of two other groups at about 0.5 and 0.7 Mev. Compton-electrons from the 0.2 Mev gamma-ray are stopped by the combined counter windows. The groups at 0.5 and 0.7 Mev appear to be of equal intensity while the most energetic group accounts for about 10 percent of the gamma-ray transitions.

In order to determine whether the more energetic gamma-radiation might be due to an impurity, two half-life measurements were made. One had just enough absorber to cut out all of the beta-rays and therefore include all the gamma-radiation. The other source was covered with 0.65 cm of lead, enough to reduce the intensity of the 0.2 Mev gamma-ray to less than 1/2000 of its original value. The same period, 49±3 days, was obtained from both curves.

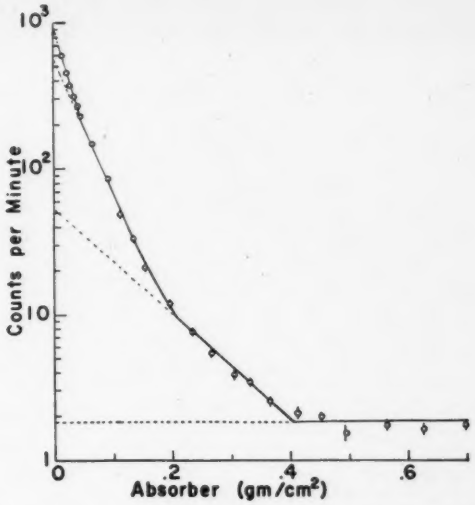

FIG. 11. Coincidence absorption of Compton-recoil electrons from In^{114}.

Very few beta-gamma-coincidences were obtained, the value of $N_{\beta\gamma}/N_\beta$ being $(0.015\pm0.005)\times10^{-3}$. Since this ratio was independent of absorber thickness, there are no less energetic beta-groups present. The smallness of the ratio excludes the possibility that the 2.05 Mev beta-ray is in coincidence with any of the above gamma-rays. In fact, it is possible that such a small coincidence rate could be due to scattered particles. The value of $N_{\gamma\gamma}/N_\gamma$ on the other hand, was much larger $(0.66\pm0.01)\times10^{-3}$. This measurement was made with enough lead in front of one counter to absorb the 0.2 Mev gamma-ray group. If the 0.5 and 0.7 Mev gamma-rays are assumed to be in cascade, the gamma-gamma-coincidence rate may be predicted from a knowledge of the counter efficiencies. This value $(0.8\pm0.1)\times10^{-3}$, is in fair agreement with that obtained experimentally. No coincidences were obtained between internal conversion electrons and beta-particles.

It appears from these experiments that there is another method of disintegration in In^{114} than the well established 0.2 Mev gamma-ray followed by a 2.0 Mev beta-ray. It is possible that this other transition goes by K-capture to two gamma-rays in cascade. The cross-over gamma-ray accounts for about 10 percent of these disintegrations. An approximate idea of the branching ratio of the two transitions above was obtained by counting both the beta-rays and gamma-rays from one source. The beta-ray singles divided by the solid angle gives essentially the disintegration rate. Then with the disintegration rate and the known efficiency and solid angle of the gamma-counter, the branching ratio was calculated as about 5 percent.

These experiments were assisted by the joint program of the ONR and the AEC. The authors wish to thank Professor A. C. G. Mitchell for his continued interest and advice in this work. They also express their appreciation to Dr. M. B. Sampson and the cyclotron crew for repeated bombardments.

Transport Phenomena in a Completely Ionized Gas in Presence of a Magnetic Field*

ROLF LANDSHOFF
University of California, Los Alamos Scientific Laboratory, Los Alamos, New Mexico
(Received June 16, 1949)

Conduction coefficients were calculated connecting the electric and heat currents with the electric field and the temperature gradient, which are both assumed at right angles to the magnetic field. The coefficients are represented in a complex fashion, the real part giving a flow in the direction and the imaginary part giving a flow at right angles to the driving force. The calculation was carried through for the nuclear charges one, two, and three and for the limit of very large nuclear charges.

I. INTRODUCTION

THE free electrons which are present in an ionized gas will cause this gas to conduct electricity and heat quite easily. This will be reduced in the presence of a magnetic field because the electrons go in circles, which limits their effective mean free path. A theory of the behavior can be given by means of the kinetic theory of gases. This theory describes the gas by giving the distribution in space and velocity for each kind of particle. These distribution functions must obey a set of equations which are due to Boltzmann.[1] A simplified treatment, which is based on the assumption that the interaction between electrons is small compared to the interaction between electrons and the nuclei, can be carried out with relatively little effort. In this case the conduction coefficients can be expressed as integrals which contain the collision frequency of the electron.[2] Such integrals were evaluated, for example,[3] for the case where the mean free path is independent of the velocity so that the collision frequency is proportional to the velocity. In a completely ionized gas, one deals with Rutherford scattering and a mean free path which goes as the fourth power of the velocity. These integrations are carried out in Section IV below as a check to the validity of the method. In view of the possible application of this theory to star atmospheres which contain a large percentage of hydrogen, it was not considered to be a safe approximation to neglect the interaction between electrons, since it is of the same order of magnitude as the interaction between electrons and protons. This makes it necessary to go through the much more elaborate theory which is the subject of this paper.

II. BOLTZMANN'S EQUATION

The equations set up by Boltzmann for a gas mixture express the rate of change of the distribution functions in terms of the flow in phase space and of jumps in phase space due to collisions. For the treatment of conduction phenomena it is sufficient to look for the stationary solutions which are obtained if these two effects just balance each other. The presence of electric fields, temperature gradients, etc. will produce a distorted Maxwell distribution. This distortion will be much smaller for the heavy nuclei than for the electrons, and we will in this treatment neglect it altogether so that we are only concerned with the distortion of the electron distribution. This is introduced by assuming the distribution functions F_i for the nuclei to be given functions. The index i refers to the specific nuclei which may be present in the mixture. There remains then one Boltzmann equation for the electron distribution function ϕ, which is of the form

$$D(\phi)=-J_{ee}(\phi)-\textstyle\sum_i J_{ei}(\phi F_i), \tag{1}$$

where the operator D represents the changes due to flow in phase space and the J's the changes due to collisions. Let us assume a magnetic field H in the y-direction and an electron field and a temperature gradient both in the $x-z$ plane. The operator D for this case is (see reference 1, 18.2)

$$D(\phi)=v_x\frac{\partial\phi}{\partial x}+v_z\frac{\partial\phi}{\partial z}-\frac{e}{m}\left(\left(E_x-\frac{v_z}{c}H\right)\frac{\partial\phi}{\partial v_x}+\left(E_z+\frac{v_x}{c}H\right)\frac{\partial\phi}{\partial v_z}\right). \tag{2}$$

The operators for collisions between electrons and nuclei have the form

$$J_{ei}(\phi F_i)=\int\int w\sigma_{ei}(w\vartheta)\times\{\phi(\mathbf{v})F_i(v_i)-\phi(\mathbf{v}')F_i(v_i')\}\,\mathbf{dv}_i d\Omega. \tag{3}$$

Let $\mathbf{w}=\mathbf{v}-\mathbf{v}_i$ and $\mathbf{w}'=\mathbf{v}'-\mathbf{v}_i'$ be the relative velocities of the two colliding particles before and after the collision. In the above relation w is the magnitude of $\mathbf{w}$ and $\mathbf{w}'$, ϑ the angle between them and $d\Omega$ is the element of solid angle in the direction of $\mathbf{v}'$. σ_{ei} is the Rutherford scattering cross section for Coulomb collisions between electrons and nuclei with charge Z_i

$$\sigma_{ei}=(Z_ie^2/mw^2)^2(1-\cos\vartheta)^{-2}. \tag{4}$$

* This document is based on work performed at Los Alamos Scientific Laboratory of the University of California under Government Contract W-7405-Eng-36 and the information contained therein will appear in the National Nuclear Energy Series as part of the contribution of the Los Alamos Scientific Laboratory.

[1] A thorough discussion of this subject is given in Chapman and Cowlings monograph: "The mathematical theory of non-uniform gases" (Cambridge University Press, London).

[2] See 18.45 in reference 1.

[3] L. Tonks and W. P. Allis, Phys. Rev. **52**, 710 (1937).

The operator for collisions between electrons is similarly

$$J_{ee}(\phi\phi)=\int w\sigma_{ee}(w\vartheta)\{\phi(\mathbf{v})\phi(\mathbf{v}_e)-\phi(\mathbf{v}')\phi(\mathbf{v}_e)\}d\mathbf{v}_e d\Omega, \quad (5)$$

with

$$\sigma_{ee}=(2e^2/mw^2)^2(1-\cos\vartheta)^{-2}. \quad (6)$$

It should be pointed out that the cross sections given in (4) and (6) lead to trouble if one were to use them for very small ϑ. This difficulty arises because of the long range of the Coulomb forces.[4] We shall discuss later how we get around this difficulty.

III. FORM OF SOLUTION

It was mentioned above that the nuclei will be assumed to be locally in a Maxwell distribution. This means we assume

$$F_i(xzV_i)=N_iB_i^3\pi^{-\frac{3}{2}}\exp(-B_i^2v_i^2), \quad (7)$$

where $N_i(xz)$ is the particle density

$$B_i=[M_i/(2kT_i(xz))]^{\frac{1}{2}}. \quad (8)$$

For the electron distribution we try the form:

$$\phi(xzv)=f(xzv)(1+v_xh_x(v)+v_zh_z(v)), \quad (9)$$

with

$$f=n\beta^3\pi^{-\frac{3}{2}}\exp(-\beta^2v^2),\qquad n=n(xz);\quad \beta=[m/(2kT_e(xz))]^{\frac{1}{2}}. \quad (10)$$

In order to perform the operation $D(\phi)$ of Eq. (3) we note that

$$\frac{1}{f}\frac{\partial f}{\partial x}=\frac{1}{n}\frac{\partial n}{\partial x}-(\tfrac{3}{2}-\beta^2v^2)\frac{1}{T_e}\frac{\partial T_e}{\partial x} \quad (11)$$

and

$$\frac{1}{f}\frac{\partial f}{\partial v_x}=-2\beta^2v_x. \quad (12)$$

The significance of the approximation of Eq. (9) is that electric fields and gradients of pressure and temperature are considered as being small. To the same degree of approximation it is sufficient to keep just the terms which are linear in v_x and v_z in the Boltzmann equation. In this way we obtain

$$D(\phi)=\left(\frac{eE_x}{kT_e}+\frac{1}{n}\frac{\partial n}{\partial x}-\frac{1}{T_e}\frac{\partial T_e}{\partial x}(\tfrac{3}{2}-\beta^2v^2)-\omega h_z\right)v_xf$$
$$+\left(\frac{eE_z}{kT_e}+\frac{1}{n}\frac{\partial n}{\partial y}-\frac{1}{T_e}\frac{\partial T_e}{\partial z}(\tfrac{3}{2}-\beta^2v^2)+\omega h_x\right)v_zf, \quad (13)$$

where we have introduced $\omega=eH/mc$. J_{ei} can be greatly simplified by the observation that the heavy particles are much slower than the electrons so that w can be replaced by v. In addition the combined effect of Coulomb scattering which favors small angles and the large mass-ratio has the effect of making the energy transfer in a collision between electron and nucleus negligible so that we can set $v_i'=v_i$, $v'=v$, and obtain:

$$J_{ei}(\phi F_i)=vf(v)\int\int\sigma_{ei}(v\vartheta)$$
$$\times[(v_x-v_x')h_x+(v_z-v_z')h_z]F_i(v_i)d\mathbf{v}_i d\Omega. \quad (14)$$

Because of

$$\int F_i(v_i)d\mathbf{v}_i=N_i$$

this leads at once to

$$J_{ei}=N_ivf(v)\int\sigma_{ei}(v\vartheta)[(v_x-v_x')h_x+(v_z-v_z')h_z]d\Omega. \quad (15)$$

We note again that $v'=v$ and carry out part of the integration

$$J_{ei}=N_ivf(v)(v_xh_x+v_zh_z)\int\sigma_{ei}(v\vartheta)(1-\cos\vartheta)d\cos\vartheta$$
$$=4\pi\lambda N_i\left(\frac{z_ie^2}{m}\right)^2\frac{v_xh_x+v_zh_z}{v^3}f(v), \quad (16)$$

where λ is the integral evaluated in Section V. From Eqs. (5) and (9) we obtain

$$J_{ee}=J_{ee}(h_x)+J_{ee}(h_z), \quad (17)$$

$$J_{ee}(h_\mu)=\int\int w\sigma_e(w\vartheta)[v_\mu h_\mu(v)+v_{e\mu}h_\mu(v_e)$$
$$-v_\mu'h_\mu(v')-v_{e\mu}'h(v_{e\mu}')]f(v)f(v_e)d\mathbf{v}_e d\Omega \quad (18)$$

since by conservation of energy $f(v)f(v_e)=f(v')f(v_e')$. Terms which are quadratic in the h are neglected.

In the integration $d\mathbf{v}_e d\Omega$ regions of integration which are obtained by reflecting $\mathbf{v}_e$ and $\mathbf{w}'$, and therefore all vectors, on an axis in the direction of $\mathbf{v}$ have equal weight. We can therefore replace $\mathbf{v}_e$, $\mathbf{v}'$ and $\mathbf{v}_e'$ by their components in the v direction and obtain[5]

$$J_{ee}(h_\mu)=(v_\mu v_j/v^2)f(v)I_j(h_\mu), \quad (19)$$

where

$$I_j(h)=\int w\sigma f(v_e)[v_jh(v)+v_{ej}h(v_e)$$
$$-v_j'h(v')-v_{ej}'h(v_e')]dv_e d\Omega. \quad (20)$$

Now let us introduce

$$A_\mu=\frac{eE_\mu}{kT}+\frac{1}{n}\frac{\partial n}{\partial\mu}+\frac{1}{T}\frac{\partial T}{\partial\mu},$$
$$B_\mu=(1/T)(\partial T/\partial\mu), \quad (21)$$
$$C=4\pi\lambda(e^4/m^2)\textstyle\sum N_iZ_i^2q,$$

[4] For a discussion of the point see reference 1, 10.33.

[5] j is used as a dummy index.

and enter (13), (16), and (19) into (1). We find that the equation can be split into two parts as follows

$$A_x-B_x((5/2)-\beta^2v^2)-\omega h_z+\frac{c}{v^3}h_x+\frac{v_jI_j(h_x)}{v^2}=0,$$
$$A_z-B_z((5/2)-\beta^2v^2)+\omega h_x+\frac{c}{v^3}h_z+\frac{v_jI_j(h_z)}{v^2}=0. \quad (22)$$

These can be recombined into one complex equation for

TABLE I. Computed values of the determinant ratios as functions of ω/ν for values of the effective nuclear charge $Z=1, 2, 3$.

	Δ_{00}/Δ		
ω/ν	$Z=1$	$Z=2$	$Z=3$
0.0	1.950	1.160	0.8431
0.2	1.588 −0.7290i	1.051 −0.3162i	0.7912 −0.1844i
0.5	0.8601 −0.9186i	0.7426 −0.5149i	0.6230 −0.3347i
1.0	0.3603 −0.7025i	0.4058 −0.5070i	0.3970 −0.3790i
2.0	0.1246 −0.4192i	0.1618 −0.3582i	0.1827 −0.3098i
4.0	0.04274 −0.2287i	0.05777 −0.2074i	0.06714 −0.1927i
6.0	0.02226 −0.1581i	0.03223 −0.1462i	0.03743 −0.1376i
	Δ_{01}/Δ		
ω/ν	$Z=1$	$Z=2$	$Z=3$
0.0	0.5546	0.4202	0.3425
0.2	0.3783 −0.2834i	0.3414 −0.1741i	0.2976 −0.1210i
0.5	0.1040 −0.2713i	0.1549 −0.2271i	0.1688 −0.1842i
1.0	−0.008086 −0.1454i	0.03030 −0.1557i	0.05244 −0.1480i
2.0	−0.02389 −0.06047i	−0.009445 −0.07675i	0.001288 −0.08094i
4.0	−0.01703 −0.01926i	−0.01425 −0.03178i	−0.009804 −0.03708i
6.0	−0.01089 −0.008093i	−0.01201 −0.01667i	−0.01011 −0.02156i
	Δ_{11}/Δ		
ω/ν	$Z=1$	$Z=2$	$Z=3$
0.0	0.6636	0.5433	0.4626
0.2	0.5278 −0.2563i	0.4638 −0.1878i	0.4114 −0.1428i
0.5	0.2737 −0.3027i	0.2681 −0.2614i	0.2627 −0.2234i
1.0	0.1208 −0.2201i	0.1172 −0.2051i	0.1207 −0.1922i
2.0	0.05364 −0.1328i	0.04708 −0.1232i	0.04591 −0.1190i
4.0	0.02507 −0.07933i	0.02276 −0.06231i	0.02053 −0.06607i
6.0	0.01467 −0.05803i	0.01538 −0.05101i	0.01422 −0.04724i

$h=h_x+ih_z$ if we set $A=A_x+iA_z$ and $B=B_x+iB_z$.

$$A-((5/2)-\beta^2v^2)B+\left(\frac{c}{v^3}+i\omega\right)h+\frac{v_jI_j(h)}{v^2}=0. \quad (23)$$

In order to solve (23) we expand h in terms of Laguerre polynomials of order $\frac{3}{2}$.[6] For convenience we shall omit writing the $\frac{3}{2}$ and use the notation $L_r(x)$. The L_r form an orthogonal set and the orthogonality relation is

$$\int_0^\infty x^{\frac{1}{2}}e^{-x}L_r(x)L_n(x)dx=\frac{\Gamma(n+r/2)}{\Gamma(n+1)}\delta_{nr}. \quad (24)$$

We note that $L_0=1$ and $L_1=5/2-x$. Let us substitute

$$h=\Sigma P_rL_r(\beta^2v^2) \quad (25)$$

into (23). We obtain:

$$A-L_1B+\Sigma P_r\left[\left(\frac{c}{v^3}+i\omega\right)L_r+\frac{v_jI_j(L_r)}{v^2}\right]=0. \quad (26)$$

[6] For a discussion see G. Szego, *Orthogonal Polynomials* (American Mathematical Society) Ch. 5; also reference 1, 7.5. In the latter reference these polynomials are called Sonine polynomials.

Now multiply (26) by $[B^5v^2/2\pi\Gamma(5/2)]\exp(-\beta^2v^2)\times L_s(\beta^2v^2)d\mathbf{v}$ and integrate to obtain

$$A\delta_{0s}-\frac{5}{2}B\delta_{1s}+i\omega\frac{\Gamma(s+5/2)}{\Gamma(s+1)\Gamma(5/2)}P_s+\Sigma P_rH_{rs}=0, \quad (27)$$

$$H_{rs}=H_{rs}{}^e+H_{rs}{}^i, \quad (28)$$

$$H_{rs}{}^e=\frac{\beta^5}{2\pi\Gamma(5/2)}\int\exp(-\beta^2v^2)L_sv_jI_j(L_r)d\mathbf{v}, \quad (29)$$

$$H_{rs}{}^i=\frac{C\beta^2}{\Gamma(5/2)}\int_0^\infty e^{-\epsilon}L_s(\epsilon)L_r(\epsilon)d\epsilon, \quad (30)$$

where in (30) we have made the substitution $\beta^2v^2=\epsilon$ and performed the angular integration. The integrals (29) and (30) are evaluated in the appendix. The problem now consists of solving the set of equations contained in (27) for the coefficients p_s. Actually we need only the first two coefficients. We can write for the electric and the heat currents:

$$j=-e\int(v_x+iv_z)\phi d\mathbf{v}=-\frac{e}{3}\Sigma p_s\int v^2L_sfd\mathbf{v}=-\frac{en}{2\beta^2}p_0, \quad (31)$$

and similarly

$$q=\int(v_x+iv_z)(m/2)v^2\phi d\mathbf{v}=(5nkT/4\beta^2)(p_0-p_1). \quad (32)$$

We shall solve for p_0 and p_1 in the approximation where we cut the matrix H_{rs} off beyond $r, s=2$ and shall check the error involved in this procedure for the case of negligible e–e scattering. In Section VI we obtain H_{rs} in the form νh_{rs} with ν given by Eq. (62). We can then write down the solution of (27)

$$p_0=\nu^{-1}\left(-\frac{\Delta_{00}}{\Delta}A-\frac{5}{2}\frac{\Delta_{01}}{\Delta}B\right),$$
$$p_1=\nu^{-1}\left(\frac{\Delta_{01}}{\Delta}A+\frac{5}{2}\frac{\Delta_{11}}{\Delta}B\right), \quad (33)$$

where

$$\Delta=\begin{vmatrix}[h_{00}+i(\omega/\nu)] & h_{01} & h_{02}\\ h_{01} & [h_{11}+(5/2)i(\omega/\nu)] & h_{12}\\ h_{02} & h_{12} & [h_{22}+(35/8)i(\omega/\nu)]\end{vmatrix}, \quad (34)$$

and $\Delta_{00}\Delta_{01}\Delta_{11}$ are minors of the determinant Δ. If $1/p(\partial p/\partial\mu)=1/n(\partial n/\partial\mu)+1/T(\partial T/\partial\mu)=0$, the electric and heat currents will be linear in the electric fields and temperature gradients. Still in complex notation we can write

$$A=\frac{eE}{KT},\quad B=\frac{1}{T}\left(\frac{\partial T}{\partial x}+i\frac{\partial T}{\partial z}\right)=\frac{1}{T}\nabla T, \quad (35)$$

so that

$$j=\sigma E+\tau\nabla T,\quad q=-\mu E-K\nabla T, \quad (36)$$

with

$$\sigma=\frac{ne^2}{m\nu}\frac{\Delta_{00}}{\Delta},\quad \tau=\frac{5}{2}\frac{nek}{m\nu}\frac{\Delta_{01}}{\Delta},$$
$$\mu=\frac{5}{2}\frac{nekT}{m\nu}\left(\frac{\Delta_{00}+\Delta_{01}}{\Delta}\right),\quad K=\frac{25}{4}\frac{nk^2T}{m\nu}\left(\frac{\Delta_{01}+\Delta_{11}}{\Delta}\right). \tag{37}$$

The determinant ratios were computed as functions of ω/ν and for values of the effective nuclear charge Z (as defined in Eq. (66)) of 1, 2, and 3. This is presented in Table I.

IV. THE CASE OF NEGLIGIBLE ELECTRON-ELECTRON SCATTERING

If one drops the last term in (23) one obtains

$$A-[(5/2)-\beta^2v^2]B+[(C/v^3)+i\omega]h=0. \tag{38}$$

Physically this means that one considers the effect of scattering of electrons by other electrons as small compared with the scattering by nuclei; that is, the case of large Z. It is of further interest to us because one can write h down at once and is therefore in a position to check the theory based on the Laguerre polynomials. Rewriting (38) we obtain

$$h=\frac{-A+BL_1(\epsilon)}{C\beta^2\epsilon^{-\frac{1}{2}}+i\omega}, \tag{39}$$

Now let

$$D_{ik}=\int\frac{\epsilon^{\frac{1}{2}}e^{-\epsilon}L_i(\epsilon)L_K(\epsilon)}{C\beta^3\epsilon^{-\frac{1}{2}}+i\omega}d\epsilon. \tag{40}$$

Then we obtain for the coefficients of expansion of h

$$P_r=\frac{\Gamma(r+1)}{\Gamma(r+5/2)}(-AD_{0r}+BD_{1r}). \tag{41}$$

If we set

$$\xi=(C\beta^2/\omega)^{\frac{1}{3}}=\{[3(\pi)^{\frac{1}{2}}/4]Z\nu/\omega\}^{\frac{1}{3}}, \tag{42}$$

and introduce

$$I_n(\xi)=\int_0^\infty\frac{\epsilon^ne^{-\epsilon}}{\xi^3+\epsilon^3}d\epsilon. \tag{43}$$

We obtain the following expressions for the D_{ik}:

$$\begin{aligned}
D_{00}&=\omega^{-1}(\xi^{\frac{1}{2}}I_3-iI_{4.5}),\\
D_{01}&=\omega^{-1}[\xi^{\frac{1}{2}}((5/2)I_3-I_4)-i((5/2)I_{4.5}-I_{5.5})],\\
D_{11}&=\omega^{-1}\{\xi^{\frac{1}{2}}[(25/4)I_3-5I_4+I_5]\\
&\qquad -i[(25/4)I_{4.5}-5I_{5.5}+I_{6.5}]\}.
\end{aligned} \tag{44}$$

The P_r given by (41) with D_{ir} given by (44) solve Eq. (38) exactly. We can now compare the P_r given by (33) which is the approximation of the previous section with the exact solution to check its validity. We want to check the above coefficients over a region of field strength where they vary by a factor of between 100 and 1000. This can be done best by giving the error in percent of the combinations $Z\Delta_{00}/\Delta$; $Z(\Delta_{00}+\Delta_{01})/\Delta$ and $Z(\Delta_{00}+2\Delta_{01}+\Delta_{11})/\Delta$. Both the real and imaginary part of each one of these combinations is directly connected with one of the I_n and does not change sign. We found that the real part of $Z\Delta_{00}/\Delta$ is off by as much as 20 percent at $\omega/Z\nu=6$. One other combination has a maximum error of 10 percent and all the other combinations have errors of less than 6 percent. In Table II we list $Z\Delta_{00}/\Delta$, $Z\Delta_{01}/\Delta$ and $Z\Delta_{11}/\Delta$ as functions of $\omega/\nu Z$.

V. TREATMENT OF DIVERGENT INTEGRALS[7]

We have to evaluate integrals of the form

$$\int\sigma(v,\vartheta)(1-\cos\vartheta)d\cos\vartheta$$

where $\sigma\sim(1-\cos\vartheta)^{-2}$.

Now let

$$\lambda=\tfrac{1}{2}\int_{\vartheta_1}^{\vartheta_2}(1-\cos\vartheta)^{-1}d\cos\vartheta=\tfrac{1}{2}\log\left(\frac{1-\cos\vartheta_2}{1-\cos\vartheta_1}\right). \tag{45}$$

This obviously diverges if $\vartheta_1=0$.

Another, less catastrophic, difficulty arises out of the uncertainty principle which excludes head-on collisions, because one has to consider an electron as being spread out over a region of the order of magnitude of its deBroglie wave-length. To remedy the situation, we, first of all, replace ϑ in (45) by the collision parameter p

TABLE II. Values of $Z\Delta_{00}/\Delta$, $Z\Delta_{01}/\Delta$ and $Z\Delta_{11}/\Delta$ as functions of $\omega/\nu Z$.

$\omega/Z\nu$	$Z(\Delta_{00}/\Delta)$	$Z(\Delta_{01}/\Delta)$	$Z(\Delta_{11}/\Delta)$
0.0	3.3906	2.0625	3.250
0.2	1.720 −1.335i	0.2645 −0.7257i	0.4778 −1.053i
0.5	0.7182 −1.139i	0.01457 −0.3345i	0.1203 −0.3770i
1.0	0.2712 −0.7254i	−0.03051 −0.1635i	0.05925 −0.1798i
2.0	0.1055 −0.4073i	−0.03463 −0.06695i	0.03674 −0.1070i
4.0	0.04206 −0.2251i	−0.02112 −0.01906i	0.01926 −0.07351i
6.0	0.02251 −0.1571i	−0.01243 −0.007394i	0.01104 −0.05639i

through

$$\operatorname{ctg}\vartheta/2=(mv^2/ze^2)p=p/p^*, \tag{46}$$

$$\lambda=\tfrac{1}{2}\log\frac{1+(p_2/p^*)^2}{1+(p_1/p^*)^2}. \tag{47}$$

[7] For a somewhat different treatment compare L. Landau, Phys. Zeits. Sowjetunion **10**, 154 (1936).

The lower limit is the deBroglie wave-length

$$p_1 \approx \hbar/mv$$

so that

$$p_1/p^* = (137/z)v/c. \tag{48}$$

The upper limit is chosen so as to exclude collisions which last longer than the time during which the electron gas would be able to rearrange its density distribution so as to give a shielding effect. The rate at which this takes place is determined by the frequency of the plasma vibrations[8]

$$\omega_{PL} = [(4\pi ne^2)/m]^{\frac{1}{2}}. \tag{49}$$

The collision parameter will thus be given to the right order of magnitude by the relation

$$p_2 \approx v/\omega_{PL}, \tag{50}$$

which leads to

$$\lambda = \tfrac{1}{2} \lg \frac{1+[1/4\pi n(e^2/mc^2)^3 z^2](v/c)^6}{1+(137/z)^2(v/c)^2}, \tag{51}$$

for high velocities and small charges this is approximated well by

$$\lambda = 36.17 - \tfrac{1}{2} \lg n + 2 \log v/c. \tag{52}$$

In view of the somewhat uncertain character of the cut-off procedure, this latter formula may be sufficient for most purposes.

VI. CALCULATION OF THE MATRIX ELEMENTS

The integral (29) can be written as:

$$H_{rs}^{e} = \frac{2n\beta^8}{3\pi^3} \int w\sigma_{ee} \exp[-\beta^2(v^2+v_e^2)] L_s \mathbf{v}\cdot(\mathbf{v}L_r(v) + \mathbf{v}_e L_r(v_e) - \mathbf{v}' L_r(v') - \mathbf{v}_e' L_r(v_e')) d\mathbf{v} d\mathbf{v}_e d\Omega. \tag{53}$$

For convenience we introduce the following notation

$$\begin{gathered} \mathbf{v}=\mathbf{v}_1; \quad \mathbf{v}_e=\mathbf{v}_2; \quad \mathbf{v}'=\mathbf{v}_3; \quad \mathbf{v}_e'=\mathbf{v}_4 \\ \mathbf{w}_1=-\mathbf{w}_2=\mathbf{w}, \quad \mathbf{w}_3=-\mathbf{w}_4=\mathbf{w}', \end{gathered} \tag{54}$$

$$M_i = \frac{2n\beta^8}{3\pi^3} \int \exp\left[-\beta^2\left(\frac{v^2}{1-\xi}+v_e^2+\frac{\eta v_i^2}{1-\eta}\right)\right] \times (\mathbf{v}_0\mathbf{v}_i) d\mathbf{u}. \tag{55}$$

Then considering the generating function of the Laguerre polynomials

$$(1-\xi)^{-5/2} \exp(-\xi\epsilon/1-\xi) = \sum_r \xi^r L_r(\epsilon), \tag{56}$$

we can write

$$\sum_r \sum_s \xi^r \eta^s H_{rs}^{e} = (1-\xi)^{-5/2}(1-\eta)^{5/2} \times \int\int w\sigma_{ee}(M_1+M_2-M_3-M_4) d\mathbf{w} d\Omega. \tag{57}$$

H_{rs}^{e} appears thus as a coefficient in expanding Eq. (57) in powers of ξ and η. The integration (55) leads to

$$M_i = A[1-Bw^2+C(\mathbf{w}\cdot\mathbf{w}_i)] \exp[-(Dw^2-E\mathbf{w}\cdot\mathbf{w}_i)] \tag{58}$$

with

$$\begin{aligned} A &= n\beta^3\pi^{-\frac{3}{2}}\left[\frac{(1-\xi)(1-\eta)}{2-\xi-\eta}\right]^{5/2}, \\ B &= \frac{1}{3}\frac{\xi+\eta-\xi\eta}{2-\xi-\eta}\beta^2, \\ C &= \frac{1}{3}\frac{2-\xi-\eta+\xi\eta}{2-\xi-\eta}, \\ D &= \frac{1}{2}\frac{2-\xi\eta}{2-\xi-\eta}\beta^2, \\ E &= \frac{1}{2}\frac{\xi\eta}{2-\xi-\eta}\beta^2. \end{aligned} \tag{59}$$

Now we form $M_1+M_2-M_3-M_4$ and expand in powers of $(1-\cos\vartheta)$. Actually we will need only the linear term of the expansion because the scattering cross section is proportional to $(1-\cos\vartheta)^{-2}$ so that contributions of large angle scattering are negligible. With σ_{ee} given by (6) we obtain for the integral in (57)

$$\int\int w\sigma_{ee}(M_1+M_2-M_3-M_4) d\mathbf{w} d\Omega = 64\pi^2\left(\frac{e^2}{m}\right)^2 AE\frac{D^2E+2D^2C-E^3-2BDE}{(D^2-E^2)^2}. \tag{60}$$

With the help of (59) this leads to

$$\sum_r \sum_s \xi^r \eta^s H_{rs}^{e} = \nu\sqrt{2}\frac{(1-\frac{1}{2}(\xi+\eta)-\frac{1}{8}\xi\eta(\xi+\eta)-\frac{3}{8}(\xi\eta)^2\xi\eta}{[1-(\xi+\eta/2)]^{5/2}(1-\xi\eta)^2}, \tag{61}$$

where

$$\nu = (4\sqrt{2}/3)\lambda n(e^2/kT)^2(kT/m)^{\frac{1}{2}}. \tag{62}$$

By expanding (61) we obtain

$$(H_{rs}^{e}) = \nu\sqrt{2}\begin{bmatrix} 0 & 0 & 0 & \cdots \\ 0 & 1 & 3/4 & \cdots \\ 0 & 3/4 & 45/16 & \cdots \end{bmatrix}. \tag{63}$$

[8] See J. D. Cobine, *Gaseous Conductors* (McGraw-Hill Book Company, Inc., New York, 1941), p. 132.

The integral (30) requires considerably less labor. As before we make use of the generating function and write

$$\sum \xi^r \eta^s e^{-\epsilon} L_s(\epsilon) L_r(\epsilon) d\epsilon$$
$$= (1-\xi)^{-5/2}(1-\eta)^{-5/2}$$
$$\times \int \exp\{-[(\epsilon/1-\xi)+(\eta/1-\eta)+1]\epsilon\} d\epsilon$$
$$= (1-\xi)^{-\frac{1}{2}}(1-\eta)^{-\frac{1}{2}}(1-\xi\eta)^{-1}. \quad (64)$$

By expanding this in powers of ξ and η we obtain

$$H_{rs}^2 = Z\nu \begin{bmatrix} 1 & 3/2 & 15/8 & \cdots \\ 3/2 & 13/4 & 69/16 & \cdots \\ 15/8 & 69/16 & 433/64 & \cdots \end{bmatrix}, \quad (65)$$

where the effective nuclear charge Z is defined by

$$Z = (\Sigma N_i Z_i^2/n). \quad (66)$$

ACKNOWLEDGMENT

I wish to thank Dr. Joseph Weinberg for his permission to use his unpublished notes which contained the work presented in Sections V and VI.

PHYSICAL REVIEW VOLUME 76, NUMBER 7 OCTOBER 1, 1949

The Disintegration of Ce^{141}

MICHEL TER-POGOSSIAN, C. SHARP COOK, C. HAROLD GODDARD, AND J. EUGENE ROBINSON
Wayman Crow Laboratory of Physics, Washington University, St. Louis, Missouri

(Received June 20, 1949)

The beta- and gamma-rays from 28 day Ce^{141} have been studied in a beta-ray spectrometer. The maximum beta-particle energy is 560 kev and gamma-rays at 146 kev and 315 kev have been found. With the additional aid of beta-gamma- and gamma-gamma-coincidence studies a disintegration scheme is proposed.

The maximum beta-energy of Pr^{143} has also been determined as 920 kev.

I. INTRODUCTION

IN view of the fact that all previous measurements[1–4] of the energies of the beta- and gamma-rays of Ce^{141} have been made by absorption methods, it seemed advisable to make a more thorough study of the isotope using a magnetic spectrometer. The investigation reported herein is such a study. From it has resulted both beta- and gamma-spectra of Ce^{141} and a beta-spectrum of Pr^{143}.

As a source of additional information both beta-gamma- and gamma-gamma-coincidence studies of Ce^{141} have also been conducted.

Using the results of the investigation, a possible decay scheme has been proposed for Ce^{141}.

II. APPARATUS

The magnetic spectrometer used in these investigations is the same as used previously[5] in an investigation of the nuclear radiations from Se^{75}. The only significant change in the instrument since the Se^{75} investigation has been the replacement of the low resistance coils used to supply the magnetic field by a set of high resistance coils[6] and the replacement of the battery current supply for these coils by an electronic constant current supply.[7]

Counters used with the spectrometer were of the same design and employed the same argon-ethylene filling mixture as before.[5] The window in the current investigation was a thin zapon window with a low energy cut-off at approximately 6 kev.

The circuit used for the beta-gamma- and gamma-gamma-coincidence studies was constructed in this laboratory by Mr. W. R. Konneker. It is built such that either instantaneous or delayed coincidences may be studied. In the present situation, only instantaneous coincidences were investigated. The resolving time for instantaneous coincidences may be varied in the range from 10^{-7} to 10^{-5} second in order that the apparatus may be used in conjunction with either scintillation or G-M counters.

III. EXPERIMENTAL DETAILS AND RESULTS

In order to obtain the sample used for the current investigation, cerium oxide powder was irradiated with slow neutrons from the Oak Ridge pile. Spectroscopic analysis (as supplied by Oak Ridge) of the sample used for the bombardment indicated no impurities in the sample except for a possible small quantity of iron. Slow neutron bombardment of iron has been known[8] to lead

[1] W. H. Burgus, Plutonium Project Report CC-680, p. 13 (May 1943) as reported by G. T. Seaborg and I. Perlman, Rev. Mod. Phys. **20**, 585 (1948).
[2] M. L. Pool and J. D. Kurbatov, Phys. Rev. **63**, 463 (1943).
[3] M. L. Pool and N. L. Krisberg, Phys. Rev. **73**, 1035 (1948).
[4] W. Bothe, Zeits. f. Naturforschung **1**, 179 (1946).
[5] Ter-Pogossian, Robinson, and Cook, Phys. Rev. **75**, 995 (1949).
[6] We are indebted to the Moloney Electric Company, St. Louis, and especially to Mr. Wooley of that organization for their kind cooperation in making the new high resistance coils for us.
[7] W. C. Elmore, AECD-2208-G, 29 (1948).
[8] G. T. Seaborg and I. Perlman, Rev. Mod. Phys. **20**, 585 (1948).

to only one radioactive isotope of iron, Fe^{59}, which has two high energy gamma-rays at 1.1 and 1.3 Mev. Neither of these gamma-rays have been found in the current investigation. It is thus concluded that no significant amount of iron impurity is present.

Cerium has four stable isotopes at mass numbers 136, 138, 140, and 142. The isotopes at 136 and 138 are of very low abundance and have not yet been found to produce a significant quantity of radioactive material through the (n, γ) process.[8] The resulting radioactive isotopes from such a process would have had half-lives sufficiently different from that of Ce^{141} that it is felt that, had a significant quantity of either Ce^{137} or Ce^{139} been present, it could have been detected in the gamma-ray measurements. The isotopes at 140 and 142 both produce radioactive products by means of the (n, γ) reaction and both of the products were present in significant quantities in the present investigation. Fortunately the Ce^{141} has a half-life of 28 days while the Ce^{143} has a half-life of only 33 hours. The Ce^{143} decays to Pr^{143} which further decays to Nd^{143} by beta-emission with a half-life of 13.8 days. The Ce^{141} can, however, be separated from the Pr^{143} both chemically and through half-life measurements.

The latter of these two methods of separation was used in the study of the gamma-radiations. The cerium oxide as received from Oak Ridge was initially placed in a small brass container built for the purpose whose walls were sufficiently thick to completely absorb all possible beta-radiation from the source. A 50 mg/cm^2 uranium foil radiator was fastened at the proper location on this container and the photoelectrons thus produced were analyzed in the magnetic spectrometer. The results are shown in Figs. 1 and 2. The open and solid circles represent two sets of data taken with approximately six days intervening. In Fig. 1 the data have been corrected for decay assuming a 28 day half-life. In Fig. 2 the correcting process assumed 13.8 days as the half-life. It takes no stretch of the imagination to see that the half-life at all parts of the spectrum is much closer to 28 days than to 13.8 days.

It seems possible to associate two groups of photoelectron lines with gamma-rays. The lines marked K_1, L_1, and M_1 appear at the correct momenta to be asso-

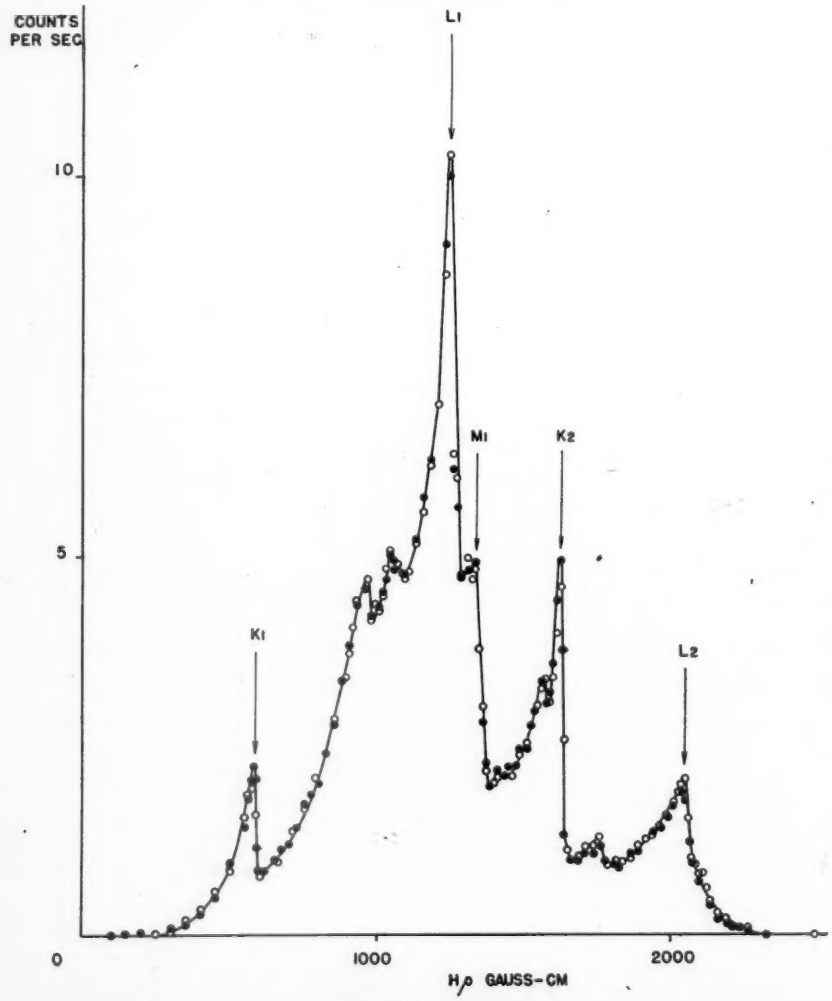

FIG. 1. Photoelectron spectrum of a source of Ce^{141} plus Pr^{143} using a 50 mg/cm^2 uranium radiator. The open and solid circles represent two sets of data taken approximately six days apart. All parts of the spectrum have been corrected for decay to an initial time by an amount appropriate to a 28 day half-life (the reported half-life of Ce^{141}). K_1, L_1, and M_1 point out the K, L, and M photo lines of the 146 kev gamma-ray and K_2 and L_2 the K and L photo lines of the 315 kev gamma-ray.

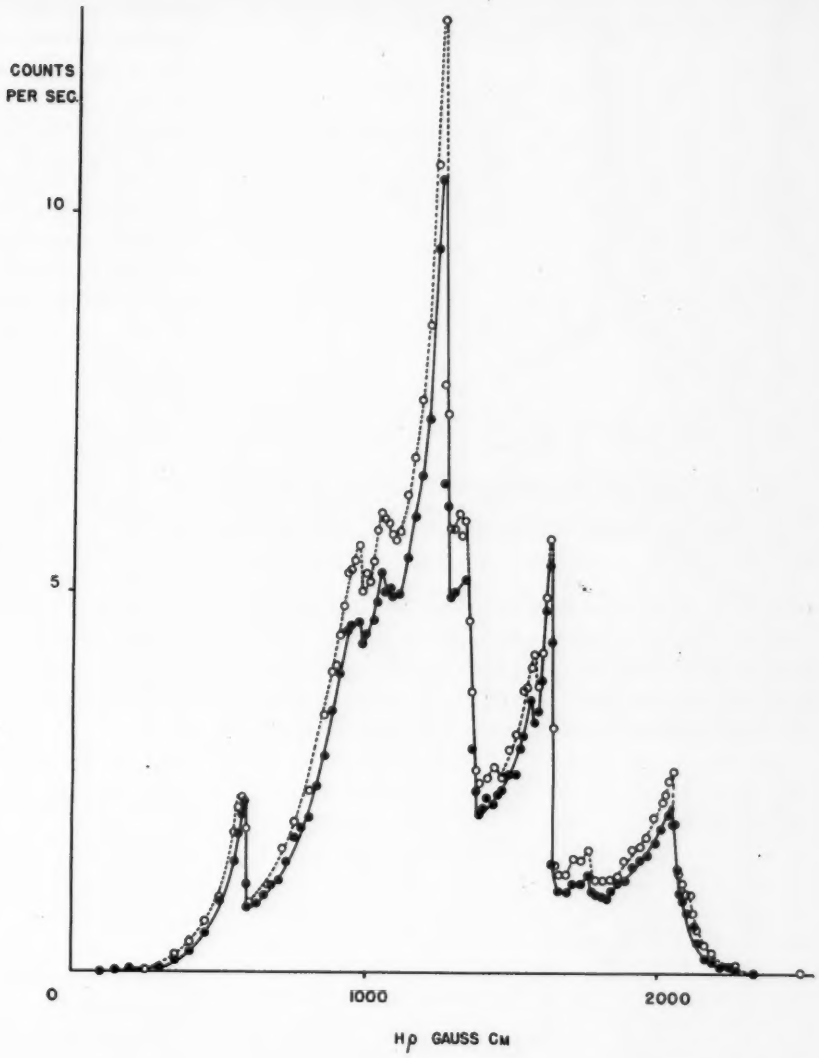

FIG. 2. Same as Fig. 1 except that the spectrum has been corrected for decay to an initial time by an amount appropriate to a 13.8 day half-life (the reported half-life of Pr^{143}).

ciated with a single gamma-ray of 146 kev energy while those marked K_2 and L_2 may in like manner be associated with a gamma-ray of 315 kev energy. Other lines of much lower intensity appear at momenta of 980, 1070, 1570, and 1768 gauss-cm. Since it has thus far been impossible to assign definitely a gamma-ray energy to any of these lines, they have not been considered in the disintegration scheme. They do, however, as can be seen in Fig. 1, appear to decay with a half-life of 28 days and would thus seem to be associated with Ce^{141}. It is assumed that the apparently low intensity of K_1 is caused by its close proximity to the low energy cut-off of the counter window.

Upon completion of the photoelectron investigation, a chemical separation was made[9] after which cerium and praseodymium were studied as beta-ray sources. The beta-spectrum of the cerium fraction is shown in Fig. 3 and that of the praseodymium (plus cerium)[9] fraction in Fig. 4. The 146 kev gamma-ray transition appears internally converted but no trace can be ob-

[9] Chemical separations were performed by Mr. A. G. Jehle, Jr. The procedure as outlined by Mr. Jehle is described in the following two paragraphs.

The impure cerium oxide was dissolved in 10 ml HNO_3 with a small drop of HF added as catalyst. When dissolved, 3 g NH_4NO_3 was added and the solution cooled to precipitate the cerium as $(NH_4)_2Ce(NO_3)_6$. The precipitate was separated and washed once by decantation with a few ml of HNO_3 containing a little NH_4NO_3. The product was reprecipitated from 5 ml HNO_3 containing a small amount of NH_4NO_3, separated and washed as before. The precipitate was dissolved in water, diluted to 50 ml, and the cerium precipitated as the oxalate. After cooling to room temperature, this was filtered and ignited to the carbonate.

In order to concentrate the praseodymium, the first set of filtrates from the nitrate separation were combined and concentrated further to precipitate as much of the $(NH_4)_2Ce(NO_3)_6$ as possible. After cooling, the supernatant liquid was removed by decantation and evaporated almost to dryness. A little water was added and the evaporation was repeated three more times to remove as much of the free HNO_3 as possible. The final residue was taken up in about 200 ml of water, boiled vigorously for an hour, and allowed to stand overnight to precipitate the basic ceric nitrate. The suspension and precipitate were separated by centrifuging. The praseodymium and the cerium remaining in solution was precipitated as the oxalate by adding a concentrated solution of oxalic acid to the hot filtrate. After standing overnight, the precipitate was filtered off and ignited to the carbonates.

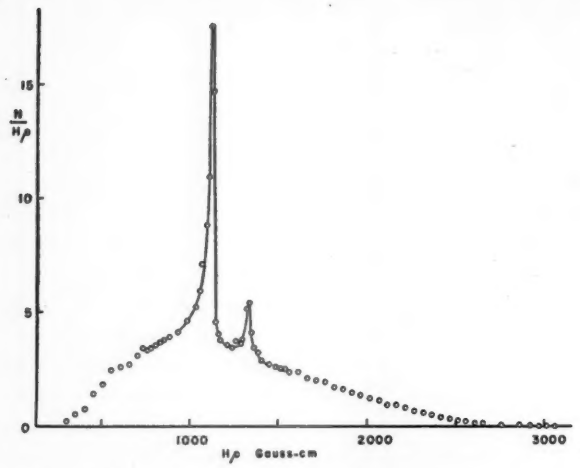

FIG. 3. Beta-spectrum of the chemically separated cerium fraction (Ce^{141}). The two internal conversion peaks correspond to the K and L peaks of the 146 kev transition in Pr^{141}. The end-point energy is 560 kev.

served of any other internally converted transition.

Both beta-ray sources were mounted on a cellulose tape backing. They were made by sprinkling the source material onto the gummed side of the tape and shaking off all material which did not stick. Weighing indicated

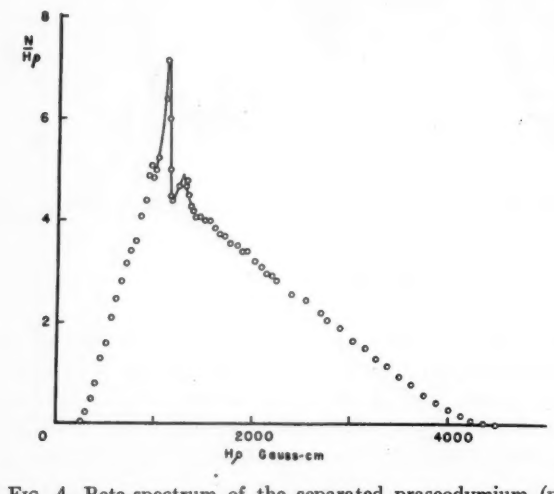

FIG. 4. Beta-spectrum of the separated praseodymium (plus cerium) fraction (see reference 9). The two internal conversion peaks are the same as those appearing in Fig. 3. The end-point energy of Pr^{143} is 920 kev.

average thicknesses of 0.8 mg/cm² for the Ce^{141} source and 0.2 mg/cm² for the Pr^{143} (plus Ce^{141})[9] source.

End-point energies for the beta-spectra have been assigned at 560±20 kev for the Ce^{141} and 920±10 kev for Pr^{143}.

FK(Fermi-Kurie)[10] plots were made of the spectra of Ce^{141} and Pr^{143} in the regions near their end-point energies. These are shown in Figs. 5 and 6. Interpretation of the shape of the FK plot of Ce^{141} will be discussed in connection with the tentative assignment of a disintegration scheme for that isotope.

Although coincidence measurements usually do not lead by themselves to accurate interpretations of disintegration schemes, their use as a supplementary tool in conjunction with beta-spectrometer measurement is a common practice.[11] In order to obtain further evidence for a possible disintegration scheme of Ce^{141} both beta-

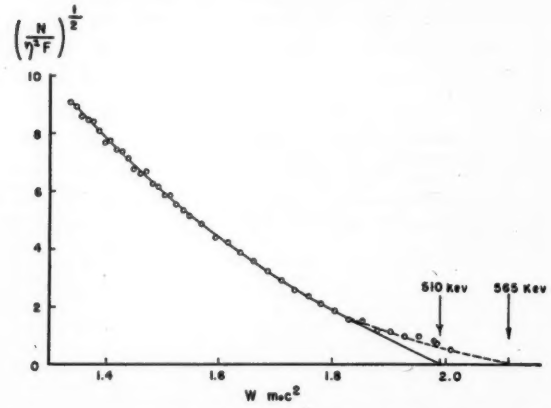

FIG. 5. Fermi-Kurie plot of the Ce^{141} beta-spectrum in the energy interval between the internal conversion lines and the spectral end point. The indicated value of 515 kev is the end point determined by a continuation of the smooth curve from the lower energy region of the plot. The end-point energy of 565 kev is the value obtained if the observed break in the curve at $W \approx 1.8$ mc² is assumed correct, and, as discussed in the text, is the case here considered correct.

gamma- and gamma-gamma-coincidence measurements were made.

All attempts failed to reveal any gamma-gamma-coincidences. It would, therefore, appear that, if the

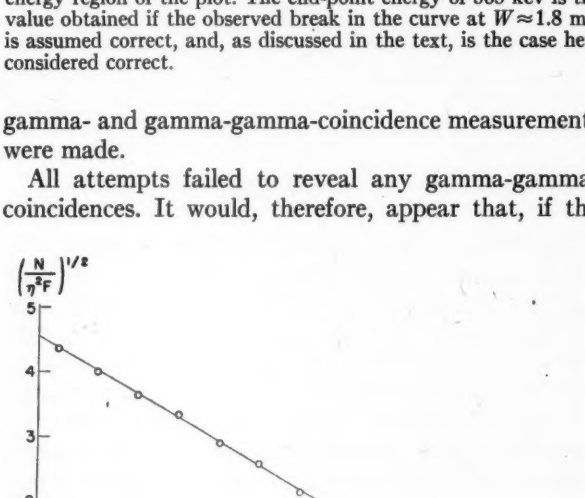

FIG. 6. Fermi-Kurie plot of the Pr^{143} beta-spectrum for energies greater than the end-point energy of the Ce^{141} spectrum.

[10] The name FK(Fermi-Kurie) for this type of plot has been suggested by Professor E. Feenberg as a means of standardization. The name Kurie plot arose from the fact that the first use of this type of analysis of experimental data was made by Kurie, Richardson, and Paxton [Phys. Rev. 48, 167 (1935)]. Later to distinguish between the respective theories the terms Fermi plot and K-U plot came into usage. Both Kurie plot and Fermi plot have been carried over into current terminology. It is possible to eliminate this dualism through introduction of the FK plot.

[11] A. C. G. Mitchell, Rev. Mod. Phys. 20, 296 (1948).

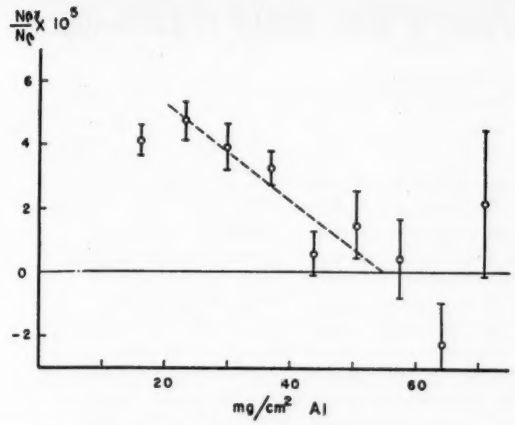

FIG. 7. Beta-gamma coincidences in Ce^{141} as a function of beta-ray energy in terms of absorber thickness.

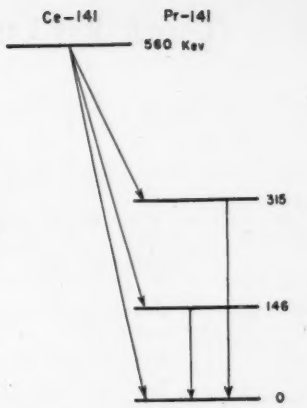

FIG. 8. Proposed disintegration scheme for the 28 day Ce^{141}. Numbers indicate the height of the energy level in kev above the ground state of the daughter Pr^{141}.

two gamma-rays mentioned above are in coincidence, one is delayed. The results of the beta-gamma-coincidence measurements are indicated in Fig. 7. It would appear from this that no beta-particle having a kinetic energy greater than 250 kev is followed immediately by a gamma-ray whereas some of those having energy below 250 kev are in immediate coincidence with a gamma-ray.

IV. DISINTEGRATION SCHEME

The experimental evidence offered does not conclusively prove the validity of the disintegration scheme proposed in Fig. 8. The proposed scheme is, however, consistent with all experimental evidence and is the only one which to date we have been able to construct which is consistent with all such evidence.[12] The 560 kev beta-ray direct to the ground state and the 240 kev beta followed by a 315 kev gamma-ray is, in addition to spectrometer measurements, a direct result of the beta-gamma-coincidence results. The 415 kev beta-ray followed by a 145 kev gamma-transition agrees with the evidence presented only if the gamma-transition is delayed. The negative results[13,14] for this isotope in the region 10^{-6} to 10^{-3} seconds indicates that the half-life of such a metastable state must be greater than 10^{-3} seconds. Because of the difficulties of the chemical separation of praseodymium from cerium[9] further evidence for a metastable state in Pr^{141} will not be immediately forthcoming.

Experimental evidence favoring the disintegration scheme seems also to be indicated by the FK plot (Fig. 5). The experimental points in the energy region below $W=1.8$ mc² may be extrapolated as indicated by the solid line to a maximum beta-particle energy of $W=2.0$ mc² (510 kev). The experimental points however deviate from this at an energy slightly greater than $W=1.8$ mc² and may be extrapolated as indicated by the dotted line to a maximum beta-particle energy at approximately $W=2.1$ mc² (565 kev). The difference between this higher maximum energy and the energy at the apparent break in the curve near $W=1.8$ mc² is, within experimental error, equal to 145 kev and therefore offers additional evidence, ever though slight, in favor of the disintegration scheme of Fig. 8.

Attempts to put quantum numbers into the tentatively proposed disintegration scheme have thus far not led to any remarkable degree of success. A measure of either the half-life of the 145 kev transition or of the spin of Ce^{141} could add significantly to the knowledge of the decay of this isotope. It must thus be concluded that the proposed scheme, although both simple and in agreement with existing evidence, cannot be finally proven without further experimental data.

We are grateful to Professor E. Feenberg for many helpful discussions.

This work has been supported by the joint program of the ONR and AEC.

Note added in proof: Since submission of the manuscript for this paper to the *Physical Review*, an article by C. E. Mandeville and E. Shapiro [Phys. Rev. **75**, 1834 (1949)] has appeared and an article by L. R. Shepherd [Research **1**, 671 (1948)] has come to the attention of the authors. Although the results obtained by Mandeville and Shapiro differ in many respects from those of the present work, Shepherd's measurements are in remarkably good agreement with those reported by us. For the Pr^{143} beta-spectrum end point Shepherd reports 930±20 kev; our results giving 920±10 kev. Shepherd's disintegration scheme for Ce^{141} gives beta-groups with maximum energies of 560 and 420 kev in excellent agreement with our two higher energy beta-transitions, the 420 kev transition subsequently going to the ground state of Pr^{141} by means of Shepherd's 141 kev (our 146 kev) gamma-transition. Since Shepherd measured only the beta-spectrum he did not observe the 315 kev gamma-transition which does not appear internally converted. Our current data neither confirm nor deny the suggestions of Mandeville and Shapiro that the 315 kev gamma-ray is an impurity with exactly the *same half-life* as Ce^{141}.

[12] Alternate disintegration schemes require either that some of the experimental data be in error or that the calculations of internal conversion coefficients by Rose, Goertzel, Spinrad, Harr, and Strong [Phys. Rev. **76**, 184 (1949)] be in serious error for some gamma-ray transitions and not for others.

[13] S. DeBenedetti and F. K. McGowan, Phys. Rev. **74**, 728 (1948).

[14] Bunyan, Lundby, and Walker, Proc. Phys. Soc. London **62**, 253 (1949).

Cosmic-Ray Experiments at High Altitudes over a Wide Range of Latitudes

A. T. BIEHL, H. V. NEHER, AND W. C. ROESCH
California Institute of Technology, Pasadena, California

(Received June 20, 1949)

A number of experiments made in a B-29 on the properties of cosmic rays are herein reported. These include the latitude effect of the following, performed along the 80th geographic west longitude from 64° geomagnetic north to the geomagnetic equator, all at a constant pressure altitude of 30,000 ft. (3.10 m of water equivalent): (1) Intensity at the vertical without and with lead absorber; (2) intensity at 45° West and 45° East both without and with lead absorber; (3) total ionization intensity; (4) extensive showers. Also measured at 48° North and at the geomagnetic equator were the following: (1) Zenith angle effect both without and with lead absorber; (2) intensity *vs.* air pressure without and with lead; (3) extensive showers *vs.* air pressure; (4) local showers. In addition to the above the variation in azimuth of the cosmic-ray intensity was measured with the various telescopes tipped at 22½°, 45°, and 67½° to the vertical at an elevation corresponding to 2.35 m of water equivalent at the geomagnetic equator. Two lead thicknesses were used, 10 and 20 cm, inserted between the counter trays. These experiments throw new light on the nature of the primary radiation and on the interaction of the primary particles with the matter through which they pass.

I. INTRODUCTION

IT has been found that the intensity of cosmic rays changes with time, especially at high altitudes.[1,2] The data taken by the Carnegie Institution of Washington[3] show that changes at or near sea level are world wide and may amount to several percent in a period of one or two months. The percentage fluctuation at high altitudes appears to be considerably greater than at sea level so that cosmic-ray data taken with balloons at one time should not be compared with those taken at another time unless such fluctuations are taken into account.

Since 1935 the group at the California Institute of Technology has made balloon flights with ionization chambers and counter telescopes in Canada, the United States, Mexico and India, measuring the ionization or counting rate as a function of depth below the top of the atmosphere. It is evident that if one point on each of the curves so obtained were simultaneously determined, the curves could be adjusted slightly and then compared. Ideally this one point should be as high on the curves as possible. For the case of no absorber, using a counter telescope, this would be at about 45,000 ft. where the peaks of the altitude curves occur. However at heights of 30,000 ft., readily reached with B-29's over great distances, the radiation near the vertical is already from one-half to two-thirds its value at the maximum. The present plan was then to fly at a constant barometric pressure to the equator covering the same latitude range or more than had been covered in previous years with balloon instruments.

Although data taken in a flight such as this at 30,000 ft. going north or south are not taken simultaneously for all latitudes, yet the time intervals involved are short since the B-29 travels over 300 m.p.h. at this altitude. Past experience has shown that except on rare occasions fluctuations over a period of a few hours are negligible. Further, the experimental values obtained on the return flight indicated no detectable change from the values going south. As an additional check, Dr. S. E. Forbush of the Carnegie Institution of Washington kindly furnished us with data taken with his continuously recording meters at Huancayo, Peru, and Cheltenham, Maryland. These showed no appreciable disturbances during this period.

In order to avoid changing longitude it was planned to fly along longitude 80° West which conveniently passes near Florida, Panama, and Peru, all of which have landing fields for B-29's. The 80th meridian further has the advantage of nearly coinciding with a geomagnetic longitude.

II. EXPERIMENTS PERFORMED

Although measurement of the latitude effect of the radiation coming in near the vertical was the primary object of this flight, a number of other measurements also were made. Since the flight took place along a nearly constant geomagnetic longitude, the heavy cosmic-ray telescopes could be rotated about a single, north-south horizontal axis to measure first the radiation coming in from the west, and then the radiation coming in from the east. Since the heading of the plane was always nearly north or south, these counter telescopes would be pointing toward geomagnetic east or west at all times.

A list of experiments performed both on the trip to Peru and return as well as on a high flight over Peru is given below. The range of latitude was from 64° geomagnetic North to the geomagnetic equator along longitude 80° geographic West.

[1] Millikan, Neher, and Pickering, Phys. Rev. **66**, 295 (1944).
[2] Biehl, Montgomery, Neher, Pickering, and Roesch, Rev. Mod. Phys. **20**, 360 (1948).
[3] S. E. Forbush and Isabelle Lange, Researchers of the Department of Terrestrial Magnetism, Vol. XIV.

A. Pressure Altitude 30,000 Ft. (310 G Cm^{-2} = 3.10 M of Water)

1. *Latitude effect*—Continuous measurements both going and coming—

a. *Vertical radiation:* Two independent telescopes; no shielding.

b. *Vertical radiation:* One telescope; 10 cm of lead absorber.

c. *Vertical radiation:* One telescope; 20 cm of lead absorber.

d. *East-West effect at 45°:* Two independent telescopes; no absorber.

e. *East-West effect at 45°:* One telescope; 10 cm of lead absorber.

f. *East-West effect at 45°:* One telescope; 20 cm of lead absorber.

g. *Wide showers:* Four trays of counters. Maximum extension 3.5 meters.

h. *Total radiation:* Continuously recording ionization chamber. Same as used in our sea level and airplane surveys.

2. *Other Experiments at 30,000 ft.*—

a. *East-West effect at equator:* Measurements made with no lead, 10 and 20 cm absorber at zenith angles of 0°, 22½°, 45°, 67½°, 90° in the East-West plane.

b. *Zenith angle measurements:* Made in North-South plane at 48° geomagnetic North on flight from Provo, Utah, to Springfield, Illinois, along a constant geomagnetic latitude. No absorber, 10 and 20 cm of lead absorber. Zenith angles: 0°, 22½°, 45°, 67½°, 90°. These same measurements were repeated on the East-West flight along the geomagnetic equator from longitude 80° West to Lima, Peru.

c. *Side showers:* To provide data on the corrections due to showers from the sides to be made to the counting rate of the counter telescopes the center tray of counters on two telescopes was displaced sideways outside the telescope aperture. This was done both at northern latitudes and at the equator.

B. Pressure Altitude 36,000 Ft. (235 G Cm^{-2}) over Peru

1. *Azimuthal experiments*—Two hexagonal courses flown, one hexagon rotated 30° with respect to the other, thus giving data every 30° in azimuth. Measurements made with no lead, 10 cm and 20 cm of lead absorber. Zenith angles: 0°, 22½°, 45°, 67½°.

2. *Wide showers also measured.*

C. Miscellaneous Experiments

1. *Counting rate versus air pressure*—At nearly all times when the plane was ascending, all telescopes were turned vertically and records were kept of outside air pressure *versus* time.

2. *Calibration checks*—On several occasions on the flight down and return all telescopes were turned vertically and long runs made for intercomparison.

III. DESCRIPTION OF APPARATUS

The apparatus used in these experiments consisted essentially of three parts; the cosmic-ray telescopes, the scaling circuits, and the recording equipment.

A. The Cosmic-Ray Telescopes

These were the same, with slight modifications, as those previously used by us in balloon experiments.[2] They consisted of three nearly equally spaced trays in triple coincidence each containing eight Geiger-Müller tubes. Each tray had an area of 650 cm^2, the spacing between extreme trays being about 80 cm. This spacing was reduced from the previously used value of one meter in order (1) to fit into the frame four equally spaced trays and (2) to increase the counting rate. This arrangement permitted the top three trays to be used as one telescope and the lower three as another. The center two trays thus were common to each telescope. This arrangement was used in the telescopes measuring the East-West effect and in the vertical telescopes containing 10 and 20 cm of lead. The two used for the total vertical intensity were separate and mounted in individual frames.

The Geiger tubes, described elsewhere,[4] were made of copper-plated steel. The steel was 0.025 cm thick bent to form a tube 3.3 cm in diameter and 25 cm long. The five walls necessary for a particle to penetrate to register as a triple coincidence thus corresponded to an average thickness of 0.20 cm of iron or very closely 1.6 g cm^{-2}.

Figure 1 shows schematically the arrangement used in the plane. The two frameworks holding the two sets of 3 trays each, forming the two telescopes without lead absorber, were mounted in the rear corners of the pressurized section of the B-29. The other three frame-

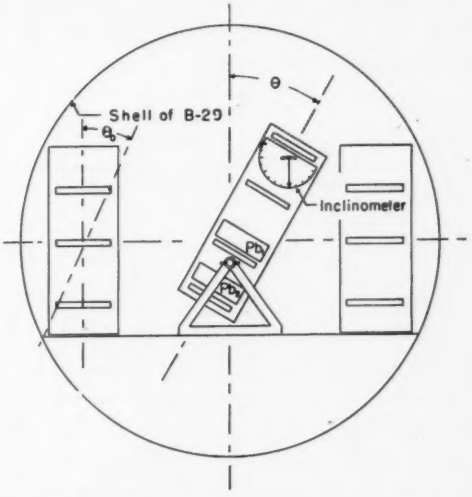

FIG. 1 Disposition of cosmic-ray telescopes in rear pressurized section of the B-29.

[4] Biehl, Montgomery, Neher, Pickering, and Roesch, Rev. Mod. Phys. **20**, 354 (1948).

works were mounted along the center of the plane. Two of these latter were used for East-West measurements. In each of these cases, Pb_1 was missing while Pb_2 was 10.2 cm of lead in one and 20.3 cm of lead in the other. For measuring the absorption of the vertical radiation, θ in Fig. 1 was kept at 0° while Pb_1 was 10.2 cm of lead and Pb_2 was another 10.2 cm of lead.

In the case of the East-West arrangement, for example, the top three trays would respond to the total radiation incident within a certain solid angle while the lower three trays would count only those particles that had sufficient energy to penetrate either 10 or 20 cm of lead incident within the same solid angle.

The trays were nearly square, being 23.1 cm by 28.5 cm. Allowing for cracks between counters, the effective area was about 600 cm². With the spacing used, the extreme half-angle θ_0 in one plane was 16° and in the other 20°. In the telescopes that were tilted the counters were mounted so that the 16° angle was in the vertical plane.

An inclinometer with a pointer was mounted on the sides of the two frames that were rotated. The graduated circles on these read to ¼° and the sensitivity of the bubble was such that a rotation of ¼° could easily be detected.

Each telescope frame was covered with 0.5-mm sheet aluminum. This performed a threefold purpose: (1) electrical shielding, (2) mechanical rigidity, and (3) physical protection. The amplifiers and coincidence circuits were the same as used on balloon flights previously.[2]

The two frames holding the four East-West telescopes and the single frame holding the two vertical telescopes containing lead were mounted along the center of the rear pressurized section of the B-29. The width of the plane was just sufficient to allow the East-West sets to be tipped until they were horizontal. The total weight of each of the two heavier pieces with the 20 cm of lead was approximately 200 kg.

B. The Scaling Circuits

The maximum coincident counting rates expected were approximately 1000 per minute. With the mechanical registers used a scale of 4 to 1 was sufficient to reduce the randomness and average rate of counting to a value where a negligible number of counts would be missed.

Each scaling circuit consisted of a multivibrator pulse shaper (Fig. 2), two scale of two circuits and a final multivibrator for driving the register. Germanium crystal diodes were used between stages of the scaling circuit for isolation purposes. The frequency response of the complete circuit was measured to be approximately 50 kilocycles per second without the mechanical register attached. The register itself would follow 50 evenly spaced pulses per second.

Ten scaling units were built, nine of which were used at any one time. A switch on the input side permitted a pulse of variable frequency to be fed in, to check the scaling circuits and registers. Another switch permitted the scaling circuit to be eliminated and the single pulses would then be recorded on the register, thus permitting checks to be made on the scaling factor.

To avoid effects of moisture in the tropics, all circuits were dipped in hot paraffin.

C. The Recording Unit

The dials of the nine registers, a clock, and pertinent information written on a small card were all photographed once every minute on a 35-mm film.

D. Auxiliary Equipment

1. A wide shower experiment was performed using four trays in quadruple coincidence. The physical arrangement is shown in Fig. 3. Four trays were necessary to reduce the accidental rate to an inappreciable value.

2. The pressure altitude of the plane was obtained by

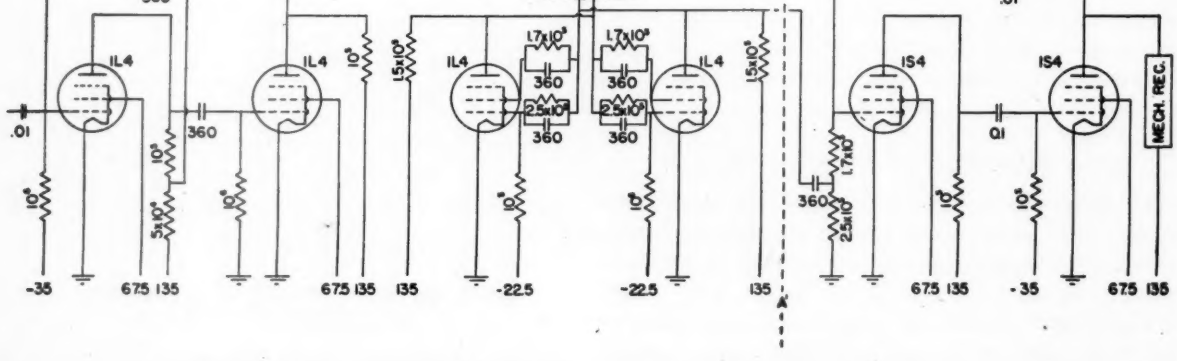

FIG. 2. Input and output multivibrators for the scales-of-two. At AA' another scale-of-two was used.

two methods: (a) The plane's altimeter and (b) a Friez aircraft continuously recording barograph suspended in the bomb bay. The plane's altimeter was calibrated prior to the flight by the Air Forces in terms of the standard atmosphere.[5]

3. An ionization chamber like that used in previous years on airplanes and on ships at sea gave a continuous record of the total intensity.[6] This instrument was placed in the pressurized section of the plane along with the other equipment and as far removed from radioactive dials as possible.

The temperature of the rear pressurized section of the B-29 was kept at about 20°C during the flights and the air pressure was maintained at a value corresponding to about 10,000-ft. elevation.

IV. INTERNAL CALIBRATIONS

All telescope data were adjusted by suitable correction factors to read what set No. 1 (one of the vertical, unshielded telescopes) would have read in the same circumstances. These calibration factors were determined as follows:

On several occasions, both on the ground and in the air, the four unshielded sets were measuring the same radiation while the cosmic-ray intensity was constant for a sufficient time to yield an accurate ratio between counting rates. There is no significant difference between the two methods of comparing the rates. Averaging the ratios so obtained using the reciprocals of the probable errors as weighting factors provided the calibration factors.

For the calibration of the telescopes containing lead absorber, data taken in the plane on the ground were used. These data gave the counting rate with the lead removed but the iron boxes which held the lead still in place. An experiment in which iron sheets were inserted between the trays of the unshielded telescopes gave the necessary correction for the metal boxes, so that the above counting rates could be compared with those of set No. 1 (see Fig. 4).

This last procedure failed in one case due presumably to the failure of a counter in the set. However, on other occasions its counting rate could be compared with another set with the same absorber.

The results of the internal calibrations were as follows:

Set No.	Ratio of No. 1 to this set
3	0.979±0.004
4	0.981±0.007
5	1.037±0.009
6	1.000±0.007
7	1.037±0.006
8	1.011±0.006
9	1.019±0.016

(Set No. 2 was used to measure extensive showers.)

[5] Report No. 538 of the National Advisory Committee for Aeronautics.

[6] Robert A. Millikan and H. Victor Neher, Phys. Rev. **50**, 15 (1936).

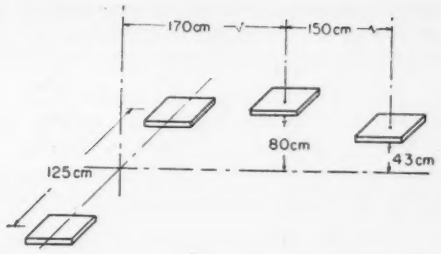

FIG. 3. Four trays of 8 counters each with 600 cm² area used to measure extensive showers had a maximum extension of about 3.5 m.

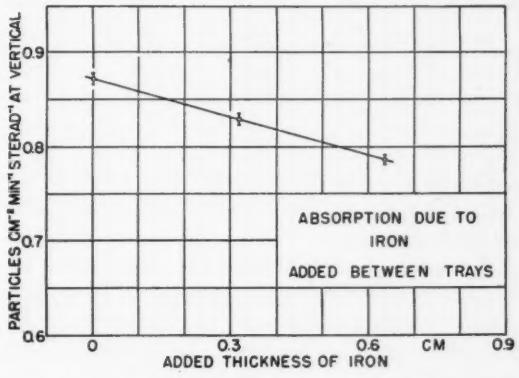

FIG. 4. Adding iron sheets between the trays at Inyokern gives an absorption of 2.0±0.2 percent g^{-1} cm^2.

The indicated probable errors are those computed from statistical errors in the calibration. The above comparison gives a good experimental check of the similarity of the geometries of the various telescopes.

V. CORRECTIONS

The following is a list of corrections to the different arrangements that need to be considered:

A. Accidental counting rates.
B. Deadtime of counters.
C. Effect of side showers.
D. Variation in pressure (altitude).
E. Efficiency of recording circuit.
F. Variation in zenith angle of the East-West sets.
G. Effects of finite telescope aperture.
H. Effect of finite thickness of counter walls and absorption in walls of plane.

These corrections will be discussed individually.

(A) The accidental counting rate was important only at the high altitudes and is due almost entirely to the real double coincidence rate between any two trays and the single counting rate of the third tray.* Using the known geometry of the counters and the counting rate of a single counter at the equator[7] we can compute this accidental rate at different latitudes. The computation depends slightly on the amount of lead between the

* This particular correction was not applied to the results using this same equipment reported in Rev. Mod. Phys. **20**, 366 (1948). We are grateful to G. Cocconi for calling our attention to this omission.

[7] H. V. Neher and W. H. Pickering, Phys. Rev. **61**, 407 (1942).

TABLE I. Total correction in counts per minute due to showers for telescopes with no lead for zenith angle z.*

Latitude	$z=0$	$22\frac{1}{2}°$	45°	$67\frac{1}{2}°$	90°
50°N	100±10	92±10	85±15	80±15	76±10
0	66±7	61±7	57±10	53±10	50±7

* No correction made for local side showers for telescopes with lead absorber.

TABLE II. Corrections to be applied to zenith angle data for finite opening of telescope (no lead absorber).

Zenith angle	48° North (3.1 m of water)	0° (2.3 m of water) N-S plane	West	East
0	0%	0%	0%	0%
$22\frac{1}{2}°$	+ 1.0	+0.1	+0.3	+0.2
45°	− 2.0	+1.1	+1.1	+0.6
$67\frac{1}{2}°$	−23	−8.0	−8.1	−9.5

trays and on the zenith angle distribution at the high altitudes but this we know from measurements made during these flights.

If I represents the number of ions cm^{-3} $sec.^{-1}$ in air at N.T.P. as measured with our thin-walled balloon ionization chambers,[8] then we compute the relative number of accidentals for any one of the unshielded telescopes to be

$$R_a = 1.52 \times 10^{-4} I.$$

This gives a value of −1.5 percent as a correction for the telescopes with no lead at the northern latitudes and −1.0 percent at the equator, both at 3.10 m of water equivalent.

(B) The correction for deadtime was determined experimentally.[4] Again this correction depends on the counting rates of the individual counters which will be proportional to I, the ionization measured by a thin-walled ionization chamber. The relative correction is given by

$$R_a = 4.3 \times 10^{-4} I.$$

This gives a correction of +4.0 percent at the northern latitudes at 30,000 ft. and +2.6 percent at the equator.

(C) The correction for side showers is somewhat more difficult to make. These showers will probably be due mostly to small, local events originating in the material in the immediate neighborhood such as the equipment and the structure of the plane or in the air outside.

When the East-West telescopes were turned over so that their axes made 90° with the vertical, the counting rate, except for scattering, should, because of the finite aperture of the telescope, be due to particles that have penetrated a minimum of 11 m of water equivalent (1100 g cm^{-2} of air). The radiation in this direction should be of about the same composition as that found at sea level, namely 30 percent soft and 70 percent penetrating particles. The 10 or 20 cm of lead in the telescopes should stop the non-penetrating particles and further, because of the shielding, it would be expected that the correction due to local side showers for the telescopes containing lead would be negligible. The average of the counting rates at northern latitudes with 10 and 20 cm of lead when the telescopes were horizontal was 21 per minute. We estimate from our extended shower measurements that about 7 counts per minute of these will be due to extended showers. Since in this position the telescopes receive particles from both ends, the number of penetrating particles incident from one end from 16° above the horizon to the horizon is 7 per minute. This is to be compared with about 800 per minute at the vertical for the telescopes with no lead or an average of 180 per minute at the vertical for 10 and 20 cm of lead. This rate when the telescopes with lead were horizontal is not far from the counting rate to be expected from the underwater data on counting rates due to radiation near the vertical coming through an equal amount of matter.

Taking this evidence that the effect of local side showers on the telescopes containing lead is negligible and assuming that the radiation coming in at these large angles is similar to that found near the vertical at sea level and below, we can compute what the rate should be in the unshielded telescopes when horizontal. This turns out to be 26 per minute. The actual counting rate under these conditions was 102 per minute. The difference, or 76 per minute, we will assume is due to local side showers.

To find the effect of side showers at other zenith angles we can use the data on the counting rate with the center tray displaced outside the aperture of the telescope. At the northern latitudes at 30,000 ft. the counting rate with the center tray displaced on the telescope with no lead was 44 per minute when the telescope was vertical. When tipped over at 45° this

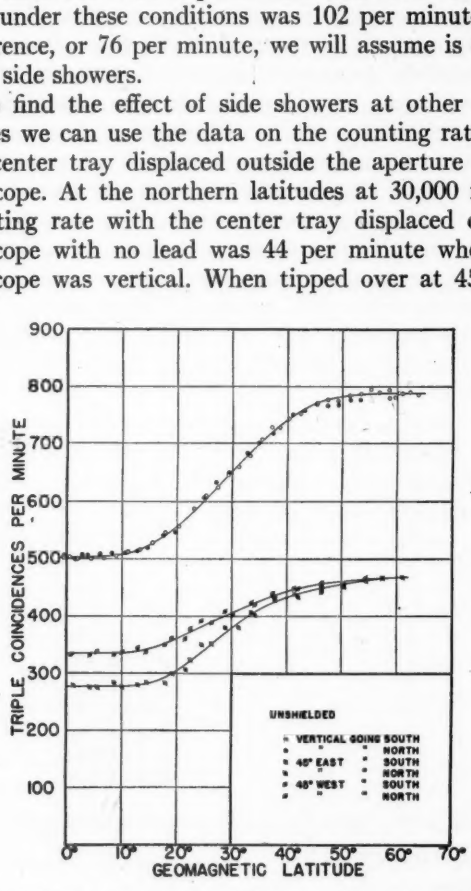

FIG. 5. Latitude effect in the radiation at the vertical, 45° West and 45° East with no absorber. No corrections applied.

Bowen, Millikan, and Neher, Phys. Rev. **53**, 855 (1938).

TABLE III.

Flight No.	Route	Time
4	Inyokern–Chicago	May 26, 1948, 0334–1004*
5	Chicago–54°N–Tampa	May 29, 1948, 1146–2100
6	Tampa–Panama	June 2, 1948, 1522–2334
7	Panama,–Lima, Peru	June 4, 1948, 0945–1839
8	Above Peru	June 6, 1948, 1505–2130
9	Lima–Panama	June 8, 1948, 1537–2324
10	Panama–Tampa	June 9, 1948, 1738–0130
11	Tampa–Chicago	June 10, 1948, 2044–0328
12	Above Illinois and Wisconsin	June 12, 1948, 1758–0118
13	Scott Field–Inyokern	July 1, 1948, 1405–2240

* Greenwich civil time.

rate dropped to 29 per minute. At the equator this latter went down to 20 per minute. (The fact that the latitude effect in these showers is about the same as for the total intensity means that most of them are not of the extended variety which show no latitude effect (see Fig. 10).)

R. A. Montgomery of this laboratory[8a] has analyzed the side showers at sea level and concludes that most of the events with three trays of counters are due to two time-associated particles, one passing through one tray and one passing through the other two considered as a wide angle telescope. Assuming a zenith angle distribution the same for these small showers as for the total radiation, it is possible to make an estimate, for a known geometry, of the dependence of such events on zenith angle and on the position of the center tray. Superimposed on the effect due to these small side showers will be the extensive or wide showers whose frequency of occurrence we also measured during these flights. The contribution of these to our telescopes we will take to be 7 per minute, independent of spacing, zenith angle, or latitude. The above kind of analysis leads us to the following scheme for the total correction due to showers for the telescopes without lead at different zenith angles (Table I). Corrections are in counts per minute and are to be subtracted from the original data (see Fig. 5). Estimates of the errors involved are based on the uncertainties in applying shower data to our particular geometry. We assume that these showers will, to a first approximation, show no asymmetry at the equator.

It should be pointed out that the relative importance of side showers should be considerably less with the large area trays made up of small diameter Geiger tubes here used, than with the usual single Geiger tube telescopes of small spacing. This is due, (1) to the relatively smaller projected areas at large angles to the axis of the telescope and (2) to the relatively large spacing between trays. It is readily seen that a telescope of large size will be less subject to showers from material in the immediate neighborhood since in general the shower is concentrated in a small solid angle.

[8a] R. A. Montgomery, Phys. Rev. **75**, 1407 (1949).

(D) Variation in pressure due to variations in the height of the plane were negligible. From previous data we calculate that at 30,000 ft. at northern latitudes the change in cosmic-ray intensity for a change of 100 ft. in altitude is about 0.6 percent for the total intensity at the vertical. The altimeter indicated that the plane was seldom off more than 100 ft. and then not for any appreciable time. Since most of our data are averaged over a period of 30 minutes such fluctuations should be negligible.

(E) A simple calculation shows that the efficiency of

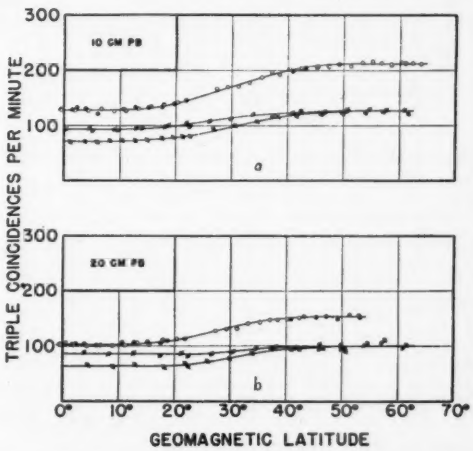

FIG. 6. Latitude effect in the radiation at the vertical, 45° West and 45° East for that part which can penetrate 10 and 20 cm of lead. No corrections applied.

the recording circuit with the scale of 4 and the register used was nearly 100 percent for the highest counting rates encountered.

(F) Effect of variation of zenith angle on the East-West sets may be calculated roughly as follows: The zenith angle dependence at 48° North and 30,000 ft. with no absorber may be represented by

$$k = k_0 \cos^{1.7} z,$$

where z is the zenith angle and k_0 is the counting rate at the vertical. At $z = 45°$ a variation in z of $\pm 1°$ will result in a variation in counting rate of 3 percent.

Except on rare occasions the roll of the plane was not more than $\pm 0.5°$ and the statistical fluctuation in the roll of the plane is estimated at $\pm 0.25°$. Thus this correction may be ignored.

The effect of variation of zenith angle on the vertically directed telescopes was at all times completely negligible.

The geometrical alignment of the trays in the east-west telescopes as well as the positioning of the inclinometer were checked by tipping the telescopes 45° North then 45° South on the ground at Inyokern and comparing the two counting rates. As originally aligned, no difference between these two rates could be found within the probable errors.

(G) Effect of finite opening of telescopes: The tele-

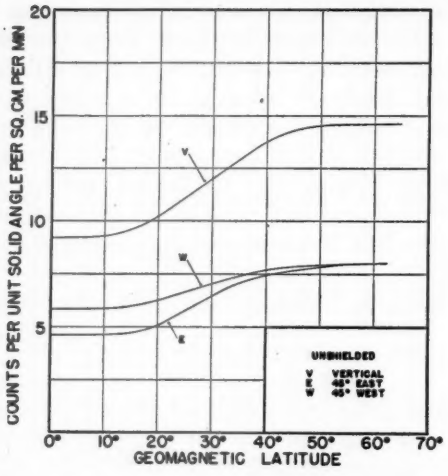

FIG. 7. Data of Fig. 5 reduced to absolute values.

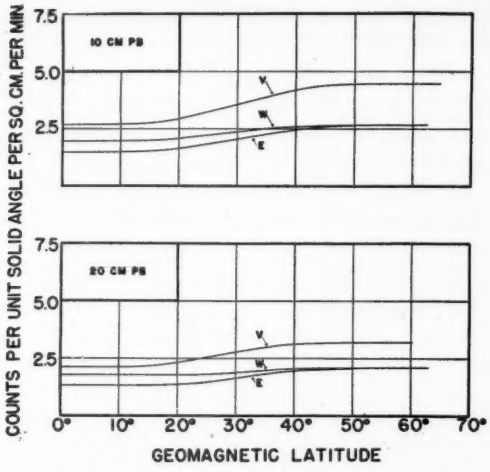

FIG. 8. Data of Fig. 6 reduced to absolute values.

scopes here used, when tipped at an angle of z to the zenith, will respond to particles coming in within the angles $z \pm 16°$ in the vertical plane and $\pm 20°$ in azimuth. The mass of air thus varies over the aperture, depending on the direction. If it is assumed that the variation of the intensity over the aperture can be represented by the vertical intensity curve for the same mass of air then a double graphical integration will give the correction for the aperture here used.

This graphical integration has been performed at 48° North and at the equator. Representative values are shown in Table II. The correction for the case where the telescope is pointed in the vertical direction has been taken into account in the absolute calibration.

It should be pointed out that for telescopes with apertures much larger than are here used the corrections for large zenith angles become quite important. A finite aperture in either azimuth or the vertical plane increases the counting rate at large zenith angles compared with that at the vertical at altitudes below the maximum of the counts *vs.* depth curve.

(H) The five wall-thicknesses of the counters that a particle needed to penetrate to trip a triple coincidence set totaled up to an average over the area of 1.6 g cm^{-2} of iron. The material of the plane added about another 1 g cm^{-2}. To find the effect of adding iron between the trays of counters on the ground two additional thicknesses were used. The results are shown in Fig. 4. The relative slope of this line is 2.0 ± 0.2 percent g^{-1} cm^2 of iron.

(I) *Summary of Corrections.*—A list of corrections made to the original data is as follows:

A. Accidentals	Maximum of	− 1.5 percent
B. Deadtime of counters	Maximum of	+ 4.0 percent
C. Side showers		
No lead absorber	Maximum of	−13.0 percent at vertical
With lead absorber		0.0 percent
D. Finite aperture (all zenith angles except 67½°)	Maximum of	2.0 percent

VI. REDUCTION TO ABSOLUTE VALUES

After the data for each telescope were corrected for accidentals, deadtime, side showers, and finite aperture, the resultant counting rate was multiplied by an appropriate factor to reduce the rate to an absolute value. Montgomery of this laboratory has made a careful determination of the absolute intensity of cosmic rays at sea level and in Pasadena with the counters here used and finds a value of 0.697 ionizing particles cm^{-2} min.$^{-1}$ steradian^{-1} at the vertical at sea level. This is in close agreement with the value given by Greisen.[9]

Comparing our geometry with that used by Montgomery we arrive at the result that our counting rates must be multiplied by 0.0208 to reduce them to particles cm^{-2} min.$^{-1}$ steradian^{-1}. If we, on the other hand, assume that the intensity of cosmic rays at sea level has not changed during the 3 or 4 months between the determinations made by Montgomery and the time

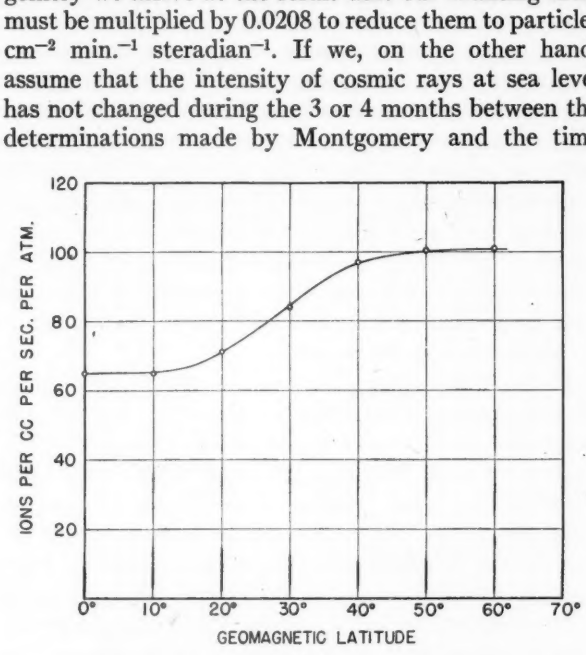

FIG. 9. Latitude effect of the total radiation as measured with a continuously recording ionization chamber.

[9] K. I. Greisen, Phys. Rev. **63**, 323 (1943).

just prior to these flights we can find the multiplying factor necessary merely by placing our unshielded telescopes outdoors in Pasadena. By such a method we find a multiplying factor of 0.0205. As a mean of these two we take the value of 0.0206.

VII. EXPERIMENTAL PROCEDURES

A. Route of the B-29

The airplane left Inyokern at 7:34 p.m. local time on May 26, 1948, and reached 30,000 ft. in one hour. The flight plan called for flying straight to Provo, Utah, follow a geomagnetic latitude from there to Springfield, Illinois, and then turn north to Chicago. On May 29 we flew northeast from Chicago to latitude 54° North, longitude 80° West, which placed us over the lower end of Hudson Bay. Turning south and flying at a constant pressure altitude of 30,000 ft. we followed the 80°W meridian to Charleston, South Carolina, where we dropped to lower elevation because of a storm, landing at Tampa, Florida. June 2 we took off from Tampa, retraced our route to Charleston to connect on to the 30,000-ft. point on the previous flight, then turning south we landed at Panama. The beginning of each flight was in this way always connected on the end of the preceding flight to leave no gaps in the records. A summary of the flights is given in Table III.

B. Procedures during Flight

(1) All telescopes were pointed vertically while gaining altitude and while descending for all flights. The rate of rise was about the same as for the balloon flights we had made in the past. This gave additional data at several latitudes on the counting rate *versus* pressure with and without lead absorber.

(2) The dials of the 9 registers, besides being photographed every minute, were read visually every 10 minutes and the rates of counting computed immediately to give a constant check on the behavior of the equipment.

(3) Frequent checks were made on the apparatus not only while in the air but on the ground. An oscilloscope was used to determine the behavior of both Geiger tubes and circuits. With the 187 miniature radio tubes and 152 Geiger tubes some difficulties were to be expected. Actually four Geiger tubes failed during the entire trip. Interruptions caused by these failures were in all cases never serious.

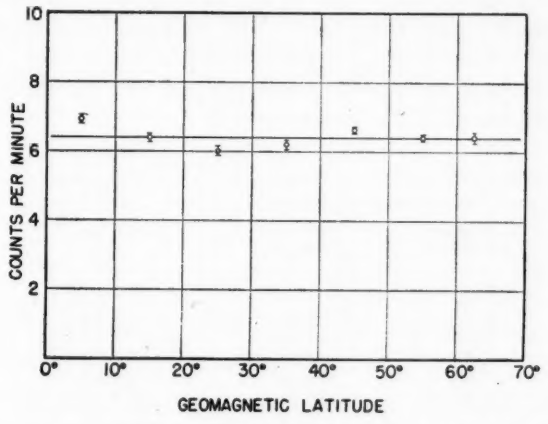

FIG. 10. Extensive showers show no latitude effect at 3.10 m of water equivalent air pressure.

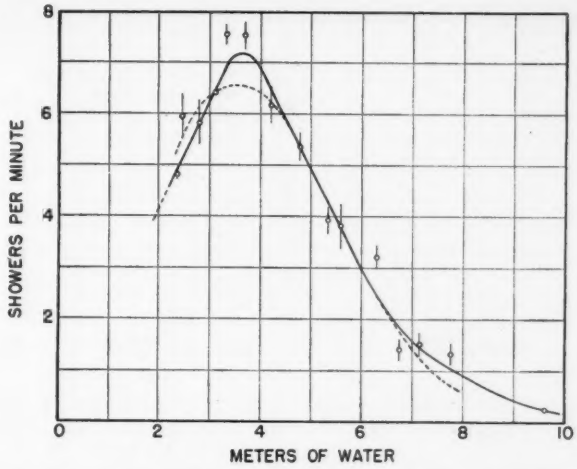

FIG. 11. Extensive showers here measured show absorption of 150 g cm^{-2} beyond the peak. Dashed curve is that obtained by Kraybill (Phys. Rev. **73**, 632 (1948)).

(4) During the flights north and south, the two observers (H. V. Neher and A. T. Biehl) shifted the two frameworks holding the four East-West telescopes every ten minutes from 45° East (or West) to 45° West (or East). Approximately 3 seconds of time were necessary to make this shift.

(5) During the azimuthal flight over Peru at 2.35 m of water equivalent the East-West sets were tipped to a given angle with the vertical and left there for two full hexagonal courses of 360°. Two full hexagonal courses were again flown with the two sets tipped at other angles. The two successive hexagons were rotated 30° with respect to each other to permit readings every 30° in azimuth. The time of flight along each side of a hexagon was approximately 10 min.

(6) A constant check was maintained on the reading of the altimeter and the heading of the plane. An inter-phone system permitted communication at any time with the pilots as well as other members of the crew.

(7) The position of the plane was determined by an experienced navigator.

(8) While flying over water the actual height of the plane was frequently determined with the radio altimeter.

VIII. EXPERIMENTAL RESULTS

A. Latitude Effect of the Vertical Radiation

(1) The counting rates of the two vertical telescopes without absorber, as a function of geomagnetic latitude, are given in the upper curve of Fig. 5. Each point on

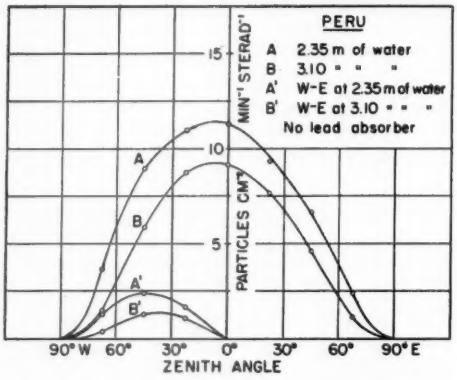

FIG. 12. Zenith angle dependence in the East-West plane at two different elevations over Peru with no lead absorber.

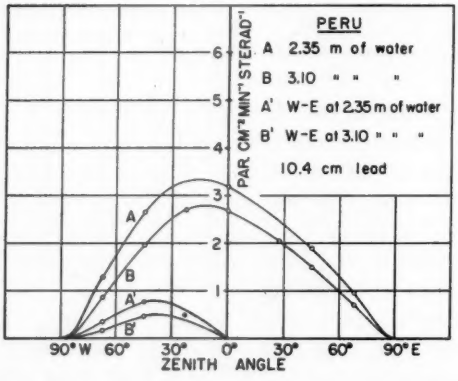

FIG. 13. Zenith angle dependence in the East-West plane at two different elevations over Peru with 10 cm lead absorber.

the curve represents the average of the two sets each averaged for a 30 minute interval of time. At the northern latitudes each point is determined by nearly 50,000 counts giving a statistical probable error of about ±0.3 percent. Thus the error in each point from the number of counts is given approximately by the radii of the circles (or dots). No corrections have been applied to these data.

The open circles represent the results of the trip south and the solid circles for the trip north. It is seen that in general the agreement is quite good indicating that the absolute value of the radiation did not change appreciably in the intervening 4 to 11 days (see Table III). There is, however, an indication of some fluctuations on the return flight at about 50° North as seen in Fig. 5.

(2) The latitude effects taken with the two telescopes with 10 and 20 cm of lead between the second and third trays of counters are given in the top curves of Fig. 6(a) and (b). The open and solid points again represent the values going south and north respectively. Since only one telescope was used for each curve, the statistical probable error over the 30-minute period at the northern latitude was ±1 percent or about one-half the radius of a circle (or dot).

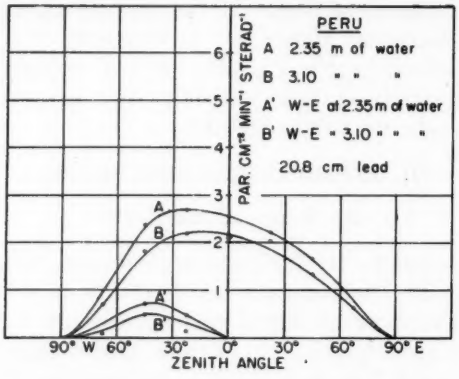

FIG. 14. Zenith angle dependence in the East-West plane at two different elevations over Peru with 20 cm of lead absorber.

B. Latitude Effect of the East-West Effect

In Figs. 5 and 6 the lower pairs of curves give the results obtained with the counter telescopes pointed east and west, without and with lead, respectively. Again the average for each point was over three intervals of 10 minutes each. The data without lead were the averages of two independent telescopes, each alternately pointing 45° East half the time and 45° West the other half. Thus each point without lead represents the counting rate obtained from about 28,000 counts at the northern latitudes.

The data with 10 and 20 cm of lead were obtained with a single telescope for each. The statistical probable error in each point is thus about ±1.2 percent or again about one-half the radius of one of the circles (or dots).

It should be noted that in certain regions of the curves with lead as shown in Fig. 6 some of the data are missing. These gaps are due to failure of the equipment but fortunately do not appear to affect the general behavior of the curves.

The above results on the latitude effect without and with lead are now corrected for side showers and multiplied by the factor 0.0206 to reduce the data to particles cm^{-2} $min.^{-1}$ $steradian^{-1}$. The reduced curves are given in Figs. 7 and 8. The side shower correction applied to the telescopes without lead amounted to, at northern latitudes, a reduction of 12.8 percent for the readings of the vertical telescopes and 18.5 percent for those tipped at 45° to the vertical.

TABLE IV. East-West asymmetry over Peru, zenith angle 45°.

M of water equivalent	Thickness of absorber	West excess* (%)
3.10	0 cm	23.3±1.1
3.10	10 cm	27.6±1.3
3.10	20 cm	30.4±1.5
2.35	0 cm	29.1±1.4
2.35	10 cm	33.0±1.6
2.35	20 cm	35.4±1.7

* Computed from the difference between West and East divided by the average.

C. Latitude Effect of the Total Radiation

The results obtained from the ionization chamber, reduced to ions cm^{-3} $sec.^{-1}$ at one atmosphere of air are given in Fig. 9. The error in each point is approximately ± 1.5 percent as determined from the scatter of the readings of the five-minute individual discharges on the film.

D. Latitude Effect of Extensive Showers

The four trays of eight counters each, connected to give quadruple coincidences, gave a counting rate of about 6 per minute. The points given in Fig. 10 are averaged over 10° of latitude. The statistical probable errors are indicated by the vertical lines through the points.

E. Altitude Effect of Extensive Showers

The altitude dependence of extended showers is shown by the solid line in Fig. 11. Since there appears to be no latitude dependence at high altitudes for wide showers, the results shown have been averaged from data collected while the plane was gaining altitude from several locations. The point at 3.10 m of water is the average for the whole trip while the one at 2.35 m of water is the result of about 2000 counts. The geometry of the four trays of counters used is shown in Fig. 3.

F. East-West Effect at the Equator

Preliminary results on the East-West effect at the equator have been reported previously[10] but for completeness are included here. The data without lead at the two elevations over Peru are given in Fig. 12. Corrections for accidentals, deadtime of the Geiger tubes, side showers, and finite opening of the telescope have been made.

The results with 10 and 20 cm of lead are given in Figs. 13 and 14, respectively, for the two different elevations over Peru. The total correction for accidentals and deadtime was about 1 percent while no corrections were made for side showers.

The data at $22\frac{1}{2}°$ with 10 cm of lead and at $67\frac{1}{2}°$ with 20 cm of lead are missing at the higher elevation because of lack of time.

The percentage west excess at 45° is given in tabular form in Table IV.

For other zenith angles the percentage West excess is plotted against angle for the higher elevation over Peru in Fig. 15.

G. Azimuthal Experiments at the Geomagnetic Equator over Peru

The variations in azimuth of the radiation at different zenith angles, z, without and with lead absorber are

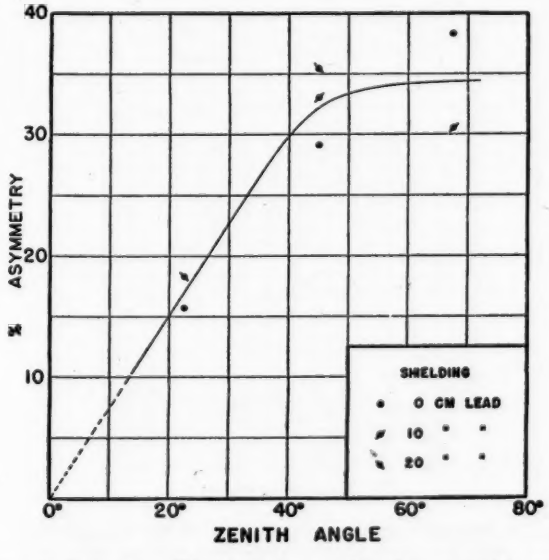

FIG. 15. Percentage West excess as a function of zenith angle with and without lead absorber.

[10] Biehl, Neher, and Roesch, Phys. Rev. 75, 688 (1949).

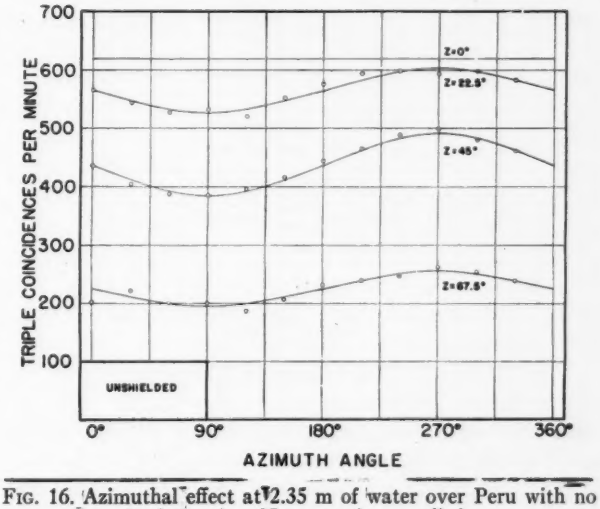

FIG. 16. Azimuthal effect at 2.35 m of water over Peru with no lead absorber. No corrections applied.

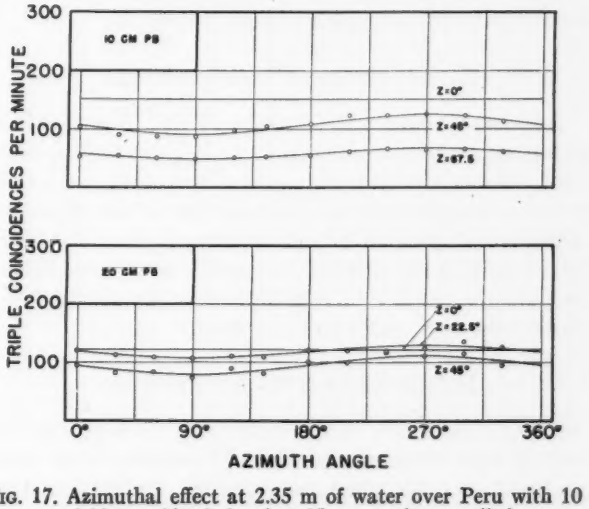

FIG. 17. Azimuthal effect at 2.35 m of water over Peru with 10 and 20 cm of lead absorber. No corrections applied.

given in Figs. 16 and 17, respectively. Each point given resulted from averaging the counting rate over a period of about 10 minutes. This results, for example, for no lead absorber in a statistical error of ±0.7 percent for each point at zenith angle of 45°. In the case of the telescopes with lead the probable error of each point at 45° is about ±2.1 percent.

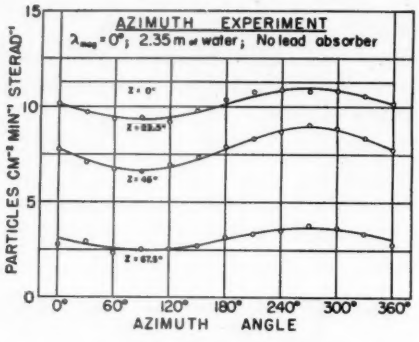

FIG. 18. Data of Fig. 16 reduced to absolute values.

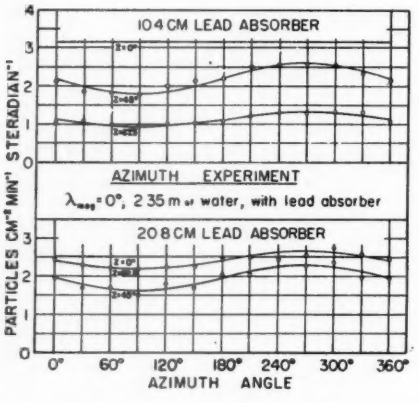
10.4 CM LEAD ABSORBER
AZIMUTH EXPERIMENT
λmag=0°, 2.35 m of water, with lead absorber
20.8 CM LEAD ABSORBER
PARTICLES CM⁻² MIN⁻¹ STERADIAN⁻¹
AZIMUTH ANGLE

FIG. 19. Data of Fig. 17 reduced to absolute values.

When corrections are made for side showers and finite opening of the telescopes as previously described and the counting rates reduced to absolute values the results obtained are given in Figs. 18 and 19.

H. Zenith Angle Measurements

At the geomagnetic latitude of 48° North while flying at 30,000 ft. between Provo, Utah, and Springfield, Illinois, the telescopes were tilted north and south to find the dependence of counting rate on zenith angle. These results are plotted in Fig. 20 for no lead absorber, 10 cm and 20 cm of lead. Corrections for side showers, accidentals, deadtime, and finite opening of the telescope have been made to these data.

I. Intensity *versus* Air Pressure

The results shown in the logarithmic plots of Figs. 21 and 22 were obtained as follows: The upper curve with no lead was obtained on gaining altitude on two occasions when leaving Chicago. The data at the equator with no lead were obtained from two flights while gaining altitude out of Lima. The data for the 10 cm and 20 cm of lead absorber were obtained in each case from the flights leaving Chicago and Lima.

The results with lead are in fair relative agreement with the values of Gill, Schein, and Yngve[11] and of Swann and Morris.[12]

J. Altitude *versus* Air Pressure

The B-29 was equipped with a radio altimeter with which true height could be readily determined while flying over water. The differences between the true height and the pressure height, as obtained from the pressure altimeter which was calibrated in terms of the standard atmosphere, are plotted at several different

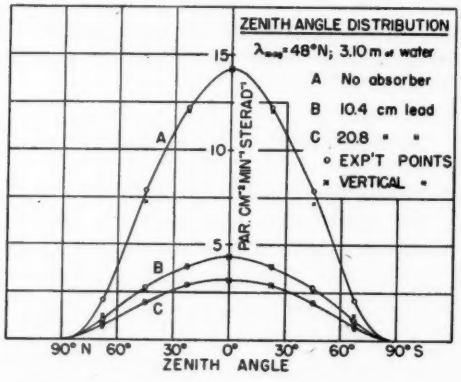

FIG. 20. Zenith angle dependence in North-South plane at 48° geomagnetic north at a pressure of 3.10 m of water. Value at 67½° with no lead through same mass of air as at vertical is about 50 percent higher.

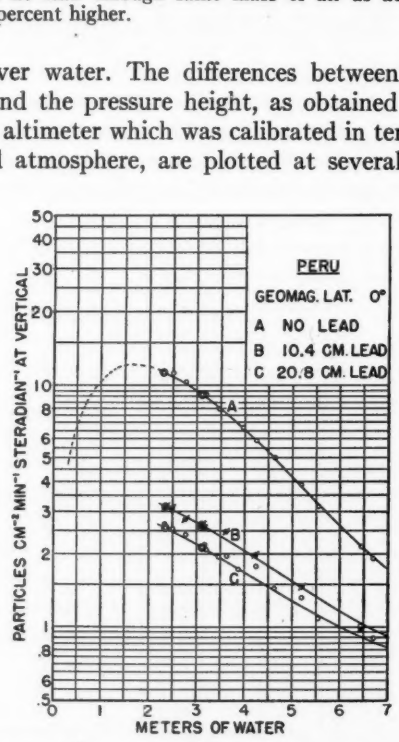

FIG. 21. Intensity at the vertical over Peru. Extended curve with no lead is that obtained from balloon data.

[11] Gill, Schein, and Yngve, Phys. Rev. **72**, 733 (1947).
[12] Second Annual Report of Bartol Research Foundation; ONR Contract N6ori-144, September 15, 1947.

latitudes in Fig. 23. This curve shows a maximum somewhat north of the geographic equator. This is not surprising since the sun was nearly at its northernmost excursion when these flights were made.

IX. DISCUSSION

A. Latitude Effect of the Radiation at the Vertical

If the latitude effect is defined as the ratio of the change of the radiation in going from the far northern latitudes to the equator at constant barometric pressure, to that existing at the far northern latitudes, then the values given in Table V are obtained.

The conclusion drawn from these values is that the latitude effect for the total radiation at the vertical is very closely the same as for the radiation that can penetrate either 10 or 20 cm of lead. This is the same conclusion arrived at by Millikan and Neher[13] for the radiation at sea level in their world survey with ionization chambers. On the several occasions in this survey when unshielded instruments and those shielded with 10 cm of lead were compared, the same latitude effect was obtained with each. This means that not only at sea level but also at a pressure of $\frac{1}{3}$ atmosphere the latitude effect in the penetrating and non-penetrating components is the same. The same conclusion for the radiation at sea level has been arrived at by Morris, Swann, and Taylor[14] for their sea level data with counters.

At sea level where the penetrating and non-penetrating components are in equilibrium an equal latitude effect for the two is easily understandable. Since, as discussed by Rossi,[15] it seems that the soft component cannot arise at high altitudes entirely from decay of mesons or collision processes there appears to be some other intimate relationship between the genesis of penetrating and non-penetrating particles which is independent of the energy of the initiating primary particle.

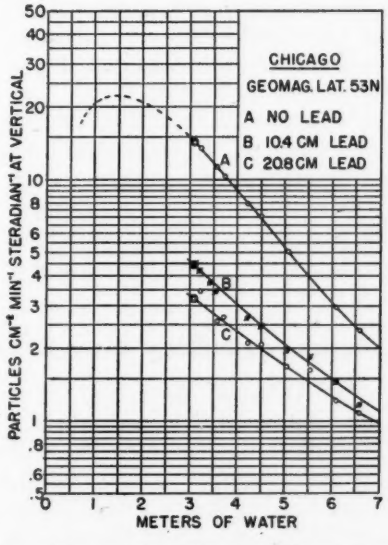

FIG. 22. Intensity at the vertical at 53° geomagnetic North. Extended curve with no lead is obtained from balloon data taken at Omaha.

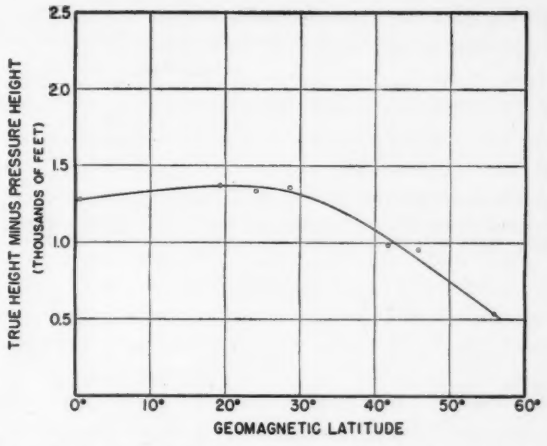

FIG. 23. At the time this flight was made (June 1948) the true altitude was always greater than the pressure altitude.

Another way of stating the above experimental fact is to say that there is the same ratio for a given pressure altitude between penetrating and non-penetrating particles at far northern latitudes as at the equator. For approximately the same mass of intervening air, covering a range of average momentum of the incoming particles of a factor of 4, some selected values are given in Table VI. This shows very clearly that in spite of the much different energy of the incoming particles that there are the same relative numbers of penetrating to non-penetrating particles.

This constant ratio of penetrating to non-penetrating particles, for the same mass of air traversed, which is independent of the energy of the primary particle up to a momentum of at least 23 Bev/c and which is also found for the radiation remaining beyond 23 Bev/c, argues for a similar type of incident particle which is responsible for the background radiation found at the equator. The effects of decay are here ignored. Later it will be shown that such effects are small at zenith angles of 45°.

B. Adjustment of Former Altitude Curves

As stated in the introduction, the original purpose of this flight was to fix one point on all the counter telescope curves taken with balloons by the California Institute group thus giving the result of having made all the balloon flights simultaneously.

Of the curves available those made at Saskatoon (Canada), Omaha, Fort Worth,[16] Acapulco[17] (Mexico) and Bangalore[18] (India) were chosen as being the most

[13] R. A. Millikan and H. V. Neher, Phys. Rev. **50**, 15 (1936).
[14] Morris, Swann, and Taylor, Phys. Rev. **72**, 1263 (1947).
[15] B. Rossi, Rev. Mod. Phys. **20**, 573 (1948).
[16] For data at Saskatoon, Omaha, and Fort Worth, see Rev. Mod. Phys. **20**, 360 (1948).
[17] Millikan, Neher, and Pickering, Phys. Rev. **63**, 234 (1943).
[18] H. V. Neher and W. H. Pickering, Phys. Rev. **61**, 407 (1942).

TABLE V.

Absorber	Latitude effect at vertical at 3.10 m of water equivalent
0	0.37
10.4 cm Pb*	0.40
20.8 cm Pb*	0.34

* Actual single thickness of lead was 10.2 cm (4 inches). Additional amount given corresponds to mass equivalent of iron holder for lead.

TABLE VI.

Geomag. lat.	Zenith angle	Mass of air	(Bev/c) min.	(Bev/c) ave.*	Penetrating ÷total 10 cm Pb	Penetrating ÷total 20 cm Pb
38°N	0°	3.1 m of water	5.4	17	0.30	0.24
0°	0°	3.1 m of water	13.2	40	0.29	0.23
0°	45°E	3.3 m of water	23.0	70	0.28	0.24

* Computed from a differential numbers distribution $p^{-2.5}dp$.

consistent and reliable. The normalization was accomplished by multiplying all values at a given latitude by a factor which made the point at 3.10 m of water equivalent agree with the present B-29 data. This procedure is justified by the following: (1) If the fluctuations at high altitudes are due to fluctuations of cosmic rays as a whole, the procedure is certainly justified. (2) If these fluctuations are due to a change in the numbers of incident particles near the minimum allowable momentum at a given latitude the procedure is justified by the fact that curves taken at two latitudes not too far apart are closely similar. A more detailed adjustment could be carried through in principle but is not found necessary due to (a) the amount of adjustment in most cases is small and (b) the errors in the experimental data do not justify further refinement. Since the areas under the curves are of primary interest,[19] this adjustment involves the least error when made near the peaks of the curves.

In transforming the Bangalore curve to the geomagnetic equator in Peru considerable adjustment needs to be made because of the longitude effect. However, as will be seen in Fig. 21, two very well determined points in Peru help to fix the curve near the maximum. Also it is found that when plotted logarithmically all these curves are close to straight lines between 3 and 7 m of water but whose slopes depend on the latitude; i.e., upon the momenta of the incident particles. This information allows an interpolation for intermediate latitudes and altitudes.

The curves of Fig. 24 represent then, the best estimate that can be made at the present time of the curves that would have been obtained at these various locations had all the flights been made simultaneously. The agreement of the present values with those obtained in 1947[16] may be seen from the fact that the adjusted value at 3.10 m of water is now 14.55 particles cm^{-2} $min.^{-1}$ $steradian^{-1}$ at Saskatoon compared with 14.37 then obtained.

A derived set of curves may be obtained from the above by plotting the counting rate as a function of latitude for constant air pressure. This has been done in Fig. 25. These results indicate that while the latitude effect appears to cease at about 53° at 30,000 ft. in going north, there is still some latitude effect at the higher altitudes beyond this latitude.

The conclusions we draw from these data are as follows: (1) There is no sharp cut-off of the primary radiation at least up to 60° geomagnetic North. While the energy being brought in by the primary particles whose momentum is less than 3 Bev/c is relatively small, there is no indication that the differential numbers distribution of the primary particles passes through a maximum. (2) That within the limits of these latitude experiments the momentum distribution of the primary particles has no sharp breaks between approximately 2 and 13 Bev/c.

The conclusion that there is no sharp cut-off of particles of low momentum is further strengthened by the balloon data taken with ionization chambers by Bowen, Millikan and Neher in 1937.[20] The flights made at Saskatoon, Canada, and Omaha, Nebraska, covered a period of two weeks during the latter part of August and the first part of September of that year. The maximum deviation from the mean at the maximum of the curve of any one 4-minute reading of the three flights made at Saskatoon on August 14, 16, and 17 was 1.8 percent. The similar measure of the consistency of the 5 flights made at Omaha on August 21 through September 5 was a maximum deviation of 2.7 percent for any one point. The measured difference in the two curves at the maximum was 7 percent. Further, the data of the Carnegie Institution meters at Huancayo and Cheltenham show that this period was very quiet in the lower part of the atmosphere.

This lack of cut-off at very high altitudes and latitudes is further confirmed by the recent work of Frier, Ney, and Oppenheimer[21] at altitudes of 70,000 to 90,000 ft. using photographic emulsions. They find evidence for particles having energies at the top of the atmosphere as low as 0.5 Bev per nucleon at a latitude of 55° North.

C. Zenith Angle Effect at the Equator

Lemaitre and Vallarta[22] have given the boundaries to the cones for certain limiting momenta of the primary particles at the equator. Of particular interest here is the cone whose boundary passes through the zenith. This boundary is tangent to the North-South direction at the zenith and bends toward the West at the larger zenith angles. From an application of Liouville's theorem it is concluded that at all zenith angles along

[19] H. V. Neher and W. H. Pickering, Phys. Rev. **61**, 410 (1942).

[20] Bowen, Millikan, and Neher, Phys. Rev. **53**, 855 (1938).

[21] Freier, Ney, and Oppenheimer, Phys. Rev. **75**, 991 (1949).

[22] G. Lemaitre and M. Vallarta, Phys. Rev. **50**, 500 (1936).

this boundary line the same numbers of particles per unit time of the same momentum distribution are incident per unit area per unit solid angle at the top of the atmosphere.

If, then, from the curves of Figs. 18 and 19 values are picked off that correspond to these azimuth angles of the same limiting momentum, the results shown in Fig. 26 are obtained. These curves correspond to those taken at 48° North as shown in Fig. 20 and give the zenith angle effect at 2.35 m of water at the geomagnetic equator.

It is possible to get the zenith angle effect also at 3.10 m of water at the equator if one assumes a sinusoidal variation in azimuth such as is found at 2.35 m of water. Experimental data were taken at the azimuth angles 0°, 90°, 180°, and 270° at the lower elevation and the assumption of a sinusoidal variation in azimuth involves only a slight correction to the North-South values. The results for no lead absorber are given in Fig. 27 together with the similar data at the same pressure taken at 48° North. The values of 48° North may be fitted rather closely with the empirical relation

$$I/I_0 = \cos^{1.70} z,$$

while at the equator the approximate relation is

$$I/I_0 = \cos^{1.62} z.$$

Plotted in Figs. 20 and 27 are the intensities at the vertical as measured with the same telescopes under the same mass of air. It will be noticed that the agreement is quite good where lead absorber is used but there is some discrepancy with no lead at 45° and still more at 67½°, the vertical values being in all cases *lower*, for the same mass of intervening air, than those measured at an angle to the zenith.

There are at least two phenomena that must be taken into account when comparing counting rates under the same mass of air but where the path lengths are different. These are decay of the meson and scattering. The effect of decay may be either to add to or subtract from the total number of ionizing particles through the same mass of air but over a greater path. If the unstable particle decays while still having considerable kinetic energy remaining, the decay electron will form a shower and thus may increase the numbers of particles that would otherwise exist. On the other hand the effect of decay should always tend to lower the corresponding numbers of penetrating particles.

Without further experimental data or an extended theoretical analysis, it is not possible at the present time to estimate the effects of decay or of scattering. Perhaps fortuitously, the combination of these two effects at these altitudes, results in nearly perfect agreement at all zenith angles for the case of the penetrating component as is seen from Fig. 20.

In connection with the effect of decay on the intensity of the meson component and how the extension of the atmosphere might affect such decay as a function of latitude, Fig. 23 is included. It will be noticed that at the altitude flown (30,000 ft.) the maximum excursion of the curve giving the difference between the true height and the pressure height is only 830 ft. Most of this change takes place at the northern latitudes.

D. Effect of Atmospheric Scattering

The effect of scattering in the atmosphere is to decrease the intensity of the secondary particles in directions where the intensity is high and to increase the intensity in the directions where it is low. Thus the zenith angle distribution found near sea level would, by this principle, be more peaked at the vertical with less intensity at large zenith angles were scattering not present.

Some indication as to the importance of scattering

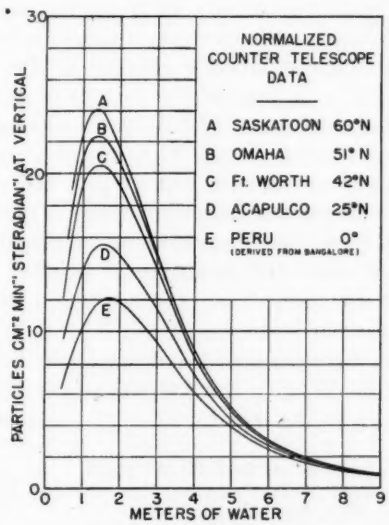

FIG. 24. Former balloon counter telescope flights normalized to present airplane data at 3.10 m of water.

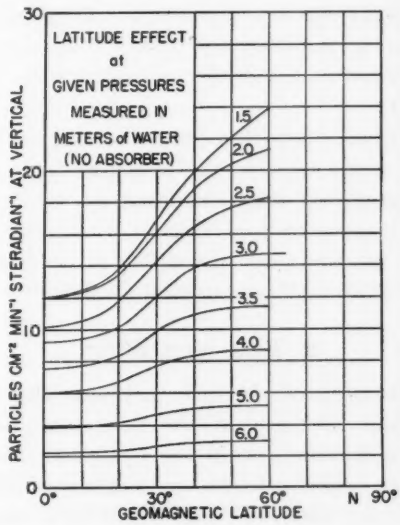

FIG. 25. Derived curves from Fig. 24 showing latitude effect at given depths in the atmosphere.

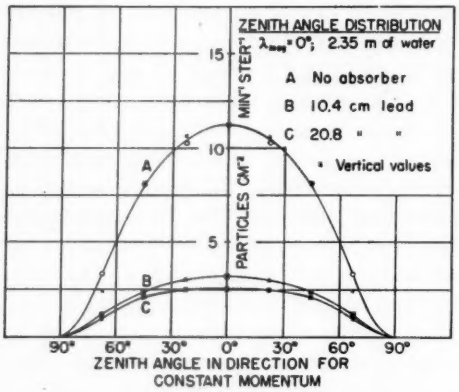

FIG. 26. Zenith angle dependence at 2.35 m of water in the direction of constant incident momentum at the equator.

may be obtained by comparing the intensity measured at large zenith angles at high altitudes with that measured near the vertical at lower altitudes and under the same mass of air. Winckler, Stroud, and Schenck[23] for example find twice the intensity at 67½° to the vertical with no lead absorber as at the vertical for one-half atmosphere of air in each case. Although no estimate, from their geometry, of the effect of finite opening of their telescope can be made, it seems reasonable that some of the excess intensity measured at this large zenith angle is due to scattering.

From our own data we see from Figs. 20 and 27 that after all corrections have been made, the intensity as measured at 67½° to the vertical with no lead absorber is from 30 to 50 percent larger than that measured in the vertical direction under the same mass of air. The effects of scattering at the other angles seem to be small and we conclude that the reduction of the values measured at the vertical because of scattering is small and probably less than 10 percent. Rossi[15] estimates the effect of scattering in the initial process, when the primary forms its first secondaries, is no larger than 10 percent in reducing the intensity at the vertical. The combined effects then will probably be less than 20 percent.

We conclude then that except for large angles the intensity at an angle to the zenith at these altitudes may be predicted from the intensity at the vertical whenever the intensity at the top of the atmosphere is the same, or when the absorption in the atmosphere gives the same effective radiation in the two cases.

E. East-West Effect

The discovery of the fact that near the magnetic equator the intensity of the secondary cosmic-ray particles is greater toward the west than toward the east has an important bearing on the assumed nature of the primary particles. While these early experiments of Johnson,[24] Alvarez and Compton,[25] Rossi,[26] and others established beyond a doubt that there was a positively charged component of the primary radiation, it was not clear whether the whole or only part of the primary particles were so charged.

A measured absence of any asymmetry in the shower producing radiation together with the small asymmetry

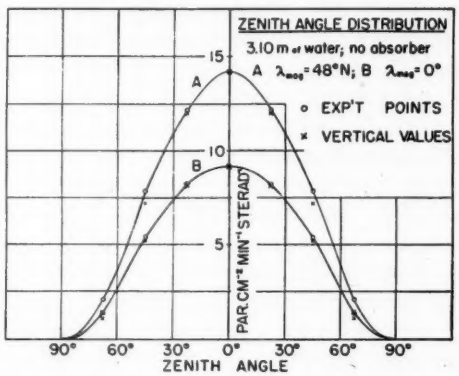

FIG. 27. Comparison of the zenith angle dependence at the equator and at 48° geomagnetic North at 3.10 m of water with no lead absorber. Differences in values through same mass of air as at vertical are most pronounced at the larger angles and northern latitudes.

of the total radiation as measured by Johnson and Barry[27] had led these authors to the conclusion that there are two kinds of primary particles, one giving rise to the penetrating component which shows asymmetry and the other giving rise to the non-penetrating component which does not show asymmetry.

The west excess of the penetrating component has been measured by Schein, Yngre, and Kraybill[28] in the geomagnetic latitude range 27° to 31° North at 34,500 ft. in a B-29. They find an asymmetry of 0.46±0.07 at a zenith angle of 45° in the particles that can penetrate 22 cm of lead. Preliminary data on the west excess were published by the present authors[10] who showed that at the highest altitude reached at the equator, corresponding to a pressure of 2.35 m of water, that the asymmetry in the total radiation was nearly equal to that in the penetrating. This means that there is approximately the same asymmetry in the non-penetrating as in the penetrating component at this altitude. Barber[29] has reported measurements at 33,000 ft. and at 25,000 ft. near the geomagnetic equator and also concludes that there is an asymmetry in the soft as well as in the hard components.

The data here presented and shown in Figs. 12–15 and in Table IV give the measurements at different zenith angles at the equator after all corrections have

[23] Winckler, Stroud, and Schenck, Phys. Rev. **74**, 837 (1948).

[24] T. H. Johnson, Phys. Rev. **43**, 381 (1933).
[25] L. Alverez and A. H. Compton, Phys. Rev. **43**, 836 (1933).
[26] B. Rossi, Phys. Rev. **45**, 212 (1934).
[27] T. H. Johnson, Phys. Rev. **56**, 219 (1939).
[28] Schein, Yngre, and Kraybill, Phys. Rev. **73**, 928 (1948).
[29] W. C. Barber, Phys. Rev. **75**, 590 (1949).

been applied. For a continuous momentum distribution of the primary particles one would expect the curve giving the difference in intensity between the west and east to start off linearly, rise to a maximum where the atmospheric absorption becomes important and approach 0 at 90°. The percentage asymmetry in the intensity for large zenith angles should, as discussed by Johnson,[30] decrease at large zenith angle due to the absorption of the atmosphere for particles in the momentum range responsible for the difference.

The near equality in the percentage of west excess for the penetrating and non-penetrating components again argues strongly for the common parentage for each. This, it will be recalled, is the same conclusion arrived at above for the relation between the penetrating and non-penetrating particles of the latitude sensitive part of the radiation.

For intermediate latitudes the East-West asymmetry is given by Figs. 5 and 6. At high latitudes the difference between east and west fades to zero both without and with lead absorber. This is to be expected since no East-West effect can exist beyond the latitude where the latitude effect, in the intensity at the vertical, ceases.

F. Azimuthal Effect at the Equator

The curves given in Figs. 18 and 19 strongly suggest a sinusoidal variation with azimuth angle for a given

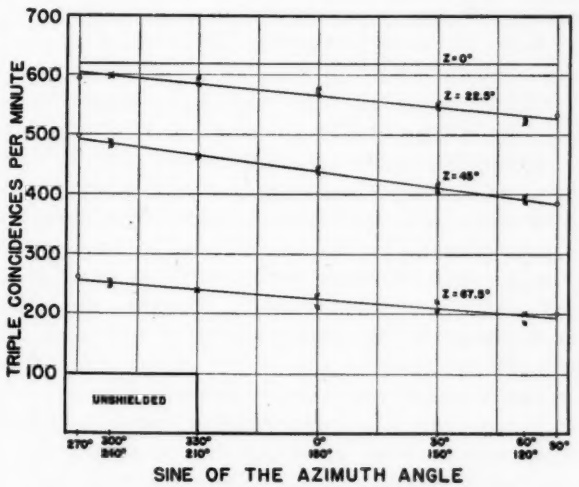

FIG. 28. Data given in Fig. 16 for no lead absorber show a sinusoidal variation with azimuth angle.

zenith angle. When plotted against the sine of the azimuth angle a straight line does in fact result within the limits of the uncertainties of the points as shown in Figs. 28 and 29.

The empirical relations that may be written down are as follows: (1) For the sine curves the number of particles per square cm per minute per steradian at the geomagnetic equator over Peru at 2.35 m of water equivalent for the different zenith angles, z, may be written in terms of the azimuth angle φ as follows:

Absorber	$z=22\frac{1}{2}°$	$z=45°$	$z=67\frac{1}{2}°$
0	$10.4-0.82\sin\varphi$	$7.83-1.14\sin\varphi$	$3.12-0.60\sin\varphi$
10.4 cm Pb	...	$2.24-0.37\sin\varphi$	$1.16-0.18\sin\varphi$
20.8 cm Pb	$2.47-0.23\sin\varphi$	$1.98-0.35\sin\varphi$	...

The above values have been corrected for deadtime of the counters, accidentals, side showers and finite opening of the telescopes.

The ranges in momentum of the primary particles covered by these azimuth experiments, according to the analysis of Lemaitre and Vallarta are as follows (eccentricity of dipole and tilt of magnetic field taken into account):

Zenith angle z	$P_{\min}$(Bev/c)	$P_{\max}$(Bev/c)
$22\frac{1}{2}°$	11.2	17.1
45°	10.0	23.0
$67\frac{1}{2}°$	9.3	32.7

In each complete revolution in azimuth, for each of the zenith angles covered, 12 points were taken; i.e., at every 30°. This means, for example, that with the unshielded telescopes, 36 ten-minute readings were taken in the momentum range 9 to 33 Bev/c. It is apparent that the multiple coverage of the momentum ranges and the consistency of the behavior of the experimental points given in Figs. 18 and 19 strongly suggest a continuous momentum distribution of the primary radiation in the range from 9 to 33 Bev/c. This conclusion combined with that arrived at for the latitude sensitive part means that so far as these experiments are concerned there is a continuous momentum distribution of the primary particles from 2 to 33 Bev/c.

G. Correlation of Latitude and East-West Effects

It is evident, from the analysis of the behavior of charged particles in the earth's magnetic field, that the latitude effect at the vertical will be due both to

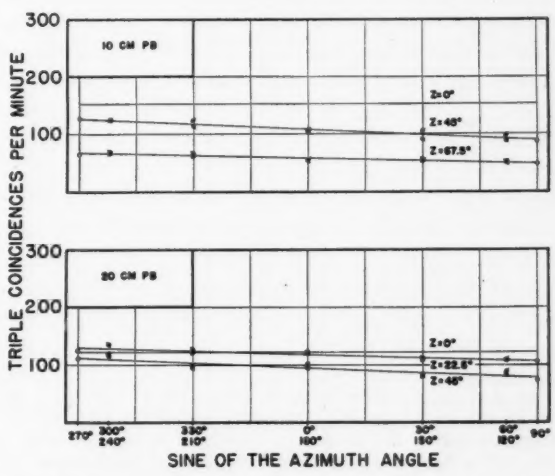

FIG. 29. Data given in Fig. 17 for 10 and 20 cm lead absorber show a sinusoidal variation with azimuth angle.

[30] T. H. Johnson, Rev. Mod. Phys. **10**, 227 (1938).

positive particles and to any negatives that may exist in this momentum range. The East-West effect on the other hand is due to the difference between the numbers of positives and negatives in the particular momentum range.

Unfortunately the existing calculations on the minimum momentum allowed at different zenith angles as a function of geomagnetic latitude are not complete enough to permit an accurate check of the above. However a rough check may be made by considering the latest curves given by Vallarta.[31]

In accordance with the instructions, we have drawn curves through the shaded region connecting his curves E_1 and E_2 for the intermediate latitudes. As drawn we find that at zenith angle 45° East the minimum momentum for positive particles at 25° North geomagnetic latitude is the same as at the vertical on the geomagnetic equator. We also find in a similar way from his curves for 45° West that the minimum momentum at geomagnetic latitude 25° North is the same as at the vertical at 29° geomagnetic north. Thus if all particles are positive we must expect the same ratio of east to west at 25° North as the ratio in vertical intensities between 0 and 29° North.** Taking the average of the values without and with lead taken from Figs. 7 and 8 we find for these ratios 0.82 for the former and 0.78 for the latter. Using the lead curves only where scattering is less pronounced we find for these ratios 0.80 and 0.78 respectively.

While these ratios are close, there is an uncertainty in just how the correct curves in Vallarta's figures should be drawn. It is evident, however, that no negative particles are necessary to correlate the east-west effect and the latitude effect in this momentum range.

While the above argument eliminates the presence of an appreciable number of negative particles in the primary radiation in the momentum range 3–13 Bev/c and the near equality in the East-West effect for the non-penetrating and penetrating particles argues for a common positive particle responsible for this difference in the momentum range 9 to 33 Bev/c, it should be pointed out that these experiments do not mean that there is but one kind of positive particle in the primary radiation. While it seems most likely that the major part of the momentum is brought in at low latitudes by protons, the presence of some α- or heavier particles cannot be excluded. The relative numbers of such particles, however, near the equator must be small in view of the constant proportionality at all altitudes between a single counter and an ionization chamber even up to 80,000 ft.[32]

[31] M. S. Vallarta, Phys. Rev. 74, 1838 (1948).

** There might be some uncertainty introduced because of the larger amount of air at zenith angle 45° compared with the vertical. We find, however, from Fig. 22, that the latitude effect at 3.10 (secant 45°) m of water is very closely the same as at 3.10 m of water.

[32] H. V. Neher and W. H. Pickering, Phys. Rev. 61, 409 (1942).

H. The Latitude Effect of the Total Radiation

The latitude effect of the total radiation as measured with the ionization chamber and shown in Fig. 9 is 36.1 percent as compared with that measured with the vertically directed unshielded telescopes of 37.0 percent. An agreement is to be expected if (1) the zenith angle distribution at this altitude does not change between the northern latitudes and the equator and (2) the relative numbers of the different kinds of particles do not change. The asymmetry at the equator will, to a close approximation, be unimportant in this comparison.

Actually it will be seen from Fig. 27 that the zenith angle distribution is somewhat flatter at the equator than at 48° North. The integrated effect over all zenith angles gives a ratio of total to vertical about 4 percent larger at the equator than at the northern latitude. This result combined with the slightly smaller latitude effect with the ionization chamber indicates that the average ionization per particle at the equator at this altitude is about 6 percent smaller than at 48° North.

I. Upward Radiation

The question as to how much upward radiation is present at the altitudes reached here has often been raised. Some data that bears on this question can be given from the experiments performed during these flights. On several occasions the two East-West frameworks were turned vertical. In one of these frameworks a threefold coincidence telescope was shielded from below by 10 cm of lead and in the other by 20 cm of lead. In each there was no absorbing material except the counter walls and the skin of the plane for the radiation coming in the downward direction. The counting rates of these telescopes could then be compared with the two telescopes which were used to measure the total radiation and had no absorber, either top or bottom. The ratio of the counting rates of the telescope shielded below with 10 cm of lead to the average of the unshielded ones at 30,000 ft. was 0.998. At Inyokern on the ground the ratio was 1.004. For the telescope shielded from below with 20 cm of lead the corresponding ratios were 0.989 and 0.983.

This agreement between relative response of telescopes with no lead below and with 10 and 20 cm of lead below means (1) that the amount of upward radiation through the unshielded telescopes at these altitudes was negligibly small, and (2) that the number of events occurring in the lead such as showers, nuclear explosions, etc., that send particles upward through the telescopes that had lead below was negligibly small.

J. Production of Penetrating Particles in the Atmosphere

Experimental data near sea level agree with theoretical calculations for the absorption of cosmic-ray mesons in various materials. In particular Rossi[15] states that a lead thickness of 167 g cm^{-2} corresponds to an

air thickness of 100 g cm^{-2} as far as total energy losses of mesons due to collisions are concerned. The absorbing layers used in these experiments including the iron box for holding the lead were 10.4 and 20.8 equivalent cm of lead. This should correspond in absorption on the above basis to 71 and 142 g cm^{-2} of air respectively.

Actually in the atmosphere, decay of the mesons plays an important part in the apparent absorption of these particles.[33,34] Using the results of Rossi, Hilberry, and Hoag, and assuming the same average momentum of the mesons at 2.35 m of water equivalent at the equator as at Mt. Evans we find that by changing altitude by an amount which adds 55 g cm^{-2} of air should be the equivalent of adding the second 10.4 cm of lead. Actually it is seen from the lead curves given in Fig. 21 that it requires an addition of 85 g cm^{-2} of air at 2.35 m of water at the equator to drop the counting rate with the 10.4 cm of lead down to that obtained with 20.8 cm of lead at the high elevation. The same situation exists for corresponding data at 50° North but here the lead curves are not as accurately determined as at the equator.

The possible interpretations of this behavior are: (1) Due to different kinds of particles at these high altitudes the absorption is different than at sea level. (2) There is production of penetrating particles taking place in the atmosphere between the two levels. This production may be taking place in the lead as well but will not show since the lead is between the counters and not above.

In terms of the total number of penetrating particles at 2.35 m of water at the equator the cross section for production of new penetrating particles is 1.0×10^{-25} cm^2. In terms of Rossi's N-rays[15] the cross section is about 4×10^{-25} cm^2. This latter number is about equal to the cross section usually taken for the nitrogen nucleus.

It seems quite likely that production of mesons is taking place in the atmosphere at these altitudes and in fact at the equator one might expect the lead curves to reach a maximum at from 1 to 2 m of water equivalent. At this point the rate of production would be just equal to the rate of absorption.

The argument for the lead curves passing through a maximum at the equator while they apparently do not at 50° geomagnetic North[35] is as follows: We take the areas under the ionization curves as a measure of the total energy being brought in by the primary particles. The data of Bowen, Millikan and Neher[36] combined with an assumed differential numbers distribution of $p^{-2.5}$ for the particles remaining at the equator show that there are incident on the top of the atmosphere at the equator only one-eighth the number at 50° North. However the lead curves at one-third atmosphere at the equator are only 35 percent less than at 50° North. We thus infer that had we taken our vertical telescopes containing lead up to very high altitudes at the equator we would have measured a value considerably lower than at our highest elevation (2.35 m of water). If 4×10^{-25} cm^2 is taken for the cross section for interaction of the primary particles with the air nuclei then the maximum might be expected at 1 to 2 m of water equivalent air pressure.

K. Latitude Effect of Wide Showers

The data given in Fig. 10 indicate that within the rather appreciable probable errors given there is no latitude effect in the extensive or wide showers. This is interpreted as meaning that the primary particles responsible for these large showers are either electrically neutral or have sufficient momenta as to be unaffected by the earth's magnetic field.

L. Altitude Dependence of Wide Showers

Kraybill[37] has reported a maximum at about 3.5 m of water in the counting rate *versus* pressure of the atmosphere curve for extended atmospheric showers at northern latitudes. The data shown in Fig. 11 where the point taken at 2.35 m of water was at the magnetic equator confirms the result of Kraybill in placing the maximum at about one-third atmosphere. Since there appears to be no latitude dependence for wide showers one would expect the same altitude dependence at all latitudes.

The increase from the ground level at Inyokern (9.60 m of water) to the peak of the curve is a factor of 33. Counter telescope data show that the particles that cannot penetrate 10 cm of lead increase by a factor of 40 in going from the altitude of Inyokern to 3.1 m of water. This is also the rate of increase of shower producing radiation and also of neutrons in the lower part of the atmosphere.

It is probably no accident that the absorption of extended shower particles at depths in the atmosphere beyond the peak of the curve is close to the same as that for the shower producing radiation. An initiating, very high energy electron or photon, near the top of the atmosphere would produce a large cascade, which in our case builds up to its maximum at 3.5 m of water. Beyond the peak, shower theory shows that the average energy of the particles is nearly independent of the energy of the initiating particle and that the absorption thickness, i.e., the thickness for the number of ionizing particles to drop to $1/e$ of their initial value, is approximately 150 g cm^{-2}. This is just the value found above for the absorption of the extensive showers at some distance beyond the peak of the curve. The presence of a small percentage of penetrating particles accompanying these extensive showers, such as are known to

[33] Rossi, Hilberry, and Hoag, Phys. Rev. **57**, 461 (1940).
[34] H. V. Neher and H. G. Stever, Phys. Rev. **58**, 766 (1940).
[35] M. A. Pomerantz, Phys. Rev. **75**, 69 (1949).
[36] Bowen, Millikan, and Neher, Phys. Rev. **53**, 859 (1938).
[37] H. L. Kraybill, Phys. Rev. **73**, 632 (1948).

exist, will not appreciably change the main features of the absorption curve.

X. SUMMARY

The cosmic-ray experiments herein reported were made in a B-29 flying along 80° West longitude at a pressure altitude of 30,000 ft. from 54° North to the geomagnetic equator during a two-week period in June of 1948. The fact that the results of the return trip from Peru agree with those taken going down indicates that no significant changes in the primary cosmic-ray intensity took place during this period. In spite of the 300-m.p.h. speed of the plane the counting rates of the Geiger counter telescopes were such that the probable error of no point on the latitude effect curves is more than 2 percent, even with 20 cm of lead absorber. To achieve this accuracy and at the same time keep a relatively small aperture, large area counter trays were used.

From the data given the following conclusions are drawn: (1) There is the same ratio between penetrating and non-penetrating radiation at 3.10 m of water equivalent at the equator as at northern latitudes, i.e., there is the same latitude effect for each. This same ratio of penetrating to non-penetrating is found at the equator for the particles causing the east-west difference. It is also found for the radiation coming in at 45° East when the mass of air penetrated is the same. From these findings we conclude that whatever the process by which the primary particles are transformed into secondaries, the relative number of penetrating and non-penetrating particles appearing after traversing one-third atmosphere of air is the same irrespective of the momentum of the primary particle. The fact that this conclusion holds also for the radiation remaining at the equator argues for these particles being the same as those showing geomagnetic effects. (2) The present data permits us to redraw our older count *versus* depth curves, normalizing them all to the present latitude curve at 3.10 m of water. After the adjustment we find no cut-off of low energy particles up to 60° geomagnetic north. This corresponds to a minimum momentum at the vertical of about 1 Bev/c. (3) From the azimuthal experiments made at 2.35 m of water over Peru we find a smooth variation in azimuth for all zenith angles, namely 22½°, 45° and 67½°. These measurements sweep across a momentum range of the primary particles (according to Vallarta *et al.*) from 9 to 33 Bev/c. This fact, taken together with the smooth variation with latitude found for the vertical radiation as well as for that coming in at 45° East and 45° West, means that, in the momentum range from about 2 to 33 Bev/c, as far as these experiments are concerned, there is a continuous momentum distribution of the particles whose effects can reach down to where these experiments were performed. (4) Comparison of the East-West effect and latitude effect, in a region where particles of the same momentum range (according to Vallarta) are involved, shows that the two are equal. This can only be so if the number of negative particles in the primary radiation, whose effects reach through one-third atmosphere, is negligible compared with the positives, in this momentum range. (5) Evidence for the production of penetrating particles at these altitudes is found when the absorption in air and lead is compared. If Rossi's "N-rays" are responsible for this production the cross section is about equal to that of the nitrogen nucleus. (6) Measurements on extended showers indicate that they are not latitude sensitive. They may thus be due either to electrically neutral primaries or, what seems to be more probable, to charged particles whose momentum is so great as to be unaffected by the earth's magnetic field. (7) The altitude dependence of extended showers shows a maximum at about one-third atmosphere. Beyond the maximum they show an absorption in the atmosphere about equal to that of either the soft component or the shower producing component. (8) The latitude effect of the total radiation as measured with an ionization chamber shows very closely the same latitude effect at 3.10 m of water as the vertical counter telescopes. This is to be expected if (a) the zenith angle effect is not latitude sensitive and (b) the relative numbers of the different kinds of particles that ionize differently at this altitude does not change appreciably with latitude. The slightly different zenith angle dependence found, together with the small difference in the latitude effect indicates an average ionization per particle at the equator slightly less than at the northern latitudes. (9) The amount of upward radiation that can be stopped by 20 cm of lead is negligible at 3.10 m of water. (10) The amount of backward scattering together with nuclear events in the lead, that result in particles ejected upward which can pass through a telescope mounted over the lead, are negligible compared with the downward radiation.

In conclusion the authors wish to thank the Office of Naval Research and the United States Air Forces for making these flights possible. Above all we wish to express our appreciation to Major W. A. Gustafson, Captain Freyer, Lt. Brandon and the other members of the crew of the B-29 for their cooperation and efforts spent in making these flights successful.

Extensive Penetrating Cosmic Ray-Showers*

JOHN ISE, JR.** AND W. B. FRETTER
Department of Physics, University of California, Berkeley, California
(Received June 23, 1949)

The density spectrum of the particles in Auger showers capable of penetrating twenty centimeters of lead has been measured at 3026-meters elevation, and found to be very nearly the same as the density spectrum of the soft component of the showers, the ratio of penetrating to soft particles apparently decreasing slowly with increasing shower density. This ratio has been measured, using the coincidences between four trays of Geiger counters, all shielded by twenty centimeters of lead, and found to be about 2.3 percent. As this value is considerably higher than the value found by other methods, some calculations on the structure of Auger showers are given, in an attempt to explain the discrepancy. It is found that any experiment using coincidences between unshielded trays, horizontally separated by a few meters, is biased strongly toward recording only the cores of the extensive showers. A cloud chamber, tripped by extensive shower counters, is used to study the structure of the extensive showers, and local production of penetrating particles in lead plates within the chamber is definitely established.

I. INTRODUCTION

SINCE the discovery[1] of the Auger cosmic-ray showers by Geiger tube coincidences, many experiments have been performed to clarify the structure and composition of these showers, and their variation with altitude and barometric pressure. Most experiments using Geiger tube coincidences have been shown[2,3] to give results agreeing with the hypothesis of the cascade origin of these showers,[4] by the bremsstrahlung and pair-production effects of high energy electrons. The existence in Auger showers of particles much more penetrating than electrons has been demonstrated by many observers,[5–10] these particles being presumably μ-mesons produced high in the air above the recording apparatus.[10] The "density spectrum," i.e., frequency of occurrence of the Auger showers as a function of average particle density (particles per unit surface area) in the showers, has been measured both directly with ionization chambers,[11] and indirectly, using coincidences between several trays of Geiger counters.[9,12,13] These experiments have established that the frequency $F(\sigma)$ of the Auger showers in which the particle density is greater than σ is given satisfactorily by the expression

$$F(\sigma)=K\sigma^{-\gamma}, \qquad (1)$$

in which K and γ are functions of the altitude above sea level, but vary only slowly with density over a large range of densities. The constant γ has been shown to be about 1.5.

It has been shown[8,9] that all Auger showers contain penetrating particles and that all extensive penetrating showers were accompanied by electron showers, but the density spectrum of the extensive penetrating showers had not been measured, nor had the relative densities of penetrating particles and electrons in Auger showers been established with certainty. Consequently experiments were carried out during the summer of 1948 at Tioga Pass (elevation 3026 meters) in Yosemite National Park on the density spectrum of the penetrating particles in Auger showers.

II. EXPERIMENTAL ARRANGEMENT

The geometrical arrangement of the experiment is shown in Fig. 1. The extensive showers were detected by means of four trays of Geiger counters A, B, C, D of equal but variable area. Threefold coincidences were recorded between trays A, B, and C, arranged in a straight line with a spacing of 4.8 meters, and also fourfold coincidences were recorded with a fourth tray D, situated on the perpendicular bisector of the line joining the threefold trays at a distance of 8.0 meters from this line. The coincidence circuits were housed in a thin-walled trailer, which also housed a large cloud

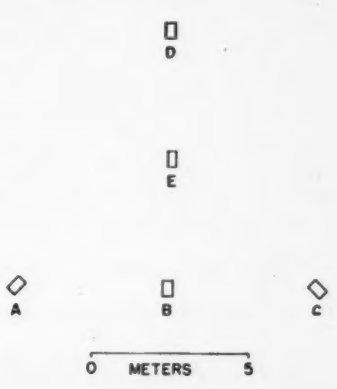

FIG. 1. Geometrical arrangement of apparatus.

* Assisted by the Joint Program of the ONR and the AEC.
** Abraham Rosenberg Fellow of the University of California.
[1] Auger, Maze, and Grivet-Meyer, Comptes Rendus **206**, 1721 (1938).
[2] H. W. Lewis, Phys. Rev. **73**, 1341 (1948).
[3] G. Cocconi, Phys. Rev. **72**, 964 (1947).
[4] G. Moliere, *Cosmic Radiation*, edited by W. Heisenberg (Dover Publications, New York, 1946).
[5] Auger, Maze, Ehrenfest, Daudin, and Robley, Rev. Mod. Phys. **17**, 238 (1939).
[6] J. Daudin, Comptes Rendus **216**, 411 (1943).
[7] A. Rogozinski, Ann. de physique **20**, 391 (1945).
[8] Cocconi, Loverdo, and Tongiorgi, Phys. Rev. **70**, 852 (1946).
[9] J. E. Treat and K. Greisen, Phys. Rev. **74**, 414 (1948).
[10] Cocconi, Cocconi, and Greisen, Phys. Rev. **75**, 1063 (1949).
[11] R. W. Williams, Phys. Rev. **74**, 1689 (1948).
[12] Cocconi, Loverdo, and Tongiorgi, Phys. Rev. **70**, 841 (1946).
[13] J. Daudin and A. Loverdo, Journal de Physique **9**, 134 (1948).

chamber E, which was used during part of the experiment. The Geiger counter trays were shielded by means of rectangular lead bricks piled above the trays, the supports being short lengths of 2-inch×4-inch lumber. The trays were placed flat on the ground with no shielding underneath, and the shielding at the ends and sides of the trays was kept constant at 10 centimeters of lead, while the shielding above the trays was varied from 5 to 20 centimeters of lead, being the same over all four trays. Measurements were also taken with no shielding above or at the sides and ends of the trays.

The thickness of 20 centimeters of lead used to absorb the soft component of the showers was based on the results of absorption measurements obtained during the course of these experiments, as well as on the results of other observers,[14–16] all of which had indicated that the absorption curve started its "tail" at thicknesses of about 15 centimeters of lead. Cocconi and collaborators[8] had used 16 centimeters of lead in the only previous work of the kind described here and had found no significant change in coincidence rate between 16 and 24 centimeters of lead. Recent results, both experimental[10] and theoretical,[17] have shown that the effects of electrons in discharging counters under lead screens are not entirely eliminated for thicknesses of lead less than 20 centimeters. This penetration in lead, much greater than formerly believed, is due to the effects of the many low-energy photons in air showers which, although possessing insufficient energy for pair-production, can nevertheless set off counters by means of Compton electrons originating in the walls of the counters. Incidentally, as pointed out by Greisen,[17] this invalidates much of the previous work done on extensive penetrating showers, in which insufficient lead shielding was used to completely absorb the soft component.

TABLE I. Observational data (the probable errors are assigned only on the basis of statistics).

Area (cm^2)	Lead thickness (cm)	3fold rate ($hr.^{-1}$)	4fold rate ($hr.^{-1}$)
350		48.9 ±0.8	30.07 ±0.70
700	0	130 ±5	80.72 ±3.88
1050		234 ±3	144.6 ±2.1
350		6.14 ±0.33	
700	5		
1050		42.1 ±0.8	
350		0.55 ±0.08	
700	10		
1050		4.01 ±0.28	
350			
700	15		
1050		1.56 ±0.09	
350		0.193±0.015	0.114±0.013
700	20	0.588±0.033	0.360±0.031
1050		1.18 ±0.064	0.706±0.056

[14] Auger, Maze, Ehrenfest, and Freon, J. de phys. et rad. **10**, 39 (1939).
[15] de Souza Santos, Pompeia, and Wataghin, Phys. Rev. **57**, 339 (1940) and **59**, 902 (1941).
[16] L. Janossy, Proc. Roy. Soc. **179**, 361 (1942).
[17] K. Greisen, Phys. Rev. **75**, 1071 (1949).

The Geiger counters used in this experiment were of the all-metal type filled with an argon-alcohol mixture. They were all of 2-inches inside diameter and 14-inches effective length. The counter trays consisted of several of these counters connected in parallel inside a light wooden tray of $\frac{1}{4}$-inch plywood. Oilcloth sheets covered each tray to keep moisture off the counters.

Counting rates of the individual trays were taken daily with an electronic pulse counter. In this way failure of one Geiger tube in a tray could be immediately detected.

The coincidence circuit was patterned after that described by Howland, Schroeder, and Shipman,[18] with a few modifications. It consisted of an input cathode follower and amplifier, a differentiating circuit and an output cathode follower. The resolving time of the coincidence circuit, measured by chance coincidences between two counters with very high rates, was 14 microseconds. The maximum correction to the observed coincidence rate, caused by this long resolving time, was of the order of 15 percent, so no serious errors were thereby introduced.

III. RESULTS AND CALCULATIONS

The data taken during the course of this experiment are shown in Table I. All counter trays had the same thickness of lead shielding and the same number of counters per tray, any variation in these last two quantities being made simultaneously in all four trays. All rates are corrected for accidental coincidences.

The absorption curve of the extensive showers in lead is shown in Fig. 2 where the threefold coincidence rate is plotted logarithmically against the lead thickness, the area of all trays being 1050 cm^2. The probable errors of all points lie within the small circles. This curve is in agreement with that given by Cocconi, Cocconi, and Greisen,[10] in that it shows a noticeable decrease in coincidence rate between 15 and 20 centimeters of lead, this decrease presumably being due to the absorption of the last of the soft component. Reynolds and Hardin[19] have obtained a similar curve by a somewhat different method, showing a slight initial rise in coincidence rate as the lead thickness is increased from zero to two centimeters, this rise being caused by the secondary multiplication of the shower electrons.

The theory underlying the determination of the density spectrum by variation of counter area was developed by Cocconi[12] and independently by Daudin.[20] It was shown by them that, assuming the density spectrum of the Auger showers to be given by Eq. (1),

[18] Howland, Schroeder, and Shipman, Rev. Sci. Inst. **8**, 551 (1947).
[19] G. T. Reynolds and W. D. Hardin, Phys. Rev. **74**, 1549 (1948).
[20] J. Daudin, Ann. de physique **18**, 238 (1943).

the n fold coincidence rate between n trays of Geiger counters, all of area S, is given by

$$C(n, S)=\int_0^\infty K\sigma^{-(\gamma+1)}(1-\epsilon^{-\sigma S})^n d\sigma. \quad (2)$$

It is tacitly assumed in the derivation of Eq. (2) that the shower density σ is the same over all counter trays. Because of the pronounced maximum of the integrand occurring at a shower density $\sigma\sim 1/S$, most of the contribution to the integral (2) comes from a comparatively narrow range of densities and hence the density-spectrum (1) need not be assumed valid much beyond this range of densities.

By varying the area S of all the counter trays the constant γ can be obtained from (2) by plotting logarithmically the coincidence rate *versus* the area S (see Fig. 3) and using

$$\gamma=\{d[\log C(n, S)]/d(\log S)\}. \quad (3)$$

Using this equation, the value of γ obtained from the unshielded rates in Table I is 1.42 ± 0.02.

An independent determination of γ can be made by observing the ratio of fourfold to threefold coincidence rates. If the integral (2) be evaluated for $n=4$ and $n=3$, it can be shown that

$$\begin{aligned} C(4, S)&=KS^\gamma(-1-\gamma)![4^\gamma-4(3)^\gamma+6(2)^\gamma-4], \\ C(3, S)&=KS^\gamma(-1-\gamma)![-3^\gamma+3(2)^\gamma-3], \end{aligned} \quad (4)$$

and from the ratio of these two rates, which is a function of γ alone, the value of γ may be obtained. From the observed ratio of fourfold to threefold unshielded coincidence rates in Table I, the computed value of γ is 1.58 ± 0.04, which is not at all in agreement with the value obtained by variation of counter area. Each of these values is in very good agreement, however, with the corresponding value obtained by Treat and Greisen,[9] who obtained, respectively, 1.40 and 1.55. A discussion of the discrepancy will be given in Section IV.

In Fig. 3 is shown a plot of the logarithm of the coincidence rate *versus* the logarithm of the counter area for the threefold and fourfold coincidence rates, both unshielded and under 20 centimeters of lead. The shielded coincidence rates have been multiplied by 100 in order that they might be shown on the same graph as the unshielded rates. The captions on the straight lines in Fig. 3 refer to threefold and fourfold coincidences, the "S" and "H" referring to "soft" (unshielded) and "hard" (shielded) showers. The values of γ as determined from the slopes of these curves are

$$\begin{aligned} (3S)\gamma&=2.425\pm 0.019, \\ (4S)\gamma&=2.428\pm 0.025, \\ (3H)\gamma&=2.65\ \pm 0.09, \\ (4H)\gamma&=2.66\ \pm 0.12. \end{aligned} \quad (5)$$

In the determination of the density spectrum (1) for the extensive penetrating showers, it is evident from (5) that the exponents γ for the hard and soft showers

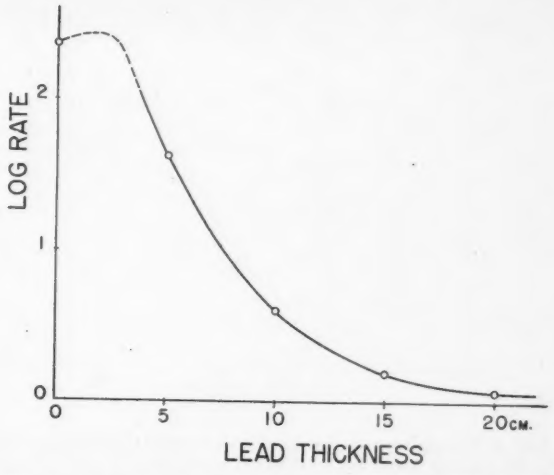

FIG. 2. Absorption in lead of extensive showers. The threefold coincidence rate between trays of area 1050 cm² is plotted as a function of the lead thickness above each tray.

apparently differ by about 0.23, which is well outside the statistical uncertainties. However, it must be remembered that the average (total) shower densities recorded with and without lead shielding differ by a factor of about forty-five because the average density of penetrating particles recorded under 20 centimeters of lead is identical to the *total* particle density recorded with no lead shielding, and the relative densities of hard and soft particles will be shown below to be about one in forty-five.

The recent very exact measurements of Cocconi and Cocconi[21] on the variation of γ with shower density have established the empirical relation

$$\gamma=1.26-0.099\log_{10}S, \quad (6)$$

where S, the area of the counter trays, is measured in square meters. For $S=700$ cm² (the middle of the range of values used in the present experiment) the value of γ as given by this equation is 1.37 (in good agreement with the value given in Eq. (5) above), while for $S=15.5$ cm² (which, because of the inverse relationship of counter area S to average shower density recorded, therefore corresponds to shower densities 45 times as large), $\gamma=1.54$. It is this last value of γ that must be compared to the value 1.65 ± 0.09 obtained for the extensive penetrating showers.

From these last two values of the density exponent γ, corresponding to penetrating and soft particles in showers of the same total density, it seems that the penetrating particles decrease slightly more rapidly than do the electrons with increasing shower density, i.e., the ratio of penetrating particles to electrons decreases slowly as the shower density increases, since

$$\text{penetrating particles/electrons}\sim\sigma^{-0.11\pm 0.09}. \quad (7)$$

The large probable error attached to the value of γ for

[21] G. Gocconi and V. Cocconi-Tongiorgi, Phys. Rev. **75**, 1058 (1949).

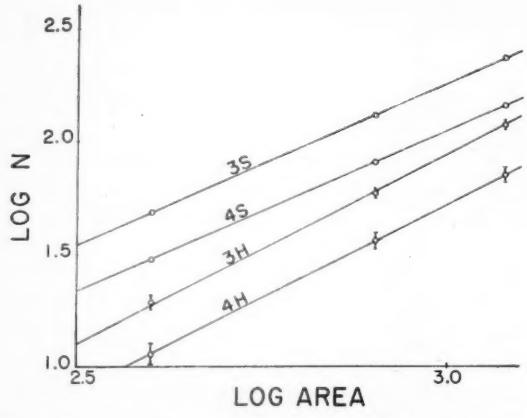

FIG. 3. Dependence of threefold and fourfold coincidence rates (N) on counter area, for unshielded counters ($3S$ and $4S$) and for counters shielded by 20 cm of lead ($3H$ and $4H$).

the penetrating showers precludes much confidence in the numerical value of the exponent in (7), but recent exact measurements of the ratio of penetrating to soft particles in extensive showers by Cocconi, Cocconi, and Greisen,[10] obtained by a somewhat different method, show that

$$\text{penetrating particles/electrons} \sim \sigma^{-0.13\pm0.02}. \quad (8)$$

It is shown in reference 10 that this relation is in accord with the provisions of the cascade theory if the assumption is made that the number of penetrating particles is proportional to the average energy of the initiating primary.

The evaluation of the relative densities of penetrating particles and electrons, which has been stated as being about one in forty-five, will now be given. The procedure will be as follows: the reduction in area of the unshielded counters necessary to produce the same coincidence rate as is obtained with the counters shielded by 20 centimeters of lead will first be found. The probability of a coincidence being recorded is a function only of the quantity σS, the average shower density times the area of the counter trays (see Eq. (2)). Therefore the new reduced area of the unshielded counters is to the area of the shielded counters as the ratio of penetrating particle density to total particle density.

We shall now calculate the area of the unshielded counters necessary to produce a threefold coincidence rate of 1.18 counts per hour, the value obtained with shielded trays of area 1050 cm². Denoting the unshielded coincidence rate by $C(3, S)$ and the surface area of the counter trays by S, we have from (3) and (6)

$$\gamma = \{d[\log C(3, S)]/d(\log S)\} = 1.26 - 0.099 \log_{10} S, \quad (9)$$

which can be immediately integrated to give

$$\log C(3, S) = 1.26 \log_{10} S - 0.0495(\log_{10} S)^2 + \text{constant}. \quad (10)$$

The constant term in (10) could be evaluated by substituting a particular set of values of $C(3, S)$ and S but in this case it is not necessary to do so. Let the subscript "1" refer to the values of $C(3, S)$ and S observed with unshielded trays of area 1050 cm² and let S_2 be the (unknown) surface area which produces the same coincidence rate $C(3, S_2) = 1.18$/hr. as do the shielded trays of area 1050 cm². Then we have

$$\begin{aligned} \log(234\pm3) &= 1.26 \log(0.105) - 0.0495(\log 0.105)^2 + \text{constant}, \\ \log(1.18\pm0.064) &= 1.26 \log S_2 - 0.0495(\log S_2)^2 + \text{constant}. \end{aligned} \quad (11)$$

By subtraction, the constant term can be eliminated and solution for S_2 gives

$$S_2 = 23.5 \text{ cm}^2, \quad \text{or} \quad S_1/S_2 = 45\pm1. \quad (12)$$

From what has been said above, the ratio of penetrating particle density to total shower density, which we shall call the "penetrating fraction" and denote by R, is then

$$R = 1/(45\pm2) = (2.25\pm0.12) \text{ percent}. \quad (13)$$

Essentially the same value is obtained by using the data at 700-cm² and 350-cm² tray area.

IV. DISCUSSION OF RESULTS AND COMPARISON WITH PREVIOUS RESULTS

A. Unshielded Data

The reasons for the discrepancy between the values of γ as obtained from the ratio of fourfold to threefold (unshielded) coincidence rates and from the variation of counter area will now be taken up in some detail, as considerable insight into the structure of Auger showers is thereby gained.

Treat and Greisen[9] had observed about the same difference in values of γ as obtained in the present experiment and listed several possible reasons for this effect. The variations in surface area of the counter trays were obtained by changing the number of cylindrical counters in parallel in each tray. The effective area of the counter trays for showers incident at angles to the vertical is therefore reduced relatively more for the larger areas. This makes the change in coincidence rate with counter area less pronounced than it actually is, or in effect, reduces the apparent value of γ. Cocconi and Cocconi-Tongiorgi,[21] in the most definitive study of the density spectrum of Auger showers to date, found no perceptible difference in coincidence rate when the counters in each tray were packed closely together and when they were separated by a distance equal to their diameter. They therefore concluded that the effect of inclined showers is negligible. This is in agreement with calculations of the present writers, who, by assuming that the frequency of Auger showers as a function of their zenith angle θ varies[22] as $\cos^8\theta$ have calculated[23] the change in the value of γ that would

[22] J. Daudin, J. de phys. et rad. **6**, 302 (1945).
[23] J. Ise, Jr., Ph.D. thesis, University of California.

be introduced by the inclined showers. It was found that, assuming a value of γ of 1.55, the *apparent* value of γ would be reduced only to 1.54. If the variation of shower frequency with zenith angle is taken as $\cos^4\theta$, the value of γ is still apparently reduced only to 1.53. Thus inclined showers cannot account for the difference in the values of γ obtained by the two methods.

Treat and Greisen also mentioned, as possible reasons for this discrepancy, the barometric effect of Auger showers,[24–26] which has been estimated as being 10 percent to 20 percent per centimeter change in barometric pressure. It is possible that this effect did introduce some error into the value of γ as measured by variation of counter area, but it is felt that such an error is small. The unshielded measurements extended over two periods of three days each, at the beginning and end of the summer, and the variations in counter area were made at intervals of about two hours, in order to intersperse the counting periods for a given counter area throughout as large a time interval as possible. The barometric effect would not be expected to introduce much error into the value of γ as determined from the ratio of fourfold to threefold coincidence rates, since these were measured simultaneously.

We believe that the true explanation of the discrepancy between the two values of γ is to be found in the geometrical structure of the Auger showers themselves. The analysis of the density spectrum of extensive showers rests upon the assumption that the average shower density σ is approximately constant over the area covered by the recording apparatus, so that the shower density is the same at all the counter trays. This assumption is by no means always correct, for, especially near the core of a shower, the density changes very rapidly with distance from the core. However, it can be shown that the calculated density spectrum is not affected by this variation in shower density from one counter tray to another, if the assumption is made that all showers are geometrically similar, and that the radial density distribution in a particular shower does not change along the downward path of the shower. This latter assumption is justified by Williams,[11] who quotes an analytic approximation, due to Bethe, for the particle density σ at a depth t below the top of the atmosphere and at a distance r from the shower axis, as

$$\sigma = N(t)(0.454/r)(1+4r)\exp(-4(r)^{\frac{1}{2}}) = N(t)f(r), \quad (14)$$

where $N(t)$ is the total number of electrons in the shower at depth t, and r is measured in units of the "characteristic scattering length," which at an altitude of 3050 meters is about 106 meters.

If it is now assumed that the differential frequency distribution of extensive showers according to the total number of particles N in the shower, at a given elevation, is

$$F(N)dN = KN^{-(\gamma+1)}dN, \quad (15)$$

then the coincidence rate between three counter trays each of area S (which must be measured in units of the square of the characteristic scattering length) is

$$C(3,S) = \int_0^\infty KN^{-(\gamma+1)}dN \int d\Sigma \prod_i (1-e^{-NSf(r_i)}), \quad (16)$$

where r_i $(i=1, 2, 3)$ are the distances of the three counter trays from the shower axis and the space integral over Σ must be extended over all relative positions of the counter trays and the shower axis, given by particular values of r_i. After this integration (16) may be written

$$C(3,S) = \int_0^\infty KN^{-(\gamma+1)}g(NS)dN$$

$$= S^\gamma \int_0^\infty KN^{-(\gamma+1)}g(N)dN, \quad (17)$$

and it is seen that, just as in the simpler analysis given in Section III, the coincidence rate varies as a power of the surface area of the counter trays. In this case the exponent γ refers not to a "density spectrum" but to the spectrum of the total number of particles in the shower. It is to be noted that, with this latter interpretation, the term "shower density" as applied to a particular shower is a meaningless term, since in any shower, regardless of the total number of particles, all shower densities are to be found, depending on the distance from the shower axis.[27] The integration indicated in Eq. (16) has been carried out numerically for the particular counter arrangement used in this experiment, i.e., three counter trays in a straight line, with a spacing a of 5 meters. If the central counter tray lies at a distance r from the shower axis, and the angle between the radius vector from the shower axis to the central tray and the line joining the three counter trays be denoted by θ (see Fig. 4), the threefold coincidence rate

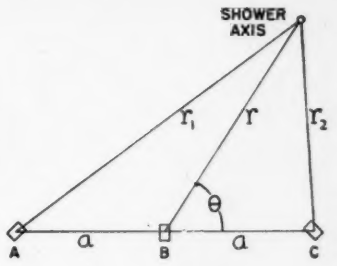

FIG. 4. Coordinates of shower axis with respect to the threefold coincidence trays *A*, *B*, *C*.

[24] M. G. E. Cosyns, Nature **145**, 668 (1940).
[25] P. Auger and J. Daudin, Phys. Rev. **61**, 91 (1942).
[26] G. Cocconi, Phys. Rev. **72**, 964 (1947).

[27] In the derivation of Eq. (16) it has not been possible to take into account the variations in shower density over the individual counter trays. This neglect should not affect appreciably the results of these calculations.

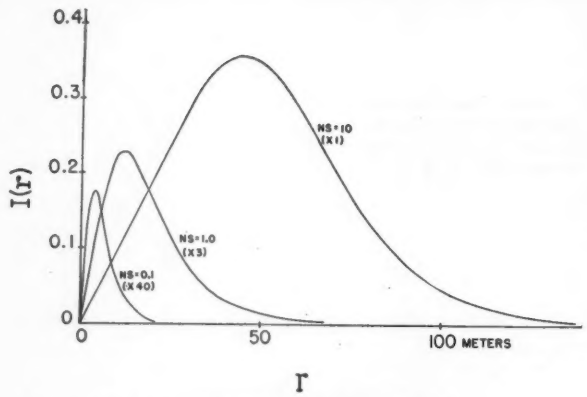

FIG. 5. Probability $I(r)$ of a threefold coincidence due to all showers striking at a distance r from the central counter tray (see Fig. 4), for various values of NS. (N=total number of particles in shower, S=counter area in units of 1.13×10^4 meter^2.)

is from (16)

$$C(3,S)=\int_0^\infty KN^{-(\gamma+1)}dN\int_0^\infty 2\pi r dr\int_0^{\pi/2}\frac{2}{\pi}(1-e^{-NSf(r)})\times(1-e^{-NSf(r_1)})(1-e^{-NSf(r_2)})d\theta, \quad (18)$$

where $r_{1,2}=(a^2+r^2\pm 2ar\cos\theta)^{\frac{1}{2}}$ and

$a=5$ meters$=0.05$ in units of the characteristic scattering length.

The function

$$I(r)=r\int_0^{\pi/2}(1-e^{-NSf(r)})\times(1-e^{-NSf(r_1)})(1-e^{-NSf(r_2)})d\theta \quad (19)$$

is shown in Fig. 5 for $NS=0.1$, 1.0 and 10. This function represents the probability of a threefold coincidence due to all showers striking at a distance r from the central counter, for a particular value of the quantity NS. It will be noted that this function falls to zero for $r=0$, in spite of the obvious fact that a shower is more likely to cause a triple-coincidence if it hits right on the central counter tray than if it hits anywhere else. This apparent paradox is due to the fact that $I(r)$ is actually the product of two separate quantities, (a) the probability that a particular shower will cause a threefold coincidence if it hits at a distance r from the central counter tray, and (b) the number of such showers, which is clearly proportional to 2π-rdr. It is this last factor which brings the curves in Fig. 5 to zero at $r=0$. Perhaps a more meaningful quality would be $I(r)/r$, which therefore represents the probability (a) above, i.e., that probability that a particular shower will cause a threefold coincidence if it hits at a distance r from the central counter (averaged over all orientations θ). This is plotted in Fig. 6, for several values of the quantity NS. It will be seen that all these curves show a maximum probability of a coincidence when the shower strikes the central counter tray, i.e., at $r=0$.

In order that the curves in Fig. 5 might be shown on the same graph, the ordinates of the curve for $NS=1.0$ have been multiplied by 3 and the ordinates of the curve for $NS=0.1$ have been multiplied by 40. These curves show that for small showers for which $NS=0.1$ the maximum contribution to the threefold counting rate comes from showers whose cores strike within a few meters of the central counter tray, while for larger showers ($NS=10$) the maximum contribution is from showers whose cores strike perhaps 50 meters from the central tray.

A graph of the function,

$$R(N,S)=N^{-(\gamma+1)}\int_0^\infty I(r)dr=[dC(3,S)/dN], \quad (20)$$

versus the logarithm of NS is shown in Fig. 7 for $\gamma=1.5$. For any value of S, this curve shows the contribution to the coincidence rate of showers of various total numbers of electrons striking at all distances from the counter trays. Although the experimental value of the exponent γ obtained in this experiment is closer to 1.42 (see Eq. (5)), the value 1.5 has been chosen in this analysis in order to be able to compare the value of the constant K in Eq. (22) below with the value obtained previously by Blatt, as quoted by Williams.[11]

The sharp maximum in Fig. 7 at $NS=0.04$ thus shows that for a tray area of 100 cm^2 the maximum contribution to the coincidence rate is from showers in which the total number of electrons is

$$N=0.04/S=0.04/0.01\times(106)^{-2}=4.5\times10^4. \quad (21)$$

Furthermore, since the maximum in Fig. 7 occurs at $NS=0.04$, it can be seen from the curve in Fig. 5 that, regardless of the surface area of the counter trays, most of the showers recorded strike within ten meters of the central tray. This is an interesting result, since the *a priori* conclusion might well have been that smaller counter areas, which therefore select larger showers, would respond to showers whose axes were

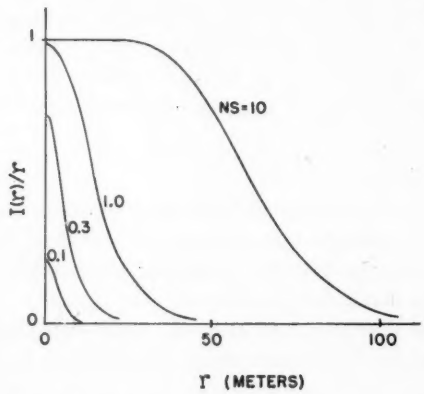

FIG. 6. Probability that a particular shower will cause a threefold coincidence if it hits at a distance r from the central counter of Fig. 4, for various values of NS.

farther from the central counter tray. Since the showers which produce threefold coincidences strike in the immediate vicinity of the central counter tray, it can be seen from the arrangement of the counter trays in Fig. 1 that on the average the fourth counter tray will be struck simultaneously with the other three trays less often than if it were nearer the central tray of the threefold set. This lowers the ratio of fourfold to threefold coincidence rates, and, as can be shown from Eqs. (4), leads to a value of γ calculated from this ratio which is too high. This explains the discrepancy between the values of γ calculated from the variation in counter area and from the ratio of fourfold to threefold coincidence rates. Cocconi and Cocconi[21] have used a more symmetrical counter geometry, with three counter trays at the vertices of an equilateral triangle and the fourth tray at the center of the triangle, and have found no significant difference in the values of γ obtained by the two methods. This is then an experimental verification of the conclusion given above, that the showers recorded almost always strike in the immediate vicinity of the recording counter trays.

With the assumption that the frequency of showers according to the total number of particles in the shower varies as given in Eq. (15) the constant K can be evaluated from Eq. (18), i.e., from the known coincidence rate at a particular value of counter area S, and from the measured area under the curve in Fig. 7, plotted on a linear scale. When this is done, the number of showers per square meter per hour with a total number of particles between N and $N+dN$ is found to be

$$F(N)dN=1.3\times10^{6}N^{-2.5}dN \text{ meter}^{-2} \text{ hr.}^{-1}. \quad (22)$$

The value quoted by Williams,[11] as obtained by Blatt from ionization chamber data is

$$F(N)dN=2.7\times10^{6}N^{-2.5}dN \text{ meter}^{-2} \text{ hr.}^{-1}. \quad (23)$$

Both these values depend on the assumption that Eq. (14) is valid for all showers, and Williams states that his value is uncertain by perhaps a factor of two. In view of this, the agreement seems very good.

B. Shielded Data

The form of the density spectrum for extensive penetrating showers obtained in this experiment agrees within the statistical uncertainties with the results of Cocconi, Cocconi and Greisen.[10] The value of the penetrating fraction R obtained in Eq. (13) is, however, almost twice as large as the value obtained in their work at very nearly the same altitude. The reason for this difference is not known but some suggestions will be discussed below.

If the penetrating fraction R is assumed to be constant throughout any shower, and the same for all showers, then its value may be obtained provided we know only the decrease in coincidence rate when a system of Geiger counter trays is shielded with at least

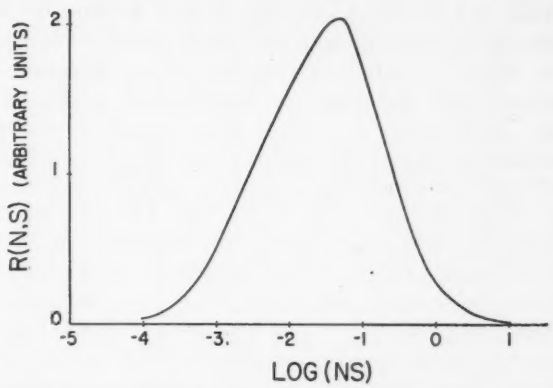

FIG. 7. Contribution to threefold coincidence rate of showers of various total numbers N of electrons striking at all distances from the central counter of Fig. 4.

20 centimeters of lead. In fact, if X is the factor by which the unshielded coincidence rate is diminished, it can be shown that

$$R=(1/X)^{1/\gamma}. \quad (24)$$

From the data in Table I, the value of X corresponding to a counter tray area of 700 cm^2 is 221. The value of γ which we must use in (24) will probably lie between 1.42 (the value obtained with no lead shielding) and 1.65 (the corresponding value under 20 centimeters of lead). Using these two extreme values of γ we find as extremal values of the penetrating fraction R, 3.9 percent and 2.2 percent, the latter of which is in good agreement with the value obtained in (13). The observed reduction factor in coincidence (221) is in very good agreement with that obtained by Cocconi, Loverdo and Tongiorgi[8] at 2200 meters elevation. It is true that these latter observers used only 16 centimeters of lead shielding, but they stated that no further change in coincidence rate occurred between 16 and 24 centimeters of lead. This last work was done using four trays of Geiger counters, all shielded.

We note further the work of Treat and Greisen.[9] They also carried out coincidence measurements between four shielded trays of Geiger counters, and obtained a value of the penetrating fraction of 3.4 percent at 3260 meters altitude. As pointed out by Cocconi, Cocconi, and Greisen,[10] Treat and Greisen had used insufficient lead shielding (14 centimeters), so that from the absorption curves in reference 10 about one third of their "penetrating particles" were really electrons and photons. With this correction, the value of the penetrating fraction becomes about 2.3 percent, in very good agreement with the value obtained in the present work at about the same altitude.

In the experiments of Cocconi and Greisen only one tray of Geiger counters was shielded, coincidences of this tray with three other unshielded trays being recorded simultaneously with threefold coincidences among these unshielded trays.

In the work of Cocconi, Loverdo, and Tongiorgi,[8]

Treat and Greisen[9] and the present writers, on the other hand, all counter trays were shielded. From what has been said above concerning the localization of showers near the recording apparatus, it is seen that any experiment in which coincidences of several unshielded trays with one shielded tray are recorded will inevitably lead to a value of the penetrating fraction R which obtains at, or very near, the core of the showers. If the penetrating particles do not have the same extreme concentration toward the shower center shown by the soft component, then an experiment in which all the counter trays are shielded will not have this bias towards recording only showers which strike in the immediate vicinity. This would consequently lead to a larger value of the penetrating fraction than obtained with unshielded counters.

It is true that in the present experiment there was no lead shielding below the counter trays, and only ten centimeters at the ends and sides. It is possible that some coincidences were caused by electrons coming through the side shielding, even when the shielding thickness above the trays was 20 centimeters of lead. This would, as seen from Eq. (24), lead to a value of R which was too high. However, in view of the low frequency of inclined showers, and the small solid angle subtended by the sides and ends of the lead piles compared to that subtended by the top, it is felt that the great majority of the coincidences under 20 centimeters of lead was due to true penetrating particles.

V. CLOUD-CHAMBER OBSERVATIONS

A large cloud chamber containing 16 one-half inch lead plates was operated during most of the summer to obtain information on local penetrating showers.[28] The cloud chamber was triggered by a set of counters sensitive not only to penetrating showers but also to ordinary electron showers. Thus 2774 pictures of electron showers were obtained during the summer. That most of these showers were components of extensive air showers was evidenced by the simultaneous tripping of an extended counter tray of 1050 cm^2 area and frequently simultaneous tripping of one or more of the four shower trays described in the first part of this paper. These events were signaled by the flashing of neon lights mounted on the cloud chamber and photographed along with the event in the chamber.

In addition to these pictures thirty-four usable pictures were obtained with the cloud chamber triggered by threefold coincidences of the shielded extended counter trays, having areas of 350 cm^2 and 20 centimeters of lead shielding. These pictures have been analyzed for penetrating particles and penetrating showers which accompany the extensive air showers.

An attempt has been made in a series of 226 shower pictures taken with the first arrangement to count the number of electrons above the top lead plate. Poor lighting in this region of the chamber and sometimes very dense showers make the count rather inaccurate but an average of 17 particles per picture was obtained and this is probably right to a factor of two. The top wall of the chamber was ½-inch brass, or 0.88 shower units; multiplication of a factor of two or so might be expected in the brass. Thus the average number of electrons incident on the chamber in these showers may have been 5 to 10. The illuminated area of the cloud chamber was 0.05 m^2 so it is seen that the average density of showers recorded by the particular counter area was very high.

In the 2774 pictures of electron showers obtained at 3027 meters elevation 482 parallel penetrating particles of the right age were observed. Using the above figures for average number of electrons, the percentage of penetrating particles comes out 1.7 percent to 3.5 percent, and in view of the inaccuracies involved must be considered in agreement with estimates made using counter data.

In addition to the penetrating particles, most of which penetrated many lead plates without noticeable interaction, some penetrating showers were observed in the midst of the electron showers. 64 of these "accompanied" penetrating showers were observed. In 28 the initiating particle could not be identified, in 3 the initiating particle was neutral, and in the other 33 the initiating particle was a charged penetrating particle. If we assume that the latter were secondary protons or π-mesons and compare the number observed to the number of ordinary penetrating particles, we see that the secondary protons or π-mesons may compose 5 to 10 percent of the penetrating component. In consideration of this figure it must be remembered that the detection of penetrating showers in the cloud chamber does not depend on very high energy or highly multiple events and that if large amounts of lead are used as in counter experiments[29] (which give a smaller nuclear component), only the very high energy nuclear components are detected. It is also probable that a fairly large fraction of the initiating particles are neutrons.

When the cloud chamber was triggered with three shielded extended counter trays as described above, six pictures showed extensive showers with a penetrating particle in the midst, twelve showed extensive showers without penetrating particles, and eight showed extensive showers in which the existence of penetrating particles is not certain. The uncertainty derives from the fact that in very dense showers, penetrating tracks might not be visible if present, and some of the pictures show penetrating tracks which may not be time-coincident with the shower. Some of the Auger showers are of very high density, one photographic negative being almost completely blackened with tracks of ionizing particles.

In four of the photographs there are either no electrons at all, or a few very weak tracks above the

[28] W. B. Fretter, Phys. Rev. 76, 511 (1949).

[29] J. Tinlot and B. Gregory, Phys. Rev. 75, 519 (1949).

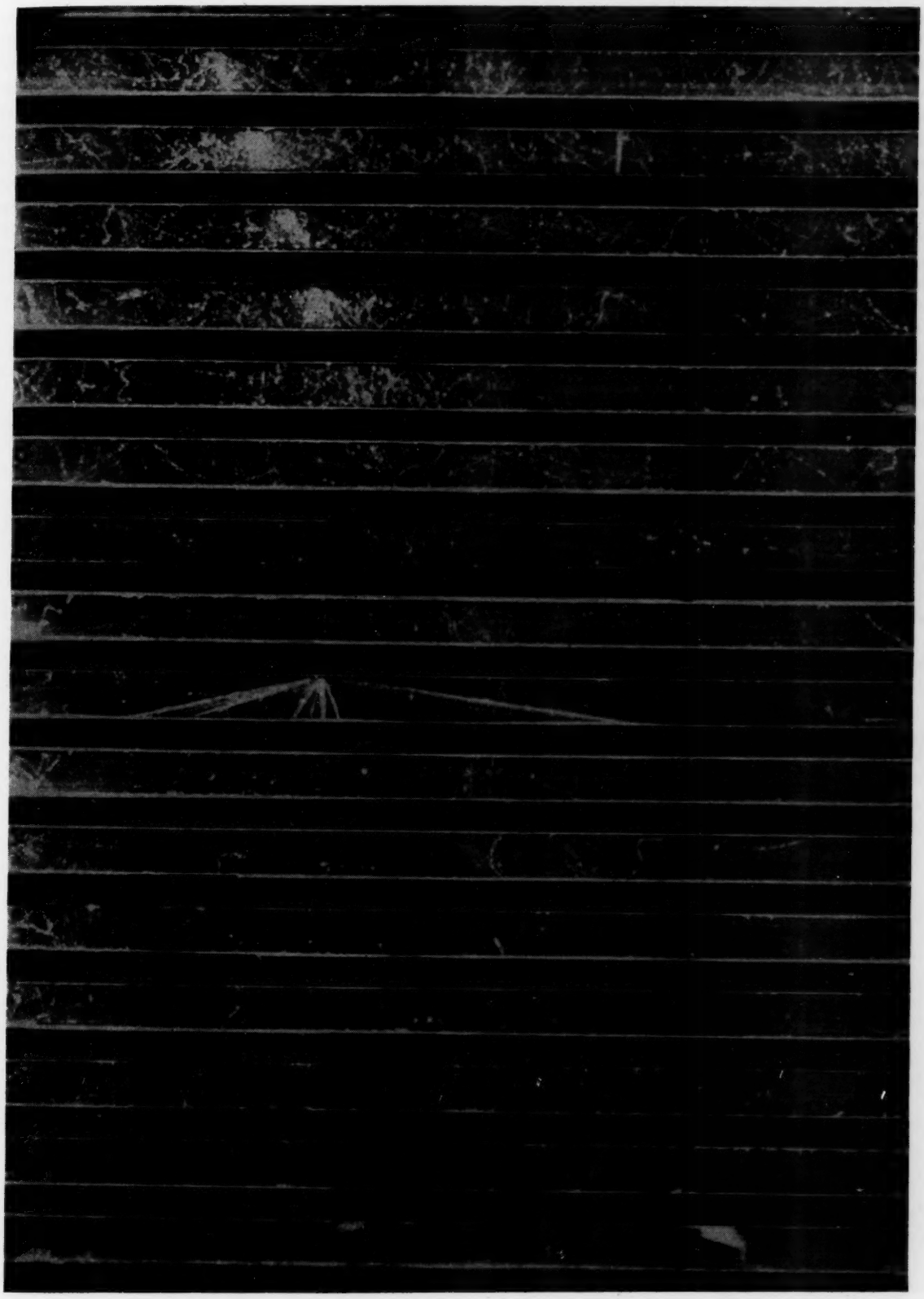

FIG. 8. Local production of penetrating particles by component of extensive shower.

topmost plate, but several tracks of penetrating particles which cannot be identified as being simultaneous with the extensive penetrating shower recorded by the threefold coincidence. Two pictures show no tracks at all, being possibly accidental coincidences.

Two pictures showed local production of penetrating particles in the lead plates of the cloud chamber and the better of these is reproduced in Fig. 8. A number of slow particles and two fast penetrating particles were created by a penetrating particle accompanying the air shower.

Although the statistics are not good, the relative number of penetrating particles and the relative number of nuclear events are the same order of magnitude in this series of pictures as in those triggered by the penetrating shower arrangement.[28]

Production of mesons by 300 Mev γ-rays has been reported[30] and it might be expected that occasionally mesons should emerge from cores of electron showers. It is difficult to identify this event in the cloud chamber because of the large amount of electronic radiation present. In any individual case one could argue that the meson pre-existed in the shower, or that it was created by a pre-existing nucleon. There were, however, 23 photographs of electron showers which could be interpreted as showing production of mesons by electronic or γ-radiation.

Calculation of a cross section for production of mesons by γ-rays from these data must necessarily be rough and may be completely wrong if the events are due to some other cause. We must take into account the minimum energy required to make a meson and try to estimate the number of γ-rays above this energy which exist in the average incident shower. The average number of high energy (150 Mev) γ-rays incident is estimated as roughly equal to the number of electrons, or 5 to 10 per picture. If half of these are capable of producing mesons, and remembering that the γ-rays degrade rapidly in the lead, we can estimate that the number of traversals of $\frac{1}{2}$-inch lead plates might have averaged 10 per picture and certainly could not have been more than 100 per picture. Using the first figure, we get that $\sigma \sim 2 \times 10^{-26}$ cm^2 per lead nucleus or $\sigma \sim 10^{-28}$ cm^2 per nucleon. This is larger than the cross section reported by McMillan and Peterson,[30] obtained with a glass target, although he predicted that the true cross section might turn out to be larger when higher energy mesons could be counted. Recent measurements by McMillan[31] support this view and indicate that the cross section is probably somewhat higher than the original estimate. It may also be that (1) there is a higher cross section in lead than in glass or carbon, (2) we underestimated the average number of γ-rays per shower capable of creating mesons, (3) some of the events we observe are due to nucleons or mesons which were already present in the shower.

VI. ACKNOWLEDGMENTS

We wish to thank Mr. Carl P. Russell, Superintendent, Yosemite National Park, and the National Park Service men at Tioga Pass for their generous cooperation in our experiment. Discussions of the results with Professor R. B. Brode have been very helpful in the preparation of this paper.

[30] E. M. McMillan and J. M. Peterson, Science **109**, 438 (1949).

[31] E. M. McMillan, private communication.

Conduction Processes in Thin Deposits of Antimony

LOUIS HARRIS AND LLOYD H. SHAFFER*,**
Department of Chemistry, Massachusetts Institute of Technology, Cambridge, Massachusetts
(Received March 28, 1949)

Sublimed antimony deposits having a resistivity 1.35 times massive resistivity have been prepared. Assuming two conduction processes in antimony, the mean free paths for the conducting processes in thin sublimed deposits of antimony were found to be 1725A and 666A. $\Delta\rho/\Delta T$ measurements for thin antimony deposits indicate that the trapping of electrons in the surface becomes important for thicknesses less than 1000A, and lend support to the concept of surface electronic states in metals.

ACCORDING to modern theories of the behavior of electrons in metals, the conductivity, σ, of a comparatively simple metal, such as sodium, can be expressed to the first approximation as

$$\sigma = ne^2l/m^*v = 1/\rho,$$

where n is the number of charge carriers per unit volume; e, the electronic charge; v, the velocity of the charge carriers; l, the mean free path of the charge carriers; and m^*, the effective mass of the charge carriers. The mean free path of the charge carriers in most metals is believed to be in the range from 200 to 2000A. It is apparent that the specific resistivity, ρ, of a thin film of a metal should increase rapidly with decreasing thickness when the thickness is less than the normal mean free path and should change much more slowly when the thickness is greater than the normal mean free path. The mean free path of the charge carriers can therefore be estimated from the variation of specific resistivity with thickness.

The outer electrons in arsenic, antimony, and bismuth are distributed between two overlapping energy bands. The unfilled energy levels in the lower band behave as positively charged carriers, n_+, while the electrons overlapping into the upper band behave as negatively charged carriers, n_-. The conductivity equation for these metals should be rewritten

$$\sigma = (ne^2l/m^*v)_+ + (ne^2l/m^*v)_-,$$

where the + and − signs refer to the holes in the lower band and the electrons in the upper band, respectively. In these metals, when pure, n_+ equals n_- and n is a small number compared to the total number of atoms. The distribution of charge carriers can be changed significantly by adding traces of impurities which may act as electron donors or acceptors. Mott and Jones[1] have estimated n_+ and n_- in bismuth from the sudden change in the magnetic anisotropy of this material when all n_- are removed by the addition of small amounts of tin and lead. In addition, the temperature dependence of the specific resistivity of bismuth was found to change sharply when all n_- are removed. In a similar manner Brown and Lane[2] have estimated n_- for antimony from measurements of the magnetic anisotropy of tin-antimony alloys. Lane and Dodd[3] have measured the temperature dependence of the specific resistivity of tin-antimony alloys and a plot of $\Delta\rho/\Delta T$ from their data shows a sharp break at one atomic percent of tin, where all n_- have been removed by the addition of this electron acceptor.

Surface energy levels[4] may have the same effect as electron acceptors in metals which have nearly filled conduction bands. Thin metal deposits offer a means of studying the effects due to the trapping of electrons in surface energy states because of the large ratio of surface to volume. The removal of conduction electrons by increasing the ratio of surface to volume should have the same effect on the properties of a metal as that produced by alloying small traces of electron acceptors. A plot of $\Delta\rho/\Delta T$ against reciprocal thickness of thin films of antimony should show a discontinuity similar to that observed for tin antimony alloys when the films are thin enough for surface electronic states to become important.

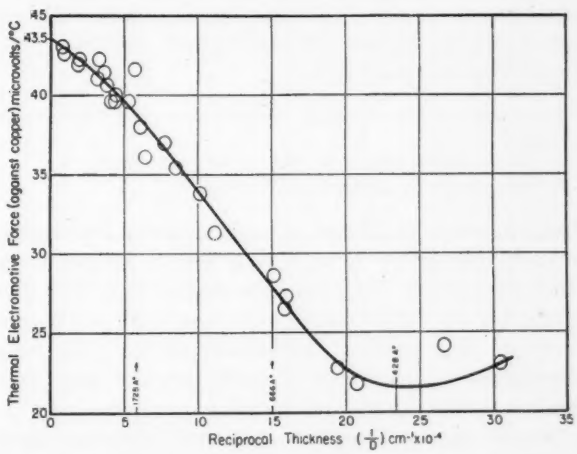

FIG. 1. Thermal e.m.f. of sublimed antimony deposits against copper between 14 and 26°C as a function of the reciprocal thickness of the antimony deposits.

* Present address, Corning Glass Works, Corning, New York.
** Work submitted by Lloyd Shaffer in partial fulfillment for the degree of doctor of philosophy.
[1] N. F. Mott and H. Jones, *The Theory of the Properties of Metals and Alloys* (Clarendon Press, London, 1936).
[2] S. H. Brown and C. T. Lane, Phys. Rev. **60**, 895 (1942).
[3] C. T. Lane and W. A. Dodd, Phys. Rev. **61**, 183 (1942).
[4] F. Seitz, *The Modern Theory of Solids* (McGraw-Hill Book Company, Inc., New York, 1940), pp. 320–326, has discussed the work that has been done on the theory of surface energy states.

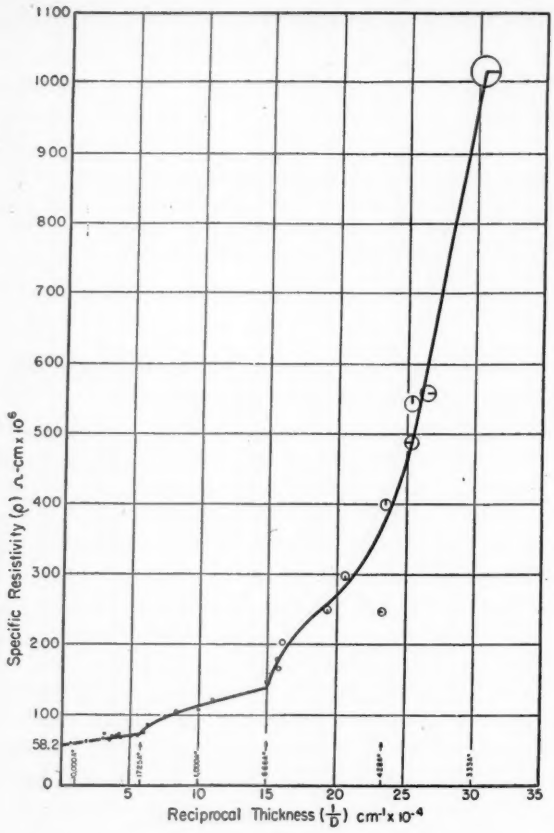

FIG. 2. Specific resistivity (at 25°C) of sublimed deposits of antimony as a function of reciprocal thickness.

EXPERIMENTAL PROCEDURE

Antimony of 99.5 percent purity was sublimed at 400°C from a folded molybdenum strip onto cellulose nitrate films weighing 130×10^{-6} g/cm². The conditions for obtaining deposits of the highest electrical conductivity were found to be:

1. pressure in the subliming chamber less than 10^{-5} mm of mercury;
2. rate of condensation less than 2×10^{-6} g/cm²/min.;
3. temperature of substrate greater than 95°C.

The amount of antimony per unit area was determined in each case either by weighing with a microbalance (to 1 microgram) or for deposits thinner than 50×10^{-6} g/cm² by an amperometric titration with potassium bromate. The nominal thicknesses of the films were obtained from the mass of antimony per unit area divided by the density of massive antimony.

Several of the thin films prepared were examined under a microscope. Except for an occasional pinhole, no flaws were found in the deposits. Lotmar[5] has published excellent photographs of thin evaporated films of antimony and the microstructure of our films was in general similar to that of the films prepared by Lotmar except that the individual crystallites, 0.1 to 0.2 mm across, were much more regular due to the method of preparation. Each crystallite observed extended through the thickness of the film.

The specific resistivity at 25°C, the change of resistivity with temperature from −78°C to 25°C and the thermal e.m.f. in the room temperature range were measured all for nominal thicknesses of antimony from 10000A to 300A.

The resistance of a deposit was first measured at 25°C. After cooling and measuring the resistance at −78°C and intermediate temperatures, the resistance at 25°C was then found to be within 0.5 percent of the original value.

The results are given in Figs. 1–4. The uncertainty in the measurements is shown by the size of the circles.

DISCUSSION OF RESULTS

1. Change of Resistivity with Thickness at 25°C

Electron diffraction studies[6,7] have shown that evaporated antimony deposits are oriented with the principal axis perpendicular to the substrate. Further confirmation of this orientation is afforded by the thermal e.m.f. measurements given in Fig. 1. The extrapolated thermal e.m.f. of thick deposits of sublimed antimony is 43.5 $\times10^{-6}$ volt/°C. This value is to be compared with the measurements on massive antimony. Bridgman[8] obtained 46.2×10^{-6} volt/°C for single crystals measured perpendicular to the principal axis (and parallel to the principal cleavage plane), and 19.5×10^{-6} volt/°C for the thermal e.m.f. parallel to the principal axis.

From Fig. 2, the extrapolated resistivity of thick deposits of sublimed antimony measured parallel to

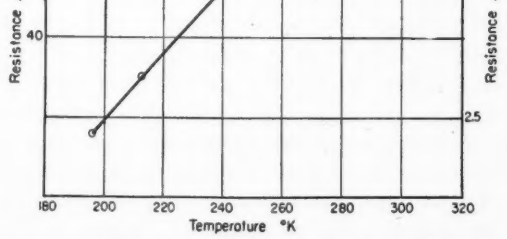

FIG. 3. The resistence of thin evaporated deposits of antimony as a function of temperature. *A*—deposits 650A thick; *B*—deposits 3500A thick.

[5] W. Lotmar, Helv. Phys. Acta **18**, 369 (1945).

[6] J. A. Prins, Nature **131**, 760 (1933).
[7] G. Hass, Kolloid Zeits. **100**, 230 (1946).
[8] P. W. Bridgman, Proc. Am. Acad. **63**, 351 (1929).

the substrate (and therefore perpendicular to the principal axis) is 58.2×10^{-6} ohm-cm at 25°C (57.3×10^{-6} ohm-cm at 20°C). The specific resistivity of massive antimony perpendicular to the crystal axis is 42.6×10^{-6} ohm-cm at 20°C.[8] We believe that the increased resistivity of thick sublimed deposits is due to additional electron scattering at the mosaic boundaries present in sublimed deposits of antimony. Lotmar[9] estimated the mosaic size in sublimed deposits to be of the order of 300A.

Figure 2, the plot of specific resistivity *vs.* reciprocal thickness, shows two distinct breaks, one at 1725 (±75)A and one at 666A. We believe that the two breaks correspond to the mean free paths of the two conducting processes in thin deposits of antimony. Assuming that both conduction processes contribute significantly to the conductivity of antimony, it is estimated that the mean free paths for the two processes in annealed *massive* antimony are 2500A and 750A, and that the mean free path due to mosaic scattering alone is 5000A. This value was obtained using the extrapolated value of the specific resistivity of the sublimed deposits at 25°C, 58.2×10^{-6} ohm-cm, and the assumption that the mosaic structure alone is the cause of the increased resistivity of the thick sublimed deposits.

Several investigators have attempted to explain the effect of thickness on the mean free path of the conducting electrons.[10–12] The results of those studies lead to the conclusion that $\Delta\rho/\Delta T$ should be temperature dependent for a thin deposit. In Fig. 3 we present the data for the −78° to 25°C temperature range for a sublimed deposit 3500A thick and for a deposit 650A thick. $\Delta\rho/\Delta T$ is temperature independent for both deposits. Those theories are therefore inadequate when applied to antimony.

2. Change of $\Delta\rho/\Delta T$ with Thickness

Figure 4, the plot of $\Delta\rho/\Delta T$ *vs.* $1/D$ shows two breaks, one at 1725A and one at 428A. The break at 1725A is to be correlated with the corresponding break in the specific resistivity plot and so is associated with the effect of thickness on the mean free path of one of the conduction processes. The measurements for Fig. 4 are probably not precise enough to show a small break which may exist at 666A. The leveling-off of the temperature derivative of resistivity for thicknesses less than 1000A and the pronounced break at 428A suggests that the effect of surface energy states become important at these thicknesses. The change in $\Delta\rho/\Delta T$ with thickness can be imagined to be governed by two main processes. The change in mean free path for these thicknesses should cause $\Delta\rho/\Delta T$ to rise as the thickness decreases, while the trapping of conduction electrons on the surface should cause $\Delta\rho/\Delta T$ to fall. The pronounced break and sharp rise in the $\Delta\rho/\Delta T$ *vs.* $1/D$ plot at 428A indicates that at this thickness all the upper zone electrons in antimony are trapped in surface states.

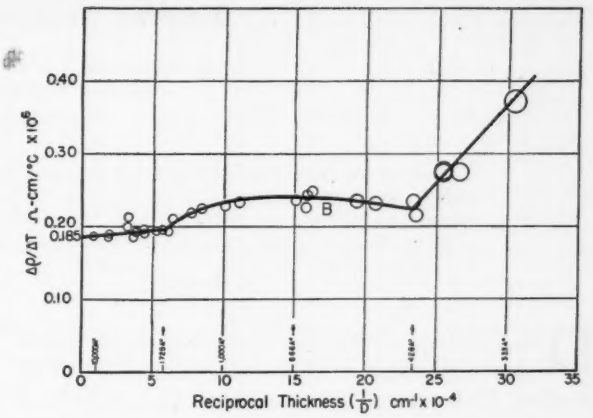

FIG. 4. The change of resistivity per degree centigrade ($\Delta\rho/\Delta T$) of sublimed deposits of antimony as a function of reciprocal thickness.

Assuming that for a layer of antimony 428A thick there is complete removal of the upper zone electrons to the surface states and that the same effect is produced by the addition of one atomic percent tin to antimony, one electron per hundred atoms of antimony are trapped in the surface or there are 1.6×10^{15} electrons trapped per square centimeter of surface.

OTHER EVIDENCE OF SURFACE STATES

In the light of our deductions it is of interest to consider the conduction processes in bismuth. It has been found[13–15] that removal of all upper zone electrons by the addition of electron acceptors to massive bismuth, cause the temperature coefficient of resistivity (at room temperature) to become negative. A negative temperature coefficient of resistivity has also been observed[16] for thin bismuth wires and similar results have been obtained[17,18] for thin evaporated bismuth deposits. By analogy to the results with antimony, negative temperature coefficient of resistivity of thin deposits of bismuth can thus also be explained by the assumption of trapping of electrons in surface states.

ACKNOWLEDGMENT

We wish to thank Professor Lane for making the detailed resistance measurements of the tin-antimony alloys available to us.

[9] W. Lotmar, Helv. Phys. Acta. **20**, 447 (1947).
[10] J. J. Thomson, Proc. Camb. Phil. Soc. **11**, 120 (1901).
[11] A. C. B. Lovell, Proc. Roy. Soc. **A157**, 311 (1936).
[12] K. Fuchs, Proc. Camb. Phil. Soc. **34**, 100 (1938).
[13] W. R. Thomas and E. J. Evans, Phil. Mag. **16**, 329 (1933).
[14] C. W. Ufford, Proc. Am. Acad. **63**, 309 (1928).
[15] N. V. Thompson, Proc. Roy. Soc. **A155**, 111 (1936).
[16] A. Eucken and F. Foster, Goettingen Nachrichten, Math. Phys. Klasse Fachgruppe **2**, **1**, 43 (1934).
[17] W. J. Tulley, Nature **157**, 372 (1946).
[18] B. H. Billings, W. L. Hyde, and E. E. Barr, J. Opt. Soc. Am. **37**, 123 (1947).

Delayed Neutrons from Thorium

L. G. CREVELING,* J. R. HOOD,** AND M. L. POOL
Ohio State University, Columbus, Ohio

(Received June 30, 1949)

Thorium has been irradiated with fast neutrons from the reaction Li(d, n). The half-lives of the delayed neutron activities were found to be: 55.6, 22.0, 4.5, 1.5, and 0.13 seconds with initial relative saturation intensities of 0.279, 1.00, 2.00, 1.83, and 1.75, respectively. The intensity of the 55.6 second activity relative to the 22.0 second activity was found to be 1.76 times greater for thorium fission than for uranium fission.

DELAYED neutrons were first observed in the fission of uranium in 1939, and exhibited a half-life of about 12 seconds.[1] Two periods of 45 and 10 to 15 seconds were later found.[2] In 1947 it was reported[3] that at least 5 periods of delayed neutrons resulted from the fission of uranium 235. Other investigations showed that these periods were also present in plutonium fission.[4,5] By extending this work with refined techniques, six periods were reported in 1948 which were as follows: 55.6 sec., 22.0 sec., 4.51 sec., 1.52 sec., 0.43 sec., and 0.05 sec.[6]

The reported investigations of delayed neutrons from the fission of thorium are few,[3] and indicate that the delayed activity was identical with that resulting from

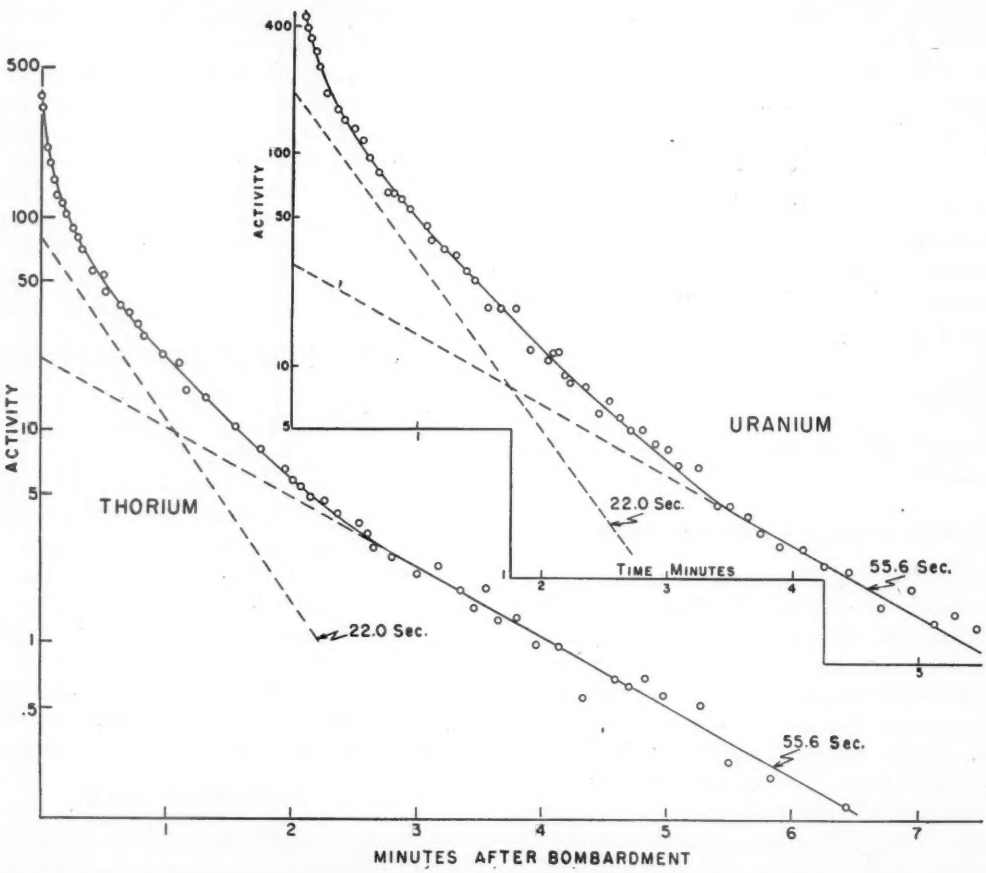

FIG. 1. Total decay curves of the delayed neutron activity resulting from the fission of natural uranium metal and thorium metal bombarded with fast neutrons from the Li+d reaction.

* First Lieutenant, USAF, research under the auspices of the USAF Institute of Technology, Wright Field, Dayton, Ohio.
** Lieutenant Colonel, USAF, research under auspices of the USAF Institute of Technology, Wright Field, Dayton, Ohio.

[1] Roberts, Meyer, and Wang, Phys. Rev. **55**, 510 (1939).
[2] Booth, Dunning, and Slack, Phys. Rev. **55**, 876 (1939).
[3] Snell, Nedzel, Ibser, Levinger, Wilkinson, and Sampson, Phys. Rev. **72**, 541 (1947).
[4] W. C. Redman and D. Saxon, Phys. Rev. **72**, 541 (1947).
[5] F. deHoffman and B. T. Feld, Phys. Rev. **72**, 567 (1947).
[6] Hughes, Dabbs, Cahn, and Hall, Phys. Rev. **73**, 111 (1948).

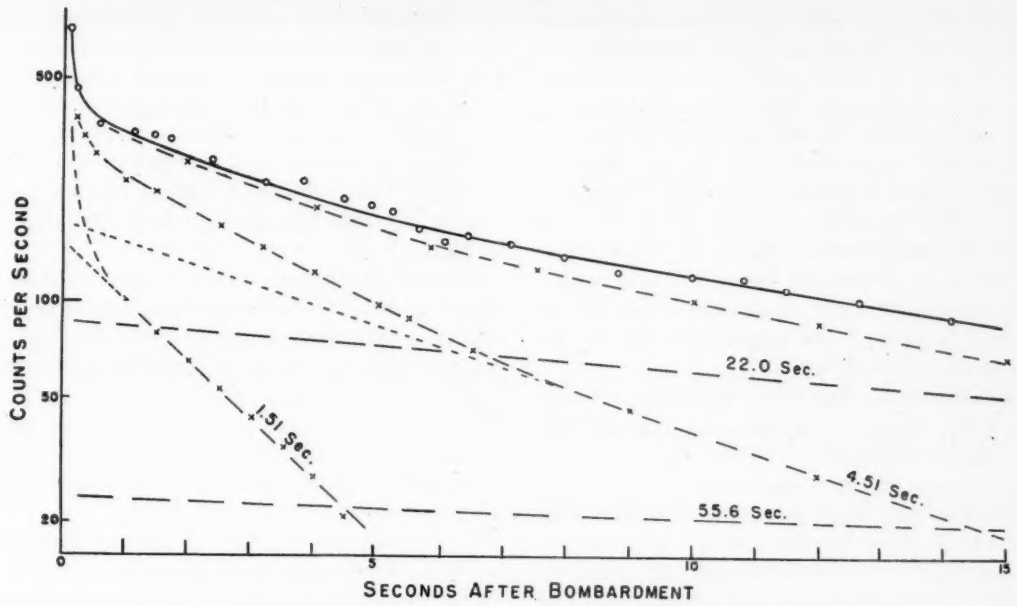

FIG. 2. First fifteen seconds of the decay curve of the delayed neutron activity resulting from the fission of thorium.

uranium. The purpose of this paper is to report in detail the values obtained for delayed neutron activity resulting from the fission of thorium with fast neutrons of energies up to 24 Mev.

10.26 grams of natural uranium metal and 10.53 grams of thorium 232 were bombarded with neutrons which were obtained from the reaction $Li^7(d, n)$. The bombarded metal was placed immediately behind the lithium target inside the cyclotron vacuum chamber. A BF_3 enriched tube, operated in the proportional region, and preamplifier were mounted near the target vacuum lock and surrounded with paraffin. Adequate thermalization of the neutrons was checked by means of a cadmium shield on the BF_3 counter. The tube voltage was set at a value sufficiently low to make the tube insensitive to gamma-rays. The detected neutron pulses were fed into a linear amplifier and a "scale of 64." The output of the scaler was fed into a photoelectric inking recorder. As a check a movie camera was used to photograph the interpolation lights of the scaler and a dial recorder. After a five-minute bombardment, the power to the cyclotron oscillator was shut off and the delayed neutrons measured while the target was still in the cyclotron.

One of the curves obtained from fast neutron fission of natural uranium is shown in the upper part of Fig. 1. The saturation intensity of the 55.6 second activity was found to be 0.150 relative to that of the 22.0 second activity. The values of the ratio of the 55.6 second activity to the 22.0 second activity obtained from slow neutron fission of uranium 235 and plutonium 239 have been reported as 0.153 and 0.14, respectively.[6] The ratio of the delayed neutron emitting fission products from uranium metal irradiated by a beam of fast neutrons therefore appears to be very nearly equal to that of uranium 235 irradiated with slow neutrons.

One of the total decay curves obtained for the delayed neutrons from thorium is shown in the lower part of Fig. 1. It is seen that the saturation value of the 55.6 second activity is 22 units and that the 22.0-second activity is 81 units. The ratio of these two values is 0.279. It is even obvious from the figure that the 55.6-second activity in the thorium curve is larger than that in the uranium curve relative to the 22.0-second activity. In the case of uranium metal the above ratio as previously mentioned is 0.150.

Figure 2 shows an enlargement of the first 15 seconds of Fig. 1. By repeated subtractions the half-lives of the delayed neutron activities from thorium were found to be: 55.6, 22.0, 4.5, 1.51, and 0.13 seconds with initial intensities of $0.279 \pm .016$, 1.00, 2.00, 1.83, and 1.75, respectively. The 0.13 second activity is probably a combination of 0.43 and 0.05-second activity which have been found[6] in uranium. Since the value 0.279 represents the ratio of the 55.6-second activity to the 22.0-second activity in thorium, and the value 0.150 represents a similar ratio in uranium, the ratio of these

TABLE I. Relative yields of delayed neutrons.

Bombarding neutrons from	Target	Relative yield for 55.6 sec.	22.0 sec.	4.5 sec.	1.5 sec.	0.4 sec.	Reference
Be *d*	U 235	0.14	1.00	1.1	0.5	0.4	3
Pile	U 235	0.153	1.00	1.28	1.45	0.51	6
Pile	U 235	0.150	1.00	1.36	1.65		4
Pile	Pu 239	0.10	1.00	1.1	1.2		4
Pile	Pu 239	0.14	1.00	1.29	1.05		5
Li *d*	Th 232	0.279	1.00	2.00	1.83	1.75	This report

numbers (1.76) may therefore be interpreted to mean that the 55.6-second activity in thorium relative to the 22.0-second activity is 1.76 times more intense than that in the case of uranium. The 55.6-second and the 22.0-second activities are believed to be due to bromine 87 and iodine 137[3] respectively, and the fission yield curve[7] indicates that 2.5 percent of the fission products are mass 87 and 6.7 percent are mass 137. If it is assumed that the production of mass 137 is the same percent in the case of thorium fission as for uranium fission, then the fission yield of mass 87 would be increased from 2.5 percent for uranium fission to 4.0 percent for thorium fission.

Table I shows a comparison of the relative saturation intensities of the delayed neutrons from uranium and plutonium previously reported. Also shown are the values from thorium reported in this paper.

When uranium and thorium were bombarded with 10-Mev deuterons directly, the delayed neutron activity obtained from both elements was small compared to that obtained when irradiated with Li neutrons. The delayed activity, however, from uranium under deuteron bombardment was approximately 5.3 times that from thorium. For neutrons between 2.4 Mev and about 10 Mev, the cross sections for uranium fission and thorium fission are 0.5 and 0.1 barn, respectively.[8] Since a (d, p) bombardment is essentially a neutron bombardment, the above observed ratio (5.3) is expected. No measurable delayed neutron activity resulted from bombarding uranium and thorium with 20-Mev alpha-particles. The threshold for alpha-particle induced fission in thorium has recently been reported as 23 to 24 Mev.[9]

Attempts were made to obtain delayed neutrons from other elements by lithium neutron irradiation. Negative results were obtained from the following elements: radium, bismuth, tungsten, and tantalum. With fast neutrons the cross section of radium for the production of delayed neutrons, if any, was less than 10^{-2} of that of uranium and less than 10^{-4} for the other elements mentioned. With 10-Mev deuterons no delayed neutrons were observed.

It is a pleasure to acknowledge the assistance given by N. L. Krisberg in setting up the electrical circuits. The authors are grateful for the support received from the Ohio State University Development Fund and the Graduate School.

[7] Plutonium Project Report, Rev. Mod. Phys. **18**, 513 (1946).

[8] Landenburg, Kanner, Barschall, and Van Voorhis, Phys. Rev. **56**, 168 (1938).

[9] Amos S. Newton, Phys. Rev. **75**, 17 (1949).

PHYSICAL REVIEW VOLUME 76, NUMBER 7 OCTOBER 1, 1949

Second Sound Velocity in Helium II*

R. D. MAURER AND MELVIN A. HERLIN
Research Laboratory of Electronics, Massachusetts Institute of Technology, Cambridge, Massachusetts

(Received June 20, 1949)

Pulse methods are applied to extend the measurements of second sound velocity in liquid helium II to a temperature of 0.86°K. The rise in velocity below 1.1°K observed by Peshkov is verified and extended to lower temperature. The theoretical implications are discussed.

I. INTRODUCTION

IT is rather generally accepted that the peculiar properties of helium II have to be explained by means of a two-fluid model. This viewpoint has two variants in the theories of Tisza[1] and Landau.[2] The theory due to Tisza is based on London's interpretation of the λ-point transition of helium as an Einstein-Bose condensation.[3] The elementary excitations of the liquid were assumed to possess translational momenta (states analogous to Bloch waves in metals) and to obey Bose-Einstein statistics. The "condensation" implied by the statistics led to a division of the liquid into a "normal" and a "superfluid" fraction, the latter having practically no entropy. This incomplete vanishing of the

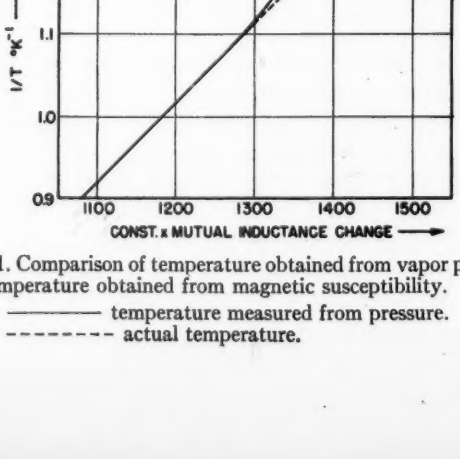

FIG. 1. Comparison of temperature obtained from vapor pressure with temperature obtained from magnetic susceptibility.
———— temperature measured from pressure.
- - - - - - - - actual temperature.

*This work has been supported in part by the Signal Corps, Air Materiel Command, and ONR.

[1] L. Tisza, Phys. Rev. **72**, 838 (1947); Comptes Rendus Acad. Sc. Paris **207**, 1035 (1938).

[2] L. Landau, J. Phys. USSR **5**, 71 (1941); **8**, 1 (1944); **11**, 91 (1947).

[3] F. London, Phys. Rev. **54**, 947 (1938).

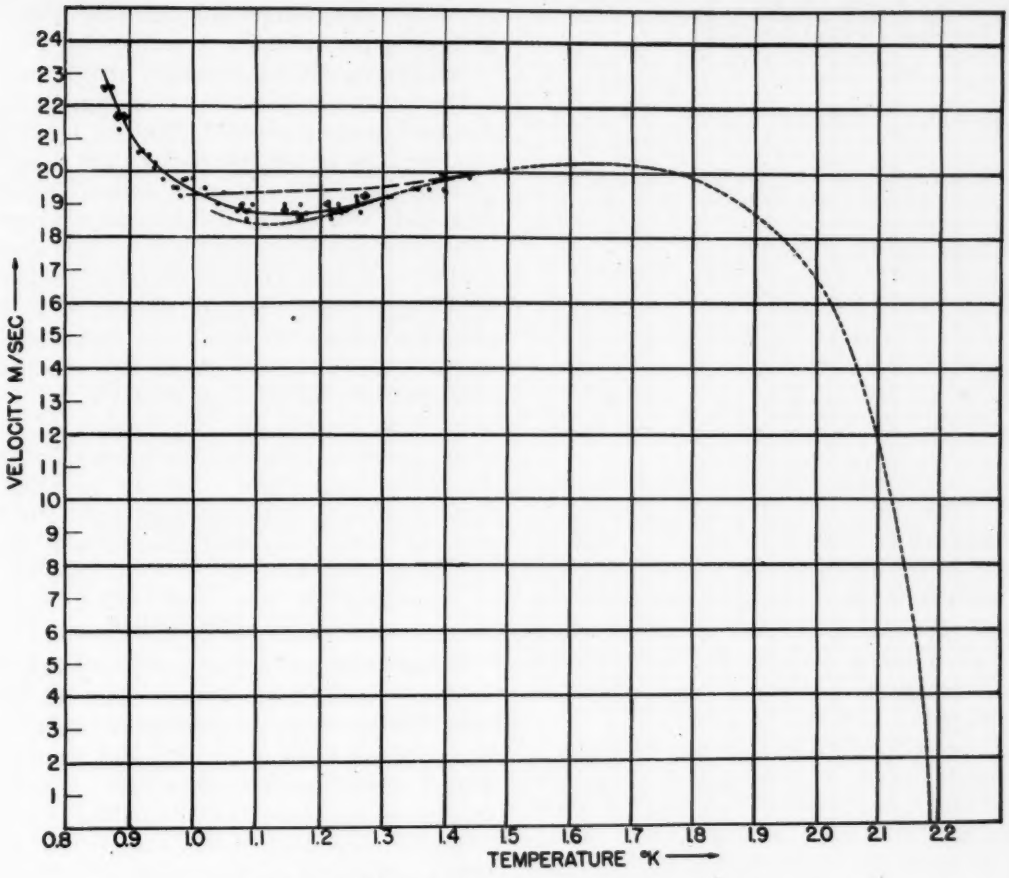

FIG. 2. Second sound velocity as a function of temperature.
— —— curve drawn from Pellam's data.
- - - - - - curve from Peshkov.
——— curve fitted to authors' data.

entropy was assumed to stem from elementary excitations of another type (phonons) contributing to the whole liquid and to the superfluid fraction in particular. This contribution could be expected to be important only below 1°K. Landau modified this theory in two respects. Denying the relevance of Einstein-Bose statistics, he concluded that the elementary excitations are phonons and rotons. Second, he assumed that these two types of elementary excitation together compose the "normal" flow of the liquid. Hence, the superfluid liquid was supposed to be entirely devoid of entropy. In spite of considerable differences in the assumed molecular mechanisms, the two theories led to essentially identical conclusions. However, differences in the conclusions do occur at temperatures where the role attributed to the phonons becomes significant.[4] Such a difference occurs in the predicted velocity of second sound below 1°K and led to the experiment reported here.

II. EXPERIMENT

Second sound may be excited by periodic or pulsed transfer of heat into liquid helium II. It was first observed by Peshkov,[5] following its theoretical prediction by Tisza[1] and Landau.[2] Peshkov measured its velocity down to 1.03°K, using a standing wave technique,[5] and other investigators have covered portions of this same region. Pellam,[6] and Osborne,[7] have developed pulse techniques, which were also employed in the present work.

The apparatus used by Pellam in this laboratory was selected for this investigation because of its low heat input and consequent possibilities for attaining very low temperatures. A Du Mont type 256D oscillograph was used to trigger a pulse generator which fed into a carbon-sheet resistor in the end of the second-sound tube. This pulse initiated the thermal wave which traveled to the other end of the tube where the change in temperature affected another carbon-sheet resistor acting as a resistance thermometer. The change in voltage across it was amplified, filtered for noise, and fed back into the vertical plates of the range scope. To reduce heat input, photographs of the scope were

[4] L. Tisza, Phys. Rev. **75**, 885 (1949).

[5] V. Peshkov, J. Phys. USSR **10**, 389 (1946); J.E.T.P. USSR **18**, 951 (1948).

[6] J. R. Pellam, Phys. Rev. **75**, 1183 (1949).

[7] D. V. Osborne, Nature **162**, 213 (1948).

TABLE I. Second sound velocity in helium II (smoothed values taken from the fitted curve of Fig. 2.)

Temperature (°K)	Velocity (m/sec.)
1.45	19.95
1.40	19.78
1.35	19.55
1.30	19.20
1.25	18.95
1.20	18.75
1.15	18.70
1.10	18.75
1.05	19.00
1.00	19.40
0.95	20.05
0.90	21.20
0.86	23.00

taken during the second or so in which the pulse switch was closed. These films could then be analyzed on a microfilm projector in order to count the crystal-controlled time markers. Inasmuch as the pulse began with the sweep, the first marker represented an elapsed time interval of 40 microseconds and each marker thereafter represented an additional interval of 50 microseconds. A fixed path length of 7.97 cm between the carbon resistors was used.

The high capacity pumping system permitted a generally simple design. A Distillation Products type MB-100 diffusion pump, rated at 110 v on the heater and operated at 220 v, was connected with two Cenco Hypervac 25 forepumps. A large-diameter brass pipe followed a semicircular path from the top of the diffusion pump to the top of the liquid helium Dewar vessel. This pipe contained the McLeod gauge entry, for vapor pressure measurement, and also the permanent shield fittings to the signal wires, so that it could be used as the electrical ground.

Two concentric double-walled Dewars were employed. The exterior one contained liquid air. The inner one was specially constructed with walls which joined at a ring seal into a single wall about 10 cm from the top. A liquid air level was maintained above the ring seal so that the conduction of heat down the inner wall to the liquid helium was greatly reduced. The high-speed pumping system made the additional complication of capillaries or diaphragms unprofitable.

A possible source of error in temperature measurement arose from the pressure gradient between the McLeod gauge entry and the liquid helium surface. To correct this, measurements of mutual inductance were made with a coil wrapped around the inner Dewar, which was filled with liquid helium and iron ammonium alum. Since the susceptibility of this salt, and hence the change in mutual inductance of the coil, varies as $1/T$ by Curie's law, comparison could be made with the McLeod gauge readings. Actually, Fig. 1 shows that no such correction was necessary above about 0.92°K.

The data are shown in Fig. 2, and agree with those of Peshkov down to about 1.2°K; but below this temperature they are slightly higher than his most recent evaluations.[5] The deviation of Pellam's results,[6] as he suggested, was due to his failure to correct for the absence of true vapor pressure readings directly over the helium surface. This was serious, since he was pumping through a small capillary. Above 1.45°K, the values given by Peshkov, Pellam, and Lane are essentially in agreement.[5,6,8] Table I shows the smoothed values obtained from the fitted curve of Fig. 2.

In these experiments, the strength of the second sound pulses was observed to increase markedly with decreasing temperature. Although the pulse strength depends on many factors, there is qualitative indication that the thermomechanical effect remains strong down to 0.86°K.

III. DISCUSSION

Recent experiments[9] with He^3, showing no superfluidity down to 1°K, seem to bear out the original Bose-Einstein hypothesis[10] rather than the roton hypothesis of Landau. On the other hand, the rise in second sound velocity reported here supports Landau's contention regarding the role of the phonons. As a result, it seems likely that a more refined form of the fluid model should contain elements of both the London-Tisza and the Landau theories—phonons and Bose-Einstein excitations both contributing to the normal flow. It may be added that our experiments bear out Landau's views regarding the role of phonons only in a qualitative way. It would be premature to conclude, as yet, that the superfluid liquid has a rigorously vanishing entropy. However, should this be true, the implications would be considerable; that is, the cooling method based on the thermomechanical effect as advanced by Kapitza[11] should prove a powerful means for reaching low temperatures.

IV. ACKNOWLEDGMENT

The authors are highly indebted to Mr. P. L. Nicholas for assistance with electronic and other apparatus; to Messrs. R. P. Cavileer and J. W. Toomey, Jr., for the production of liquid helium; and to Professor L. Tisza for theoretical discussion.

[8] Lane, Fairbank, Schultz, and Fairbank, Phys. Rev. **70**, 431 (1946); **71**, 600 (1947).
[9] Osborne, Weinstock, and Abraham; Phys. Rev. **75**, 988 (1949).
[10] F. London, Nature **163**, 694 (1949).
[11] P. L. Kapitza, J.E.T.P. USSR **5**, 59 (1941).

Electromagnetic Interactions of a Vector Meson with a Scalar Excited State*

MARSHALL N. ROSENBLUTH**
University of Chicago, Chicago, Illinois
(Received May 19, 1949)

A relativistically invariant formalism is presented for a theory of a meson possessing a vector and a scalar state of different mass which are tightly coupled by the electromagnetic field. It is found that the theory reduces formally to the theory of a five-dimensional vector meson, with the constant which couples the states playing the role of a fifth component of the energy-momentum vector. With a large coupling constant there is a high probability for producing excited-state mesons, and hence decay photons, in electromagnetic processes; e.g., by Rutherford scattering on passage of a beam of mesons through heavy material. The production of many photons in nucleon-nucleon scattering, such as has been reported at Berkeley, might possibly be interpreted as resulting from the decay of excited-state mesons which are produced directly. It is also found that the existence of a scalar excited state aggravates the high energy divergences of vector meson cross sections for such electromagnetic processes as Compton effect, so that the validity of the Christy-Kusaka argument against the μ-meson having spin 1 is not affected by the possible existence of a scalar excited state.

I. INTRODUCTION

RECENT experimental work has forced the abandonment of the idea that by the assumption of one simple-type meson field (such as vector, scalar, etc.) all the phenomena of cosmic rays and nuclear forces could be explained. Instead all evidence points to a picture of great complexity. It was therefore considered worthwhile to investigate the consequences of a theory which treated particles possessing several states of different spin and mass. In particular, it is the purpose of this paper to develop a convenient formalism for a relativistically invariant field theory of a meson possessing a vector state and a scalar state of differing mass. The states are assumed connected by the electromagnetic field and our main interest will be centered on the electromagnetic cross sections of this meson.

In 1941 Christy and Kusaka[1] showed that cosmic-ray (μ) mesons must have spin 0 or $\frac{1}{2}$ since the electromagnetic interaction of high energy vector mesons is much too strong to be compatible with experimental evidence.

We shall inquire whether the assumption of a scalar excited state with an appropriately chosen coupling to the vector ground state can alter this conclusion. We might expect that the assumption of excited states would lower the theoretical cross section for a vector meson if we consider the latter as being simply the ground state of a system of two tightly bound spin $\frac{1}{2}$ particles. This system may be supposed to have a number of discrete states and a continuum of unbound states, so that for the limit of infinitely high energy the system behaves like two free spin $\frac{1}{2}$ particles, hence has a relatively weak interaction with the electromagnetic field. In this paper, however, we restrict ourselves to the consideration of a single scalar excited state and find that in this case the additional terms lead to an increase in the high energy cross sections. Moreover, the additional mechanism for photon production which is provided by the possibility of Rutherford scattering to the excited state followed by decay to the ground state also leads to an amount of burst production incompatible with cosmic-ray evidence.

It should also be mentioned here that some work on the problem of a "vector-scalar" meson has been done by the Russian physicist V. L. Ginsburg[2] who used the usual wave theory formalism. He, however, never developed the theory much beyond the qualitative stage.

II. DEVELOPMENT OF MATRIX FORMALISM

A. Introduction of Coupling

In this paper we shall use the matrix formalism originated by Kemmer.[3] While this formalism at first appears unnecessarily complex, the spur techniques which it makes possible are invaluable in a calculation of this kind. We first write down the relativistically invariant Lagrangian density.

$$\left.\begin{aligned} L&=L_{\text{vector}}+L_{\text{scalar}}+L_{\text{coupling}};\\ L_{\text{vector}}&=ihc[\psi_v{}^{+}B_\mu{}^{v}(\partial\psi_v/\partial X_\mu)+(M_v c/\hbar)\psi_v{}^{+}\psi_v];\\ L_{\text{scalar}}&=ihc[\psi_s{}^{+}B_\mu{}^{s}(\partial\psi_s/\partial X_\mu)+(M_s c/\hbar)\psi_s{}^{+}\psi_s];\\ L_{\text{coupling}}&=-ghc(\psi_v{}^{+}\gamma\psi_s+\psi_s{}^{+}\gamma^{+}\psi_v). \end{aligned}\right\}$$

Here ψ_v is the ten component vector meson wave function (four-vector potential and associated antisymmetric tensor); ψ_s is the five component scalar wave function (scalar potential and its four-gradient); M_v and M_s are respectively the vector and scalar masses; the $B_\mu{}^{v}$'s are Kemmer's ten by ten matrices; the $B_\mu{}^{s}$'s are his five by five matrices. γ is a ten by five matrix which we introduce to couple the vector and scalar states. We shall deduce its properties later. Also

$$\psi^{+}=i\psi^{*}N_4. \quad (N_\mu=2B_\mu{}^{2}-1).$$
$$\gamma_{ij}{}^{+}=\gamma_{ji}{}^{*}.$$

* This paper was written as a Ph.D., thesis in the Department of Physics, University of Chicago, Chicago, Illinois.
** National Research Council Fellow. Now at Stanford University.
[1] R. Christy and S. Kusaka, Phys. Rev. **59**, 414 (1941).
[2] V. L. Ginsburg, J. Phys. U.S.S.R. **8**, 33 (1944).
[3] N. Kemmer, Proc. Roy. Soc. London **173**, 91 (1939).

The B's follow the commutation rule:

$$B_\mu B_\nu B_\lambda + B_\lambda B_\nu B_\mu = B_\mu \delta_{\nu\lambda} + B_\lambda \delta_{\nu\mu}. \tag{1}$$

The omission of the superscript v or s implies that the law is true both for vector and scalar matrices.

We can now express the Lagrangian in a neater form by adopting a 15 by 15 formalism. We set:

$$L = \hbar c\{i[\psi^+ B_\mu(\partial\psi/\partial X_\mu) + \psi^+ K\psi] - g\psi^+ D\psi\}, \tag{2}$$

where

$$B_\mu = \left(\begin{array}{c|c} B_\mu{}^v & \\ \hline & B_\mu{}^s \end{array}\right),$$

$$\psi = \left(\begin{array}{c} \psi_{v1} \\ \vdots \\ \psi_{v10} \\ \hline \psi_{s1} \\ \vdots \\ \psi_{s5} \end{array}\right),$$

$$K = \left(\begin{array}{c|c} \dfrac{M_v c}{\hbar} & \\ \hline & \dfrac{M_s c}{\hbar} \end{array}\right), \tag{3}$$

$$D = \left(\begin{array}{c|c} 0 & \gamma \\ \hline \gamma^+ & 0 \end{array}\right).$$

Our equations of motion become:

$$B_\mu(\partial\psi/\partial X_\mu) + (K + igD)\psi = 0, \tag{4}$$

$$(\partial\psi^+/\partial X_\mu)B_\mu - \psi^+(K + igD) = 0. \tag{5}$$

It is obvious that the new B_μ's still obey the commutation rules (1). It should also be noted that the rest masses of the vector and scalar states are no longer given simply by M, since the coupling introduces a "mesomatic" mass which we shall derive later.

B. Properties of the Coupling Matrix

We next consider the properties of D as determined by the conditions of relativistic invariance. First we consider invariance of the Lagrangian (2) under an infinitesimal Lorentz rotation. As Pauli[4] has shown, it is sufficient that L be invariant under the transformation $\psi' = S\psi$; $\psi^{+\prime} = \psi^+ S^{-1}$ where

$$S = 1 + \tfrac{1}{2}\mathcal{E}_{\mu\nu}(B_\mu B_\nu - B_\nu B_\mu),$$

($\mathcal{E}_{\mu\nu} = -\mathcal{E}_{\nu\mu}$ = magnitude of rotation) provided that the B's obey the commutation rules (1). The first two terms in (2) are invariant just as in the pure scalar or vector case. In order that the term $\psi^+ D\psi$ remain invariant we must require:

$$(B_\mu B_\nu - B_\nu B_\mu)D - D(B_\mu B_\nu - B_\nu B_\mu) = 0. \tag{6}$$

At this point it will prove useful to summarize some of the formulas easily derivable from the commutation rules (1). These are:

$$\begin{array}{ll} B_\mu B_\nu B_\mu = 0;\ (\mu \neq \nu) & N_\mu = 2B_\mu{}^2 - 1; \\ B_\mu{}^2 B_\nu + B_\nu B_\mu{}^2 = B_\nu;\ (\mu \neq \nu) & N_\mu B_\mu = B_\mu N_\mu = B_\mu; \\ B_\mu{}^3 = B_\mu; & N_\mu B_\nu = -B_\nu N_\mu;\ (\mu \neq \nu). \end{array} \tag{7}$$

[4] W. Pauli, Rev. Mod. Phys. 13, 227 (1941).

We now consider the problem of invariance under a reflection about the X_ν axis, i.e., $X_\mu' = -X_\mu$ $(\mu \neq \nu)$; $X_\nu' = X_\nu$. Pauli has shown that the proper transformation law is $\psi' = \pm N_\nu \psi$, the sign being dependent on the desired reflection properties of ψ. It can be shown that $\psi' = N_\nu\psi$ is the desired law for scalar or pseudo-vector; $\psi' = -N_\nu\psi$ for pseudo-scalar or vector. We are interested in vector coupled to scalar so our transformation matrix is:

$$S = \left(\begin{array}{c|c} -N_\nu{}^v & \\ \hline & N_\nu{}^s \end{array}\right).$$

Using this and (3) we find that invariance of $\psi^+ D\psi$ requires:

$$N_\nu D + DN_\nu = 0. \tag{8}$$

From (6) and (8) we can derive the properties of D. From (6):

$$B_\mu B_\nu D + DB_\nu B_\mu - B_\nu B_\mu D - DB_\mu B_\nu = 0.$$

Multiply by $B_\mu{}^2$ from front and rear and remember $B_\mu B_\nu B_\mu = 0$; $B_\mu{}^3 = B_\mu$. Then

$$B_\mu B_\nu DB_\mu{}^2 + B_\mu{}^2 DB_\nu B_\mu = 0.$$

But since N_μ anti-commutes with D and B_ν,

$$\begin{aligned} B_\mu B_\nu DB_\mu{}^2 &= B_\mu B_\nu D(N_\mu + 1/2) = B_\mu B_\nu(-N_\mu + 1/2)D \\ &= B_\mu(N_\mu + 1/2)B_\nu D = B_\mu B_\nu D. \end{aligned}$$

Therefore

$$B_\mu B_\nu D + DB_\nu B_\mu = 0. \tag{9a}$$

Similarly, multiplying (6) front and rear with B_μ

$$B_\mu DB_\nu + B_\nu DB_\mu = 0. \tag{9b}$$

Also we have from (8):

$$N_\mu D + DN_\mu = (2B_\mu{}^2 - 1)D + D(2B_\mu{}^2 - 1) = 0.$$

Therefore

$$B_\mu{}^2 D + DB_\mu{}^2 = D. \tag{9c}$$

Multiplying (9c) front and rear with B_μ

$$2B_\mu DB_\mu = B_\mu DB_\mu = 0. \tag{9d}$$

It can be shown that rules (9a–d) and the condition that D contain only terms coupling vector to scalar, i.e., no diagonal terms which only represent a change of mass, uniquely determine D. This may be most easily seen by considering the usual wave theory formalism where it is apparent that the requirement of relativistic invariance allows one to choose only an expression of the form $g\psi \cdot \nabla_4 \varphi$ as a bilinear, first-derivative coupling term in the Lagrangian. (ψ here is the vector four-potential, φ is the scalar potential.)

From this uniquely determined D one can, by using a special representation, also show:

$$DB_\mu D = 0; \quad D^2 B_\mu + B_\mu D^2 = B_\mu; \quad D^3 = D. \tag{9e}$$

It will now be observed that rules (9a–e) are precisely of the form of the commutation rule (1); i.e.,

that (1) is still valid if we consider $D=B_5$. Thus we may regard Eqs. (4) and (5) as a five-dimensional analog of the usual four-dimensional vector meson theory. The fifteen component wave function may be interpreted as a five-vector with associated ten antisymmetric tensor. Such a five-dimensional vector would have four possible orientations of spin—the three vector states and the one scalar state. It should be noted that in Eq. (4) the constant $g\hbar$ appears in a way exactly analogous to another momentum component, i.e., $g\hbar=-i\hbar(\partial/\partial X_5)$. This symmetry often leads to simplifications in the carrying out of computations.

C. Development of Canonical Formalism

We are now in a position to set up the energy-momentum tensor, Hamiltonian, etc. For this purpose we use the usual four-dimensional representation.

From Eqs. (4) and (5) we see that the current may be defined as:

$$S_\mu=e(\psi^+B_\mu\psi), \text{ since } (\partial S_\mu/\partial X_\mu)=0. \tag{10}$$

This means that charge density is proportional to $\psi^+B_4\psi$, and that in a way exactly analogous to that used in the Dirac theory we may define the expectation value of an operator ω by $\bar{\omega}=\int\psi^+\overline{\overline{\omega B_4}}\psi d\tau$. Here the double bar represents some type of appropriate symmetrization. Remembering that the momentum p_ν is given by $(\hbar/i)(\partial/\partial X_\nu)$ we are led to assume for the energy-momentum tensor:

$$T_{\mu\nu}=(\hbar c/i)\psi^+B_\nu(\partial\psi/\partial X_\mu),$$

satisfying the requirement $(\partial T_{\mu\nu}/\partial X_\nu)=0$.

This, however, is not a symmetric form of the energy-momentum tensor, so we now apply the standard symmetrization procedure[4] and obtain after some work:

$$\theta_{\mu\nu}=i\psi^+(B_\nu B_\mu+B_\mu B_\nu-\delta_{\mu\nu})Mc^2\psi. \tag{11}$$

From the energy-momentum tensor we can write down the spin matrix (from the angular momentum):

$$S_{ik}=\frac{B_iB_k-B_kB_i}{i}, \tag{12}$$

and the Hamiltonian:

$$H=\theta_{44}=-i\psi^+N_4Mc^2\psi=\psi^*Mc^2\psi. \tag{13}$$

D. Supplementary Condition and Second Quantization

Our next step should be to quantize the field. We must, however, be careful only to quantize those components which represent independent states of the system. For while we have a fifteen component wave function it is clear that there are only eight independent states of the system—four positive ones (three vector and one scalar), and four negative ones. Since the charge density is given by $e\psi^+B_4\psi$ and we wish to quantize the theory in terms of charged particles, it is convenient to eliminate the seven components corresponding to a zero eigenvalue of B_4^2, and quantize $B_4^2\psi$ directly. We see, in fact, that the seven components corresponding to a zero eigenvalue of B_4^2 may be expressed in terms of the eight components corresponding to eigenvalue 1. First, we multiply the wave Eq. (4) from the left by $1-B_4^2$:

$$(1-B_4^2)[\partial_\mu B_\mu\psi+(K+igD)\psi]=0.$$

Here we have written $\partial_\mu=\partial/\partial X_\mu$. But

$$B_4^2B_\mu+B_\mu B_4^2=B_\mu+B_4\delta\mu_4. \tag{7}$$

Therefore

$$\{\partial_kB_kB_4^2+(1-B_4^2)K+igDB_4^2\}\psi=0,$$

k to be summed from 1–3, and

$$\psi=K^{-1}(K-\partial_kB_k-igD)B_4^2\psi.$$

Similarly,

$$\psi^+=\psi^+B_4^2(K+\partial_kB_k-igD). \tag{14}$$

We now quantize the field in the usual way and set:[5]

$$\begin{aligned}B_4^2\psi=1/h^3\int\sum_{k=1}^{4}\{&a_k(\mathbf{p})B_4^2U_k^+)\exp(-iE_k(\mathbf{p})t/\hbar)\\&+b_k^*(\mathbf{p})B_4^2U_k^-(\mathbf{p})\exp(iE_k(\mathbf{p})t/\hbar)\}\\&\times\exp(i\mathbf{p}\cdot\mathbf{r}/\hbar)d\mathbf{p},\end{aligned} \tag{15}$$

$$\begin{aligned}\psi^*B_4^2=1/h^3\int\sum_{k=1}^{4}\{&a_k^*(\mathbf{p})U_k^+(\mathbf{p})^*B_4^2\exp(iE_k(\mathbf{p})t/\hbar)\\&+b_k(\mathbf{p})U_k^-(\mathbf{p})^*B_4^2\exp(-iE_k(\mathbf{p})t/\hbar)\}\\&\times\exp(-i\mathbf{p}\cdot\mathbf{r}/\hbar)d\mathbf{p}.\end{aligned}$$

Here $a_k(\mathbf{p})$ and $a_k^*(\mathbf{p})$ are annihilation and creation operators for positive mesons of momentum $\mathbf{p}$ and polarization k and $b_k(\mathbf{p})$ and $b_k^*(\mathbf{p})$ are the corresponding quantities for negative mesons of momentum $-\mathbf{p}$ and polarization k. They satisfy the usual commutation rules, e.g.,

$$[a_k(\mathbf{p})a_l^*(\mathbf{p}')-a_l^*(\mathbf{p}')a_k(\mathbf{p})]=\delta_{kl}\delta_{\mathbf{p},\mathbf{p}'}.$$

The $U_k(\mathbf{p})$'s are particular 15 component c-number solutions of the wave Eq. (4), corresponding to a momentum $\mathbf{p}$ and polarization k.

Substituting (14) and (15) in our fundamental Eq. (4), and remembering that $B_4(\mathbf{p}\cdot\mathbf{B})B_4=0$:

$$\begin{aligned}&[-E_k(\mathbf{p})B_4+Mc^2+(\mathbf{p}\cdot\mathbf{B}+g\hbar D)M^{-1}\\&\qquad\times(\mathbf{p}\cdot\mathbf{B}+g\hbar D)]B_4^2U_k^+(\mathbf{p})=0,\\&[E_k(\mathbf{p})B_4+Mc^2+(\mathbf{p}\cdot\mathbf{B}+g\hbar D)M^{-1}\\&\qquad\times(\mathbf{p}\cdot\mathbf{B}+g\hbar D)]B_4^2U_k^-(\mathbf{p})=0.\end{aligned} \tag{16}$$

It should be noted that $E_k(\mathbf{p})$ is different for vector and scalar states, as will be shown later. We now choose the U_k's to be orthogonal and normalize in such a way

[5] F. Booth and A. H. Wilson, Proc. Roy. Soc. London **175**, 490 (1940). Much of the subsequent calculation parallels this paper.

that the Hamiltonian (13) represents the energy of the system.

$$U_k^* Mc^2 U_l = E_k \delta_{kl} = U_k^* B_4^2 (Mc^2 + (\mathbf{p}\cdot\mathbf{B} + g\hbar D) M^{-1} \times (\mathbf{p}\cdot\mathbf{B} + g\hbar D)) B_4^2 U_l. \quad (17a)$$

Multiplying (16) from the left by $U_l^* B_4^2$ and using (17a) we find:

$$U_l^* B_4 U_k = \rho_{kl}. \quad (17b)$$

We have used the fact that $B_4^3 = B_4$. Here

$$\rho_{kl} = \delta_{kl} \text{ for } k = 1 \cdots 4,$$
$$= -\delta_{kl} \text{ for } k = 5 \cdots 8,$$

where $k = 1 \cdots 4$ applies to positive, $k = 5 \cdots 8$ to negative states. We now consider the eight linearly independent vectors $B_4^2 U_k$ as forming an eight by eight non-singular matrix $B_4^2 U$. We note from (17b) that the inverse matrix for $B_4^2 U$ is given by $\rho(U^* B_4^2) B_4$. The equation $(B_4^2 U)(B_4^2 U)^{-1} B_4 = B_4$ then gives the inverse orthogonality relation:

$$\sum_{k,\, l = 1 \cdots 8} B_4^2 U_k \rho_{kl} U_l^* B_4^2 = B_4. \quad (18)$$

E. Introduction of the Electromagnetic Field and Writing Down of the Hamiltonian

The next step is to introduce the electromagnetic field which we do in the usual gauge-invariant way, replacing $\partial\psi/\partial X_k$ with $(\partial\psi/\partial X_k) - (ie/\hbar c) A_k \psi$ and $\partial\psi^+/\partial X_k$ with $(\partial\psi^+/\partial X_k) + (ie/\hbar c)\, A_k \psi^+$ where A_k is the 4-vector potential of the electromagnetic field:

$$\mathbf{A} = 1/h^3 \sum_{\mathbf{k},\lambda} (2\pi\hbar^2 c/k)^{\frac{1}{2}} \mathbf{e}_{\mathbf{k},\lambda} [q_{\mathbf{k},\lambda} \exp(i\mathbf{k}\cdot\mathbf{r}/\hbar) + q_{\mathbf{k},\lambda}^* \exp(-i\mathbf{k}\cdot\mathbf{r}/\hbar)]. \quad (19)$$

Here q and q^* are the photon annihilation and creation operators.

Substituting (19), (15), and (14) into the Hamiltonian (13), integrating over the volume, and expanding in powers of the electric charge e, we obtain:

$$\bar{H}_0 = \int H_0 d\mathbf{r} = c^2 \sum_{k,\, l = 1 \cdots 4} \int [a_l^*(\mathbf{p}) U_l^+(\mathbf{p})^* + b_l(\mathbf{p}) U_l^-(\mathbf{p})^*] B_4^2 [M - (i/c)\mathbf{p}\cdot\mathbf{B} - (ig\hbar/c) D] \times N_4 M^{-1} [M - (i/c)\mathbf{p}\cdot\mathbf{B} - (ig\hbar/c) D] B_4^2 \times [a_k(\mathbf{p}) U_k^+(\mathbf{p}) + b_k^*(\mathbf{p}) U_k^-(\mathbf{p})] d\mathbf{p}. \quad (20a)$$

$$\bar{H}_1 = -\frac{1}{2\pi} \frac{e}{(\hbar c)^{\frac{1}{2}}} \frac{1}{(|\mathbf{p}' - \mathbf{p}|)^{\frac{1}{2}}} \sum_{k,\, l = 1 \cdots 4,\ \lambda = 1,\, 2} \int\int [a_l^*(\mathbf{p}') U_l^+(\mathbf{p}')^* + b_l(\mathbf{p}') U_l^-(\mathbf{p}')^*] B_4^2 \times \{ q_{\mathbf{p}'-\mathbf{p},\lambda} [(\mathbf{e}_{\mathbf{p}'-\mathbf{p},\lambda}\cdot\mathbf{B}) M^{-1} (\mathbf{p}\cdot\mathbf{B} + g\hbar D) + (\mathbf{p}'\cdot\mathbf{B} + g\hbar D) M^{-1} (\mathbf{e}_{\mathbf{p}'-\mathbf{p},\lambda}\cdot\mathbf{B})] + q^*_{\mathbf{p}-\mathbf{p}',\lambda} [(\mathbf{e}_{\mathbf{p}-\mathbf{p}',\lambda}\cdot\mathbf{B}) M^{-1} (\mathbf{p}\cdot\mathbf{B} + g\hbar D) + (\mathbf{p}'\cdot\mathbf{B} + g\hbar D) M^{-1} (\mathbf{e}_{\mathbf{p}-\mathbf{p}',\lambda}\cdot\mathbf{B})] \} \times B_4^2 [a_k(\mathbf{p}) U_k^+(\mathbf{p}) + b_k^*(\mathbf{p}) U_k^-(\mathbf{p})] d\mathbf{p} d\mathbf{p}'. \quad (20b)$$

$$\bar{H}_2 = \frac{1}{4\pi^2} \frac{e^2}{\hbar c} (1/kk')^{\frac{1}{2}} \sum_{\substack{l,\, m = 1 \cdots 4 \\ \lambda,\lambda' = 1,2}} \int\int\int\int [a_l^*(\mathbf{p}') U_l^+(\mathbf{p}')^* + b_l(\mathbf{p}') U_l^-(\mathbf{p}')^*] B_4^2 [M^{-1} (\mathbf{B}\cdot\mathbf{e}_{\mathbf{k},\lambda})(\mathbf{B}\cdot\mathbf{e}_{\mathbf{k}',\lambda'})] \times [q_{\mathbf{k},\lambda} q_{\mathbf{k}',\lambda'} \delta(\mathbf{p} - \mathbf{p}' + \mathbf{k} + \mathbf{k}') + q_{\mathbf{k},\lambda} q^*_{\mathbf{k}',\lambda'} \delta(\mathbf{p} - \mathbf{p}' + \mathbf{k} - \mathbf{k}') + q^*_{\mathbf{k},\lambda} q_{\mathbf{k}'\lambda'} \delta(\mathbf{p} - \mathbf{p}' - \mathbf{k} + \mathbf{k}') + q^*_{\mathbf{k},\lambda} q^*_{\mathbf{k}',\lambda'} \times \delta(\mathbf{p} - \mathbf{p}' - \mathbf{k} - \mathbf{k}')] \times B_4^2 [a_m(\mathbf{p}) U_m^+(\mathbf{p}) + b_m^*(\mathbf{p}) U_m^-(\mathbf{p})] d\mathbf{k} d\mathbf{k}' d\mathbf{p} d\mathbf{p}'. \quad (20c)$$

In addition if there is an external potential ϕ we have a term:

$$\bar{H}_{\text{static}} = \int \rho\phi d\mathbf{r} = e \sum_{k,\, l = 1 \cdots 4} \int\int [a_l^*(\mathbf{p}') U_l^+(\mathbf{p}')^* + b_l(\mathbf{p}') U_l^-(\mathbf{p}')^*] B_4^2 B_4 \phi(\mathbf{p}' - \mathbf{p}) B_4^2 \times [a_k(\mathbf{p}) U_k^+(\mathbf{p}) + b_k^*(\mathbf{p}) U_k^-(\mathbf{p})] d\mathbf{p}' d\mathbf{p}; \quad (20d)$$

where

$$\phi(\mathbf{p}' - \mathbf{p}) = \int \exp(-i(\mathbf{p}' - \mathbf{p})\cdot\mathbf{r}) \phi(\mathbf{r}) d\mathbf{r}.$$

F. Calculational Techniques

With the Hamiltonian (20) we may select matrix elements for any desired process and carry out the calculations in a manner entirely analogous to that used in the usual Dirac electron theory. As in the Dirac theory one eventually reduces the calculation to a summation of the matrix element of some operator over all eight states corresponding to a given momentum, and then uses the rule derived from (19):

$$\sum_{k = 1 \cdots 8} U_k^* B_4^2 \theta B_4^2 U_k \rho_{kk} = \text{Spur}(U^* B_4^2) \theta (B_4^2 U) \rho = \text{Spur} B_4 \theta.$$

As in the Dirac theory it is necessary to introduce annihilation operators so that a summation over a small number of states may be replaced by a summation over all eight states.

In our case it is necessary to introduce two types of annihilation operators, one to separate vector and scalar states, the other to distinguish between positive and negative mesons. We first discuss the annihilation operator for distinguishing between spin states.

Consider a solution U_k of the wave Eq. (4). If we can find a transformation matrix S such that SU_k has only $1 \cdots 10$ components if k is a vector state, and $11 \cdots 15$ components if k is a scalar state, then:

$$B_4^2 S^{-1} Z S U_k = B_4^2 U_k \text{ if } k \text{ is a vector state,}$$
$$= 0 \text{ if } k \text{ is a scalar state,} \quad (21)$$

where Z is the matrix

$$Z=\left(\begin{array}{ccc|c} 1 & & & \\ & \ddots & & \\ & & 1 & \\ \hline & & & 0\cdots 0 \end{array}\right). \tag{22}$$

We shall show that

$$S=\exp\left(igK^{-1}\left(\frac{K_vK_s}{g^2+K_vK_s}\right)^{\frac{1}{2}}D\right) \tag{23}$$

is such a matrix. The wave Eq. (4) tells us that for a plane wave solution U_k we have

$$[-E_kB_4+ic\mathbf{p}\cdot\mathbf{B}+Mc^2+ig\hbar cD]U_k{}^+=0.$$

(We have assumed that U_k is a positive state. This in no way affects the argument below.) Then

$$[S(-E_kB_4+ic\mathbf{p}\cdot\mathbf{B}+Mc^2+ig\hbar cD)S^{-1}]SU_k{}^+=0.$$

Using (23) for S and the commutation rules (1), (7), and (9), we arrive after some algebra at the equation:

$$\left\{-E_kB_4+ic\mathbf{p}\cdot\mathbf{B}+Mc^2\left(\frac{g^2+K_vK_s}{K_vK_s}\right)^{\frac{1}{2}}\right.$$
$$\left.+ig\left(\frac{K_vK_s}{g^2+K_vK_s}\right)^{\frac{1}{2}}K^{-1}(-E_kB_4+ic\mathbf{p}\cdot\mathbf{B})D\right\}SU_k{}^+=0.$$

We now prove that the term containing D is separately equal to zero. From the last equation we have:

$$SU_k{}^+=-\left(\frac{K_vK_s}{g^2+K_vK_s}\right)^{\frac{1}{2}}\frac{1}{c^2}M^{-1}\{-E_kB_4+ic\mathbf{p}\cdot\mathbf{B}\}$$
$$\times\left\{1+ig\left(\frac{K_vK_s}{g^2+K_vK_s}\right)^{\frac{1}{2}}K^{-1}D\right\}SU_k{}^+.$$

$\therefore\ (-E_kB_4+ic\mathbf{p}\cdot\mathbf{B})DSU_k{}^+=0$, since $B_\mu DB_\mu=0$.

So we finally obtain

$$\left[-E_kB_4+ic\mathbf{p}\cdot\mathbf{B}+Mc^2\left(\frac{g^2+K_vK_s}{K_vK_s}\right)^{\frac{1}{2}}\right]SU_k{}^+=0. \tag{24}$$

If we now consider the special representation (3) we see that in Eq. (24) the ten-component wave function and the five-component wave function have been uncoupled so that the wave Eq. (24) for SU_k is simply the sum of the vector and scalar wave equations. If SU_k is to represent a vector state it must satisfy the vector wave equation, hence have only $1\cdots10$ components. Thus we have proven that (23) is the desired transformation matrix.

Using (23) and remembering that $ZD+DZ=D$ while Z commutes with all other matrices we find after algebra:

$$\begin{aligned}B_4{}^2S^{-1}ZSU_k&=B_4{}^2[Z+(2Z-1)\\&\quad\times(g/g^2+K_vK_s)D(\mathbf{p}\cdot\mathbf{B}/\hbar)]B_4{}^2U_k,\\&=B_4{}^2U_k \text{ if } k \text{ is a vector state,}\\&=0 \text{ if } k \text{ is a scalar state.}\end{aligned} \tag{25}$$

Thus the quantity in square brackets in (25) is the desired annihilation operator.

In order to separate positive and negative states we use (16) which tells us:

$$\begin{aligned}&(1/2E_k)B_4[E_kB_4+Mc^2+(\mathbf{p}\cdot\mathbf{B}+g\hbar D)M^{-1}\\&\times(\mathbf{p}\cdot\mathbf{B}+g\hbar D)]B_4{}^2U_k\\&\quad=B_4{}^2U_k \text{ if } U_k \text{ is a positive state,}\\&\quad=0 \text{ if } U_k \text{ is a negative state.}\end{aligned} \tag{26}$$

Equipped thus with the commutation rules (1) and (9), the inverse orthogonality relation (18), and the annihilation operators (25) and (26) we are able to reduce all calculations to taking the spur of a matrix. This implies that we always sum or average over the different vector polarizations. Using a special representation like (3) it can be shown that if $D=B_5$, then

$$\begin{aligned}S_pB_i{}^2&=8;\\S_pB_i{}^2B_j{}^2&=4(i\neq j);\\S_pB_i{}^2B_j{}^2B_k{}^2&=2(i\neq j\neq k);\\S_pB_i{}^2B_j{}^2B_k{}^2B_l{}^2&=1(i\neq j\neq k\neq l);\\S_pB_i{}^2B_j{}^2B_k{}^2B_l{}^2B_m{}^2&=0(i\neq j\neq k\neq l\neq m).\end{aligned} \tag{27}$$

Also the spur of any matrix containing an odd power of one of the B's must vanish.

G. Physical Interpretation of $\bar{H}_0$

We now apply these techniques to the evaulation of the Hamiltonian $\bar{H}_0$ (20a) and find after some calculation:

$$\bar{H}_0=\sum_{k=1\cdots4}\int E_k(\mathbf{p})[a_k{}^*a_k+b_k{}^*b_k+1]d\mathbf{p}, \tag{20e}$$

where

$$\begin{aligned}E_k(\mathbf{p})&=(M_v{}^2c^4+g^2\hbar^2c^2(M_v/M_s)+p^2c^2)^{\frac{1}{2}}\\&\qquad\text{if } k \text{ is a vector state;}\\E_k(\mathbf{p})&=(M_s{}^2c^4+g^2\hbar^2c^2(M_s/M_v)+p^2c^2)^{\frac{1}{2}}\\&\qquad\text{if } k \text{ is a scalar state.}\end{aligned} \tag{28}$$

Thus we see that the coupling has given a "mesomatic" mass to the states. The mass as defined by (28) [(i.e., from $E=(\mu^2c^4+p^2c^2)^{\frac{1}{2}}$] is clearly to be considered as the physical mass, with M merely being an auxiliary constant without obvious physical significance.

It should be noted that we have effectively uncoupled the vector and scalar states by writing the Hamiltonian in the form (20e). That is, we would have obtained the identical Hamiltonian if we had assumed uncoupled vector and scalar states of the appropriate masses. The

term $\bar{H}_1$, however, cannot be separated in this way, so that we have not merely made a trivially different formalism. The physical meaning of this is clear. There can be no transition from a vector to a scalar meson unless we introduce another particle so as to conserve angular momentum. Such a particle is the photon, and it is precisely this effect of the excited state on electromagnetic interactions that we are seeking.

III. ELECTROMAGNETIC INTERACTIONS

A. Lifetime of Excited State

From the expression (20b) for the Hamiltonian $\bar{H}_1$ we see that it is possible for a meson in an excited state to decay with emission of a photon to the ground state. If we assume, for example, that the scalar of mass μ_s is the excited state, then a positive scalar meson at rest can decay into a vector meson of mass μ_v and momentum $\mathbf{p}$, and a photon of momentum $-\mathbf{p}$. Conservation of energy tells us:

$$\mu_s c^2=(\mu_v^2c^4+p^2c^2)^{\frac{1}{2}}+pc.$$

The lifetime for such a transition is given by:

$$1/\tau=(2\pi/\hbar)|\bar{H}_{vs}|^2\rho_E,$$

with the matrix element:

$$\bar{H}_{vs}=-\frac{1}{2\pi}\frac{e}{(\hbar c)^{\frac{1}{2}}}\frac{1}{(p)^{\frac{1}{2}}}U_v^+(\mathbf{p})^*B_4^2[(\mathbf{e}_{-\mathbf{p},\lambda}\cdot\mathbf{B})M^{-1}g\hbar D+(\mathbf{p}\cdot\mathbf{B}+g\hbar D)M^{-1}(\mathbf{e}_{-\mathbf{p},\lambda}\cdot\mathbf{B})]B_4^2U_s^+(0).$$

Using the spur techniques discussed previously we may evaluate the lifetime and find:

$$1/\tau=\tfrac{1}{4}(e^2/\hbar c)K^2(\mu_vc^2/\hbar)(\mu_s/\mu_v-\mu_v/\mu_s)^3, \quad (29)$$

where we have written $K^2=(g^2\hbar^2/M_vM_sc^2)$, a dimensionless constant which represents the strength of the coupling between vector and scalar states. We see that for any "strong-coupled" case, i.e., a case where $K^2\approx1$, the lifetime of the excited state will be very short unless the energies are very close together. For example, if $\mu_vc^2=200$ Mev; $\mu_sc^2=400$ Mev; $K^2=1$, then $\tau=5\times10^{-22}$ sec. Hence the excited state is unobservable directly.

The photons which have been observed at Berkeley might possibly be such decay photons. Further experimental evidence is needed to decide this point. The coincidence measurements to determine whether the photons are produced singly or in pairs are of crucial importance in this connection.

B. Rutherford Scattering

An experiment by which the existence of such an excited state might be detected is scattering by a Coulomb field. Let us image a vector (ground state) meson of mass μ_v, charge e, and momentum $\mathbf{p}$ impinging on a fixed scattering center of charge Ze. Then, using the static Hamiltonian (20d), we find for the Born approximation scattering cross section:

$$\sigma(\theta,\varphi)=\sigma_v(\theta,\varphi)+\sigma_s(\theta,\varphi),$$

where $\sigma_v(\theta,\varphi)$ represents the cross section for the final state being vector, $\sigma_s(\theta,\varphi)$ for it being scalar. $\sigma_v(\theta,\varphi)$ is the usual vector cross section:

$$\sigma_v(\theta,\varphi)=\left(\frac{Ze^2}{2\mu_vv^2}\right)^2\left[\left(1-\frac{v^2}{c^2}\right)+\tfrac{1}{6}\sin^2\theta\frac{v^4}{c^4}\right]\frac{1}{\sin^4(\theta/2)}d\Omega,$$

while

$$\sigma_s(\theta,\varphi)=\tfrac{1}{3}K^2\left(\frac{Ze^2}{\mu_vc^2}\right)^2\left[\frac{pp'[(c^2/v^2)-1]}{p^2+p'^2-2pp'\cos\theta}+\frac{pp'^3\sin^2\theta}{(p^2+p'^2-2pp'\cos\theta)^2}\right]d\Omega.$$

Here p' is the momentum of the outgoing scalar meson as given by the conservation of energy:

$$p'^2=p^2+\mu_v^2c^2-\mu_s^2c^2.$$

$\sigma_s(\theta,\varphi)$ is of course zero for $p^2+\mu_v^2c^2-\mu_s^2c^2<0$.

This cross section for production of excited-state mesons is proportional to K^2, hence will be appreciable only for a "strong-coupled" theory. As we have already seen, in such a theory the excited state decays almost instantaneously if the mass difference is at all appreciable. Hence the total cross section σ_s represents the cross section for production of decay photons. We find for this cross section:

$$\sigma_s=\int\sigma_s(\theta,\varphi)d\Omega=(\pi/3)K^2(Ze^2/\mu_vc^2)^2\times\{[2(c^2/v^2)-1+(p'^2/p^2)]\times\ln(p+p'/p-p')-2(p'/p)\}. \quad (30)$$

In the case where the scalar is the ground state, we have exactly the same matrix element for the transition, and we find for the cross section for excited-state production;

$$\sigma_{s\to v}=\pi K^2(Ze^2/\mu_sc^2)^2\{2[(c^2/v^2)-1]\ln(p+p'/p-p')+(\mu_s/\mu_v)^2[(1+(p'^2/p^2))\ln(p+p'/p-p')-2(p'/p)]\}.$$

As in the previous case, p' refers to the momentum of the excited state meson.

In the non-relativistic region this is appreciable, and is considerably larger than the bremsstrahlung cross section, so that the existence of a low lying strongly coupled excited state would manifest itself by the production of many photons on passage of a meson beam through a heavy target.

In the relativistic limit the ratio of the cross section (30) to the bremsstrahlung cross section for a vector meson is a factor of the order of magnitude $K^2(\hbar c/e^2)(\mu_vc^2/E)$. Thus for $E\approx137\mu_vc^2$, the upper limit of reliability of the theory, a strongly coupled scalar excited state would lead by Rutherford scattering alone

to burst production too great to be compatible with the experimental evidence on μ-mesons. This would not be true, however, if the mass difference of the states either were great enough so that the excited state could not be produced, or small enough so that the decay photons had very low energy.

For the degenerate case where $\mu_v=\mu_s$ we obtain for the Rutherford cross section:

$$\sigma_{\mu_v=\mu_s}=(Ze^2/2\mu v^2)^2[(1-v^2/c^2)+\tfrac{1}{4}K^2(v^2/c^2)(1-\cos\theta)+\tfrac{1}{8}(1+K^2)(v^4/c^4)\sin^2\theta](1/\sin^4\theta/2)d\Omega. \quad (31)$$

For this case both initial and final states may be either vector or scalar, with the average over the initial state taken such that the vector is given weight three, the scalar weight one.

C. High Energy Compton Effect

As is well known, the total Compton effect cross section for vector mesons behaves like E^2 at high energies in the barycentric system.[6] It has been shown by Wilson[7] that this result is not cut down by radiation damping until $E>(137)^{\frac{1}{2}}\mu c^2$, so that the Christy and Kusaka argument against the μ-meson having spin 1 is still valid.

We will inquire whether the assumption of a scalar excited state allows for destructive interference and cancellation of the E^2 terms as discussed in the Introduction. The calculation is very tedious and has only been carried out for the case $E\gg\mu_s c^2\geq\mu_v c^2$.

The scattering may occur directly through the two-quantum Hamiltonian $\bar{H}_2$, or via any of four possible intermediate states, through $\bar{H}_1$. These are:

(1) Absorption of the incident photon by the meson, followed by emission of the scattered photon;
(2) Emission of the scattered photon followed by absorption of the incident photon;
(3) Absorption of the incident photon, accompanied by creation of a meson pair, followed by annihilation of one member of the pair with the original meson, accompanied by emission of the scattered photon;
(4) Emission of the scattered photon accompanied by creation of a meson pair, followed by annihilation of one member of the pair with the original meson and absorption of the incident photon.

Initially the meson is assumed to be in the ground (vector) state, while the intermediate and final states may be either vector or scalar.

After a very long calculation we find for the total cross section in the case $E\gg\mu_s c^2\geq\mu_v c^2$:

$$\sigma=(5\pi/9)(e^2/\mu_v c^2)^2(E/\mu_v c^2)^2(1+\tfrac{3}{2}K^2+\tfrac{1}{2}K^4)=(1+\tfrac{3}{2}K^2+\tfrac{1}{2}K^4)\sigma_{\text{vector}}, \quad (32)$$

where σ_{vector} is the ordinary vector meson cross section.

For the degenerate case $\mu_v=\mu_s$,

$$\sigma=\tfrac{3}{4}\sigma_{\text{vector}}(1+2K^2+K^4). \quad (33)$$

The results of this special case thus tend to indicate that the high-energy divergences of the electromagnetic cross sections of higher spin particles are made worse rather than alleviated by the assumption of excited states.

I would like to thank Professor E. Teller who suggested this problem and Professor G. Wentzel, Dr. G. F. Chew, and Dr. C. N. Yang for many stimulating discussions.

[6] W. Pauli, Rev. Mod. Phys. **13**, 230 (1941).
[7] A. H. Wilson, Proc. Camb. Phil. Soc. **37**, 311 (1941).

Radiations from Hf^{181}

ERLING N. JENSEN
*Institute for Atomic Research and Department of Physics, Iowa State College, Ames, Iowa**

(Received June 3, 1949)

The radiations from Hf^{181} have been examined with a magnetic lens spectrometer. Four gamma-rays were found having energies of 0.087, 0.134, 0.347, and 0.485 Mev. There is evidence for the existence of a fifth gamma-ray. The maximum energy of the beta-rays was estimated to be 0.41 Mev. The three higher energy gamma-rays were found to have intensities proportional to 11, 29, and 100, respectively. The total internal conversion coefficient for the 0.134-Mev transition was calculated to be 11. Calculations on the lifetime and the ratio of the conversion electrons in the K and L shells indicate that in the transition from the metastable state the nucleus undergoes a spin change of three units.

I. INTRODUCTION

A NUMBER of authors[1–6] have examined the radiations from Hf^{181} by means of absorption and coincidence techniques. In addition, Cork, Shreffler, and Fowler[7] have examined the internal conversion spectrum with a 180° spectrograph. They also looked for higher energy gammas by absorption in copper and aluminum. Benes, Ghosh, Hedgran, and Hole[8] and Chu and Wiedenbeck[9] have reported on the radiations as found with a magnetic lens and semicircular spectrometer, respectively.

The results reported in this paper are those obtained by examining the radiations from Hf^{181} by means of a thin magnetic lens spectrometer previously described,[10] and provide evidence for an additional gamma-ray that has not been reported previously. In addition, calculations have been made on the intensity ratios of the gamma-rays, the total internal conversion coefficient for one of the gamma-rays, and the spin change of the nucleus in the transition from the metastable state as predicted from the lifetime and the ratio of the conversion electrons in the K and L shells. The spectrometer was calibrated by means of the F conversion line of ThB ($1385H\rho$) and the annihilation radiation from Zn^{65}. The resolution of the spectrometer was 2.1 percent (half-width).

TABLE I. Gamma-ray energies of Hf^{181}.

Gamma-ray	Electron energy (corrected) Mev	Conversion shell	Gamma-ray energy Mev	Relative weight	Average energy Mev
1	0.0708	Pb(L)	0.0866	5	0.087
2	0.0458	Pb(K)	0.1334	10	
	0.1206	Pb(L)	0.1364	10	
	0.1310	Pb(M)	0.1348	5	
	0.0641	Ta(K)	0.1315	10	
	0.1227	Ta(L)	0.1344	10	0.134
4	0.2600	Pb(K)	0.3476	10	
	0.3335	Pb(L)	0.3493	5	
	0.2794	Ta(K)	0.3468	10	
	0.3300	Ta(L)	0.3417	1	0.347
5	0.3975	Pb(K)	0.4851	10	
	0.4706	Pb(L)	0.4864	5	
	0.4158	Ta(K)	0.4832	10	
	0.4730	Ta(L)	0.4847	5	0.485

II. PHOTOELECTRON SPECTRUM

The composite spectrum of photoelectrons and Compton electrons ejected from a lead foil of surface density 37.0 mg/cm² is shown in Fig. 1. The 46-day[11] Hf^{181} was obtained by neutron bombardment of HfO_2 in the Clinton pile. The Hf^{181} was placed in a Lucite holder and covered with an aluminum cap of sufficient thickness to absorb all electrons emitted. A lead foil having a surface density of 37.0 mg/cm² was fastened to the aluminum cap. Curve 1 of Fig. 1 was obtained with a Geiger counter having a mica window of surface density 4.0 mg/cm², while curve 2 was obtained with a mica counter window of surface density 1.1 mg/cm² and was run 49 days later than curve 1. The curves have not been corrected for window absorption.

The gamma-ray energies calculated from the data shown in Fig. 1 are given in Table I as conversions in lead.

III. INTERNAL CONVERSION SPECTRUM

The composite spectrum of internal conversion electrons and beta-rays from Hf^{181} is shown in Fig. 2. This curve has not been corrected for window absorption. The source had a surface density of about 15 mg/cm² and was mounted on mica of surface density 2.8 mg/cm². This is too large a surface density for accurate beta-ray work, but is of no particular disadvantage in

* Work was performed at the Ames Laboratory of the AEC.

[1] H. Neuert, Zeits. f. Naturforschung **2a**, 432 (1947).
[2] L. Madansky and M. L. Wiedenbeck, Phys. Rev. **72**, 185 (1947).
[3] A. F. Voigt and B. J. Thamer, AECD 2083 and Phys. Rev. **74**, 1264 (1948).
[4] S. DeBenedetti and F. K. McGowan, Phys. Rev. **74**, 728 (1948).
[5] Bunyan, Lundby, Ward, and Walker, Proc. Phys. Soc. London **61**, 300 (1948).
[6] Mandeville, Scherb, and Keighton, Phys. Rev. **75**, 221 (1949).
[7] Cork, Shreffler, and Fowler, Phys. Rev. **72**, 1209 (1947).
[8] Benes, Ghosh, Hedgran, and Hole, Nature **162**, 261 (1948).
[9] K. Y. Chu and M. L. Wiedenbeck, Phys. Rev. **75**, 226 (1949).
[10] Jensen, Laslett, and Pratt, Phys. Rev. **75**, 458 (1949).
[11] Seren, Friedlander, and Turkel, Phys. Rev. **72**, 888 (1947).

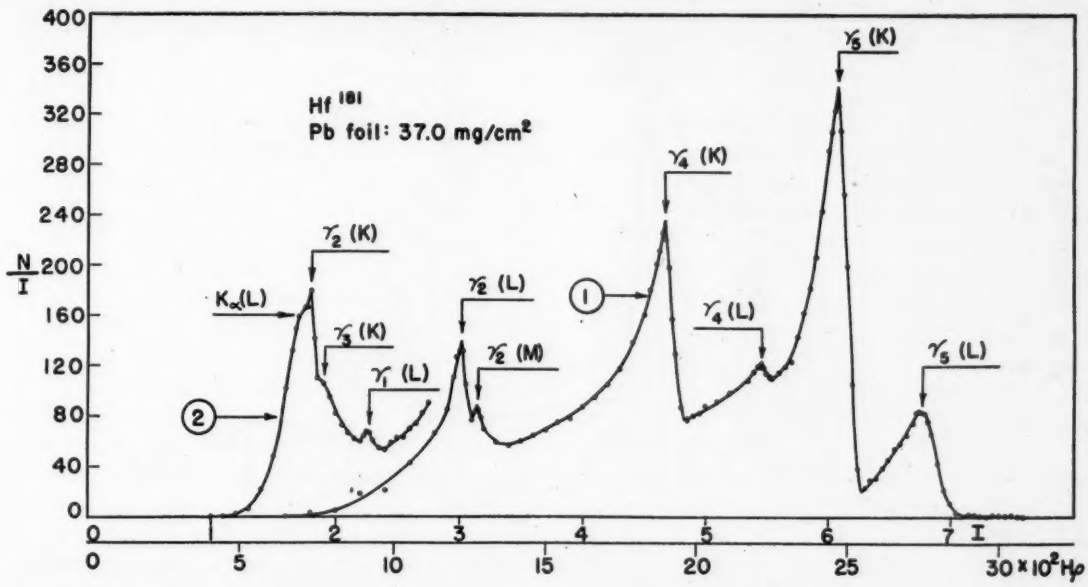

FIG. 1. Composite spectrum of photoelectrons and Compton electrons ejected from 37.0 mg/cm² lead foil by the gamma-rays from Hf^{181}. N is the counting rate in counts/min. and I is the current in the spectrometer coil.

determining gamma-ray energies from internal conversion lines if a correction is applied for the thickness of the source.[10] There is a distinct advantage in a thick conversion source since the intensity is increased appreciably. The counter window was a thin film of Formvar of surface density about 0.3 mg/cm².

The gamma-ray energies calculated from the data shown in Fig. 2 are given in Table I as conversions in Ta, since Hf^{181} decays by beta-emission.

In calculating the gamma-ray energies given in Table I, the data were corrected for the earth's magnetic field, the surface density of the source and the resolution of the spectrometer as explained in reference 10. The probable error is estimated to be 1 percent.

The maximum energy of the beta-rays, as determined from Fig. 2, is estimated to be 0.41±0.02 Mev.

IV. DISCUSSION

A. Energies of Gamma-Rays

The gamma-ray energies listed for γ_2, γ_4, and γ_5 in Table I are in fairly good agreement with those given by Benes, Ghosh, Hedgran, and Hole[8] (0.128, 0.342, and 0.472 Mev), Cork, Shreffler, and Fowler[7] (0.132, 0.344, and 0.479 Mev), and three of the four gamma-rays reported by Chu and Wiedenbeck[9] (0.130, 0.337 and 0.471 Mev). Chu and Wiedenbeck report a fourth gamma-ray with an energy of 0.134 Mev, which was observed in their internal conversion spectrum. This gamma-ray was not observed in the internal conversion spectrum of this investigation, but the hump labeled $\gamma_3(K)$ in the photoelectron spectrum of Fig. 1 is presumably due to this gamma-ray. Cork, Shreffler, and Fowler[7] report that absorption measurements in copper and aluminum give evidence for the existence of an additional gamma-ray at an energy of about 0.60 Mev. A search was made for a gamma-ray of about this energy, but no evidence was obtained for its existence.

Gamma-ray number 1 has not been reported by other investigators. There is some uncertainty in determining the conversion shell for this gamma-ray, due to the low intensity of the conversion electrons. The assignment given in Table I seems to be consistent with the data from both the internal conversion and photoelectron spectra. An impurity of Zr^{95} was found in the sample by Voigt and Thamer[3] of this laboratory, but the intensity of the radiations was too low to account for the observed line. Furthermore, no gamma-ray with an energy of 0.087 Mev has been reported for Zr^{95} or its daughter Cb^{95}.

The peculiar shape of the $\gamma_2(K)$ photoelectron line is due to the photoelectrons $[K_\alpha(L)]$ produced by the characteristic x-rays from Ta following the internal conversion of the gamma-rays, and also to the photoelectrons $[\gamma_3(K)]$ produced by the gamma-ray of energy 4 kev higher than γ_2, which has been reported by Chu and Wiedenbeck.[9] Chu and Wiedenbeck[9] did not observe the photoelectron lines of γ_2 and cite this as further evidence that γ_2 is highly converted.

B. Intensities of Gamma-Rays

For Fig. 1 the spread in momentum due to the surface density of the lead foil was greater than the momentum spread which the spectrometer could accept.[10] In this case, neglecting scattering, the maximum counting rate for any line is proportional to the number of such quanta emitted from the atom, the photoelectric absorption coefficient, the transmission of the counter window and inversely proportional to the spread in momentum produced by the lead foil. Using the K

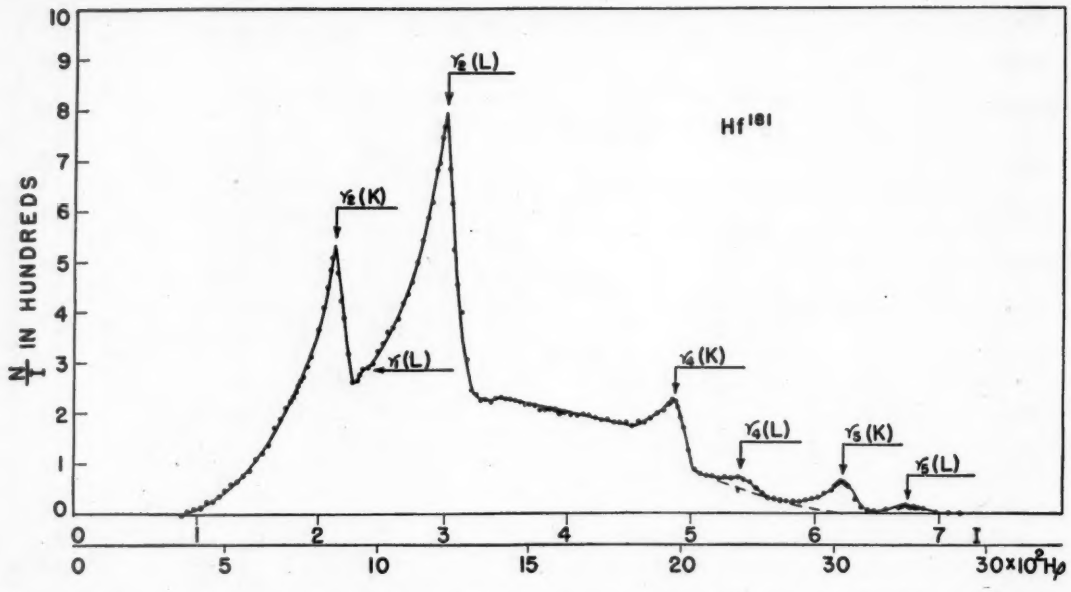

FIG. 2. Composite spectrum of internal conversion electrons and beta-rays from Hf^{181}. N is the counting rate in counts/min. and I is the current in the spectrometer coil.

photo-lines of γ_4 and γ_5 and the L photo-line of γ_2, after subtracting the Compton background, the gamma-ray intensities were found to be proportional to 11, 29, and 100 for γ_2, γ_4, and γ_5, respectively. In these calculations it was assumed that the photoelectric absorption coefficient for the L shell of γ_2 was 0.23 of that for the K shell as is the case for γ_5. The photoelectric absorption coefficients were calculated by means of Gray's[12] empirical formula and the spread in momentum produced by the lead foil by means of a formula given by Heitler,[13]

Chu and Wiedenbeck[9] have proposed a decay scheme, based on coincidence measurements, which is reproduced in Fig. 3. The gamma-ray energies are those determined in this investigation with the exception of γ_3 which is taken as 4 kev greater than γ_2 as determined by Chu and Wiedenbeck.[9] In this decay scheme, the number of transitions for γ_3 and γ_4 should be equal. From the spectra determined in this investigation and those of Chu and Wiedenbeck, this does not seem to be the case. It is possible that there are other weak radiations which together with γ_1 are in parallel with γ_2. For this to be a single gamma-ray, the energy should be 51 kev and the internal conversion line from the L shell should be at 1.7 amp. As Fig. 2 indicates, it was not possible to resolve a line at this current value. If the gamma-ray exists, it undoubtedly has a low intensity.

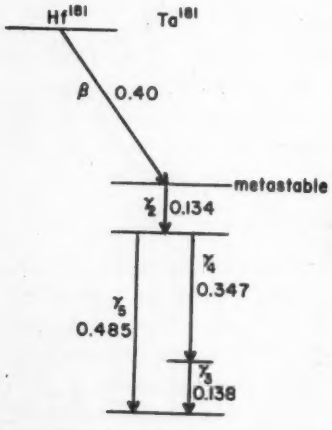

FIG. 3. Proposed decay scheme by Chu and Wiedenbeck (see reference 9). The energies are given in Mev.

C. Internal Conversion Coefficient of γ_2

The total internal conversion coefficient is defined as the ratio Ne/Nq, where Ne is the total number of conversion electrons and Nq the number of quanta emitted from the atom for this transition. Assuming the decay scheme shown in Fig. 3, Ne/Nq can be calculated from the ratios of the intensities of the gamma-rays.

Neglecting the small internal conversion coefficients of γ_4 and γ_5, Ne/Nq for γ_2 is calculated to be 10.8. Taking into account the conversion coefficients determined by Chu and Wiedenbeck[9] for γ_4 and γ_5, the total conversion coefficient Ne/Nq is 11.5.

D. Multipole Order of Radiations

DeBenedetti and McGowan[14] report a half-life of 22μ sec. for the short-lived isomer of Ta^{181*}. This has been confirmed by Madansky and Wiedenbeck.[2] The

[12] L. H. Gray, Proc. Camb. Phil. Soc. **27**, 103 (1931).
[13] W. Heitler, *The Quantum Theory of Radiations* (Oxford University Press, New York 1944), second edition, p. 219.
[14] S. DeBenedetti and F. K. McGowan, Phys. Rev. **70**, 569 (1946).

lifetime of a metastable state is given by Bethe[15] as

$$\tau = 5\times 10^{-21} l\,!^2 (20/\hbar\omega)^{2l+1} \text{ sec.}, \quad (1)$$

where $\hbar\omega$ is the energy of the emitted radiation in Mev and l is the change in angular momentum of the nucleus. Hebb and Uhlenbeck[16] have suggested that Eq. (1) should be divided by $(1+Ne/Nq)$ in order to allow for the increased decay probability due to internal conversion. Wiedenbeck[17] has shown that this correction improves the agreement between the lifetimes calculated by means of Eq. (1) and those determined experimentally. The corrected half-life, as calculated from Eq. (1), for a metastable state of 0.134 Mev and a spin change of three units is 17μ sec. This is in fairly good agreement with the experimental value of 22μ sec.[14] The corrected half-lives for $l=2$ and 4 are 8.2×10^{-11} sec. and 5.9 sec., respectively.

For the internal conversion spectrum of Fig. 2, the ratio N_K/N_L of the conversion electrons for γ_2 in the K and L shells is 1.19.

Hebb and Uhlenbeck[16] and Dancoff and Morrison[18] have calculated the conversion coefficients for the K shell for electric and magnetic multipole radiation. Hebb and Nelson[19] have made similar calculations for the L shell. From these calculations the ratio N_K/N_L can be determined. These calculations are for elements with atomic numbers less than about 50. However, it is of interest to apply these formulas to Ta^{181} for which Z is 73.

The calculated values of N_K/N_L for γ_2 are 0.10 for electric 2^4 radiation and 4.05 for magnetic 2^3 radiation. Since the experimental value of 1.19 is between the two calculated values, the radiation is presumably a mixture of magnetic 2^3 and electric 2^4 radiation. This is consistent with the calculation of the lifetime with a spin change of three units. Hence, the Ta^{181*} nucleus appears to undergo a spin change of three units with the emission of γ_2(0.134 Mev). Using a formula due to Nelson,[20] it is found that the γ_2-radiation is a little less than half (~42 percent) electric and the rest (~58 percent) magnetic.

For γ_4 and γ_5, the experimental values of N_K/N_L are 5.0 and 5.2, respectively, while the calculated values for electric quadrupole radiation ($l=2$) are 6.0 and 6.9, respectively. This suggests that γ_4 and γ_5 are perhaps electric quadrupole radiations.

V. ACKNOWLEDGMENTS

The author wishes to express his appreciation to Dr. A. F. Voigt for preparing the samples; Dr. L. Jackson Laslett, Dr. J. M. Keller, and Mr. William W. Pratt for helpful discussions on the problem; Messrs. R. T. Nichols and G. O. Pickens for assistance in operating the spectrometer, and Mr. E. R. Rathbun, Jr. for the construction of the Geiger-Müller counters.

[15] H. A. Bethe, Rev. Mod. Phys. **9**, 226 (1937), Eq. (733).
[16] M. H. Hebb and G. E. Uhlenbeck, Physica **5**, 605 (1938).
[17] M. L. Wiedenbeck, Phys. Rev. **69**, 567 (1946).
[18] S. M. Dancoff and P. Morrison, Phys. Rev. **55**, 122 (1939).
[19] M. H. Hebb and E. Nelson, Phys. Rev. **58**, 486 (1940).
[20] E. Nelson, cited by A. C. Helmholtz, Phys. Rev. **60**, 415 (1941).

Measurement of *f*-Values in the Iron Spectrum with Applications to Solar and Stellar Atmospheres

W. W. CARTER*
California Institute of Technology, Pasadena, California
(Received June 20, 1949)

The relative *f*-values of 47 spectral lines of Fe I have been derived from measurements of intensities in emission of lines excited in an electric furnace. The measurements were made photoelectrically. The *f*-values were measured relative to King's previously determined values and are on the same scale. Lines with excitation potential of low term up to 3.5 volts are included.

The *f*-values derived have been used to plot a solar curve of growth. The scatter of the points for high energy level lines is large. This is due mainly to the fact that lines whose low term is of odd parity are apparently consistently too strong in the sun and those of even parity too weak. On the other hand curves of growth for the giant stars γ-Cygni and α-Persei exhibit a much smaller scatter of points and no evidence of odd-even difference. Measurements of laboratory pressure shifts show systematic odd-even differences. These tests indicate that the effect observed in the sun is real and suggests that it may be due to the relatively high pressure in the solar atmosphere. If this is true the practice of using relative *f*-values derived from the solar curve of growth in the study of stellar atmospheres should be reconsidered.

INTRODUCTION

OSCILLATOR strengths, or *f*-values, for atomic transitions have previously been determined both theoretically and experimentally. The *f*-values for hydrogen lines have been accurately calculated by quantum mechanics,[1] and other simple atoms have been treated by approximate methods. Few attempts to calculate *f*-values for complex spectra have been made, although recently W. M. Gottschalk[2] has used an approximate method with restrictive assumptions to calculate line strengths for lines of Fe I in the multiplets of $3d^7(^4F)4s-3d^7(^4F)4p$ and $3d^7(^4P)4s-3d^7(^4P)4p$. The agreement between Gottschalk's results and experimental values is fair. Experimental methods for measuring *f*-values have been described by A. Unsold[3] and by Mitchell and Zemansky.[4] Prior to 1935 the *f*-values of fewer than two dozen lines had been measured. Starting in 1935 A. S. King and R. B. King[5–7] applied the method of *total absorption* to the measurement of *f*-values of many lines in the spectra of several of the more refractory elements, e.g., iron, nickel, titanium, and vanadium. These values have found wide applications in problems of astrophysics and spectrographic analysis. Practical limitations have so far restricted these measurements to lines of low excitation potential. In the present work the *f*-values of 47 spectral lines of Fe I have been derived from measurements of emission intensities. Lines are included whose low terms have excitation potentials up to 3.5 volts.

APPARATUS

The principal components of the apparatus used in the present investigation are (A) a furnace to vaporize and excite the iron atoms, (B) a spectrograph, and (C) a sensitive element to measure directly spectral line intensities.

(A) The electric resistance furnace described by A. S. King[8] was used to vaporize the iron and excite the neutral iron spectrum. The heating element of this furnace is a graphite tube 10 in. long, $\frac{1}{2}$ in. I.D. and $\frac{3}{4}$ in. O.D. Currents ranged from 500 to 1300 amps. During the measurements the tube was in kinetic and radiative thermodynamic equilibrium. The temperature distribution along the furnace tube is uniform (to within 5° at 2500°K) except very near the ends of the tube. Tests by King[5] showed that a true Boltzmann distribution among the low energy states was attained by the iron atoms. These tests were extended by the writer to higher energy states and temperature with satisfactory results.

The intensities of furnace emission lines from low energy levels were strongly affected by self-reversal due to absorption by the cooler vapor at the end of the tube. Tests showed that this self-reversal could be entirely eliminated by passing a stream of helium backward through the furnace tube thus preventing a layer of cooler iron vapor from collecting at the end of the tube.

(B) The spectrograph used was the 15 foot Rowland grating spectrograph of the Mt. Wilson Observatory. All measurements were made in the first order with a dispersion of 3.7 A./mm.

(C) A 1P21 photo-multiplier tube was used as a sensitive indicator to measure the spectral line intensi-

* Now at Los Alamos Scientific Laboratories, Los Alamos, New Mexico.

[1] H. Bethe, Handbuch der Physik 24, part 1, 443–469.

[2] W. M. Gottschalk, Astrophys. J. 108, 326 (1948).

[3] A. Unsold, *Physik der Sternealmosphären* (Verlag Julius Springer, Berlin, 1938).

[4] Mitchell and Zemansky, *Resonance Radiation and Excited Atoms* (Cambridge University Press, London, 1934), p. 145.

[5] R. B. King and A. S. King, Contribution from the Mt. Wilson Observatory No. 528; Astrophys. J. 82, 377 (1935).

[6] R. B. King and A. S. King, Contribution from the Mt. Wilson Observatory No. 581; Astrophys. J. 87, 24 (1938).

[7] R. B. King, Contribution from the Mt. Wilson Observatory Nos. 655, 656; Astrophys. J. 95, 78 (1942).

[8] A. S. King, Contribution from the Mt. Wilson Observatory No. 247; Astrophys. J. 56, 318 (1922).

ties. The output of the tube was applied directly to a type R galvanometer whose sensitivity was about 2×10^{-10} amp./mm. The sensitivity of this simple arrangement approached the noise level of the multiplier tube. The addition of external amplification would have yielded small gain unless the photo-cell had been refrigerated to lower the noise level. Without amplification the photo-multiplier and galvanometer could detect any spectral line that could be photographed in an exposure time of 5 to 10 minutes. By moving the photo-multiplier along tracks in the focal plane of the spectrograph and with a defining slit in front of the photo-cell, the relative intensities of several spectral lines could be measured in rapid succession. The photo-cell was mounted with a lateral slide adjustment that permitted easy interchange with a viewer equipped with cross-hair and wave-length scale.

In the measurement of furnace emission line intensities, direct photoelectric recording appears to offer the following advantages over photographic photometry: (a) Fewer sources of error. The errors of non-linearity of response and non-uniformity of the photographic emulsion are eliminated. (b) Permits the study of rapid changes in excitation conditions in the furnace. (c) Potentially more rapid and less laborious. In many spectral regions the measurements can proceed at the rate of 2 or 3 lines per minute and the reduction of the data is simpler and faster than the photographic method.

RELATIVE ADVANTAGES OF ABSORPTION AND EMISSION LINE PHOTOMETRY

In the measurement of f-values by spectrophotometry with a photo-multiplier tube there are several possible advantages to be gained if the measurements can be made on absorption lines rather than on emission lines. The principal advantage is the possible increase in sensitivity in absorption line measurements. For an emission line the galvanometer deflection is directly proportional to the strength of the line, which in turn is usually directly proportional to the number of emitting atoms. Thus the galvanometer deflection can be increased only by increasing the number of emitting atoms. On the other hand, the depth of an absorption line, for a given number of absorbing atoms, is a constant fraction of the intensity of the continuum. Therefore, by increasing the intensity of the continuum, the difference between galvanometer deflections for continuum and absorption line can be amplified. The continuum can be bucked out between the photo-multiplier tube and the galvanometer so that the absorption line depth can be measured on as high a sensitivity range as necessary, up to the full sensitivity of the photo-cell circuit. However, this requires that the continuum and bucking out current be exceedingly steady, i.e., there must be no noise in the frequency range 0 to 0.5 c.p.s. passed by the galvanometer.

To observe lines in absorption, the brightness temperature of the continuous source must be considerably higher than the temperature of the furnace. For a furnace temperature of about 2800°K, which is required to vaporize sufficient iron and to populate appreciably the upper energy levels, a lamp of brightness temperature greater than 3100°K is required. An extensive search for a source of continuous radiation of very high brightness temperature and extreme steadiness was unsuccessful. Therefore, the measurements described here were made on emission lines.

PROCEDURE AND EXPERIMENTAL RESULTS

With the photo-multiplier tube the intensities of all iron emission lines in a short region of the spectrum

TABLE I. Measured f-values of iron lines.

λ	Transition	gf	f	No obs.	Notes
4219.364	$a^1H_5-y^3I_6^0$	25800.	4.34×10^{-1}	4	
4222.219	$z^7D_3^0-e^7D_3$	1320.	3.48×10^{-2}	6	
4227.434	$z^5F_5^0-e^5G_6$	22300.	3.75×10^{-1}	4	
4231.525	$a^3D_3-v^3G_3^0$	11000.	2.90×10^{-1}	1	
4232.732	$a^5D_1-z^7P_2^0$	0.231	1.42×10^{-5}	7	
4233.608	$z^7D_1^0-e^7D_2$	2790.	1.72×10^{-1}	7	
4235.942	$z^7D_4^0-e^7D_4$	4620.	9.48×10^{-2}	7	
4238.816	$z^5F_3^0-e^5G_4$	11100.	2.95×10^{-1}	1	
4239.847	$a^5F_2-z^3F_3^0$ $a^3G_5-y^3G_5^0$	2.57	6.79×10^{-5}	2	1
4247.432	$z^5F_4^0-e^5G_5$	9880.	2.03×10^{-1}	6	
4248.228	$c^3P_1-x^3P_2^0$	4640.	2.86×10^{-1}	3	
4250.125	$z^7D_2^0-e^7D_3$	3190.	1.18×10^{-1}	12	
4260.479	$z^7D_5^0-e^7D_5$	8130.	1.37×10^{-1}	25	
4271.159	$z^7D_3^0-e^7D_4$	4180.	1.11×10^{-1}	14	
4282.406	$a^5P_3-z^5S_2^0$	2280.	6.03×10^{-2}	10	
4299.242	$z^7D_4^0-e^7D_5$ $(b^3H_5-y^3H_5^0)$	2120.	4.35×10^{-2}	9	1
4430.618	$a^5P_1-x^5D_0^0$	22.2	1.37×10^{-3}	1	2
4435.151	$a^5D_2-z^7F_1^0$	0.575	2.13×10^{-5}	14	
4442.343	$a^5P_2-x^5D_2^0$	644.	2.38×10^{-2}	5	
4443.197	$b^3P_0-x^3D_1^0$	12570.	2.32	7	2
4445.48	$a^5D_2-z^7F_2^0$	0.133	4.92×10^{-6}	5	2
4447.722	$a^5P_1-x^5D_1^0$	709.	4.37×10^{-2}	4	
4450.320	$c^3P_0-y^3S_1^0$	29600.	5.48	7	2
4454.383	$b^3P_2-x^3D_2^0$	2470.	9.13×10^{-2}	1	
4459.121	$a^5P_3-x^5D_3^0$	1070.	2.83×10^{-2}	15	
4466.554	$b^3P_2-x^3D_3^0$ $a^5D_1-z^7F_0^0$	0.978	3.62×10^{-5}	12	1
4476.021	$b^3P_1-x^3D_2^0$	2500.	1.54×10^{-1}	6	
4494.568	$a^5P_2-x^5D_3^0$	1240.	4.60×10^{-2}	18	
4528.619	$a^5P_3-x^5D_4^0$	2100.	5.55×10^{-2}	7	
4531.152	$a^3F_4-y^5F_4^0$	96.4	1.98×10^{-3}	7	
5191.460	$z^7P_2^0-e^7D_1$	2460.	9.10×10^{-2}	7	
5192.350	$z^7P_3^0-e^7D_3$	3610.	9.53×10^{-2}	24	
5194.943	$a^3F_3-z^3F_3^0$	52.2	1.38×10^{-3}	12	
5202.339	$a^5P_2-y^5P_3^0$	105.	2.76×10^{-3}	4	
5216.278	$a^3F_2-z^3F_2^0$	53.8	1.99×10^{-3}	14	
5225.531	$a^5D_1-z^7D_1^0$	0.0966	5.96×10^{-6}	15	
5232.946	$z^7P_4^0-e^7D_5$	5250.	1.08×10^{-1}	27	
5247.065	$a^5D_2-z^7D_2^0$	0.0589	2.18×10^{-6}	5	
5250.211	$a^5D_0-z^7D_1^0$	0.0693	1.28×10^{-5}	5	
5250.650	$a^5P_2-y^5P_3^0$	61.1	2.26×10^{-3}	4	
5254.956	$a^5D_1-z^7D_2^0$ $(b^1D_2-y^1F_3^0)$	0.105	6.47×10^{-6}	4	1
5266.562	$z^7P_3^0-e^7D_4$	2550.	6.73×10^{-2}	4	
5307.365	$a^3F_2-z^3F_3^0$	8.00	2.96×10^{-4}	4	
5324.185	$z^5D_4^0-e^5D_4$	7150.	1.47×10^{-1}	5	
5328.534	$a^3F_3-z^3D_3^0$	99.2	2.62×10^{-3}	8	
5332.903	$a^3F_3-z^3F_4^0$	10.9	2.88×10^{-4}	6	
5341.026	$a^3F_2-z^3D_2^0$	79.7	2.95×10^{-3}	5	

[1] Two possible identifications.
[2] These lines consistently off the solar and stellar curves of growth.

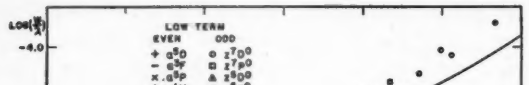

FIG. 1. Solar curve of growth.

were measured in rapid succession. Observations of the furnace temperature were made with an optical pyrometer at frequent intervals during a run. Relative f-values of the lines were derived from the intensity measurements. In each region a high energy level line was selected as a standard and the f-values of other lines were determined relative to this. Measurements on the standard line were usually made twice as frequently as other lines. A plot of these and of the furnace temperature as a function of time permitted the f-values to be corrected for changing furnace conditions. At least one line whose f-value was known from King's work was included in each region. The new values, first of the unknown standard line and then of the others, were found relative to King's values.

The results are given in Table I. In Column 3 are listed the relative gf-values obtained from the emission intensity measurements. These gf-values are on the same arbitrary scale as those of King and King.[6] It should be noted that the f-value observed in emission is equal to the ratio (g lower state/g upper state) times the f-value observed in absorption. The values tabulated in Column 4 are values of f-absorption on the absolute scale determined by King.[7] The accuracy of the f-values varies from line to line between 3 percent and 15 percent.

APPLICATIONS OF RESULTS

The measured f-values were used to plot a curve of growth (Fig. 1) for lines of Fe I in the solar atmosphere. A curve of growth is the functional relationship between the *total absorption* or *equivalent width* of lines absorbed by a layer of gas and the number of atoms active in absorbing the lines.* The solar equivalent widths, W, for all lines plotted in Fig. 1 were taken from C. W. Allen's tables[9] determined from the central intensities. The abscissa scale, $\log X$, is an abbreviation for $\log(gf\lambda e^{-E/kT})$. An excitation temperature of 4850°K[10] was used. The solid line shown is the curve given by K. O. Wright[10] based on the laboratory gf-values of King for Fe I and Ti I, and solar equivalent widths measured by Allen. It should be noted that all of King's values are for lines of low excitation potential whose low terms have even parity.

The new points extend down the curve almost onto the linear portion. King's Fe I values lie on the damping and upper Doppler part of the curve entirely. The lower half of the solid curve was determined by Wright from King's Ti I points fitted onto the iron points used to form the upper, or damping, part of the curve. The general fit of the new points onto Wright's composite curve is reasonably good.

The symbols used in Figs. 1 and 2 distinguish lines whose low terms have odd parity from those whose low terms have even parity. A closed symbol (i.e., one enclosing an area) represents a line whose low term is odd; an open symbol one whose low term is even. Examination of Fig. 1 shows that the new measurements for low level lines generally agree within the accuracy of the observations with Wright's curve. However, the new high level lines diverge from this curve very considerably and in systematic ways. The lines whose low terms have odd parity lie above Wright's curve, and those whose low terms have even parity lie below it. The higher the excitation potential the greater is the deviation. If the equivalent width as determined from the line's contour (tabulated in Allen for some, but not all, of the lines) was used instead of the equivalent width derived from the central intensity, a slightly greater odd-even difference was noticed. Extensive tests on the furnace and several independent checks showed the deviations to be due to effects in the sun.

Selective pressure broadening of solar absorption lines would appear as lateral displacements in the uppermost, damping, part of the curve of growth. Greater pressure broadening contributes to a higher damping constant. Consequently no pressure effects should appear on the linear or truly Doppler portions. This means that the points lying above the curve (odd low term) could be attributed to greater pressure broadening. Likewise those points from even low terms lying below Wright's curve of growth, but above the curve of growth for zero damping, could be explained by smaller pressure effects. If the differences are due to pressure effects, this might mean that there is a larger interaction (i.e., larger perturbation of states) when the two colliding atoms are of opposite parity, since most of an iron atom's neighbors would be in states of even parity. The large majority of the atoms found in stellar atmospheres are in states of even parity because the ground state of most of the elements and all the states of Fe I and Fe II up to 2.4 volts are even states.

Another tentative explanation of the larger solar equivalent widths of the lines with low term odd is a departure from thermal equilibrium in the solar atmosphere. Then the population of the odd states could be greater than that predicted by the Boltzmann equation. One mechanism might be the preferential population of

* The curve of growth for stellar atmospheres has been described in detail elsewhere [see A. Unsold (reference 3), and K. O. Wright (reference 10)].

[9] C. W. Allen, Commonwealth Solar Observatory, Memoir No. 5, parts 1 and 2 (1934).

[10] K. O. Wright, Pub. Dominion Astrophysical Observatory, 8, No. 1 (1948).

these states in the formation of Fe I by recombination of an electron and an Fe II ion. There is much more ionized iron than neutral iron in the sun's atmosphere. All the low terms of Fe II are of even parity, so if the electron is captured in an *s* wave the combination results in an even state. Then since the energy is probably given off by dipole radiation, the neutral atom is left in an odd state.

The fact that the solar atmosphere is not in strict thermal equilibrium has been discussed by R. v. d. R. Wooley.[11] One reason for this condition is that the atmosphere is bathed in radiation of a higher temperature than its own local temperature and from one side only.

In order to throw more light on the subject, several independent sources of information were considered. In Allen's catalogue of solar equivalent widths are 142 iron lines for which the equivalent widths were determined from contours (W_e) as well as from central intensities (W_r). By forming the ratio (W_e-W_r/W_r), a measure of each line's sharpness was obtained. The average value of this ratio for all the iron lines with odd low term is +0.062, and for all the iron lines with even low term +0.0058. This means that the iron lines from odd low terms are wider for the same central intensity than Allen's average for solar lines of all elements while iron lines from even low term are about the same width as the average line. It is generally true in iron that the even states have lower excitation than the odd states, so this correlation could almost be reduced to the previously known fact[9] that the lower energy states are sharper than the higher. Nevertheless in the region of overlap (2.4 to 3.0 volts), there is still a systematic difference between lines from odd and even terms.

A second independent verification of the reality of the odd-even differences was found in H. D. Babcock's measurements of the pressure shifts of iron lines.[12] Babcock measured the pressure shift due to one atmosphere air pressure of iron lines excited in an arc. If a line's wave-length is shifted by pressure, certainly the line has been broadened considerably also. Babcock computes the pressure depression of each term and finds that the curve of term depression *vs.* excitation potential follows a second degree parabolic equation. The pressure shift of a line is the difference of the shifts of the upper and lower states, but the pressure width of a line is the sum of the pressure widths of the two terms. Hence the pressure width of a line should increase more rapidly with excitation potential than the pressure shift. Separation of the 138 lines in Babcock's data according to excitation potential and odd or even low term, gives the results shown in Table II. The average pressure shift in 10^{-3} cm^{-1} for each group is shown first, followed in parentheses by the number of lines in each group. Here it is evident that in the energy level regions where both odd and even terms occur, there is a difference in behavior between the odd and even states. To illustrate the small dispersion of pressure shifts within any one group, the average deviation of the shift of a single line from the value given in Table II in the group 2.2 to 3.4 volts odd low term is 2.9×10^{-3} cm^{-1}, and of the same excitation potential but even low term is 1.8×10^{-3} cm^{-1}. In 3.4–4.7 volt odd group there are included two multiplets with consistently small shifts. They are $z^5G^0-e^5H$ and $z^3G^0-e^3H$. The average shift of the 9 lines involved is 7.9×10^{-3}, whereas the average shift of the rest of that group is 23.6×10^{-3} cm^{-1}. The average shift of all the odd lines except the 2 discordant multiplets is 22.98 $\pm0.08\times10^{-3}$ cm^{-1}.

TABLE II. Average pressure shifts of lines of Fe I (Babcock).

E.P. (volts)	0–1.0	1.0–2.2	2.2–3.4	3.4–4.7
Odd	*	*	22.7 (41)	18.0 (25)
Even	7.6 (23)	10.5 (24)	10.3 (16)	11. (1)

* There are no odd terms below 2.4 volts.

The most conclusive proof that the deviations of the points on the solar curve of growth are due to solar causes was found when the same laboratory data were applied to the giant stars γ-Cygni and α-Persei. The equivalent widths of the stellar lines were kindly supplied by K. O. Wright in advance of publication. The curve of growth for γ-Cygni is shown in Fig. 2. Here the points lie very consistently on a single curve and no odd-even difference appears. γ-Cygni is a giant star of spectral type *cF7*, very close to the sun's *dG2*. In constructing the curve of growth, an excitation temperature of 4850°K[10] was adopted, as for the sun. The major difference is that γ-Cygni is a giant while the sun is a dwarf. Consequently the atmosphere of γ-Cygni has a much lower pressure than that of the sun. All the points fall on the Doppler portion of γ-Cygni's curve of growth, where pressure effects would not be seen if it is still a true Doppler region. No damping or pressure portion of the curve has been observed so far. The solid line is Wright's curve[10] based on King's *f*-values for low level, even term Fe I lines. The consistency of the points in Fig. 2 tends to confirm the accuracy of both Wright's measurements of equivalent widths and the laboratory *f*-values.

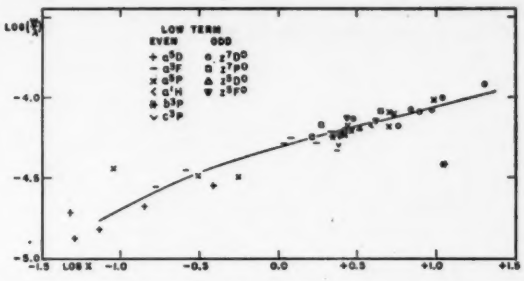

FIG. 2. Curve of growth for γ-Cygni.

[11] R. v. d. R. Wooley, M.N.R.A.S. **94**, 631 (1934).
[12] H. D. Babcock, Astrophys. J. **67**, 240 (1928).

The curve of growth for Fe I for α-Persei was also plotted using the furnace f-values and Wright's equivalent widths. α-Persei is a giant star of spectral type $cF4$ and excitation temperature about 5100°K,[10] and hence differs from the sun slightly more than γ-Cygni. The scatter of points is slightly greater than for γ-Cygni, but less than that for the sun, and no systematic difference between lines from odd and even low terms is apparent.

Since the only previously known f-values for Fe I were those of King for the low energy level lines, it has been the practice to use Wright's solar curve of growth to obtain additional iron f-values. The common procedure is to measure the solar equivalent width of some line in the Utrecht Atlas,[13] or to use Allen's tabulated value, and then from the solar curve of growth read off the value of $\log X$ for the line. Since all the other quantities involved in X are at least approximately known, the relative f-values can be derived. The atmospheres of several stars have been studied with the aid of these solar f-values. Examples are Wright's[10] and Sahade and Cesco's[14] curves of growth for γ-Cygni, and Th. Walraven's curve for δ-Cephei.[15] However, if real systematic deviations of individual lines from the solar curve exist, then this method obviously is open to serious question. The deviations that exist in the sun will be superposed, in inverse position, on the stellar curves of growth. This is strikingly illustrated by a comparison of the published curves for γ-Cygni of Wright and of Sahade and Cesco with Fig. 2, which shows that the scatter of points is very greatly reduced when the furnace f-values are used. The points on Walraven's curve of growth for the Cepheid type variable star δ-Cephei not only have large dispersion, but they also reflect the systematic deviations found by the present writer in the solar curve of growth. These deviations, as would be expected, are in the opposite sense from those observed in the sun. Walraven himself remarks that lines with low term odd seem to lie consistently below those with low term even! This appears to be the only instance in which this effect has been previously noted.

New curves of growth were plotted for the variable star δ-Cephei using Walraven's equivalent widths and the new furnace f-values. One curve was made for observations near maximum phase, and another for minimum phase. There is a general shift of the curves between maximum and minimum (discussed by Walraven), and also a smaller scatter of points for minimum phase. Although the points for both maximum and minimum phases appear to lie on the Doppler part of the curve of growth, it seems possible that the greater scatter at maximum might be due to selective pressure broadening. Evidence that the pressure in the atmosphere of the variable star is greatest at maximum phase is given by Walraven and also by M. Schwarzschild.[16]

The results described above indicate that the solar curve of growth does not provide a reliable standard from which to obtain new f-values. They also indicate that it would be preferable to use the atmosphere of a giant star such as γ-Cygni for this purpose. This would require an extensive catalogue of stellar equivalent widths, but Wright's table for γ-Cygni, which contains about 800 lines, is a good start. If the deviations in the sun are indeed due to pressure effects, then the phenomenon should provide a tool for the study of pressures in other stellar atmospheres. That the pressure effect will also be dependent on the excitation potential as well as on the odd or even nature of the low term is understandable from Babcock's pressure shift data. The odd-even differences have no theoretical explanation as yet. In addition, Dr. R. Minkowski has pointed out that pressure broadening is commonly explained as a Stark effect,[17] and that Stark effect is not dependent on the parity of the states. If the odd-even differences are due to pressure influences, as the evidence indicates, then perhaps the mechanisms of pressure broadening should be reconsidered.

ACKNOWLEDGMENTS

I wish to express my grateful appreciation to Professor R. B. King, who suggested this problem and guided the work to completion. The work was done in the laboratory of the Mt. Wilson Observatory, whose facilities were generously made available to me. Dr. K. O. Wright of the Dominion Astrophysical Observatory, Victoria, B.C., kindly provided me with prepublication lists of equivalent widths of lines in γ-Cygni and α-Persei.

[13] Minneart, Mulders, and Houtgast, *Photometric Atlas of the Solar Spectrum* (Schnabel, Kampert, and Helm, Amsterdam, 1940).
[14] Sahade and Cesco, Astrophys. J. **104**, 133 (1946).
[15] Th. Walraven, Pub. of The Astronomical Institute of the University of Amsterdam, No. 8 (1948).
[16] Schwarzschild, Schwarzschild, and Adams, Astrophys. J. **108**, 207 (1948).
[17] A. Unsold, Zeits. f. Astrophys. **12**, 56 (1936).

A New Method of Analysis of the Beta-Ray Spectrum

MITSUO SAKAI AND SEITARO NAKAMURA
Department of Physics, University of Tokyo, Tokyo, Japan
(Received June 8, 1949)

A new method of analysis is developed for taking into account the beta-ray spectrum as a whole. Stress is layed on the point of maximum intensity of the spectrum, rather than the lower or the upper end. Tentative conclusions drawn by this method are as follows: (1) Experimental spectra now available show some deviations from Fermi theory which should be considered as a standard reference. (2) These deviations are found to manifest a certain tendency without any distinction between the allowed and the forbidden transitions. (3) These deviations tend to increase with the atomic number of the elements and are hardly related to the upper end of the spectrum. Hence, the forbidden correction factors are not likely to explain these deviations. A possible elucidation is discussed which is due to the Coulomb effect.

I. THE POINT OF MAXIMUM INTENSITY

SINCE the measurement of the Cu^{64} beta-ray spectrum, which was given by Backus,[1] presented a serious problem concerning the deviation from Fermi theory at the lower energy end of the spectrum, detailed attacks have been carried out on this problem with refined tools, both experimental and theoretical. In these discussions the drifts of the spectrum near the lower energy end were matters of first considerations. Great care has been taken for eliminating experimental errors in spite of weakness of the intensity in this energy region. The relativistic and the screening effects for the electron wave were successfully taken into account to explain the net drift at the lower energy end, at least in the case of Cu^{64}. However, the shape of the beta-ray spectrum as a whole, which should be essential to the fate of the theory, has been passed over. In this paper the shift of the point at maximum intensity of the spectrum is adopted as a measure of analysis of the beta-ray. Original shape of the spectrum is used for comparison with Fermi theory, in place of Kurie plot.

As is well known, the predicted number of the electrons per unit momentum per second is given by Fermi as follows:

$$Nd\eta = MC(Z,\eta,\eta_0)F(Z,\eta)P(\eta,\eta_0)d\eta, \qquad (1)$$

where η, η_0 are the momentum of the electron or its upper limit, respectively; $C(Z,\eta,\eta_0)$ is the correction factor which, in the case of the forbidden transitions, contributes to the shape of the spectrum and was precisely given by Konopinski and Uhlenbeck.[2] M involves the coupling constant of the beta-decay and the nuclear matrix elements which are considered to have little bearing on the spectrum. $F(Z,\eta)$ is a Coulomb factor, which will be discussed later. P is a statistical factor and is given as follows:

$$P=\eta^2\{(1+\eta_0^2)^{\frac{1}{2}}-\langle 1+\eta^2\rangle_{Av}\}^{2n}, \qquad (2)$$

where n is equal to 1 or 2, according to the case of the original Fermi theory or to the modified theory of Konopinski and Uhlenbeck. Thus, if we denote by η_{max} the value of η which corresponds to the maximum value of P, a simple calculation yields from (2):

$$\eta_{max}=\tfrac{1}{8}([(\eta_0^2+1)(\eta_0^2+9)]^{\frac{1}{2}}+\eta_0^2-3)^{\frac{1}{2}}\text{(Fermi)}, \qquad (3)$$

$$\eta_{max}=\tfrac{1}{8}([(\eta_0^2+1)(\eta_0^2+25)]^{\frac{1}{2}}+\eta_0^2-5)^{\frac{1}{2}}\text{(K.U.)}, \qquad (4)$$

Here η_{max} is given by the function of η_0 only. On the other hand, the value of η at the maximum point of the curve N/F, which is presented by the experimental spectrum divided by the computed Fermi function $F(Z,\eta)$, will be determined for every beta-ray emitter. We shall designate this η by $\eta_{max\ obs.}$ $\eta_{max}-\eta_{max\ obs}$ in each case can be considered as a measure of Fermi theory concerning the spectrum as a whole, with reference to the allowed shape. This method of analysis is almost free from various experimental error, since the intensity of the particles in question is apparently strong which makes the measurement less ambiguous.

II. ANALYSIS OF EXPERIMENTAL SPECTRA

In response to the technical advance in the measurements more reliable data have recently become available which have succeeded in eliminating the scattering and absorption of the particles or in decreasing the thickness of sources. Still the number of available data seems to be rather meager to attain decisive conclusions. Al-

TABLE I. Experimental spectra used for our analysis.

Elements	Grouping of transitions	Authors	Papers
C^{14}	2 *A*	Cook and Langer	Phys. Rev. **74**, 548 (1948)
Na_1^{24}	1 *A*	Lawson	Phys. Rev. **56**, 131 (1939)
Na_2^{24}	1 *A*	Siegbahn	Phys. Rev. **70**, 127 (1946)
P_I^{32}	2 *A*	Lawson	Phys. Rev. **56**, 131 (1939)
P_{II}^{32}	2 *A*	Siegbahn	Phys. Rev. **74**, 548 (1948)
S^{35}	0 *A*	Cook and Langer	Phys. Rev. **70**, 127 (1946)
$Cu^{64}(+)$	0 *B*	Cook and Langer	Phys. Rev. **73**, 601 (1948)
$Cu^{64}(-)$	0 *B*	Cook and Langer	Phys. Rev. **73**, 601 (1948)
In^{114}	0 *B*	Lawson	Phys. Rev. **57**, 982 (1940)
I^{128}	1 *B*	Siegbahn and Hoyle	Phys. Rev. **70**, 133 (1946)
RaE	1 *C*	Neary	Proc. Roy. Soc. **175**, 71 (1940)
RaE	1 *C*	Flammersfeld	Zeits. f. Physik **112**, 727 (1939)

[1] J. Backus, Phys. Rev. **68**, 59 (1945).
[2] E. J. Konopinski and G. E. Uhlenbeck, Phys. Rev. **60**, 308 (1941).

TABLE II. The average energies of the recoil nucleus.

Elements	Grouping of transitions	E_{max}	$\langle PR^2\rangle/P^2_{max}$	Authors
Li^8	1 *A*	12 Mev	0.600	Christy *et. al.*, Phys. Rev. **72**, 698 (1947)
Kr^{88}	1 *B*	2.4 Mev	0.565	Jacobsen and Kofoed-Hansen, Phys. Rev. **73**, 216 (1948)
P^{32}	2 *A*	1.7 Mev	0.32	Scherwin, Phys. Rev. **73**, 216 (1948)
Y^{90}	2 *B*	2.16 Mev	0.35	Scherwin, Phys. Rev. **73**, 1173 (1948)

though a criticism of reliability of the data should be done in advance, we shall tentatively call attention to the following data given in Table I. In the column, "Grouping of Transitions," 0, 1, 2, means the allowed, the first, and the second forbidden transitions, respectively, and *A*, *B*, *C*, the light, middle, and heavy elements, respectively, which were classified by Konopinski.[3] $\eta_{max\ obs}$ given in these data are plotted in Fig. 1 where η_{max} in (3) and (4) are also shown as functions of η_0. It will be evident that almost every point of $\eta_{max\ obs}$ clusters along the Fermi line of η_{max}, and not with the K.U. line. This result speaks strongly against K.U. theory and in favor of the original Fermi theory, which is in accordance with the current discussions.

Further, it may be argued that the drift of the points from the Fermi line, which is now taken as a standard reference, becomes more noticeable for the elements of higher atomic number. For instance, the drifts of the lighter elements, such as P^{32}, Cu^{64}, Na^{24}, and C^{14}, are apparently exceeded by those of the heavier elements, such as RaE, I^{128}, and In^{114}, as is shown in Fig. 1.

In order to make the nature of this tendency of the drifts more concrete, we define the deviation factor of the beta-ray spectrum by the following formula,

$$\delta=(\eta_{max}-\eta_{max\ obs})/\eta_{max}. \tag{5}$$

In Fig. 2 the values of δ indicated by the percentages as a function of Z are shown. In the $(N/F-\eta)$ diagram,

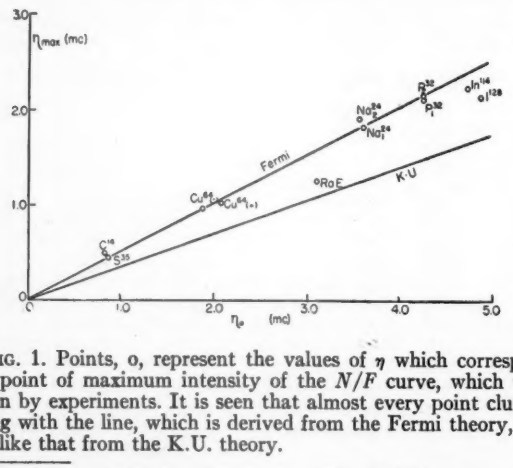

FIG. 1. Points, o, represent the values of η which correspond the point of maximum intensity of the N/F curve, which were given by experiments. It is seen that almost every point clusters along with the line, which is derived from the Fermi theory, and not like that from the K.U. theory.

[3] E. J. Konopinski, Rev. Mod. Phys. **15**, 209 (1943).

the point of maximum intensity in each case is determined by the following method: Firstly, two lines are drawn parallel to the η-axis near the summit of the curve at about 90 percent of its height; secondly, the centers of the two intercepts of these two lines with the curve are lined and stretched to meet the curve at a point which is required. As mentioned above, it is generally claimed that the measurements are more reliable in the vicinity of the summit of the spectrum, since either the value of the energy or the intensity of the particles is greater in almost every case, however, differences are seen between each author, such as in the case of P_1^{32} and P_2^{32}, or Na_1^{24} and Na_2^{24}. On the basis of present data (Fig. 2), the deviation factors, δ, are roughly considered to increase with the atomic number of the elements. This consideration is rather striking, since this tendency is confirmed either in the case of the allowed or of the forbidden transitions, and what is more, correlations are hardly found between δ and η_0. The latter discussion seems to be at variance with the current theory of the forbidden transitions, where the correction factors depend generally upon η_0, as was given by Konopinski and Uhlenbeck.[2]

III. DISCUSSIONS

The deviation of the point of the maximum intensity of the spectrum from the prediction of Fermi theory should essentially be attributable to the following three considerations:[4]

(1) The modification of the Coulomb correction factor to include the effects of screening by atomic electrons.

(2) The relativistic effect for the electron wave, which is defined as the refinements of Fermi function from Nordheim Yost's approximation.

(3) The correction factors of the forbidden transitions.

Firstly, the screening effects are found to make no appreciable change in the point of maximum intensity of the spectrum. This is easily seen from calculations of

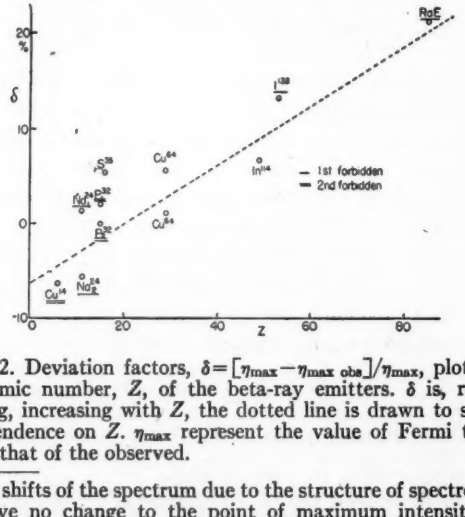

FIG. 2. Deviation factors, $\delta=[\eta_{max}-\eta_{max\ obs}]/\eta_{max}$, plotted to the atomic number, Z, of the beta-ray emitters. δ is, roughly speaking, increasing with Z, the dotted line is drawn to suggest its dependence on Z. η_{max} represent the value of Fermi theory, $\eta_{max\ obs}$ that of the observed.

[4] The shifts of the spectrum due to the structure of spectrometer used give no change to the point of maximum intensity. See G. E. Owen and H. Primakoff, Phys. Rev. **74**, 1406 (1948).

C. Longmire and H. Brown,[5] and independently by M Kotani and K. Tomita.[6] In fact, the screening correction for the electron spectrum of RaE is only 1.8 percent at 500 kev; for the positron spectrum of Cu^{64}, 0.1 percent; and for the electron spectrum of Cu^{64}, negligible.

Secondly, the effect of the relativistic treatment for the electron wave, which was given by Bethe and Bacher, is expressed by the factor $(d^2+\frac{1}{4})^{s-1}$ in the following formula:[7]

$$F(Z,\eta)=F_N(Z,\eta)(d^2+\tfrac{1}{4})^{s-1} \qquad (6)$$

where

$$S=(1-\gamma^2)^{\frac{1}{2}}, \quad d=_N(1+\eta^2)^{\frac{1}{2}}/\eta, \quad \gamma=Z/137.$$

Longmire and Brown have tabulated $(d^2+\frac{1}{4})^{s-1}$ for the case of S^{35}, Cu^{64}, and RaE. One can roughly estimate the drift of the point of maximum intensity of the spectrum due to the relativistic correction by means of their table; thus δ should be changed by 0.5 percent for RaE, 0.4 percent for Cu^{64}, and 0.6 percent for S^{35}, if one takes into account the factor of $(d^2+\frac{1}{4})^{s-1}$. Therefore, the screening effects and the relativistic effects are both insufficient to explain the shifts of the maximum points.

Thirdly, the forbidden correction factors are known to be effective for the change of the shape of the spectrum as a whole. In order to know the contributions exactly, the values of the nuclear matrix elements are to be determined in advance.[8] On the basis of Fig. 2 the shift of Cu^{64} is apparently outstripped by that of In^{114}. The difference between them cannot be explained by the forbidden correction, because both electron activities belong to the allowed transitions. On the other hand, the shifts of the experimental maximum points show, roughly speaking, a linear dependence on Z, almost masking a dependence on η_0. This fact, also, seems to be at variance with the forbidden theory, since the latter predicts, in general, correction factors which depend on η_0, as well as on Z. One more correction factor dependent exclusively on Z may certainly be needed, if the above discrepancy of the theory could be established.

The difficulties of the Fermi theory have appeared thus far in the analysis of the selection rule for the long-lived decay of C^{14}, of the forbidden spectrum of Be^{10}. We shall add another example to this problem. The average energy of the recoil nucleus calculated by Kofoed-Hansen[9] showed different dependence at the upper end of the beta-ray energy, in response to the different interaction type and different degree of transitions. On the other hand, the average energy of the recoil nucleus can be deduced from the measurements of Li^8, Kr^{88}, P^{32}, and Y^{80}.[10] (See Table II.) The results are indicated with those of the theoretical values in Fig. 3. Here almost every point given by these experiments lies along the allowed lines, in spite of their forbidden life times. This fact again speaks against the forbidden theory. If we take into account that there is included a branching process of transmuting into the excited state of Rb^{88} emitting a gamma-ray in the beta-decay of Kr^{88}, the actual average energy will be less than that estimated above.[9] This is in agreement with our discussions. Of course, it may be a hazardous step to derive the average energy from Scherwin's experiment. Nevertheless it is certain that the above value in Table II is not underestimated, since the low momentum particles will partly be missed in his experiment.

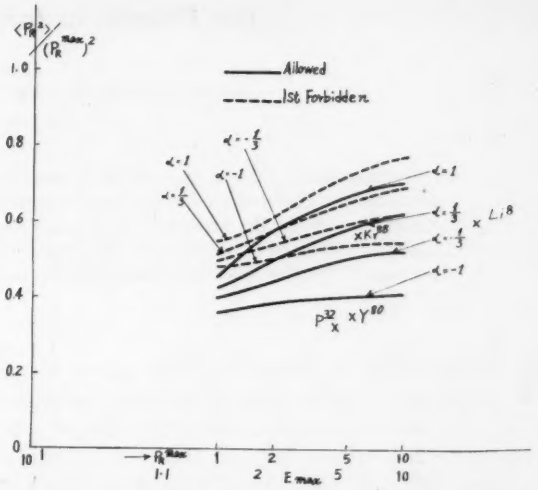

FIG. 3. Comparison of the average momentum of the recoil nucleus which was observed, with that which is given by the Fermi theory; it is noticeable that the observed values belong to within the allowed lines in spite of their forbidden life times.

Finally, we should like to suggest that, in analyzing the beta-ray spectrum, original shapes are to be presented with Kurie plot, which makes the comparison between theory and experiments, with regard to the point of maximum intensity of the spectrum, feasible. It seems to us that our method of analysis may offer a new tool, which is an advancement over the current method with respect to easy and accurate measurements.

[5] C. Longmire and H. Brown, Phys. Rev. **75**, 264 (1948); **75**, 1102 (1948).

[6] M. Kotani and K. Tomita, Lecture at the Annual Meeting on May 1949 of the Phys. Soc. of Japan.

[7] We have used as Fermi function the following expression, $F_N(Z,\eta)=[2\pi d/1-\exp(-2\pi d)]$, in calculating N/F. This is recognized as a non-relativistic approximation, which should be modified by the relativistic correction, $(d^2+\frac{1}{4})^{s-1}$.

[8] The interesting spectrum of Y^{91}, where a unique shape is predicted, differing from the allowed shape by the factor, $a\sim\{(\eta_0^2+1)^{\frac{1}{2}}-(\eta^2+1)^{\frac{1}{2}}\}^2+\eta^2$, is very important. It is keenly interesting to study the original shape of Y^{91} spectrum whether or not its maximum point drifts from the N/F curve. See L. M. Langer and H. C. Price, J. Phys. Rev. **75**, 1109 (1949).

[9] O. Kofoed-Hansen, Phys. Rev. **74**, 1785 (1948).

[10] Jacobsen and Koefoed-Hansen, Phys. Rev. **73**, 675 (1948).

The Process of Ionization in Active Nitrogen

K. T. CHAO AND H. P. CHANG
Department of Physics, National Peking University, Peiping, China
(Received June 20, 1949)

Average energy and concentration of electrons along the axis of a nitrogen afterglow tube have been measured by means of a movable Langmuir probe. Electrons with energies of more than 20 volts have been found throughout the afterglow. The experimental curves of potential and electron density distribution could be explained by solving the diffusion equation. It is shown that a part of the ions in the afterglow is produced by the collision of fast electrons with N_2 molecules.

ACCORDING to Mitra's theory,[1] active nitrogen consists of positive ions of nitrogen molecules in the $N_2^+(X')$ state. Because of the absorption of a layer of nitrogen molecules or atoms, the walls of the containing vessel are so conditioned that they have a very high reflection coefficient for electrons and ions. The long-life of the nitrogen afterglow is ascribed to the slow process of three-body recombination in the volume of the gas. It is as follows,

$$N_2^+(X')+e+N_2 \rightarrow N_2(B)+N_2(A),$$

which explains the emission of the characteristic spectrum of the Lewis-Rayleigh afterglow and some features of the Kaplan afterglow, as recently reported.[2] The source of ionization in the afterglow is, however, still not clear. The experiments of Rayleigh[3] show that the ionization is not produced either by the bombardment of any metallic surfaces by the active nitrogen particles or by the photoelectric emission in the volume of the gas. The present note is a report of some experiments to show that the ionization in the afterglow is produced in the gas partly by the collision of fast electrons with N_2 molecules, and is derived partly from the main discharge into the observation vessel through ambipolar diffusion.

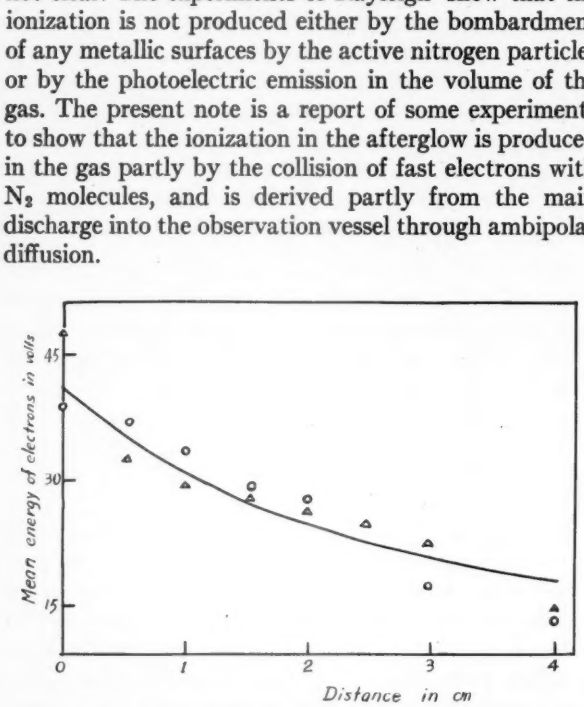

FIG. 1. Mean energy of electrons along afterglow tube. Voltage across discharge tube, 635 volts. Discharge current, 2.7 ma. Gas pressure, 0.48 mm Hg.

[1] S. K. Mitra, *Active Nitrogen—A New Theory* (Indian Association for the Cultivation of Science, Calcutta, 1945).
[2] S. K. Mitra, Phys. Rev. 74, 1637 (1948).
[3] Lord Rayleigh, Proc. Roy. Soc. A180, 123 (1942).

In a cylindrical discharge tube with plane parallel disk electrodes, a side tube of the same diameter as the latter was fixed perpendicularly onto the main tube near the cathode. When a d.c. potential of about 600 volts was applied across the tube with a gas pressure of pure nitrogen of 0.5 mm Hg, the glowing gas was observed to extend a considerable distance into the side afterglow tube.

By means of a movable cylindrical probe mounted along the axis of the afterglow tube, the mean kinetic energy of electrons has been measured from the center of the main tube to 4 cm in the afterglow tube. The result is shown in Fig. 1. One notices that the electrons with energies of more than 20 volts have penetrated far into the afterglow tube. These electrons are able to produce ionization and even simultaneous excitation of N_2 molecules for the emission of the first negative bands.

The potential distribution and the concentration of electrons measured along the afterglow tube are represented in Figs. 2 and 3. These results could be explained by assuming that both the positive ions and electrons are diffused into the afterglow tube from the main discharge. Within the afterglow tube the potential was found to be decreasing linearly. Since electrons diffuse much faster than ions because of their smaller mass, a decreasing potential might be created along the tube axis. If the constant electric field is E, the potential V

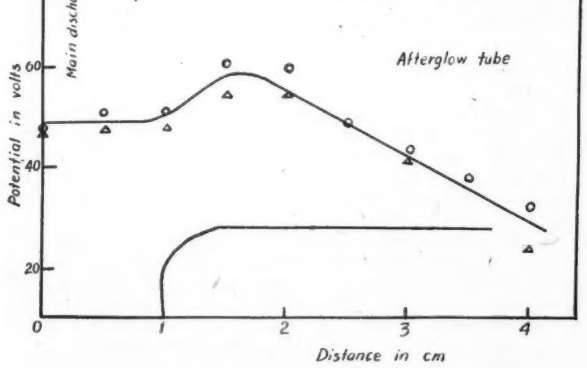

FIG. 2. Potential distribution along afterglow tube.

at any position z along the tube axis can be expressed as $V=V_0-Ez$, where V_0 is the value of V at $z=0$.

The distribution of electrons along the tube in Fig. 3 could be obtained by considering the solution of the following diffusion equation for the electron concentration n,

$$D_a \text{ div grad} n+qn=0.$$

In this equation q is the number of electrons produced per sec. per unit volume due to ionization by collision of each fast electron in the volume of the gas. D_a, the coefficient of ambipolar diffusion, is given by

$$D_a=(D_+b_-+D_-b_+)/(b_++b_-),$$

where D_-, b_- are the diffusion coefficient and mobility of electrons, respectively, and D_+, b_+ those for positive ions. If cylindrical coordinates are used, the equation can be solved subject to the condition that in the steady state the diffusion current along the axis of the tube is equal to that due to drift. The result obtained is given as

$$n=n_0J_0([(b_-E/D_-)^2+(q/D_a)]^{\frac{1}{2}}r)\exp(-b_-Ez/D_-),$$

where J_0 is the Bessel function of order zero and n_0 is the value of n when $z=0$ and $r=0$. A plot of log$n$ *versus* z using values from the curve in Fig. 3 gave a fair straight line, the slope of which, after division by E (from Fig. 2), gives $b_-/D_-=0.041$ volt^{-1}; but $b_-/D_-=e/kT_e$, where T_e is the electron temperature and e and k have their usual significance. Since the slope of log$n$ *versus* z plot is constant, T_e must be independent of z in the afterglow tube, which is nearly so from experiment as shown in Fig. 1. If now, from Fig. 1, the value of 25 volts is taken as the mean energy of electrons in the tube, we have $b_-/D_-=e/kT_e=0.059$ volt^{-1}, which is approximately checked with the value obtained in the other way.

The electron distribution along a radius of the afterglow tube was not measured. However, an estimate of the value of q could be made by taking measured values in the main tube. From Fig. 3 we have $n/n_0=0.24$

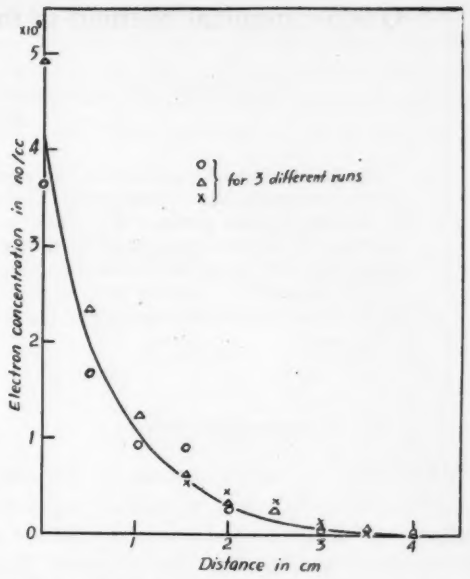

FIG. 3. Variation of electron concentration along afterglow tube.

at $r=1$ cm, the radius of the tube, and then

$$[(b_-E/D_-)^2+q/D_a]^{\frac{1}{2}}=1.9.$$

If the existing experimental value[4] $b_+=9.7\times10^2$ cm/sec./volt/cm is used, one gets $q=3.85\times10^4$ electrons produced per sec. per cc by each electron in the volume of the gas. These are probably mostly slow electrons, and they may play an important role in the process of the three-body collision, as the coefficient of recombination for fast electrons is very small according to Thomson's theory of collision.[5]

The authors wish to thank Professor Y. T. Yao, the director of the Physics Laboratory, for his constant encouragement and interest in the problem.

[4] A. v. Engel and M. Steenbeck, *Elektrische Gasentladungen* (Verlag. Julius Springer, Berlin, 1934), Vol. 1, p. 182.
[5] J. J. Thomson, Phil. Mag. **47**, 337 (1924).

Quasi-Chemical Method in the Statistical Theory of Regular Mixtures

YIN-YUAN LI*
Department of Physics, Carnegie Institute of Technology, Pittsburgh, Pennsylvania
(Received May 23, 1949)

The quasi-chemical equations in the statistics of "regular" mixtures are deduced by assuming non-interference among local configurations. This method is capable of yielding higher and higher approximations by choosing a larger group of lattice sites as the local configuration under consideration. The comparative accuracy of different approximations can be judged by a simple criterion. Further applications to ferromagnetism and to the order-disorder transition in alloys, and their results are discussed. Equations for ternary mixtures or mixtures of even more components are given. The asymmetry of solubility of one solute in two immiscible solvents and the order effect of Ag_2HgI_4 serve as the interesting examples of the ternary case.

1. INTRODUCTION

A MIXTURE containing atoms (or molecules) of two or more kinds will be called a regular one if it satisfies the following conditions: (a) All the atoms are located on a set of lattice points (or sites). Each site has the same number of nearest neighbors. (b) The kinetic energy is either separable from the potential energy, or else of no importance. And (c) the fields of force of the atoms are spherically symmetric; and the interaction energy of the whole system can be expressed as the sum of closest neighbor contributions. The latter condition implies that the interaction fields of different atoms are almost equal at distances greater than that between two nearest neighbors. The typical examples of this model are of course substitutional alloys. It may also apply to the so-called "regular" liquid mixtures (of the hypothetical scheme adopted by Hildebrand[1] and later by Guggenheim[2] and others) and liquids considered from the viewpoint of the "hole" scheme[3] in which the unoccupied sites (holes) act as atoms of one kind. Other examples are ferromagnetism, solutions of hydrogen in palladium, and monolayer (localized) surface adsorptions. The existence of unoccupied sites leaves the theory under consideration perfectly unchanged as far as condition (a) is concerned.

A statistical method proposed by Alfred and Mark[4] for binary regular mixtures may be briefly stated as follows. The configuration of the system is described by specifying the occupants of the nearest pairs whose constituent sites taken together constitute the lattice, rather than by specifying the occupants of each individual lattice site. Assuming that the configurational energy of the binary system is the sum of the interaction energy of these nearest pairs multiplied by the ratio of the total number of pairs in the binary system to that of the reference set of pairs, they obtain the combinatory factor of the partition function of the binary system by considering the permutation of the reference pairs. Their result leads to an equation similar to that of a quasi-chemical equilibrium introduced first by Guggenheim to the theory of regular solution.

Recently Miller[5] gave a critical analysis of the Alfred-Mark method. By clarifying the meaning of their assumption, he has shown that it amounts to neglecting the restriction on the allocation of the nearest pairs of different kinds (namely, *A-A*, *B-B*, and *A-B* when the atoms of different kinds are denoted as *A*'s and *B*'s). This restriction is basically inherent in the arrangements of *A* and *B* atoms on the lattice sites. In other words, Alfred and Mark have unknowingly adopted the so-called assumption of non-interference of local configurations. The term "non-interference," which was first used by Fowler and Guggenheim, comes from the fact that actually the closest pairs are interlocked, i.e., they "interfere" with each other. Fowler and Guggenheim[6] proved even earlier (1940) that their quasi-chemical equation can be deduced by using this assumption.

By using the same assumption, the present author will develop a statistical method capable of yielding successively higher approximations and accessible to regular mixtures containing more than two different kinds of atoms. His procedure can be applied with a slight complication to the problem of superstructure of alloys. The results turn out to be the set of equations first obtained by Yang and recently generalized by Li on the general quasi-chemical theory of superstructure.[7] We shall notice that the "pair" approximation (Fowler-Guggenheim, Alfred-Mark) reaches qualitatively incorrect results for lattices with nearest interactions among the first shell sites and larger local groups offer solutions. Therefore, the general theory for successive approxima-

* Now at the University of Illinois, Urbana, Illinois.
[1] J. Hildebrand, J. Am. Chem. Soc. **51**, 66 (1929).
[2] E. A. Guggenheim, Proc. Roy. Soc. **A148**, 304 (1935); G. S. Rushbrooke, Proc. Roy. Soc. **A166**, 296 (1938): Also R. H. Fowler and E. A. Guggenheim, *Statistical Thermodynamics* (Cambridge University Press, London, 1939), pp. 351–366.
[3] J. Frenkel, Trans. Faraday Soc. **33**, 58 (1937). Bresler, Acta Physicochim. U.R.S.S. **10**, 491 (1939).
[4] T. Alfred and H. Mark, J. Chem. Phys. **10**, 303 (1942). This article will be cited as TA-HM.
[5] A. R. Miller, J. Chem. Phys. **15**, 513 (1947).
[6] R. H. Fowler and E. A. Guggenheim, Proc. Roy. Soc. **A174**, 189 (1940).
[7] C. N. Yang, J. Chem. Phys. **13**, 66 (1945). C. N. Yang and Y. Y. Li, J. Chinese Phys. **7**, 59 (1947), Y. Y. Li, J. Chem. Phys. **17**, 447 (1949). These articles will be cited as Ref. I, II, and III, respectively.

tions is not only useful but very necessary if this statistical method should be good also for more tightly packed lattices.

2. STATISTICAL METHOD

Let us consider a group of sites in a lattice which is occupied by the atoms of a binary system. The whole system is conceived as a superposition of such groups, all of identical form. Each group consists of a (connected) set of sites, but two different groups may have sites in common. Alfred and Mark selected the simplest and smallest groups. In addition they adopted a very particular manner of taking them by cutting the lattice of N sites into $N/2$ nearest pairs in such a way that no two pairs have a site in common. We intentionally generalize the choice of local groups to any shape and size, and also generalize the manner of taking them.

We denote[8] the total number of atoms in the binary mixture by N; $N\theta$ of them being A atoms and $N(1-\theta)$ being B atoms. N is also the total number of lattice sites. Let z be the number of nearest neighbors of each site. In a given choice of the groups let there be n sites and p nearest pairs in each group, and let the total number of groups be M. The sites in each group will be labeled by $1, 2, \cdots, n$, in one and the same way. We shall let $q_i (i=1, 2, \cdots, n)$ specify the occupant of the ith site; $q_i=1$ if the ith site is occupied by an A atom, $q_i=0$ if it is occupied by a B atom. In a given distribution of atoms in the whole lattice let $[q_1, q_2, \cdots, q_n]M$ be the number of groups having $q_i A$ atoms in the ith site $(i=1, 2, \cdots, n)$. Since the total number of sample groups is M, we have

$$\sum_q [q_1, q_2, \cdots, q_n]=1, \tag{2.1}$$

where the summation is taken over all possible values of the q's. When the distribution of A and B atoms on the whole lattice is purely random, the probability of finding an A atom on the ith site of any one of the M groups is simply θ. Consequently, we have

$$\sum_q q_i[q_1, q_2, \cdots, q_n]=\theta, \tag{2.2}$$

giving n equations (with $i=1, 2, \cdots, n$). The number of ways of arranging the indistinguishable groups is

$$\sum_{[q_1, \cdots, q_n]} \frac{M!}{\prod_q \{M[q_1, \cdots, q_n]\}!},$$

with the summation $\sum_{[q_1, \cdots, q_n]}$ taken over all possible values of $[q_1, q_2, \cdots, q_n]$'s which are subjected to the limitation (2.1) and (2.2).

If there were no interlocking among the local configurations (so far called groups), these M groups together should duplicate the binary system by a factor $(Nz/2Mp)$, in which $Nz/2$ and pM are, respectively, the total number of closest pairs in the binary system and that in the M groups. Therefore, the assumption of non-interference permits us to write the configurational part of the partition function of the binary mixture as

$$\begin{aligned} P(N, \theta, T) &= \sum_{[q_1, \cdots, q_n]} g(N, \theta)\left\{\frac{M!}{\prod_q (M[q_1, \cdots, q_n])!}\right\}^{Nz/2Mp} \\ &\quad \times \exp\left\{-\frac{Nz}{2Mp}\sum_q M[q_1, \cdots, q_n] \right. \\ &\qquad \left. \times \chi(q_1, \cdots, q_n)/kT\right\} \\ &= \sum_{[q_1, \cdots, q_n]} g(N, \theta)\frac{\left(\frac{Nz}{2p}\right)!}{\prod_q \left(\frac{Nz}{2p}[q_1, \cdots, q_n]\right)!} \\ &\quad \times \exp\left\{-\frac{Nz}{2p}\sum_q [q_1, \cdots, q_n] \right. \\ &\qquad \left. \times \chi(q_1, \cdots, q_n)/kT\right\} \end{aligned} \tag{2.3}$$

where χ is the configurational energy which depends on the atomic distribution $(q_1, \cdots, q_n)$. Stirling's approximation

$$\left\{\frac{(r+s)!}{r!s!}\right\}^{\alpha} = \frac{\{\alpha(r+s)\}!}{(\alpha r)!(\alpha s)!} \tag{2.4}$$

for large number r and s has been used. The factor $g(N, \theta)$ is to be adjusted so that the total number of configurations of the system is given by

$$\frac{N!}{(N\theta)!(N[1-\theta])!} = P(N, \theta, \infty). \tag{2.5}$$

It is not a surprise that $g(N, \theta)$ cannot be dispensed with, for the assumption of non-interference of local configuration should not be perfectly correct.

The most probable (equilibrium) value of the fraction $[q_1, \cdots, q_n]$ can be obtained by maximizing the general term of (2.3) under the condition (2.1) and (2.2). Using Stirling's approximate formula and undetermined Lagrange's multipliers, we get

$$[q_1, q_2, \cdots, q_n]_{eq} = \frac{\mu_1^{q_1}\mu_2^{q_2}\cdots\mu_n^{q_n}\exp[-\chi(q_1, q_2, \cdots, q_n)/kT]}{\sum_q \mu_1^{q_1}\mu_2^{q_2}\cdots\mu_n^{q_n}\exp[-\chi(q_1, q_2, \cdots, q_n)/kT]} \tag{2.6}$$

[8] In this section we adopt almost the same nôtations as were used in Ref. II.

with $\mu_1, \cdots, \mu_n$ to be determined by (2.2). By putting

$$\varphi=\sum_q \mu_1^{q_1}\mu_2^{q_2}\cdots\mu_n^{q_n}\exp[-\chi(q_1, q_2, \cdots, q_n)/kT],$$

(2.2) and (2.4) may be written as

$$\mu_i\frac{\partial \ln\varphi}{\partial\mu_i}=\theta, \tag{2.2'}$$

and

$$[q_1, q_2, \cdots, q_n]_{eq}=\frac{1}{\varphi}\mu_1^{q_1}\mu_2^{q_2}\cdots\mu_n^{q_n}\times\exp[-\chi(q_1, q_2, \cdots, q_n)/kT]. \tag{2.4'}$$

Yang (Ref. II) has pointed out that a proof of the uniqueness of the solution for the μ's of an equation of the type (2.2') follows easily from Lemma 2.42 in Fowler's *Statistical Mechanics*, second edition.

(2.4') must reduce to the Alfred-Mark result when the groups are nearest pairs as taken by them. With $\mu_1=\mu_2$ given by (2.2') for this case we have the number of *A-B*, *A-A*, and *B-B* pairs, respectively,

$$X_{AB}=\frac{Nz}{2}\{[0, 1]_{eq}+[1, 0]_{eq}\}=\frac{Nz}{\varphi}\mu_1\exp\{-V_{AB}/kT\}, \tag{2.7a}$$

$$X_{AA}=\frac{Nz}{2}[1, 1]_{eq}=\frac{Nz}{2\varphi}\mu_1^2\exp\{-V_{AA}/kT\}, \tag{2.7b}$$

$$X_{BB}=\frac{Nz}{2}[0, 0]_{eq}=\frac{Nz}{2\varphi}\exp\{-V_{BB}/kT\}, \tag{2.7c}$$

and so

$$X_{AB}^2=4X_{AA}X_{BB}\exp\{-2V/kT\}=(N_A-X_{AB})(N_B-X_{AB})\exp\{-2V/kT\}, \tag{2.8}$$

where V_{AB}, V_{AA}, and V_{AB} are, respectively, the interaction energy between *A-B*, *A-A*, and *B-B* nearest atoms; and $V=\frac{1}{2}(V_{AA}+V_{BB}-2V_{AB})$ is the "energy of mixing," or $2V$ is the amount of energy gain by creating an *A-A* pair and a *B-B* pair at the expense of two *A-B* pairs. (2.8) is seen to be the same as the quasi-chemical equation used by Guggenheim, but rather is different from Alfred-Mark result. The latter has the exponential $(-2Vz/kT)$ instead of simply $(-2V/kT)$. However, this extra factor z is erroneous due to a minor mistake in the procedure of formulating their statistical method. Unfortunately, Miller did not pay much attention to this difference between Eq. (11) of TA-HM and Guggenheim's quasi-chemical equation but just omitted the extra factor z in writing Eq. (14) of his article.

The present method is capable of yielding different approximations by choosing different groups. Consequently, we need a criterion to examine which group will give the better result. We may consider the factor $g(N, \theta)$ as representing to some degree the accuracy of the approximation. $g(N, \theta)$ should be equal to one, if the assumption on non-interference of local groups were

TABLE I. Order-disorder transitions of the second kind calculated with the quasi-chemical equations. E_0 = the energy of transformation from perfect order to complete randomness, T_c = the critical temperature of the order-disorder transition, and ΔC_v = the discontinuity of molar specific heat during the transition. The numerical values of the quantities given in the Table are for the atomic ratio $\theta=\frac{1}{2}$. The range of θ gives the limits within which the superstructure may be formed. The "pair" approximation and "center and first shell" give the same results as Bethe's method. Local configurations are named as square, rhombus, or tetrahedron, when the lattice points and the nearest interactions included in the local groups consist of, respectively, the vertices and the sides (or edges) of a square, etc.

Lattice	Quadratic $z=4$			Simple cubic $z=6$				Body-centered cubic $z=8$			
E_0	NV			$3/2\,NV$				$2\,NV$			
Local group	Pair	Center and first shell	Square	Pair	Center and first shell	Square	Unicell	Pair	Center and first shell	Rhombus	Second shell incomplete[a]
$zn/2p$	4	5/2	2	6	7/2	3	3/2	8	9/2	4	15/8
RT_c/E_0	1.443	Same as "pair"	1.386	1.644	Same as "pair"	1.624	1.613	1.738	Same as "pair"	1.736	1.698
$\Delta C_v/R$	1.93		1.99	1.78		1.80	1.83	1.70		1.70	1.80
Superstructure range of θ	0.25 −0.75		0.2696 −0.7304	0.1667 −0.8333		0.1705 −0.8295	0.1762 −0.8238	0.1250 −0.8750		0.1265 −0.8735	0.1360 −0.8640
Source of the above data	Ref. I	Unpublished elsewhere	Ref. I	Ref. I	Unpublished elsewhere	Unpublished elsewhere	Unpublished elsewhere	Ref. I	Unpublished elsewhere	Unpublished elsewhere	Unpublished elsewhere

[a] See Fig. 1.

TABLE II. Order-disorder transitions of the first kind calculated by the quasi-chemical equations. Q is the latent heat of the order-disorder transition. The numerical values of Q and RT_c/E_0 given above are for the stoichiometric atomic ratio $\theta=\frac{1}{4}$ and $\frac{1}{2}$, respectively, for the two different lattices.

Lattice	Face-centered cubic $\alpha\beta_3$-type			Face-centered tetragonal* $\alpha\beta$-type		
E_0	$3NV/4$			NV		
Local group	Pair	Rhombus	Tetrahedron	Pair	Rhombus	Tetrahedron
$zn/2p$	12	6	4	12	6	4
RT_c/E_0	No superstructure can be shown by this approximation	Same as "pair" approximation	1.097	No superstructure can be shown by this approximation	Same as "pair" approximation	0.7306
Q			$0.294E_0$			$0.288E_0$
Superstructure range of θ			0.17–0.34 and 0.66–0.83			0.43–0.57
Source of the above data	Unpublished elsewhere	Unpublished elsewhere	Ref. I, II	Unpublished elsewhere	Unpublished elsewhere	Ref. III

* Only a slight deviation from cubic form is treated as a cubic lattice in its energy interactions among atoms.

correct. From (2.5) we obtain

$$\ln g(N,\theta)=-N\theta\ln\theta-N(1-\theta)\ln(1-\theta)$$
$$+\frac{Nz}{2p}\sum_q[q_1,\cdots,q_n]_{eq}(T=\infty)$$
$$\times\ln[q_1,\cdots,q_n]_{eq}(T=\infty)$$
$$=N\left(\frac{nz}{2p}-1\right)[\theta\ln\theta+(1-\theta)\ln(1-\theta)]. \quad (2.9)$$

In the derivation of the foregoing expression we have replaced as usual the summation of (2.3) by its maximum term and used (2.2), (2.4′) and the solution of (2.2′) at $T=\infty$, i.e.,

$$(\mu_i)_{T=\infty}=\theta/1-\theta, \quad (2.10)$$

and

$$(\varphi)_{T=\infty}=1/(1-\theta)^n. \quad (2.11)$$

Now we see that $g(N,\theta)=1$ only when $nz/2p=1$, or $p=np/2$, i.e., only when the local group is comparable in size to the binary system. In practical applications of the present theory, the use of a large group introduces troublesome calculations; therefore, we have to work with groups having $nz/2p$ rather larger than 1. The criterion which offers a guide in choosing the group, may be stated as follows: *A given approximation yields a result that is not less accurate than another if the former has a smaller* $nz/2p$. It is quite interesting to notice the following consequences: (a) A group containing a given number of sites may yield a result less accurate than another group with *less* sites, since the ration n/p acts as the gauge of accuracy not n itself. (b) A new group obtained by adding a corner site[9] to another group, with $p>n$, yields a less accurate result, since

$$\frac{z(n+1)}{2(p+1)}-\frac{zn}{2p}=\frac{z(p-n)}{2p(p+1)}.$$

By a corner site is meant a site having only one nearest neighbor in the group.

Finally we have the free energy function

$$F(N,\theta,T)=-kT\ln P$$
$$=-\frac{Nz}{2p}kT\left\{\ln\varphi-\sum_i\theta\ln\mu_i+\left(n-\frac{2p}{z}\right)\right.$$
$$\left.\times[\theta\ln\theta+(1-\theta)\ln(1-\theta)]\right\}. \quad (2.12)$$

3. THEORY OF SUPERSTRUCTURE

It is commonly observed phenomena that many substitutional alloys[10] exhibit order at not too high tem-

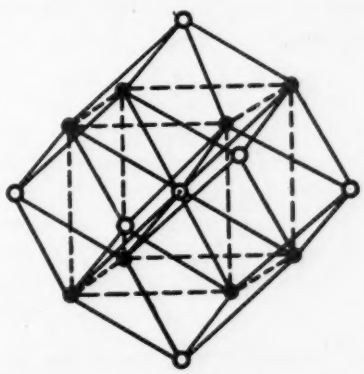

FIG. 1. A local group taken from a body-centered lattice containing a center site, denoted by ⊙ in the figure, its first shell sites, ●'s, and 6 sites, ○'s, from the second shell. Solid lines stand for the nearest interactions and dotted lines for the lattice frame.

[9] For a special consideration on corner sites see Theorem (iv) of Ref. I.

[10] See the review article by F. C. Nix and W. Shockley, Rev. Mod. Phys. **10**, 1 (1938).

peratures. We shall consider a binary system and designate the atoms by A and B. We may regard that the lattice sites as consisting of different sets of sublattices. Under suitable conditions the A atoms and B atoms distribute themselves unevenly on the different sublattices. In case of highly ordered states, some of the sublattices have their sites completely occupied by A atoms and the others by B atoms. The degree of the so-called long-range order can be described by giving the probability of finding A (or B) atoms on the sites of sublattices. The division of lattice sites into suitable sublattices must be made in such a manner that the resulting free energy successfully describes the system. For simpler cases only two sublattices (so called α- and β-sites) are needed. Here we leave the number of sublattices, m, unspecified.

Let[11] the number of sites on the sublattices L_h be $Nr_h(h=1, 2, \cdots, m)$. In a given distribution of atoms among the lattice sites, the number of A atoms on L_h is denoted by $Nr_h\theta_h$. The M groups may now fall into l different types with Mc_λ groups of the type $\lambda(\lambda=1, \cdots, l)$, because it may happen that the ith site is on L_1 in one group but on L_2 in another group. In the place of (2.1) and (2.2) we now get the limitation on the distribution of atoms in the M groups at given θ_h's in the form

$$\sum_q [q_1, \cdots, q_n]_\lambda = c_\lambda, \tag{3.1}$$

$$\sum_q q_i[q_1, \cdots, q_n]_\lambda = c_\lambda\theta_{\lambda i}. \tag{3.2}$$

Where $M[q_1, \cdots, q_n]_\lambda$ is, of course, the number of groups of type λ with q_i A atom in the ith site. $\theta_{\lambda i}=\theta_h$ when the ith site of the group of type λ is on L_h. Further, we have

$$\sum_h r_h\theta_h = \theta. \tag{3.3}$$

By the same procedure used in the preceding section, we get

$$P(N, \theta_1, \cdots, \theta_m, T) = \sum_{[q_1, \cdots, q_n]_\lambda} g(N, \theta_1, \cdots, \theta_m) \times \frac{\left(\frac{Nz}{2p}\right)!}{\prod_{q,\lambda}\left(\frac{Nz}{2p}[q_1, \cdots, q_n]_\lambda\right)!} \times \exp\left\{-\frac{Nz}{2p}\sum_{q,\lambda}[q_1, \cdots, q_n]_\lambda \times \chi(q_1, \cdots, q_n)/kT\right\}, \tag{3.4}$$

$$[q_1, \cdots, q_n]_{\lambda(eq)} = \frac{c_\lambda}{\varphi_\lambda}\mu_{\lambda 1}^{q_1}\cdots\mu_{\lambda n}^{q_n} \times \exp\{-\chi(q_1, \cdots, q_n)/kT\}, \tag{3.5}$$

where

$$\varphi_\lambda = \sum_q \mu_{\lambda 1}^{q_1}\cdots\mu_{\lambda n}^{q_n}\exp\{-\chi(q_1, \cdots, q_n)/kT\}, \tag{3.6}$$

with μ's to be determined by

$$\mu_{\lambda i}\frac{\partial \ln\varphi_\lambda}{\partial\mu_{\lambda i}} = \theta_{\lambda i}.$$

Further, we have

$$g(N, \theta_1, \cdots, \theta_m)\left\{\frac{\left(\frac{Nz}{2p}\right)!}{\prod_{q,\lambda}\left(\frac{Nz}{2p}[q_1, \cdots, q_n]_{\lambda(eq)}!\right)}\right\}_{T=\infty} = \frac{N!}{\prod_h (N\theta_h)!(N[1-\theta_h])!},$$

or

$$\ln g(N, \theta_1, \cdots, \theta_m) = N\left(\frac{nz}{2p}-1\right)\sum_h r_h \times [\theta_h \ln\theta_h + (1-\theta_h)\ln(1-\theta_h)]. \tag{3.7}$$

The derivation of the foregoing is quite similar to (2.9) but one more relation

$$\sum_{\lambda, i} c_\lambda f(\theta_{\lambda i}) = n\sum_h r_h f(\theta_h),$$

has been used. Finally, we replace the summation of (3.4) by its maximum term as usual and write the configurational free energy function

$$F(N, \theta_1, \cdots, \theta_m, T) = -kT\ln P = -\frac{Nz}{2p}kT\left\{\sum_\lambda \ln\varphi_\lambda - \sum_{\lambda, i}\theta_{\lambda i}\ln\mu_{\lambda i} + \left(n-\frac{2p}{z}\right)\sum_h r_h[\theta_h\ln\theta_h + (1-\theta_h)\ln(1-\theta_h)]\right\}. \tag{3.9}$$

We see that our Eqs. (3.2′), (3.6), and (3.9) coincide with those of Ref. III. The reader is referred to Ref. III for further work of finding equilibrium long-range order and allied physical quantities.

[11] In this section we adopt almost the same notation as was used in Ref. III.

In the opinion of this author the argument of the present theory is obviously more straightforward than that of Yang's theory which employed a chemical analogy and a mathematical trick of solving an integration by a Legendre transformation. Nevertheless, the fundamental assumptions of these two methods are only superficially different. By drawing an analogy between the local groups and the molecules in an ideal gaseous system, Yang implicitly followed the exact line of the hypothesis of non-interference of local configurations. He also tried to deduce his quasi-chemical method by adopting the hypothesis although with little success (§6 of Ref. I).

Although the statistical theory presented in this paper does not obtain new equations it leads to a useful criterion on the successive approximations. Because the factor $g(N, \theta_h)$ is hidden behind the scenes in Yang's deduction, no criterion has been established in Ref. I–III. In order to show the effectiveness of the criterion, we collect the calculated results of different approximations for several different kinds of lattices in Tables I and II. (See also Fig. 1.) For the procedure of calculations involved our readers are referred to Ref. I–III. In order to conserve space no details can be given here.

Those with the order-disorder *transition of the second kind* are shown in Table I which exhibits that in all cases T_c and $nz/2p$ vary in the same direction and ΔC_v in the opposite direction. Therefore, we may expect that higher approximations would yield larger ΔC_v in better agreement with experimental data. In Table II the simplest group which shows the superstructure phenomenon of a face-centered lattice is the tetrahedron. Both the "pair" approximation and "rhombus" are absolutely uncapable of describing the phenomena. It is interesting to see that these two local groups do not include in themselves the characteristic feature of a face-centered lattice that there are nearest neighbors among the first-shell sites of any site. On the other hand, the simple cubic or the body-centered cubic lattice has no nearest interactions among the nearest neighbors of any site. This difference in their lattice structure might be interpreted as the reason why the order-disorder transition of a face-centered cubic lattice is a transition of the first kind[12] (a sudden vanishing of long-range order with the appearance of latent heat), while that of a simple or a body-centered cubic lattice is a transition of the second kind (continuous change to disorder without latent heat). Calculations with different methods (Bethe, Kirkwood, Fowler-Guggenheim, and Yang-Li) have shown that an order-disorder transition is of the second kind whenever there is no nearest interactions among the nearest neighbors of any lattice site. It would be interesting if we could prove *in general* that *the order-disorder transition of a superlattice with nearest interactions among the nearest neighbors of a site occurs as one of the first kind*. It roughly means that the order-disorder transition happens much more abruptly than would be the case if there were no nearest interactions among the first shell sites. Work has been done only for a particular case, Cu-Au alloy system (Table II or Ref. III). Another important example is the Mg-Cd alloy system (close-packed hexagonal structure).

Incidentally, we may mention that the usual classification of the superstructures into those of $\alpha\beta$-type (designated as "with equivalent sublattices" by Fowler and Guggenheim[13]) and those of $\alpha\beta_3$-type ("with non-equivalent sublattices") is unessential and leads one to the incorrect conclusion that order-disorder transition of that with equivalent sublattices occurs as one of the second kind for any crystal structure. We have shown the incorrectness of the latter conclusion (Ref. III).

4. FERROMAGNETISM IN THE ISING MODEL

As remarked a few years ago by Peierls,[14] the theory of ferromagnetism can be presented in parallel with that of the order-disorder of alloys and this parallel is even closer when the Ising model[15] is assumed. In this model the spin of $\frac{1}{2}$ per atom is oriented either parallel or antiparallel to a specified direction. It is equivalent to disregarding the quantum mechanical combination of two spins $\sigma=\sigma_1+\sigma_2=1$ and $\sigma_z=0$, with the z axis being the specified direction. Now we can think of two kinds of atoms, A with a spin of $+\frac{1}{2}$ and B with a spin of $-\frac{1}{2}$, although they are actually of the same chemical element. The potential interaction of a nearest pair is taken as

$$\begin{aligned} V&=-2JS_1S_2-2(S_1+S_2)\beta H,\\ V_{AA}&=-\tfrac{1}{2}J-2\beta H,\\ V_{BB}&=-\tfrac{1}{2}J+2\beta H,\\ V_{AB}&=\tfrac{1}{2}J, \end{aligned} \tag{4.1}$$

where J is the exchange integral,[16] β the Bohr magneton $e\hbar/2mc$, and H the external field. Evidently we may shift the zero level of energy by replacing V_{AA}, V_{BB}, and V_{AB}, respectively, with $-J-2\beta H$, $-J+2\beta H$, and 0 in order to make the evaluation simpler.

$(2\theta-1)N\beta/v$ gives the magnetization M with v as the volume of the domain under consideration. The atomic ratio θ now varies with the temperature instead of remaining constant as it does in chemical mixtures. Elsewhere nothing is different from that discussed in Section 2. Therefore, the equilibrium value of θ can be determined by

$$\partial F/\partial\theta=0 \quad \partial^2F/\partial\theta^2>0, \tag{4.2}$$

[12] In a transition of the nth kind, the free energy function of the two phases have the same derivatives up to the $(n-1)$th order, whereas the nth derivatives are different. The zeroth derivative of a function is, of course, the function itself.

[13] R. H. Fowler and E. A. Guggenheim, *Statistical Thermodynamics* (Cambridge University Press, London, 1939), pp. 566, 598.

[14] R. Peierls, Proc. Roy. Soc. **A154**, 207 (1936).

[15] E. Ising, Zeits. f. Physik **31**, 253 (1925).

[16] See J. H. Van Vleck, *Electric and Magnetic Susceptibility* (Oxford University Press, Teddington, 1932), Chapter XII.

where F is given by (2.12). We find directly that

$$\sum_i \ln\mu_i = \left(n-\frac{2p}{z}\right)\ln\frac{\theta}{1-\theta}, \tag{4.3a}$$

and

$$\sum_i \frac{\partial \ln\mu_i}{\partial\theta} > \left(n-\frac{2p}{z}\right)\frac{1}{\theta(1-\theta)}, \tag{4.3b}$$

in the place of (4.2).

When the external field H does not exist, $\theta=\frac{1}{2}$ (and so $M=0$) offers a solution of (4.3a) for any temperature and this is the only solution for $T=\infty$. The mathematical proof of this statement can be easily obtained from the following relations, which are derived from (2.2′).

$$\mu_i(\theta)\mu_i(1-\theta)=1 \quad i=1, 2, \cdots, n, \tag{4.4}$$

and

$$\mu_i(T=\infty)=\frac{\theta}{1-\theta}.$$

Consequently, we conclude that at very high temperatures ferromagnetism must disappear and it can only exist below a critical temperature at which a root of (4.3a) other than $\frac{1}{2}$ starts to show the lowest free energy. Above the critical temperature magnetization only appears when an external field exists (paramagnetism). The transition at the Curie temperature T_c occurs as one of the second kind if $\theta=\frac{1}{2}$ is a double root of (4.3a) at T_c; i.e., when

$$\sum_i \left(\frac{\partial\mu_i}{\partial\theta}\right)_{\theta=\frac{1}{2}} = 4\left(n-\frac{2p}{z}\right). \tag{4.5}$$

However, the transition may occur as one the first kind, if two minima of the free energy $F(\theta=\frac{1}{2}, T)$ and $F(\theta\neq\frac{1}{2}, T)$ become equal at a temperature higher than that for which $\theta=\frac{1}{2}$ gives a double root of (4.3a). For examples of the latter kind found in the order-disorder transition see Fig. 7 of Ref. III.

Let us first take the "pair" approximation ($n=2$, $p=1$). The two sites are symmetric and so $\mu_1=\mu_2=\mu$. We have

$$\varphi = X+2\mu+\mu^2X, \tag{4.6}$$

where

$$X=\exp(J/kT), \tag{4.7}$$

(2.2′) reduces to

$$\mu(1+\mu X)=\theta(X+2\mu+\mu^2X). \tag{4.8}$$

From (4.5) the critical temperature T_c is given by

$$J/kT_c=\ln(z/z-2), \tag{4.9}$$

which indicates that a positive exchange interaction is necessary for the ferromagnetism to appear. Using (4.3a) we find that the equilibrium θ below T_c is determined by the implicit equation

$$\frac{(2\theta-1)\theta^{1-1/z}(1-\theta)^{1/z}}{\left[\theta^{1-1/z}(1-\theta)^{1/z}\right]^2-\theta(1-\theta)}=X. \tag{4.10}$$

The reduced saturation magnetization $M(T)/M(T=0)$ is simply equal to $2\theta-1$.

From these established results we draw the following conclusions: (a) Ferromagnetic transitions are transitions of the second kind; the spontaneous magnetization of domains vanishes gradually at a certain Curie temperature. (b) The linear chain ($z=2$) should not exhibit ferromagnetism at any temperature and two-dimensional lattices should show ferromagnetism. And (c) different lattice structures with equal coordinate number z, such as the hexagonal layer and the simple cubic lattice, should have the same ferromagnetic characteristics. Weiss[17] obtained similar results by applying Bethe's method to the Ising model. Our method is capable of seeking higher approximations with ease. Higher approximations have been tried. The results are more sensitive to the lattice geometry; hence, conclusion (c) is incorrect owing to the roughness of the "pair" approximation. (a) and (b) remain true in higher approximations. However, the improvements offered by higher approximations are not very significant, because we are working with the Ising model which does not agree with reality and only serves to show the characteristics of the mathematical theory of ferromagnetism. For example, (b) has been disproved by both Bloch's method of spin function[18] and the Bethe-Weiss method. They show that only three-dimensional lattices can ever exhibit ferromagnetism.

It remains to be seen how we can modify the quasi-chemical method to fit the quantum-mechanical spin vector. This work will not only offer an alternative method to the Bethe-Weiss method but will be more effective in applications. Because the interactions among the first shell sites introduce involved calculations, Weiss did not carry out the work on the face-centered cubic and the close-packed hexagonal lattice. From Ref. I–III we have seen that the quasi-chemical method solves the face-centered cubic lattice without much more trouble than the simple cubic or body-centered cubic lattice.

Urbain *et al.*[19] have found that the ferromagnetism of metallic gadolinium (close-packed hexagonal structure) disappears suddenly at about 16°C (a transition of the first kind). This phenomenon cannot be understood by various theories so far established. Among them Stoner's collective electron theory,[20] which employs the band scheme of electron energy on a "standard" form, predicts in any case a continuous vanishing of ferromagnetism at the critical temperature. Bloch's method, being rigorous only at very low temperatures, has nothing to do with phenomena near the critical temperature. The Bethe-Weiss method suffers from involved calculations in the case of a closed-packed hex-

[17] P. R. Weiss, Phys. Rev. **74**, 1493 (1948); also U. Firgau, Ann. d. Physik **40**, 295 (1941).
[18] F. Bloch, Zeits. f. Physik **61**, 206 (1930).
[19] Urbain, Weiss, and Trombe, Comptes Rendus **200**, 2132 (1935).
[20] E. C. Stoner, Proc. Roy. Soc. **A165**, 372 (1938).

agonal structure, although this recent work improved Heisenberg's theory quite a lot by taking the actual energy levels instead of a Gaussian distribution. Perhaps the future work of a modified quasi-chemical method could explain the phenomenon mentioned above. Otherwise this experiment finding should be re-examined.

5. REGULAR MIXTURES CONTAINING MORE THAN TWO COMPONENTS

Ternary alloys (substitutional) and complex salts such as Ag_2HgI_4 (with Ag, Hg atoms and vacancies, or so called holes, distributed on a face-centered cubic lattice[21]) are the important examples of the systems to be considered in this section. So far no theoretical work has been done with them. Now let us consider a k component mixture in general, with k unspecified. We denote the atom of the Sth kind with A_s and their number by $N\theta_S(S=1, \cdots, k)$. The designation of distribution $(q_1, \cdots, q_n)$ of Section 2 has to be replaced by $(As_1, \cdots, As_n)$ when the ith site of the group is occupied by an A_{Si} atom $(S_i=1, \cdots, k)$. Here we may confine ourselves to the case of a random distribution, since the theory of order can be formed by merely a refinement. The conditions (2.1) and (2.2) now become

$$\sum_A [As_1, \cdots, As_n]=1, \tag{5.1}$$

$$\sum_{S_i=S} [As_1, \cdots, As_n]=\theta_s, \tag{5.2}$$

where $\sum_A$ is taken over all possible local configurations and $\sum_{S_i=S}$ over the possible configurations with the ith site occupied by an A_s. By an almost the same procedure as that employed in Section 2 we obtain the following equations:

$$[As_1, \cdots, As_n]=\frac{1}{\varphi}\mu(As_1)\cdots\mu(As_n) \times\exp[-\chi(As_1, \cdots, As_n)/kT], \tag{5.3}$$

$$\varphi=\sum_A \mu(As_1)\cdots\mu(As_n) \times\exp[-\chi(As_1, \cdots, As_n)/kT], \tag{5.4}$$

and

$$\mu_i(A_s)\frac{\partial \ln\varphi}{\partial\mu_i(A_s)}=\theta_s. \tag{5.5}$$

Each $\mu_i(A_s)$ may be regarded as a k-dimensional quantity and we may choose $\mu_i(A_k)=1(i=1, \cdots, n)$ without any loss of generality (as we did in Section 2). Altogether we have $n(k-1)$ parameters μ's.

The ternary equilibrium with a solute in two immiscible solvents usually has an asymmetric solubility. A theoretical approach to this problem can be attempted by applying the equations obtained in this section under the supposition that all the atoms involved are non-electrolytic and that the model of "strict regular" liquids may be adopted.

The practical calculation of a problem with atoms of more than two different kinds would be much more involved than the applications we have made to binary systems. For binary mixture we can write χ as $V(=\frac{1}{2}[V_{AA}+V_{BB}-2V_{AB}])$ times an integer number by suitably choosing the zero level of the potential energy, but in the case of ternary mixtures χ consists of terms of the type $V_1=\frac{1}{2}(V_{AA}+V_{BB}-2V_{AB})$, $V_2=\frac{1}{2}(V_{BB}+V_{CC}-2V_{BC})$, and $V_3=\frac{1}{2}(V_{CC}+V_{AA}-2V_{CA})$. It is mainly the difficulties arising from this source instead of those arising from the presence of more variable μ's that makes the practical calculations for ternary mixtures cumbersome.

It is a pleasure to express my sincere thanks to both Dr. F. Seitz and Dr. J. S. Koehler for their interest in this work and their kind help.

[21] J. A. A. Ketelaar, Zeits. f. physik. Chemie **26B**, 327 (1934); **30B**, 53 (1935). At low temperatures Ag, Hg atoms, and "holes" form a highly ordered superlattice which gives the minimum energy when nearest interactions ($V_{Hg\cdot Hg}>V_{Hg\cdot Ag}>V_{Ag\cdot Ag}$) are counted.

Letters to the Editor

PUBLICATION of brief reports of important discoveries in physics may be secured by addressing them to this department. The closing date for this department is five weeks prior to the date of issue. No proof will be sent to the authors. The Board of Editors does not hold itself responsible for the opinions expressed by the correspondents. Communications should not exceed 600 words in length.

Neutrons from Deuterons on Lithium (6)*

C. E. MANDEVILLE, C. P. SWANN, AND S. C. SNOWDON
Bartol Research Foundation of the Franklin Institute, Swarthmore, Pennsylvania
August 12, 1949

ASIDE from the early qualitative observations[1] of the energy distribution of the neutrons from Li^6 plus deuterons, no further measurements have been published. Consequently, with the availability of highly concentrated Li^6, a more exact study seemed advisable.[2]

When Li^6 is irradiated by deuterons, the emitted neutrons are related to the following two reactions:

(1) $Li^6+D\rightarrow Be^7+n^1+3.34$ Mev,
(2) $Li^6+D\rightarrow He^4+He^3+n^1+1.72$ Mev.

Reaction (1) suggests, of course, the possibility of producing excited states in the residual nucleus, Be^7. Other nuclear reactions such as $Li^7(p,n)Be^7$ (bombarding energy as high as 3.66 Mev)[3] and $B^{10}(p,\alpha)Be^7$ (bombarding energy 630 kev)[4] have yielded no evidence for an excited state in Be^7.

In order to investigate the energy distribution of the neutrons from $Li^6(d,n)Be^7$, a thin target of $Li_2{}^6SO_4$ (300 micrograms/cm^2, 100 kev at the bombarding energy employed) was irradiated for 15 microampere hours by deuterons of mean energy 0.90 Mev supplied by the Bartol van de Graaff generator. Recoil protons were observed in Ilford C_2 photographical emulsions located 10 cm from the target and making an angle of 90° in the laboratory system with the incident deuterons. In choosing the tracks of the recoil protons, an acceptance angle of 12° in the forward direction was used. The energy distribution of the recoil protons thus noted is shown in Fig. 1 where the distribution of low energy neutrons related to reaction (2) is present along with a group centered at 3.40 Mev, corresponding to formation of Be^7 in the ground state. The Q-value, taking into account the two percent additive correction introduced by the acceptance angle of 12 degrees, is 3.30 Mev in reasonably good agreement with that calculated from mass values.[5] From a consideration of the half-width of the ground state group and the statistical accuracy of the measurements, it is estimated that in reaction (1) no level in Be^7 between 0.5 Mev and 1 Mev above the ground state is excited by more than ten percent of the disintegrations or by more than two percent on the interval between 1 Mev and 2 Mev.

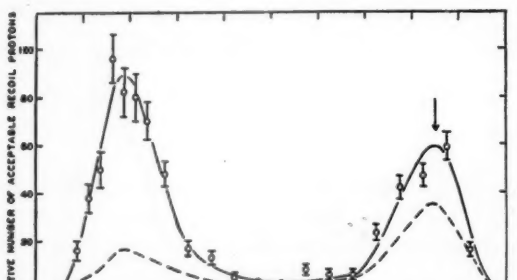

FIG. 1. Distribution in energy of the neutrons from the disintegration of Li^6 by deuterons.

The broken line is the distribution curve corrected for acceptance probability and n-p scattering cross section. From the areas under the two peaks, it is estimated that the neutron yields of reactions (1) and (2) are in the ratio of 2:1.

* Assisted by the Joint Program of the ONR and the AEC.
[1] Rumbaugh, Roberts, and Hafstad, Phys. Rev. **54**, 657 (1938).
[2] Separated Li^6 supplied from the Carbide and Carbon Chemicals Company Y-12 plant Oak Ridge, Tennessee, allocated by the Isotopes Division, U.S.A.E.C. The concentration of Li^6 was 99.4 percent.
[3] Freier, Lampi, and Williams, Phys. Rev. **75**, 901 (1949).
[4] W. E. Burcham and J. M. Freeman, Nature **163**, 167 (1949).
[5] H. A. Bethe, *Elementary Nuclear Theory* (John Wiley and Sons, Inc., New York, 1947).

The Signs of the Magnetic Moments of Neutron and Proton*

E. H. ROGERS AND H. H. STAUB
Stanford University, Stanford, California
August 16, 1949

WE have made a direct comparison between the signs of the neutron and proton magnetic moments by obtaining nuclear resonances in purely rotating radiofrequency magnetic fields. In addition to the relative sign, the absolute signs of these moments have been determined.

In order to make these sign determinations, the observation of two effects was necessary. The nuclear induction effect provided the means for determining the proton sign, while the sign of the neutron moment was obtained from observation of the depolarization at resonance of an originally polarized neutron beam. It will be recalled[1,2] that both of these effects demand a radiofrequency magnetic field which rotates about a fixed field H_0, the proper direction of rotation being determined by the sign of the magnetic moment of the nucleus under consideration. A principal deviation of our method from previous ones[3-5] lay in the technique involved in setting up the required rotating field. Our field was derived from two pairs of crossed coils placed at right angles to one another geometrically, and fed by two r-f currents differing in phase by 90°. The phase shifts was obtained by a simple delay line with lumped constants. The resultant rotating field was quite satisfactory as to homogeneity over the large volume of the neutron beam, and the power requirements were reduced by working at a low frequency (2.30 mc) for both nuclei.

In observing the proton nuclear induction signals, a difficulty peculiar to this type of arrangement had to be overcome. The usual procedure in nuclear induction involves deriving the rotating r-f field from one component of a purely oscillatory field, the important advantage being that the "leakage" flux through the receiver coil can be minimized by placing this coil at right angles to the transmitter coil. In our arrangement the axis of one pair of transmitter coils was of necessity aligned with the axis of the receiver coil, the other pair of transmitter coils being in the usual perpendicular position. Two series coils, the one with many turns so as to compensate the very large induced voltage in the receiver by the parallel component of the transmitter field, the other with few turns for compensating the perpendicular component, were linked with corresponding coils of the transmitter. The fine adjustment for both was achieved by the familiar use of "paddles." Since no information as to the shape of the signal was desired, we observed only the second harmonic (1000 c.p.s.) of the nuclear induction signal, thereby minimizing microphonics to a very large extent.

The magnet for procuding the constant H_0 field was fed by a well-stabilized current. This field was rather inhomogeneous over the region of appreciable values of the r-f field. The magnitude of the constant field was determined by an auxiliary nuclear induction apparatus.

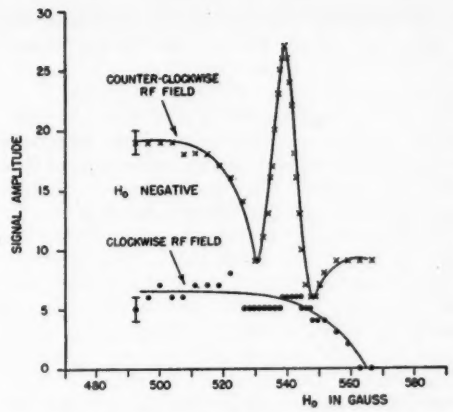

FIG. 1. Proton nuclear induction signals for the two directions of rotation ($\nu = 2.300$ mc).

Figure 1 shows the result of reversing the direction of r-f field rotation in the nuclear induction effect. (The notation "H_0 negative" simply refers to an arbitrarily assigned H_0 field direction. Similarly, the words "counter-clockwise r-f" and "clockwise r-f" refer to arbitrarily assigned directions of rotation of the radiofrequency field about the direct current field.) It will be observed that the proton nuclear induction signal appears only for a particular combination of the two magnetic fields, and is completely absent for the reverse combination.

After establishing the sign dependence of the nuclear induction effect, we removed the proton sample and passed a beam of partially polarized neutrons through the rotating field region. Figure 2 shows the results of this experiment. (Smooth curves were

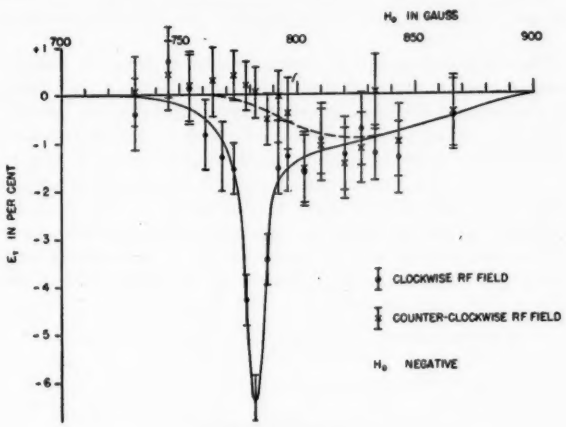

FIG. 2. Neutron transmission effect for the two directions of rotation ($\nu = 2.278$ mc).

drawn to fit the experimental points.) It will be observed that for the same direction of the H_0 field as for the protons, the neutron resonance occurs for the *opposite* direction of rotation of the r-f field. The immediate conclusion is that the neutron and proton have magnetic moments of opposite sign. The slight hump to the right of the main neutron resonance dip can be explained by the known inhomogeneities of the r-f and H_0 fields. This has been verified by an approximate calculation.

The absolute signs of the moments were determined by establishing the actual direction of the H_0 field and the true sense of rotation of the r-f field. The former was ascertained in two ways: first, from the known direction of the cyclotron magnetic field as inferred from the relative positions of target and deflector; and secondly, from the observed deflection of a current-carrying wire. The direction of rotation was determined as follows: two small probe coils oriented at right angles to one another were placed in the center of the r-f field, and the induced voltages therein mixed with a single local oscillator voltage. The resultant 80 kc voltages, for which relative phase shifts as to sign and magnitude were preserved, were applied separately to an oscilloscope whose linear sweep was synchronized with one of these voltages. The observed phase difference of the two voltages, combined with a knowledge of the sense of the probe coil windings, provided the information desired. We assumed the convention that a rotating positive charge will have a positive magnetic moment μ parallel to its angular momentum J. The absolute determination showed unambiguously that the proton moment is positive and the neutron moment is negative.

A detailed account of this work will appear in a forthcoming issue of Helvetica Physica Acta. One of us (E.H.R.) is indebted to the National Research Council for a Predoctoral Fellowship.

* Assisted by the Joint Program of the ONR and the AEC.
[1] F. Bloch, Phys. Rev. **70**, 460 (1946).
[2] I. I. Rabi, Phys. Rev. **51**, 652 (1937).
[3] P. N. Powers, Phys. Rev. **54**, 827 (1938).
[4] S. Millman, Phys. Rev. **55**, 628 (1939).
[5] Bloch, Nicodemus, and Staub, Phys. Rev. **74**, 1025 (1948).

On the Angular Distribution of D−D Reaction Products

YOSHIHIRO NAKANO
Department of Physics, Hokkaidô University, Sapporo, Japan
August 5, 1949

THE angular distribution of the D−D reaction products was given hitherto by

$$I(\theta) = A(1 + B\cos^2\theta).$$

The dependences of A and B on the energy of the incident deuteron have been explained theoretically by Konopinski and Teller,[1] taking up to the incident P waves into account. According to the recent experiment of Blair *et al.*,[2] however, an alternative formula

$$I(\theta) = A(1 + B\cos^2\theta + C\cos^4\theta)$$

holds in the region of the higher energy of the incident deuteron, i.e., 1–3.5 Mev, where the calculation of Konopinski and Teller does not seem to be sufficient. Thus, the present author has taken up to the D waves in their line of calculation. Precisely, the transitions

$$^1S_0 - {}^1S_0,\ {}^3P_2 - {}^3P_2,\ {}^3P_1 - {}^1P_1,\ {}^3P_2 - {}^3F_2,\ {}^1D_2 - {}^1D_2,\ {}^1D_2 - {}^3D_2$$

have been considered. With the same notations as Konopinski and Teller, the differential cross section becomes

$$d\sigma = d\omega\,|(\sigma_0/9)^{\frac{1}{2}}\alpha_0 Y_{0,0} + (\sigma_1/3)^{\frac{1}{2}}(\textstyle\sum_m \alpha_{1,m} Y_{1,m} + (\frac{5}{6}\tfrac{1}{2})^{\frac{1}{2}}\alpha_{P-F} Y_{3,-1}) + (\sigma_2/9)^{\frac{1}{2}}\textstyle\sum_m \alpha_{2,m} Y_{2,m}|^2$$
$$= d\omega(4\pi)^{-1}\pi\lambda^2 A'(1 + B\cos^2\theta + C\cos^4\theta),$$

$\cos^6\theta$-terms being neglected, where

$$A' = A_0P_0 + A_1P_1 + A_2P_2 + A_{02}(P_0P_2)^{\frac{1}{2}},$$
$$B = B_1P_1 + B_2P_2 + B_{02}(P_0P_2)^{\frac{1}{2}},$$
$$C = C_1P_1 + C_2P_2.$$

The coefficients A_0, etc. are the definite functions[3] of $\alpha_{l,m}$'s and phase angles. The nuclear penetrabilities P_l's have been evaluated numerically as functions of the incident energy by means of Bethe's formula,[4] assuming the value $7 \cdot 10^{-13}$ cm for the distance of the closest approach. The following values of the coefficients

$$A_0 = 0.849 \cdot 10^{-3},\quad A_1 = 1.313 \cdot 10^{-3},\quad A_2 = 17 \cdot 86 \cdot 10^{-3},$$
$$A_{02} = 4.40 \cdot 10^{-3},\quad A'B_1 = 5.12 \cdot 10^{-3},\quad A'B_2 = -144.8 \cdot 10^{-3},$$
$$A'B_{02} = 27.9 \cdot 10^{-3},\quad A'C_1 = -4.83 \cdot 10^{-3},\quad A'C_2 = 197.2 \cdot 10^{-3}$$

can reproduce the experimental data of Blair *et al.*, and furthermore, in the lower energy region, the earlier experiments as well

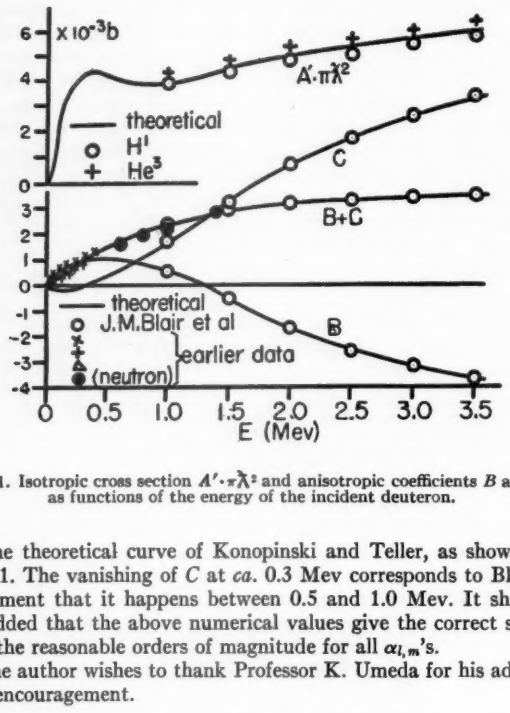

FIG. 1. Isotropic cross section $A' \cdot \pi\lambda\!\!\!^{-2}$ and anisotropic coefficients B and C as functions of the energy of the incident deuteron.

as the theoretical curve of Konopinski and Teller, as shown in Fig. 1. The vanishing of C at *ca.* 0.3 Mev corresponds to Blair's statement that it happens between 0.5 and 1.0 Mev. It should be added that the above numerical values give the correct signs and the reasonable orders of magnitude for all $\alpha_{l,m}$'s.

The author wishes to thank Professor K. Umeda for his advice and encouragement.

[1] E. J. Konopinski and E. Teller, Phys. Rev. **73**, 822 (1948).
[2] Blair, Freier, Lampi, Sleator, and Williams, Phys. Rev. **74**, 1599 (1948).
[3] The full expressions will be given shortly in J. Faculty Sci. Hokkaidô University, Sapporo, Japan.
[4] H. A. Bethe, Rev. Mod. Phys. **9**, 178 (1937).

Current Densities in the Cathode Spots of Transient Arcs

J. M. SOMERVILLE AND W. R. BLEVIN
New England University College, Armidale, New South Wales, Australia
August 9, 1949

IT has recently been suggested that the current densities of arc cathode spots may exceed hitherto accepted values by at least an order of magnitude. From observations of the tracks left by rapidly moving cathode spots on oxidized metal surfaces, Cobine and Gallagher[1] derived current densities of the order of 5×10^4 amp./cm². Using a Kerr cell shutter and exposures of the order of a microsecond to photograph the cathode spot, Froome[2] obtained current densities of about 10^6 amp/cm².

We have struck high current arcs of short duration in air at atmospheric pressure on aluminum, copper, magnesium, nickel, tin, and tungsten cathodes. Using a number of pulse-forming lines, we could pass currents of up to 200 amperes in square pulses varying in duration from 1 to 200 microseconds.

The arc strikes readily and leaves a clear, well-defined spot on clean tin, on aluminium which has not recently been scraped clean, and on oxidized copper, nickel, magnesium, and tungsten cathodes. The spots are roughly circular in shape, some typical examples being shown in Fig. 1. A single pulse usually gives a single spot although cases of multiple spot formation occur in aluminium, copper, and tungsten, particularly at high currents. Measured areas of spots obtained with the same current and pulse length vary about the mean with a standard deviation of 0.05 to 0.1 of the mean.

For a given pulse length the mean spot area is proportional to the current strength and so for each metal the ratio (current/spot area), which we may call the apparent current density, is a function of the pulse length. In all cases the apparent current density increases as the pulse length falls, as shown in Table I.

TABLE I. Current density (amp/cm²).

Pulse length	1 μsec.	5 μsec.	20 μsec.	50 μsec.	200 μsec.
Aluminium	160,000	65,000	40,000	40,000	Unreliable
Copper	780,000	390,000	114,000	90,000	35,000
Magnesium	$>10^6$	1,000,000	320,000	140,000	35,000
Nickel	480,000	175,000	67,000	56,000	18,000
Tin	340,000	33,000	19,000	19,000	9000
Tungsten	1,600,000	340,000	75,000	22,000	Unreliable

Our experiments are in agreement with those of Froome is indicating that, in arcs of short duration at least, current densities of the order of 10^6 amp/cm² may prevail. It is possible, of course, that the markings on our cathodes for longer pulse lengths are the result of the motion of one or more smaller spots like those observed by Froome, but our experiments give no information about this. It may also happen that, particularly in the case of the lower melting point metals, an area is melted greater than the area from which the current is drawn, leading to low apparent current densities. For these reasons we regard our measurements as giving only a lower limit to the real current density.

[1] J. D. Cobine and C. J. Gallagher, Phys. Rev. **74**, 1524 (1948).
[2] K. D. Froome, Proc. Phys. Soc. **60**, 424 (1948).

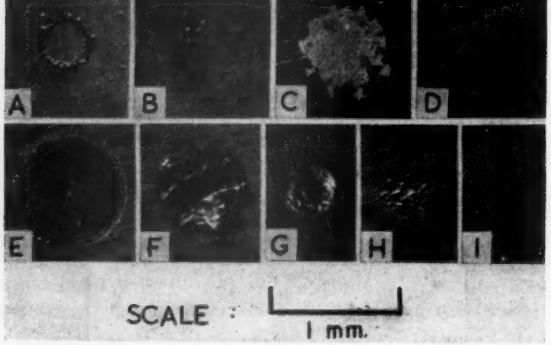

FIG. 1. Cathode markings for high current transient arcs in air at atmospheric pressure.

Top.—Cathode material: (A) copper; (B) magnesium; (C) aluminium; (D) nickel. Current: 80 amperes. Duration: 20 μsec.
Bottom.—Cathode material: Tin. Current: 50 amperes. Duration: (E) 200 μsec.; (F) 50 μsec.; (G) 20 μsec.; (H) 5 μsec.; (I) 1 μsec.

The Beta-Spectrum of Tl^{204}, Magic Numbers, and Neutron Pairing

D. SAXON AND J. RICHARDS
Argonne National Laboratory, Chicago, Illinois
August 16, 1949

THE β-spectrum of the 3 yr. Tl^{204} is of special interest because the nuclei involved lie close to the magic numbers 82 for protons and 126 for neutrons.[1] According to the most recent nuclear shell work,[2] Tl^{204} may be useful in deciding whether high angular momentum neutrons are added in pairs in the heavy element region. Both the neighboring isotopes Tl^{203} and Tl^{205} have the low spin ½, while the daughter substance Pb^{204} probably has spin 0. Therefore the shape of the β-spectrum of Tl^{204} will give strong evidence for or against the high angular momentum neutron pairing.

Thallium nitrate was irradiated in the Hanford pile; the particular sample used had been cooling for over 2 years so that all short-lived activities had disappeared. As a further precaution, a chemical purification was performed involving the conversion to the chloride followed by a final extraction.[3] The 180° spectrometer was used at 2 percent resolution in $H\rho$.

In Fig. 1 is shown the relativistic Fermi function Kurie plot using the daughter Pb, $Z=82$. For both sources, the data essentially agree, showing the same bulging at high energies and the large upward deviation at the low end. The shape is very much like that found recently for various lower Z isotopes.[4] In Fig. 2 are shown Kurie plots, the upper one corrected for the 2 percent spectrometer resolution,[5] while the lower has the $(G)^{\frac{1}{2}}$ factor[6] which for $G-T$ selection rules goes with first forbidden, $\Delta l=2$, and parity change. The resolution correction leaves the high energy bulge, while the $(G)^{\frac{1}{2}}$ factor takes it out. Both corrections have been made in Fig. 3, where the linear range now extends

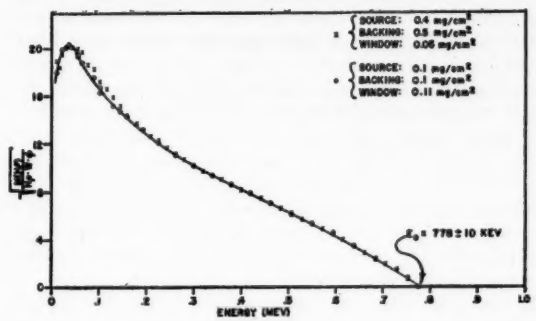

FIG. 1. Relativistic Fermi function Kurie plot for Tl^{204} (uncorrected).

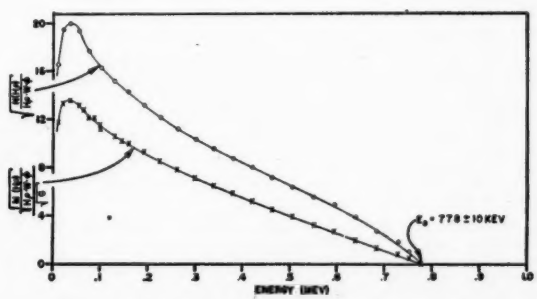

FIG. 2. Kurie plots for Tl^{204}. Upper curve, corrected for the 2 percent spectrometer resolution; lower curve, corrected for $(G)^{\frac{1}{2}}$.

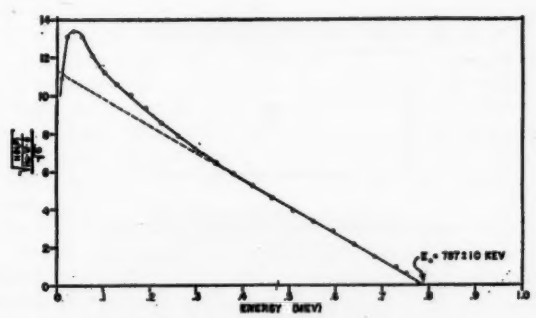

FIG. 3. Kurie plot for Tl^{204}. Corrections made both for resolution and $(G)^{\frac{1}{2}}$.

down to ~350 kev. Below this the large deviation upward is still present. We find it difficult to ascribe this to residual scattering in view of the close agreement between the two sources used. Also a low energy β-component seems improbable since there is no trace of the expected difference γ-ray.[7]

Another possibility is that the transition is actually second forbidden, the ft value of 5.0×10^9 being large enough for this. In this case, the only correction factors that would give the linear allowed shape are the scalar and axial vector interactions for $\Delta l=2$, with no parity change.[8]

It seems clear then that for Tl^{204} $\Delta l\geq2$, the parity being still in doubt. This evidence would support the conjecture concerning the pairing of the higher angular momentum neutrons in the heavy element region.

It is to be noted that the resolution correction raises the end point slightly.[5] Our final value using the average, from before and after correction, is 783±10 kev.

[1] M. G. Mayer, Phys. Rev. **74**, 235 (1948); E. Feenberg, Phys. Rev. **75**, 320 (1949).
[2] L. W. Nordheim, Phys. Rev. **75**, 1894 (1949); E. Feenberg and K. C. Hammack, Phys. Rev. **75**, 1877 (1949); M. G. Mayer, Phys. Rev. **75**, 1969 (1949).
[3] We wish to thank F. Hagemann for the source material and for performing the chemical purification.
[4] F. B. Shull and E. Feenberg, Phys. Rev. **75**, 1768 (1949).
[5] G. E. Owen and H. Primakoff, Phys. Rev. **74**, 1406 (1948).
[6] The authors wish to thank F. B. Shull for his kindness in pointing out the details of the high $Z(G)^{\frac{1}{2}}$ correction.
[7] K. Fajans and A. F. Voight, Phys. Rev. **60**, 619 (1941).
[8] E. J. Konopinski and G. E. Uhlenbeck, Phys. Rev. **60**, 308 (1941).

Frequency of Stars of Different Sizes Produced by the Cosmic Radiation in Photographic Plates Exposed at 29,000 Meters

MARGHERITA ADDARIO AND SARA TAMBURINO
Institute of Physics, University of Catania, Catania, Italy
August 15, 1949

THANKS to the kindness of Professor Frank Oppenheimer (University of Minnesota, Minneapolis, Minnesota), we had the opportunity of examining nuclear photographic plates (unloaded Ilford C2, 100 micron thickness) which had been carried aloft up to 29,000 m above sea level, in balloons launched at 55°N geomagnetic latitude (Minneapolis). The balloons remained above 27,500 m for 5.3 hours, and spent 2.2 hours between sea level and 27,500 m. The plates were arranged with the plane of the emulsion vertical, in an aluminum sphere 1 mm thick and 76 cm in diameter.

So far 1.120 cm^3 of emulsion have been examined. In this volume 488 stars with 3 or more prongs have been observed, which indicates a star frequency of 1960 $cm^{-3}\cdot d^{-1}$.

From the comparison of this frequency with that observed by Bernardini, Cortini, and Manfredini[1] at 3500 m, it can be derived that the radiation which produces stars with 3 or more prongs is

TABLE I. Total number of stars and their frequency per cubic centimeter.

1	2	3	4	5	6
Number of prongs	Stars observed at 29,000 m	Frequency $cm^{-3}\cdot d^{-1}$ at 29,000 m	Frequency $cm^{-3}\cdot d^{-1}$ at 3500 m	λ $g\cdot cm^{-2}$	Percent freq. at 29,000 m / Percent freq. at 3500 m
3	126	506	5.9	149	0.66
4	113	454	4.3	143	0.82
5	57	229	2.2	144	0.78
6	47	189	1.1	129	1.35
7	30	120	0.44	118	2.19
8	29	116	0.32	113	2.32
9	22	88	0.23	112	3.0
10	14	56	0.17	115	2.5
11	13	52	0.15	113	2.78
12	14	56	0.15	112	2.99
13	6	24	0.09	118	2.23
14	3	12	0.03	111	3.19
15	7	28	0.03	97	7.59
16	3	12	0.09	135	1.04
18	1	4			
19	1	4			
20	1	4			
24	1	4			

absorbed in air, between 3500 and 29,000 m, with a mean free path of $\sim 137\ g \cdot cm^{-2}$. We have found that the frequency of the stars with 4 or more prongs is 1450 $cm^{-3} \cdot d^{-1}$, in agreement with the figure $\sim 2000\ cm^{-3} \cdot d^{-1}$ obtained by Salant *et al.*[2] for the same kind of stars at 30,500 m.

The total number of stars we observed and their frequency per cubic centimeter, *versus* star size are given in columns 2 and 3 of Table I. In column 4 the star frequencies observed by Bernardini *et al.*[1] are given for comparison. The figures in column 5 are the absorption mean free paths λ in air, between 3500 and 29,000 m elevation, of the star primaries, deduced from the data in columns 3 and 4. Column 6 gives the ratios between the percent star frequencies at 29,000 and at 3500 m. Such percent frequencies have been calculated using the total number of stars with 3 or more prongs. Our data for percent star frequencies *versus* star size, as well as Bernardini's, are also plotted in Fig. 1.

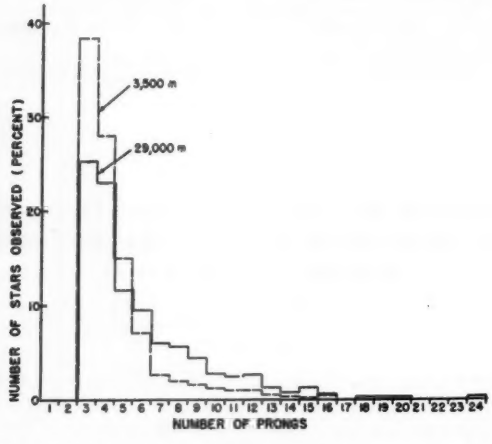

FIG. 1. Number of stars observed at 29,000 m *versus* star size.

Both the results in column 5 of Table I and the data given in Fig. 1 clearly show a decrease of λ when the star size increases; hence, an absorbability in air for the radiation capable of generating the largest stars greater than for the radiation that produces stars of small size.

This confirms the conclusions reached by Salant *et al.*,[2] comparing their data (at 30,500 m) with Wambacher's[3] (at 2300 m). We wish to point out, however, that both our and Salant's conclusions require the assumption that the data taken at the ground (Bernardini and Wambacher) are not influenced by the effect of the ground itself,[4] hence comparable with the data taken in the free atmosphere.

From Fig. 1, one can see that the percent frequencies of stars with less than 5 prongs are larger at 3500 m than at 29,000 m, while the percent frequencies of the stars with 5 or more prongs show the opposite behavior. Gardner and Peterson[5] have found that the percent frequency of the stars with 3 prongs, generated in the Berkeley cyclotron by deuterons with energies between 35 and 190 Mev, decreases when the energy increases; the percent frequencies of the stars with 4 or more prongs, instead, increases with increasing energy.

This leads us to think that the different size distribution of the stars observed at different altitudes can be explained by assuming that the star primaries have the same nature at both elevations, but greater energies at higher altitudes.

From the results in column 5 of Table I one might also deduce that the cross section for star production increases when the energy of the star primaries increases.

[1] Bernardini, Cortini, and Manfredini, Phys. Rev. **74**, 845 (1948).
[2] Salant, Hornbostel, and Dollmann, Phys. Rev. **74**, 694 (1948).
[3] H. Wambacher, Wien. Ber. **149**, 157 (1940).
[4] J. J. Lord and M. Schein, Phys. Rev. **75**, 1956 (1949).
[5] E. Gardner and V. Peterson, Phys. Rev. **75**, 364 (1949).

Meson Background in Penetrating Shower Experiments

GIUSEPPE COCCONI
Laboratory of Nuclear Studies, Cornell University, Ithaca, New York
August 15, 1949

DURING the past year experiments have been performed both at Ithaca (260 m) and at Echo Lake (3260 m) to study the interaction mean free path of the ionizing particles that generate penetrating showers.[1] The interpretation of the results of these experiments with the assumption that all the penetrating showers observed are due to the nucleonic component created rather serious difficulties.

In order to clarify the problem, during the past winter further experiments have been performed at Ithaca inside a tunnel, under a thickness of rocks equivalent to 2000 $g \cdot cm^{-2}$ water (2 atmospheres).* The purpose of these experiments was to determine whether ionizing particles different from nucleons give an appreciable contribution to the showers recorded with our apparatus. At 2000 $g \cdot cm^{-2}$ underground the nucleonic component should be reduced by a factor larger than 10^4, hence any "penetrating showers" observed at such a depth have to be related to the mesonic component, which there is reduced only by a factor 4.

The showers were firstly observed with the same apparatus used in the research of the past year (see Fig. 1). Coincidences $A+B+C+D$ revealed the showers in which at least two particles are present capable of penetrating more than two inches of lead. When only one of the 20 counters E was discharged (event $A+B+C+D+1E$), it was assumed that the showers originated in the lead P.

The rate of coincidences $A+B+C+D+1E$, as it resulted from 1638 hours of observation, was $0.114/h^{-1}$, practically independent of the thickness of lead (0 and 8 in.) put in Σ.**

The facts that the rate observed under 2000 $g \cdot cm^{-2}$ water equivalent is about $\frac{1}{3}$ of the rate observed in the same conditions outside the tunnel, and that the presence or absence of the lead in Σ does not affect it, lead us to think that the primaries of the showers we observed inside the tunnel are mostly mesons.

A further experiment has been performed in the same tunnel with the arrangement drawn in Fig. 2. The showers were again detected by coincidences $A+B+C+D$; counters E gave, here, information about the number of particles generated in the lead P, capable of penetrating the absorber Σ.

Coincidences $A+B+C+D+1E$, $A+B+C+D+2E$, $A+B+C+D+\geq 3E$ were recorded. Measurements have been taken with the absorber Σ equal to: (a) 2 in. Pb, (b) 2 in. Fe, (c) 5 in. Pb, (d) 6 in. Fe. Absorber (a) is practically equivalent to (b), and absorber (c) to (d), for particles losing their energy through ionization,

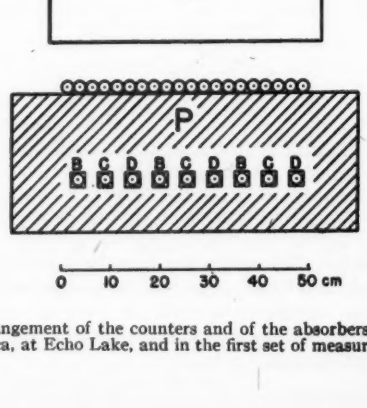

FIG. 1. Arrangement of the counters and of the absorbers in the experiments at Ithaca, at Echo Lake, and in the first set of measurements underground.

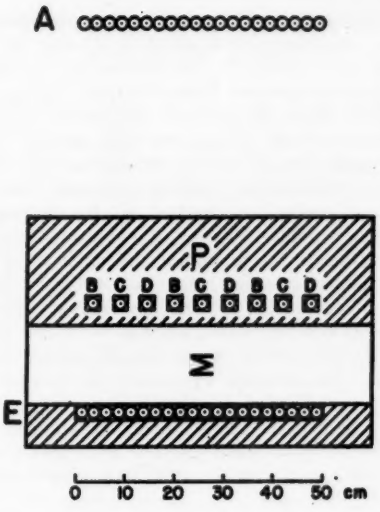

FIG. 2. Arrangement of the counters and of the absorbers in the second set of measurements underground.

while (a) and (c) are more effective than (b) and (d) in stopping electrons and photons.

In 2340 hours of observation the following results have been obtained:

$\Sigma=$	2 in. Pb	2 in. Fe	5 in. Pb	6 in. Fe
$A+B+C+D+\ 1E(h^{-1})$	0.086±.01	0.05 ±.01	0.10 ±.01	0.058±.008
$A+B+C+D+\geq 3E(h^{-1})$	0.041±.01	0.074±.015	0.011±.004	0.021±.005

Coincidences $A+B+C+D+1E$ are mostly due to mesons which have created in P a shower fully absorbed in Σ. The fact that these coincidences are more frequent when the absorber is lead shows that the particles created in the showers are more strongly absorbed in lead than in iron. The situation is reversed for coincidences $A+B+C+D+\geq 3E$, that represent instead the events in which at least two of the particles created in the showers are capable of crossing the absorber Σ.

Hence, both results agree in indicating that the particles created in the showers we observed underground are mostly electrons and photons, generated by mesons through knock-on and/or radiation processes. The same conclusion has been reached by Mr. D. Hudson, who in the same tunnel studied bursts produced in ion chambers.

On the basis of the information acquired in these experiments, some of the conclusions given in reference 1 must be modified. In fact, it is clear now that we overestimated in the previous paper the arguments which led us to disregard the contribution of showers created by mesons. Those arguments could only show that most, not all, of the showers recorded were due to nucleons. Actually a not negligible fraction of the showers we observed both at Ithaca and at Echo Lake were due, not to the nucleonic component, but to mesons.

The experiments underground allow us to make an estimate of this meson background. Though the total meson component is reduced in the tunnel by a factor 4, the energetic mesons that produce the showers we observed are likely reduced by a smaller factor, say between 2 and 3. This leads us to assume that the meson background in the showers detected at Ithaca is close to 0.3 h^{-1}, 30 percent of the total rate recorded with $\Sigma=0$. At Echo Lake only 3 to 5 percent of the rate registered in the same conditions can be accounted for by such a background. By subtracting the meson background, the absorption curves obtained both at Ithaca and at Echo Lake approach pure exponential shape, and indicate interaction mean free paths for the ionizing nucleonic component that produces penetrating showers practically equal to the ones deduced from the initial slopes of the uncorrected curves obtained at Echo Lake, i.e., 160 g·cm^{-2} in Pb, and 100 g·cm^{-2} in C. This correction eliminates the disturbing variation of the mean free paths with the thickness of the absorbers, which was so hard to understand. The absorption mean free path in air of the nucleonic component, after correction for meson background, is found to be ~120 g·cm^{-2}.

We wish finally to emphasize the importance of the evaluation of an eventual contribution due to mesons in all experiments on penetrating showers. Probably some of the discrepancies among the results of various authors are due to such a spurious effect.

[1] G. Cocconi, Phys. Rev. **75**, 1074 (1949).
* We are grateful to the Gun Company, Ithaca, New York, for allowing the use of the tunnel and furnishing the power.
** The rate of the coincidences in which two or more of the counters E were discharged (events $A+B+C+D+\geq 2E$) was 30 percent of the rate $A+B+C+D+1E$.

Addendum: Heat Flow in Metals Below 1°K and a New Method for Magnetic Cooling

J. G. DAUNT AND C. V. HEER
Mendenhall Laboratory, Ohio State University, Columbus, Ohio
August 11, 1949

USING the results of experiments on the new method of magnetic cooling briefly described in a previous letter,[1] it is it is possible to calculate the effectiveness of the following heat pump for transferring heat from a low temperature bath B (see Fig. 1) maintained at temperatures below 1°K to a higher temperature bath A, say at 1°K. A and B are connected to a paramagnetic salt D via two superconducting wires, S_1 and S_2, having a high transition temperature (e.g., Ta, Pb, Cb). S_1 and S_2 are removed some distance from D but kept in good thermal contact with D through copper posts, C. During the magnetization of D by the field $N-S$, S_1 is converted to the normal state by a magnetic field, H_1 (see Fig. 1), and the heat of magnetization is conducted through S_1 to A. Meanwhile S_2 is superconductive and therefore presents a thermal barrier to the flow of heat to B. The field H_1 next to reduced to zero; D is demagnetized and a magnetic field H_2 is placed around S_2 sufficient to convert it into the normal state; thereby placing D and B in effective thermal contact. S_1, having previously become superconductive on the removal of the field around it maintains D and B well isolated from A. This process of operation can be repeated cyclically by alternately switching on and off the three magnetic fields in the correct order.

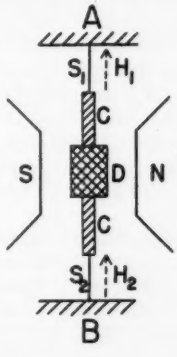

FIG. 1. Diagram of suggested heat pump.

In this manner it is estimated that, using 10 cc of salt, heat could be removed from B at 0.1°K at a rate of 10^5 ergs/cycle or more, using readily accessible magnetic fields and equipment, and that the repetition rate could be 1 cycle/min. or higher. By using therefore one or more such heat pumps, either in parallel or in series or both (as can be arranged to operate without increasing the number of magnetic fields required), a continuous cyclic

method of maintaining constant temperature baths well below 1°K is available which may prove of value for low temperature research. Moreover such an arrangement used as a two or three stage magnetic cooling system should enable the lowest temperatures to be attained without the use of intense magnetic fields.

We wish to thank The Research Corporation for their support and the Office of Naval Research for their assistance in later stages of the work by a contract with the Ohio State University Research Foundation. We also wish to thank Dr. K. W. Taconis and Professor J. de Boer for valuable discussions.

[1] J. G. Daunt and C. V. Heer, Phys. Rev. **76**, 854 (1949).

The Neutrinos from the Sun and the Source of the Earth's Heat

D. Saxon
Argonne National Laboratory, Chicago, Illinois
August 16, 1949

SINCE Bethe's classic paper on the carbon-nitrogen cycle as the source of stellar energy,[1] it has been conjectured that the sun may produce a considerable neutrino flux even at distances as far as the earth. Bethe estimated that the neutrinos in the N^{13} and O^{15} disintegrations carry off as much as 7 percent of the total energy production. Whether these neutrinos get outside the sun depends on their interaction cross section.

From the average result of neutrino interaction or closely related experiments,[2] the limit of $\leq 10^{-31}$ cm² can be made for the neutrino cross section. Crane[3] has estimated that the region 10^{-34} to 10^{-35} cm² is also eliminated; for if it were not, both the sun's surface temperature gradient and the heating of the earth would be excessive, far from known equilibrium conditions. However, Benfield[4] has since pointed out that the geophysical argument is far from secure, due to the present non-equilibrium conditions in the earth's surface gradient. In view of this, the question of the role of the sun's neutrinos in the heating of the earth seems open to further experimental work.

Although neutrino interaction experiments are difficult because of the limited sources available, there are reactions which are equivalent, which involve the same coupling constant and give the same theoretical cross section within an order of magnitude.[5,6]

The following inverse β-reaction:

$$e^- + H^1 \rightarrow n + \nu,$$

has been tried using a small van de Graaff generator. The 1.0-Mev electron beam from the generator passed out through a 2 mil (13.6 mg/cm²) Al window and was stopped in paraffin. The neutrons that might be produced ($E_n \sim 300$ ev) were moderated in the same paraffin geometry and counted in a B^{10} lined and $B^{10}F_3$ filled proportional counter. A fast preamplifier and amplifier were used in conjunction with the usual scale of 64. During the taking of data all pulses were monitored in an oscilloscope, so that neutron pulses could be distinguished from electrical pick-up or bremsstrahlung pile-up. When the generator was turned on for the first time, the bremsstrahlung pile-up was high enough to jam the mechanical recorder. By placing Pb shielding between the paraffin and counter, by removing all high Z substances from near the beam path, and finally by speeding up the preamplifier and amplifier, it was possible to run at 20μ-amp. and still keep the bremsstrahlung below the amplifier clipping level. The counter geometry efficiency was estimated to be 5×10^{-3} at 300 ev. This value was extrapolated from two known sources at higher energies, γ (Sb, Be)n at 25 kev, and γ (Ra, Be)n at $\sim$1 Mev.[7] The number of atoms of H^1 effective in the inverse β-reaction 3×10^{22} was estimated from the thickness of paraffin to slow the 1.0-Mev electrons down to 0.29 Mev, the threshold for the reaction.

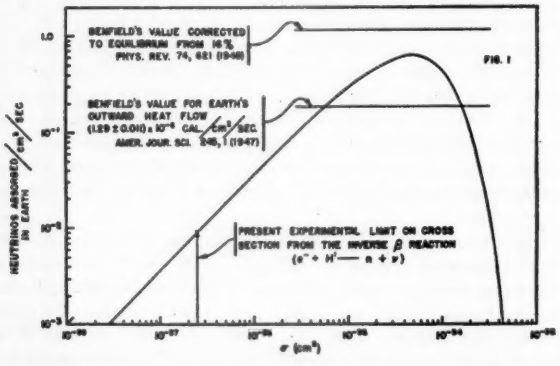
BENFIELD'S VALUE CORRECTED TO EQUILIBRIUM FROM 16% PHYS. REV. 74, 621 (1948)
FIG. 1
BENFIELD'S VALUE FOR EARTH'S OUTWARD HEAT FLOW
AMER. JOUR. SCI. 245, 1 (1947)
PRESENT EXPERIMENTAL LIMIT ON CROSS SECTION FROM THE INVERSE β REACTION
NEUTRINOS ABSORBED IN EARTH
σ (cm²)

FIG. 1. Neutrino absorption as a function of the interaction cross section.

At the maximum beam current used, 20μ-amp. there was no observable effect beyond statistics. The estimated error of 0.28 counts/min. when used with the other data gives a cross-section limit of $\leq 2.5\times10^{-37}$ cm².

In Fig. 1 is shown the neutrino absorption/cm²/sec. in the earth as a function of the interaction cross section. The solid curve was calculated assuming a point source model[1] for the sun's neutrinos; exponential absorption in the sun, and homogeneous absorption in the earth. The two horizontal lines represent the observed level for the earth's heat losses in equivalent neutrino absorptions. Assuming the equivalence of the observed cross section to that for neutrinos, it follows from Fig. 1 that at most 4 percent (and probably only 1 percent) of the observed earth's heat losses could be attributed to the absorption of the sun's neutrinos. If the further assumption is made that other neutrino interactions such as inelastic scattering are negligible, then the present result eliminates the sun's neutrinos as a significant source of the earth's heat. It should be mentioned that Crane's results[3] for the neutrino heating effect seem to be larger than the present one by a factor of 10. The particular solar model and constants used can influence the results radically. With the observed limit on the cross section, already most of the neutrinos escape the sun, giving a flux at the earth of $\sim 3.5\times10^{11}$/cm²/sec.

The ultimate cross section that can be detected by the present method is considerably smaller than 2.5×10^{-37} cm². By using a more efficient detector with lower background, and also higher beam currents it should be possible to reach 10^{-38} to 10^{-39}.

The author wishes to thank M. Burgy for many stimulating discussions, from the inception of the experiment to its completion. Also, many thanks to L. Johnson and T. Brill's group for the flawless performance of counter and circuits. The van de Graaff generator was used under the guidance of S. Rocklin.

[1] H. A. Bethe, Phys. Rev. **55**, 434 (1939).
[2] E. O. Wollan, Phys. Rev. **72**, 445 (1947); H. R. Crane, Phys. Rev. **55**, 501 (1939); R. L. Burling and F. N. D. Kurie, Phys. Rev. **74**, 109 (1948).
[3] H. R. Crane, Rev. Mod. Phys. **20**, 294 (1948).
[4] A. E. Benfield, Phys. Rev. **74**, 621 (1948).
[5] H. A. Bethe and R. F. Bacher, Rev. Mod. Phys. **8**, 196 (1936).
[6] H. Primakoff, Phys. Rev. **74**, 110 (1948).
[7] The photo-neutron source calibration was kindly done for us by A. Wattenberg and his group.

Radioactivity in Holmium 166, Thulium 170, and Lutecium 177

J. M. Cork, H. B. Keller, and A. E. Stoddard
University of Michigan, Ann Arbor, Michigan
August 19, 1949

SPECIMENS of holmium, thulium, and lutecium of high purity, prepared by Dr. G. E. Boyd, were made available by the AEC and were irradiated in the Oak Ridge pile. Conversion electron lines in each of the elements were recorded photographically. Observations were also made of the half-lives and

TABLE I. Data connected with the beta-disintegration of Ho 166, Tm 170 and Lu 177.

Z	Element symbol	Half-life	Electron energy	Interpretation	Gamma calculated	Energy probable
67	Ho 166	27.7*H*	71.7 kev	*LI, II* (9.25 kev)	81.0 kev	
			72.6	*LIII* (8.35)	81.0	
			79.0	*M* (2.22)	81.2	
			80.6	*N* (0.45)	81.0	81.0 kev
69	Tm 170	120 *D*	22.9	*K* (61.4 kev)	84.3	
			73.9	*LI* (10.5)	84.4	
			74.3	*LII* (9.95)	84.3	
			75.3	*LIII* (8.94)	84.3	
			82.2	*M* (2.41)	84.6	
			83.8	*N* (0.50)	84.3	84.3
71	Lu 177	6.7*D*	47.6	*K* (65.4 kev)	113.0	
			102.5	*LI, II* (10.7)	113.2	
			103.6	*LIII* (9.6)	113.2	
			110.5	*M* (2.60)	113.1	
			112.4	*N* (0.54)	113.0	113.1
			143.2	*K* (65.4 kev)	208.6	
			197.5	*LI, II* (11.3)	208.8	208.6

the beta- and gamma-energies by absorption. The low energy gamma-ray in each element gave rise to electron lines attributable not only to the *K*, *M*, and *N* levels but also to the sub groups of the "*L*" level. Thus in thulium the single gamma-ray gives rise to six clearly resolved lines. Failure to recognize this complexity of structure for low energy gamma-rays has led to the assumption by the present authors of non-existent gamma-rays in certain other heavy elements.

Holmium. Previous studies[1] on holmium 166 report a half-life at values from 27.0 to 35 hours, with a beta-upper limit from 1.6 to 1.9 Mev and no gamma-rays. In this investigation the decay is followed through eight octaves and the half-life is found to be 27.7 hours. By absorption in aluminum (0.724 g/cm²) the upper limit of the beta-spectrum appears to be 1.64 Mev. In addition to the low energy gamma-ray shown in Table I, absorption in lead indicates a high energy gamma at 0.92 Mev.

Thulium. Thulium 170 has been previously reported[1,2] to decay with a half-life between 105 and 127 days and a beta-upper limit of 0.98 to 1.1 Mev and a high energy gamma-ray of 0.83 Mev. An apparent half-life in the present investigation of 120 days must be confirmed by longer observation. The beta-absorption in aluminum (0.323 g/cm²) indicates an upper energy limit of 0.9 Mev. No high energy gamma-ray appeared to be present, and the beautiful agreement in the energy of the converted gamma-ray by the many electron lines is shown in Table I.

Lutecium. The half-life of lutecium 177, previously reported[1,3] between 6.6 and 6.98 days, appears in this investigation to be 6.8 days. The beta-upper limit by absorption in aluminum (0.092 g/cm²) is 0.46 Mev. The electron lines (see Fig. 1) with their

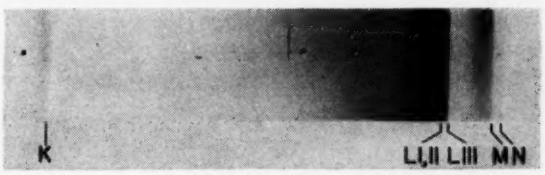

FIG. 1. Showing the electron lines associated with the 113.1 kev gamma-ray from hafnium 177, resulting from the beta-disintegration of lutecium 177.

unmistakable interpretation showing gamma-rays of energy 113.1 and 208.6 kev are presented in Table I.

This investigation was made possible by the joint support of the Atomic Energy Commission and the Office of Naval Research.

[1] W. Bothe, Zeits. Naturzorch 1, 173 (1946); M. Inghram and R. Hayden, Phys. Rev. 71, 130 (1947).
[2] G. Wilkinson and H. Hicks, Phys. Rev. 75, 1370 (1949); D. Saxon and J. Richards, Phys. Rev. 76, 186 (1949).
[3] G. Wilkinson and H. Hicks, Phys. Rev. 74, 1733 (1948); D. G. Douglas Phys. Rev. 75, 1960 (1949).

Dynamic Probe Measurements in the Ionosphere

A. REIFMAN AND W. G. DOW
University of Michigan, Ann Arbor, Michigan
July 25, 1949

EXPERIMENTAL volt-ampere characteristics obtained from a V-2 rocket in the lower part of the *E* layer on December 8, 1947, have been recently analyzed using a technique reported earlier.[1]

The experimental method involves applying a scanning voltage between two collectors on the rocket and transmitting the resulting volt-ampere characteristic to the ground. In this early experiment, the voltage was applied between a cylindrical ring on the nose and the rocket warhead. Utilizable data was obtained on the ascent from around 99 to 103.5 km. Characteristics for three different altitudes are shown plotted in Fig. 1.

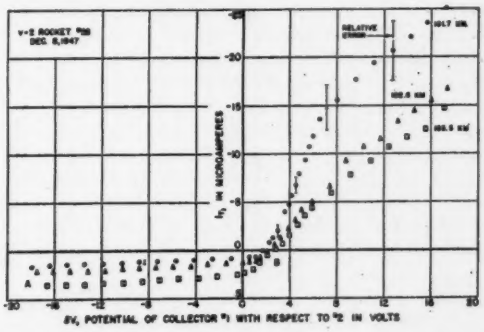

FIG. 1. Experimental volt-ampere characteristics for various altitudes.

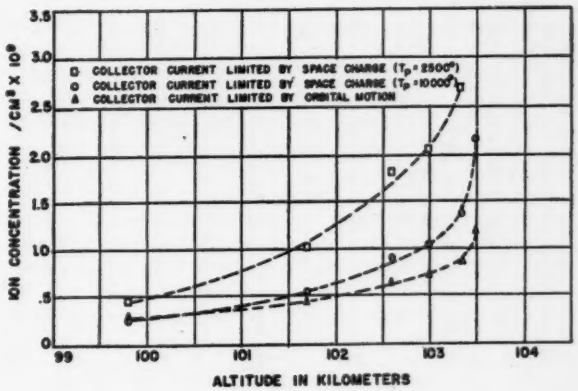
□ COLLECTOR CURRENT LIMITED BY SPACE CHARGE (T_p = 2500°)
○ COLLECTOR CURRENT LIMITED BY SPACE CHARGE (T_p = 10000°)
△ COLLECTOR CURRENT LIMITED BY ORBITAL MOTION
ION CONCENTRATION /CM³ X 10⁵
ALTITUDE IN KILOMETERS

FIG. 2. Ion density *vs.* altitude.

The ion density is calculated from the region *AB* using a method which is based upon the linearity of the i_T^2 plot as a function of δV. The experimental data for this firing gives rise to fairly good straight lines. Dependent on the initial ion energy (which was not measured in this experiment), the ion density may be evaluated directly from the slopes of these lines. Figure 2 is a plot of the ion density as a function of altitude for a range of initial ion energies.

The lower curve is based upon initial ion energies high enough to establish orbital current limitation. This would be satisfied for energies greater than 3 volts. The other two curves are based upon ion energies small enough to establish more nearly a sheath area current limitation. All of the curves in Fig. 2 have been calculated considering edge effects, which are quite large in this experiment.

Indications of a very little ionization occurred around 70 km. However the sensitivity of the instrument did not permit any quantitative evaluation until an altitude of around 99 km was

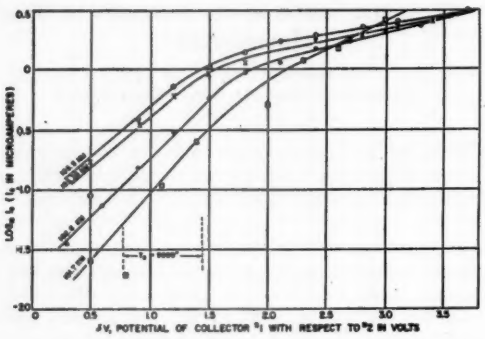

FIG. 3. $\text{Log}_{10} i_e$ *vs.* δV for a range of altitudes.

attained. Over the measurable range, 99 to 103.5 km, the results of all three calculations show progressively increasing ion density with altitude. The curves agree within order of magnitude, in spite of the uncertainty in ion energy.

At the time of this firing, the Bureau of Standards radio propagation measurements indicated a virtual E layer height of 110 km and a maximum electron density of $1.45\times10^5/\text{cm}^3$. This is in good agreement with the experimental results shown in Fig. 2.

In Fig. 3, the logarithm of the electron current measured as a function of the retarding potential δV is also calculated from the region AB of the experimental data in Fig. 1. These plots are essentially integrated electron energy distributions for only the high energy range of the distribution.

For small values of δV (more retarding field), the $\log i_e$ curve is very nearly linear. At slightly higher δV, the dependence becomes more quadratic with δV. Beyond 3 volts, the variation with voltage is affected by the current to the rocket.

These curves indicate roughly a distribution which is more nearly Davydov than Maxwellian. Under such circumstances it is not possible to assign a temperature to the electrons. However, as a first approximation, this condition can be interpreted roughly as a Maxwellian distribution with a superimposed drift. The linear portion indicate a temperature for the Maxwellian distribution of around 5000°K. This does not appear to undergo any change with altitude. The existence of a drift tends to make this temperature, calculated from the slope, too high. For an estimated drift around 4 electron volts, a more conservative estimate of the electron temperature would be about 2500°K. The displacement of the $\log i_e$ curves, the quadratic dependence on δV, and the voltage for $i_T=0$ in Fig. 1 provide strong evidence for such a drift.

A complete account of the work is being prepared for publication in the very near future. Improved experiments are also planned which should provide more accurate results as to ion density and electron energy distribution.

[1] A. Reifman and W. G. Dow, Phys. Rev. **75**, 1311A (1949).

A Cloud-Chamber Study of Fission Fragment Ranges in Air

J. K. BØGGILD, L. MINNHAGEN, AND O. B. NIELSEN
Institute for Theoretical Physics, University, Copenhagen, Denmark
August 22, 1949

THE mean ranges in air of the ^{235}U fission fragments have been measured by means of a 25-cm cloud chamber. The experimental arrangements were similar to those used in previous investigations of fission fragment ranges in other gases.[1] The uranium layer (thickness about 0.5 mg/cm^2) was evaporated on an extremely thin gold foil and suspended in the middle of the chamber. The gas mixture was air and the vapors of a mixture of ethyl alcohol and water in equal parts, the total pressure being about 20 cm of Hg. The stopping power was determined by means of polonium alpha-particles and was controlled by the tracks of the slow neutron-induced disintegration, $^{14}\text{N}(n,p)^{14}\text{C}$. A photograph of a complete pair of fission fragment tracks is shown in Fig. 1(a) together with two small photographs, Figs. 1(b) and 1(c), showing examples of $^{14}\text{N}(n,p)^{14}\text{C}$ tracks, picked out among numerous such tracks appearing in the same series of about 10,000 pictures.

Figure 2 gives the range distribution of 40 complete pairs of fission fragment tracks and, furthermore, the range statistics of the $^{14}\text{N}(n,p)^{14}\text{C}$ tracks and the UI and UII alpha-groups. The latter groups also check the experimental technique since the mean ranges measured were found to be 26.3 and 31.9 mm of air, respectively, in good agreement with the values given by Holloway and Livingstone,[2] *viz.*, 26.5 and 32.1 mm.

The mean ranges of ^{235}U fission fragments in air at S.T.P. were found to be short range group, 19.5 mm; long range group, 25.4 mm; range in total, 44.9 mm.

The method of radiochemical analysis of individual fission products has been used by several authors for determining ranges in air. For the ^{235}U fission masses 139 and 91, Finkle, Hoagland, Katcoff, and Sugerman[3] report maximum ranges of 18.5 and 25.8 mm, respectively. The corresponding mean ranges are bound to be appreciably shorter than those indicated by our cloud-chamber value given above, which should represent the most probable fission masses 139 and 94.

These authors, moreover, report ranges of ^{239}Pu fission fragments, but the values are considerably smaller than those found in recent measurements by Katcoff, Mishel, and Stanley[4] in their extensive study of extrapolated and mean ranges in air of ^{239}Pu

(a)

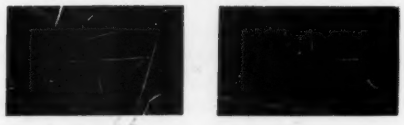

(b) (c)

FIG. 1(a). Complete pair of fission fragment tracks in air $+\frac{1}{2}C_2H_5OH$ $+\frac{1}{2}H_2O$, total pressure about 20 cm of Hg. (b) and (c). Tracks, in the same magnification as (a), of the slow neutron-induced disintegration, $^{14}\text{N}(n,p)^{14}\text{C}$ recognizable by their appearance as proton tracks starting from the small lumpy track of the recoiling ^{14}C nucleus.

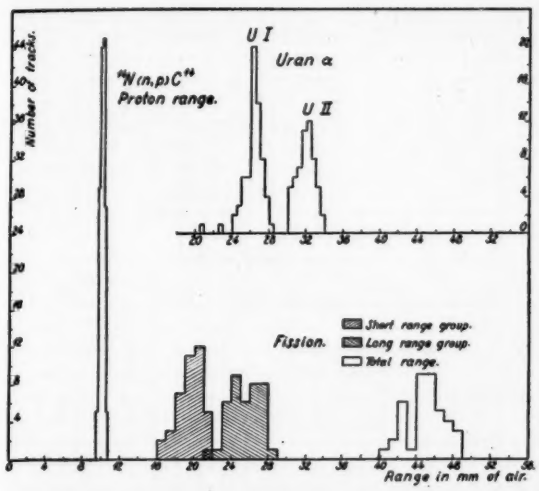

FIG. 2. Histogram of the range distribution of 40 complete pairs of ^{235}U fission fragment tracks and of the ^{14}N$(n,p)^{14}$C tracks used as controls. The range statistics of the UI and UII alpha-groups is given in a separate histogram. Mean range of the combined ^{14}N$(n,p)^{14}$C tracks 10.3 mm; UI and UII 26.3 and 31.9 mm, respectively; heavy and light fragment group 19.5 and 25.4 mm, respectively, and mean total range of paired fragment 44.9 mm.

fission fragments. Since the discrepancy here is ascribed to non-uniformity of the plutonium layer used in the work of Finkle *et al.*, similar defects might possibly be responsible for the diverging results of their and our values.

A closer comparison of our values with those of Katcoff *et al.* is hardly feasible as the two fission processes are somewhat different; however, it is noteworthy that their mean range values of 19.3 and 25.1 mm for the masses 131 and 94, respectively, in the ^{239}Pu fission are rather close to our values for the two groups of ^{235}U fission fragments, *viz.*, 19.5 and 25.4.

Measurements of the mean total range of ^{235}U fission fragments in photographic emulsions were made by various observers.[5] In Ilford nuclear research emulsions B1 and C2, the mean total track length was found to be about 24–25μ, which is about 1835 times smaller than the total range in air of 44.9 mm given above. The corresponding figures for UII alpha-particle tracks in these emulsions, as examined by Green and Livesey[5] and Lattes, Fowler, and Cuer,[6] were found to be about 1680 times smaller than the range in air. This means that the relative stopping power of the emulsion is somewhat different for fission fragments and for UII alpha-particles and, as an average over the range, about 8 percent larger for the fragments.

Keeping in mind that the stopping characteristics of the emulsion due to its large content of silver and bromine is similar to those of heavy gases, this is in agreement with present and previous cloud-chamber studies. Here the range of fission fragments in argon and xenon as compared with the range of polonium alpha-particles was found to be shorter than in air by about 3.5 and 9 percent, respectively. Incidentally, it may also be noted that the content of hydrogen is expected to contribute moderately to the diminution of the fragment ranges in the emulsion, since the fragment ranges relative to the range of alpha-particles were found shorter in hydrogen than in any other substance.

The authors wish to express their hearty thanks to Professor Niels Bohr for his continual interest and advice during these investigations.

[1] Bøggild, Arrøe, and Sigurgeirsson, Phys. Rev. **71**, 281 (1947).
[2] M. G. Holloway and M. S. Livingston, Phys. Rev. **54**, 18 (1938).
[3] Finkle, Hoaglund, Katcoff, and Sugarman, Manhattan Project Report CK-1806, 1944; Plutonium Project Record IX B, 662, 1946, cited in reference 4.
[4] Katcoff, Mishel, and Stanley, Phys. Rev. **74**, 631 (1948).
[5] L. L. Green and D. L. Livesey, Nature **158**, 272 (1946). San-Tsiang, Zah-Wei, Chastel, and Vigneson, J. de phys. et rad. **8**, 165, 200 (1947). P. Demers, Phys. Rev. **70**, 974 (1946).
[6] Lattes, Fowler, and Cuer, Proc. Phys. Soc. **59**, 883 (1947).

Erratum: Bremsstrahlung in High Energy Nucleon-Nucleon Collisions

[Phys. Rev. **76**, 58 (1949)]

J. ASHKIN AND R. E. MARSHAK
University of Rochester, Rochester, New York

THROUGH an unfortunate oversight one set of intermediate states was omitted in the matrix element for the γ-emission accompanying proton-proton or neutron-neutron collisions. With the approximations of neglecting the nucleonic recoil energies in the energy denominators and of neglecting the γ-ray momentum compared to $\mathbf{p}_0 \pm \mathbf{p}$ in the Fourier transforms of the nuclear potential, there is found to be *no* γ-emission in the collision of like particles. (Equations (8) and (9) are incorrect.) For the magnetic emission this might have been anticipated from the fact that in the neutron-proton collision the effect is proportional to $(\mu_P - \mu_N)^2$. For the electric emission in the collision of two protons it is evident that in the center of mass system the total electric dipole moment is initially zero and remains zero if the recoil due to the γ-emission is neglected. There is therefore no electric dipole emission with the approximations made.

This classical argument in the electric case can be justified by the fact that the formula (6) given for the electric emission in the neutron-proton collision can be deduced from a completely classical treatment of the bremsstrahlung. According to classical electromagnetic theory the total energy radiated by a charged particle with trajectory $\mathbf{x}(t)$ (velocity $\mathbf{v}(t)$) is distributed in frequency and direction according to

$$dQ_{\nu,\Omega} = \nu^2 d\nu d\Omega / 4\pi^2 c^3 |\mathbf{I}|^2,$$

where

$$\mathbf{I} = \int\int d\mathbf{r} dt \mathbf{n} \times e\mathbf{v} \delta(\mathbf{r} - \mathbf{x}(t)) \exp[i\nu(t - \mathbf{n}\cdot\mathbf{r}/c)]$$
$$= e\int_{-\infty}^{\infty} dt \mathbf{n} \times \mathbf{v} \exp[i\nu(t - \mathbf{n}\cdot\mathbf{x}/c)]$$
$$= \frac{ie}{\nu}\int_{-\infty}^{\infty} ds \exp[i\nu s] \frac{d}{ds}\left[\frac{\mathbf{n}\times\mathbf{v}}{1 - \mathbf{n}\cdot\mathbf{v}/c}\right].$$

Here $\mathbf{n}$ is the direction in which the radiation propagates. A change from t to the variable $s = t - \mathbf{n}\cdot\mathbf{x}/c$ and a partial integration yields the last expression for $\mathbf{I}$. Let the trajectory describe a collision of short duration in a region of dimensions a (the range of the nuclear forces). If we restrict ourselves to frequencies for which $\nu a/c \ll 1$ or to wave-lengths larger than a (γ-ray energies smaller than 137 $mc^2 = 70$ Mev) the integral $\mathbf{I}$ becomes

$$\mathbf{I} = \frac{ie}{\nu}\Delta\left[\frac{\mathbf{n}\times\mathbf{v}}{1 - \mathbf{n}\cdot\mathbf{v}/c}\right],$$

where Δ means the change in the quantity as a result of collision. The formula (6) for the electric emission results if the classical radiation formula (with the $\mathbf{n}\cdot\mathbf{v}/c$ in the denominator neglected) is multiplied by the quantum mechanical cross section for a given change in velocity as a result of the nuclear collision. $\mathbf{n}\times\Delta\mathbf{v}$ becomes $\mathbf{n}\times(\mathbf{p}_0 - \mathbf{p})$ times $1/M$ and its square gives directly the angular dependence expressed in (6).

For a collision of two protons the integral $\mathbf{I}$ is a sum of two terms corresponding to the change in velocity of each proton. Neglecting the recoil due to the photon and the $\mathbf{n}\cdot\mathbf{v}/c$ in the denominator, we obtain zero for the total. These approximations are clearly no longer valid for relativistic energies of the nucleons.

The Existence of Stable Nuclei as Related to the Principle of Regularity and Continuity of Series and the Ends of Nuclear Shells

WILLIAM D. HARKINS AND MARTIN POPELKA, JR.
University of Chicago, Chicago, Illinois
August 12, 1949

IN 1916, when the atomic nucleus of Rutherford was only five years old, Harkins submitted a paper[1] which introduced a new

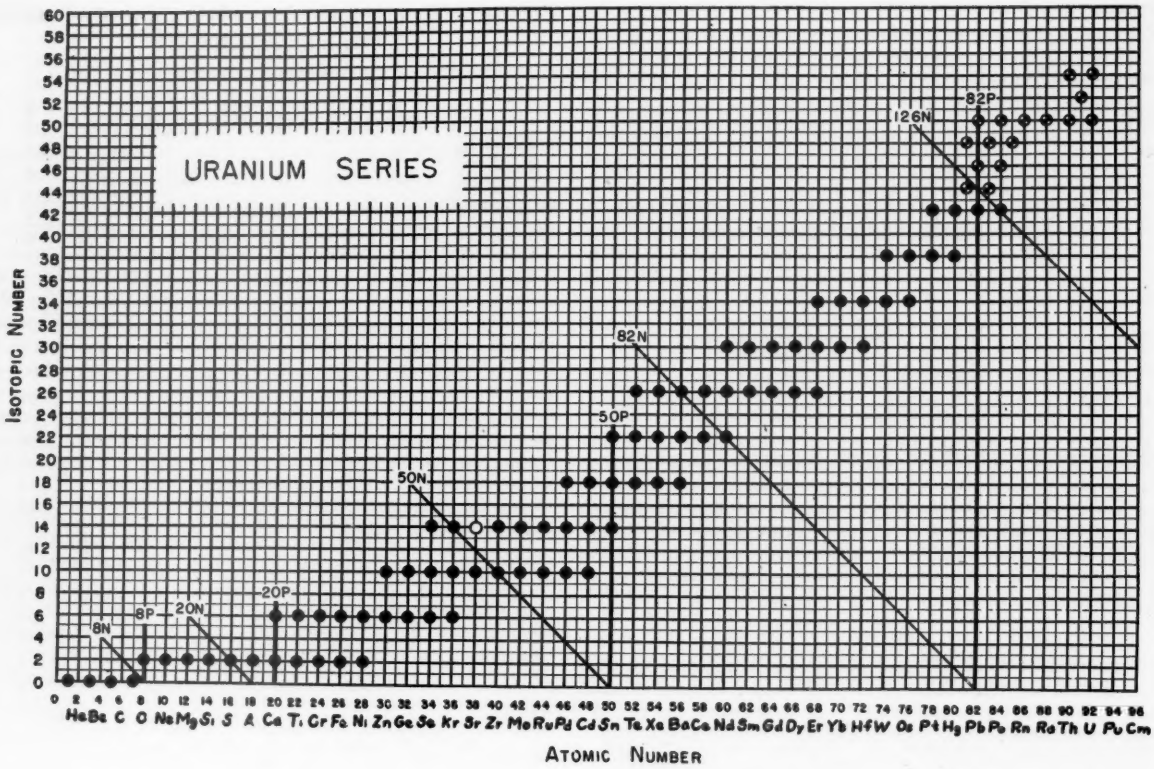

FIG. 1. Uranium series. The ends of neutron and proton shells are indicated by heavier lines at values 8, 20, 50, 82 and 126. The one unstable species is strontium of isotopic number 14, designated by an open circle.

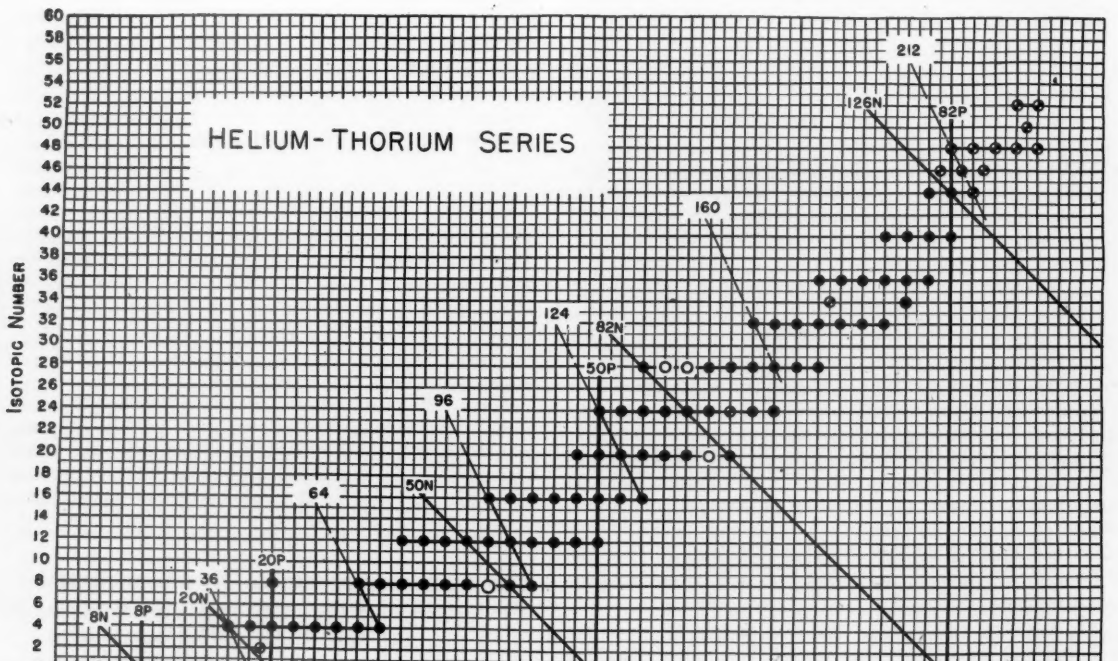

FIG. 2. Helium-thorium series. Symbols same as Fig. 1.

general principle into nuclear science. This indicated that the abundance of elements in the meteorites, earth and stars, taken as a whole, is dependent on nuclear relations, and not upon those which are chemical. It was shown that in the meteorites and in the rare earths each element of even number is much more abundant than either of the two adjacent elements of odd number. In a series of papers[2-14] (1920–23) the same was shown for neutrons. With respect to the number of neutrons (N) and of protons (P) the abundance is related to four classes.

4. Every species specified by a principle of continuity, considered later, exists and is stable, except in the relatively few cases in which some other principle intervenes and the nucleus is unstable (5 and 6 below).

5. For the even–even (N and P) series the stability and abundance are in general higher at the end of nuclear shells than for adjacent species not at the end of shells. The least stable and abundant species are adjacent in proton and neutron content to the ends of shells. For example in the uranium or $n+2$ series 83

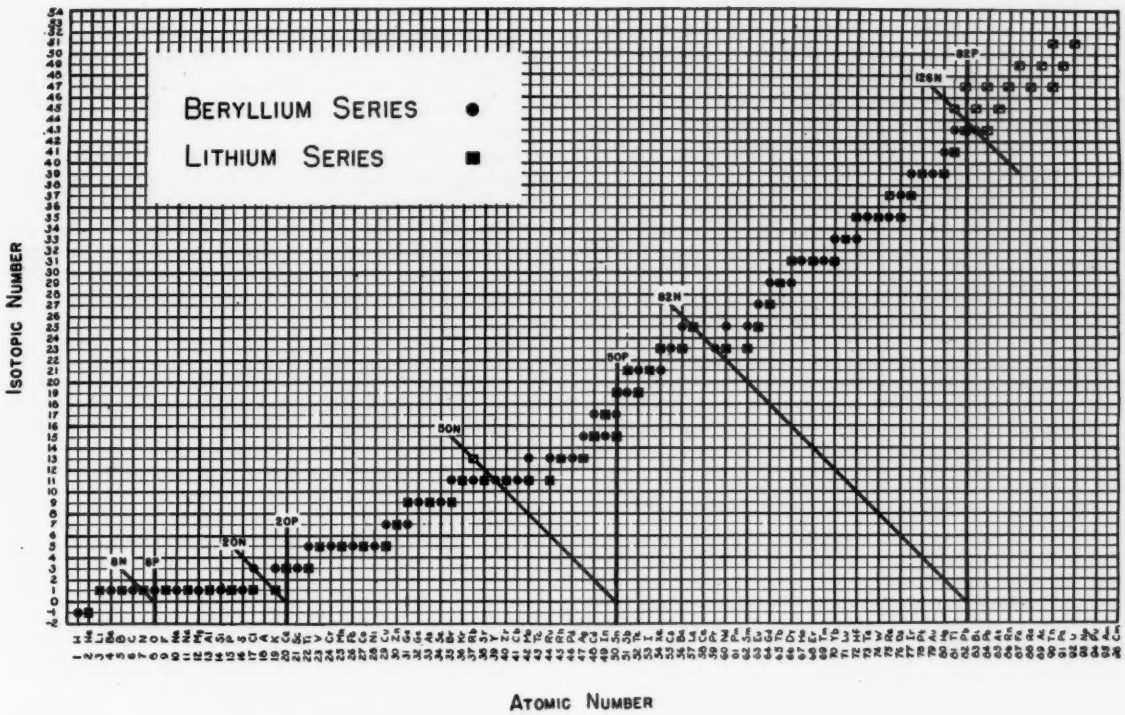

FIG. 3. Odd series of stable species. Radioactive species designated by a different symbol.

With respect to cosmic abundance almost all atoms (hydrogen excluded) belong to I (Even N–Even P), relatively few to II (Even N–Odd P) and III (Odd N–Even P), and none to IV (Odd N–Odd P). An exception to IV is that if $N=P$ odd–odd nuclei occur up to $P=7$ for nitrogen, an abundant atomic species in the universe. Similarly, for $N=P$ Ca^{40}, $N=20$, $P=20$ is the highest species.

It was shown also that all stable nuclei exist in a relatively narrow valley of stability. This is prominent when N/P *vs.* P is plotted.

These relations are basic for what is termed here the principle of regularity and continuity of series. This is illustrated here by Figs. 1 and 2, which represent the two even series of masses $4n+2$ and $4n$. These occupy a much wider region of the valley of stability than the even–odd and odd–even series of Fig. 3, which represents the $4n+3$ and $4n+1$ series.

Now it is extremely remerkable that:

1. No stable nuclear species is known *outside* the limits of these series in terms of proton (P) and neutron (N) content.

2. No stable species is known *inside* the series, except those specified by the series.

3. For even mass (M) both the number of protons and of neutrons is always even. No exception is known except for 4 species in which $N=P$ with P very small (7 or less). For odd mass ($P+N$) either P or N may be odd, but not both. All other nuclei are excluded from the system of stable nuclei.

positions are available, 82 are filled, and the one unfilled position is adjacent to the end of a shell.

6. In the even–odd and odd–even series, to the non-occurrence of adjacent isobars. In these series 106 positions are filled, 10 are unfilled by the non-occurrence of adjacent isobars. Elements 42 and 61 are excluded, as are the odd isotopes of argon (see their peculiar pattern in Fig. 3). Several of these are also close to the end of an 82 neutron shell.

7. In Fig. 2 (helium-thorium series) it appears as though three atomic species predicted by the theory of continuity, of isotopic number 8, and with atomic numbers 22, 24, and 26, are missing as stable isotopes. However, these are not predicted by the theory, since the irregularity is due to the occurrence of the highest isotope of calcium of isotopic number 8, whose stability is related to the fact that it lies at the end of a 20-proton shell.

[1] W. D. Harkins, J. Am. Chem. Soc. 39, 856 (1917).
[2] W. D. Harkins, J. Am. Chem. Soc. 42, 1956 (1920).
[3] W. D. Harkins, J. Am. Chem. Soc. 43, 1038 (1921).
[4] W. D. Harkins, Phil. Mag. 42, 305 (1921).
[5] W. D. Harkins and S. L. Madorsky, Phys. Rev. 29, 135 (1922).
[6] W. D. Harkins, J. Franklin Inst. 194, 165 (1922).
[7] W. D. Harkins, J. Franklin Inst. 194, 329 (1922).
[8] W. D. Harkins, J. Franklin Inst. 194, 521 (1922).
[9] W. D. Harkins, J. Franklin Inst. 194, 654 (1922).
[10] W. D. Harkins, J. Franklin Inst. 194, 783 (1922).
[11] W. D. Harkins, J. Franklin Inst. 195, 67 (1923).
[12] W. D. Harkins, J. Franklin Inst. 195, 533 (1923).
[13] W. D. Harkins, J. Franklin Inst. 195, 591 (1923).
[14] W. D. Harkins, J. Am. Chem. Soc. 45, 1426 (1923).

On the Abundance of I^{129}, Te^{118}, and Pt^{190}

WALLACE T. LELAND*
Department of Physics, University of Minnesota, Minneapolis, Minnesota
August 17, 1949

EVIDENCE that I^{129} must have a very long half-life, of the order of 10^8 years, has been presented by Katcoff.[1] From his value for the neutron capture cross section of I^{129} and the I^{130} yield of normal iodine irradiated with slow neutrons, he obtains an upper limit of from 0.3 to 3 parts per 10^6 as the amount of I^{129} present in normal iodine. Nier[2] has reported an upper limit of 25 parts per 10^6 based on mass spectrographic analysis.

In the present work a 60° mass spectrometer was used, the design being similar to one already described by Nier.[3] Iodine vapor was introduced into the spectrometer through a capillary leak and ionized by electron impact. The separated ion beams were detected and amplified by an electron multiplier of a design similar to that described by Allen.[4] Examination of I^+ ions revealed a small peak in the mass 129 position less than 1 part in 3×10^6 relative to the 127 peak. The 129 peak found, however, can be attributed to DI^+ ions whose presence was signaled by a HI^+ peak about 0.2 percent as large as the I^{127+} peak. It is concluded that if I^{129} does exist in nature its abundance must be less than 3 parts in 10^6 relative to I^{127}.

In a recent article H. Duckworth[5] pointed out that on the basis of regularities in a plot of the atomic number *versus* atomic weight of the lightest stable isotope of elements with even atomic number one would predict the existence of Pt^{190}, Te^{118}, and Gd^{150}. The same author and co-workers[6] conducted a mass spectrographic analysis of Pt and found Pt^{190}. Their measurements were made using a double focusing mass spectrograph similar to Dempster's and employed photographic plates for the detection of ions. They report the abundance of Pt^{190} as 0.006 percent with an accuracy of 20 percent.

Using the same 60° spectrometer mentioned above but with the usual ion collector and electrometer current amplifier,[3] the existence of Pt^{190} has been confirmed but the abundance found to be greater than reported by the discoverers. Pt vapor was obtained by evaporation of metallic Pt from a heated Pt coated tungsten filament. This type of source did not provide a sufficiently constant ion beam to permit the usual accuracy of measurement and also there were small amounts of impurity present. Correlation of the Pt^{190} peak to the Pt^{192} peak with a variation of five in intensity indicated, however, that within the accuracy of the measurements the impurities were negligible. Figure 1 shows a typical spectra obtained in the mass region 188–200. Assuming the abundance of Pt^{192} to be 0.78 percent[7] the abundance of Pt^{190} is found to 0.012 percent with an accuracy of about ten percent.

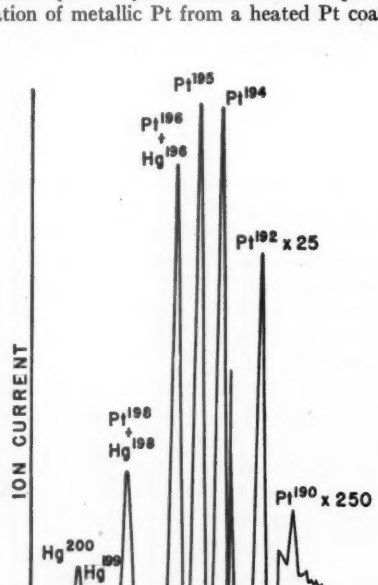

FIG. 1. Mass spectrum of platinum showing new isotope Pt^{190}. The mercury peaks are due to residual vapor in the apparatus.

In the case of Te no Te^{118} was found, but an upper limit of 0.0003 percent was placed on its abundance. Te vapor was obtained by evaporating the metal in a small oven. Examination of Te^+ spectrum revealed small peaks at mass 118 and at neighboring masses. Lack of correlation with the known Te peaks, however, indicated they were due to impurities. In any event the limit set on the Te^{118} abundance corresponds to the height of the observed 118 impurity peak.

The writer wishes to express his sincere appreciation to Professor A. O. Nier under whose guidance the work was carried out. The instrument used in this work was built with a grant from the Graduate School. The research was supported by the joint program of the Office of Naval Research and the Atomic Energy Commission. Assistance was also given by the University of Minnesota Technical Research Fund.

* AEC Fellow.
[1] S. Katcoff, Phys. Rev. **71**, 826 (1947).
[2] A. O. Nier, Phys. Rev. **52**, 937 (1937).
[3] A. O. Nier, Rev. Sci. Inst. **18**, 398 (1947).
[4] J. S. Allen, Rev. Sci. Inst. **18**, 739 (1947).
[5] H. E. Duckworth, Phys. Rev. **75**, 1438 (1949).
[6] Duckworth, Black, and Woodcock, Phys. Rev. **75**, 1438 (1949).
[7] Inghram, Hess, and Hayden, Plutonium Project, Report ANL-4012, p. 7 (July, 1947).

The Zenith Angle Dependence of Flux of the Hard Cosmic-Ray Component up to 36,000 Feet*

J. F. JENKINS, JR.
Applied Physics Laboratory, Johns Hopkins University
Silver Spring, Maryland
August 18, 1949

THE counting rates of Geiger tube telescopes containing 8 and 10 cm of Pb absorber were measured in B-29 aircraft in the neighborhood of Inyokern, California, (43°N geomagnetic latitude) from 2250 to 36,000 feet during April 1947. These telescopes were similar to one used by Schein and Wilson[1] (see corner of Fig. 1) and the dimensions are given as follows:

(1) All copper walled Geiger tubes; 2.54-cm outside diameter, 2.38-cm inside diameter and 13.9 cm in effective length, (2) Pb absorber between *A* and *B* and between *C* and *D*, 2-cm thick, (3) Pb absorber between *B* and *C*, 6-cm thick, (4) Pb absorber on sides of *C*, 2-cm thick by 6-cm high each side.

The Geiger tube outputs were connected such that all tubes bearing the same letter were in parallel; the tubes numbered C_1 and C_2 were also independent. The data were taken at a zenith angle setting of 0° and in the geographical north, east, south, and west directions with a zenith angle setting of 45°, where the zenith angle was measured between the vertical and the plane of symmetry of the telescopes parallel to the axis of revolution of the Geiger tubes. A paper tape recording was made, at each altitude, of the coincidence counting rates ABC, BCD, $(ABC+BCD)C_1C_2$ and $(ABC+BCD)E$. From this recording, it was then possible to find the net counting rates, due to single particles, for telescope ABC and telescope BCD.** It is felt that this is a realistic assignment of single particle events since the counting rates $(ABC+BCD)C_1C_2$ and $(ABC+BCD)E$ account for a high percentage of the multiple particle events of narrow and wide angular spread, respectively.

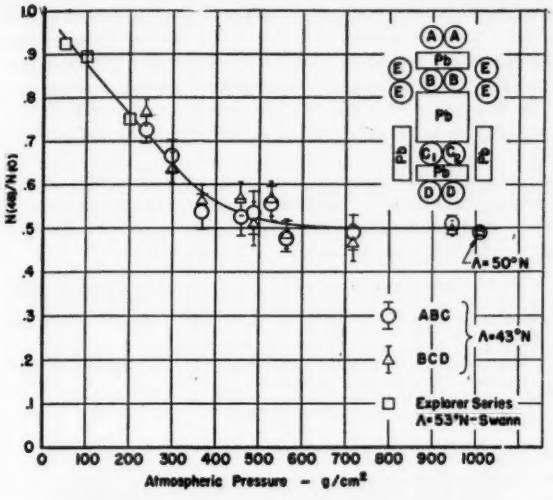

FIG. 1. Variation of the ratio of counting rates at zenith angles 45° and 0° with atmospheric pressure.

The variation with atmospheric pressure of the ratio of the penetrating particle counting rate at zenith angle setting 45° to that of 0° for the telescopes *ABC* and *BCD* is shown in Fig. 1, and this ratio is seen to be essentially the same for these two telescopes. The counting rate used for the numerator of this ratio was the average of the counting rates in the north, east, south, and west directions. The vertical bars indicate the statistical probable error of each point. The over-all correction made for counter dead-time, resolving time, counter efficiency, and recording circuit efficiency was less than 1 percent for the highest counting rate. The percentage of multiple particle events subtracted was the same for the case where the zenith angle setting was 0° as for the case where it was 45° for each of the two telescopes. These events accounted for from 1 percent at sea level to 18 percent of the net counting rate at 36,000 feet in the case of the *ABC* telescope and from 1 percent at sea level to 24 percent of the net counting rate at 36,000 feet in the case of the *BCD* telescope. Similar data, multiple particle events not excluded, obtained with narrow angle, non-leaded telescopes in the Explorer Balloon Flight Series[2] are shown for comparison.***

It is interesting to note the agreement between the zenith angle dependence of the total flux (Explorer Series) and that of the hard component (present work) at 200 g/cm^{-2}.

The assumption of a cosine power law variation of directional flux with zenith angle is suggested by the well-established $\cos^2\theta$ zenith angle dependence of the hard component flux at low altitudes.[3] Thus, if it is assumed that the directional flux, $J(\theta)$ (particles cm^{-2} sec.$^{-1}$ steradian^{-1}), at zenith angle θ, independent of azimuth, has the form:

$$J(\theta)=J(0)\cos^n\theta, \quad 0\leqq\theta\leqq\pi/2,$$
$$J(\theta)=0, \quad \pi/2<\theta\leqq\pi;$$

then from consideration of Fig. 1, the exponent, n, must vary with altitude.

To find the manner in which the exponent, n, varies with altitude, the ratio of the counting rates of these telescopes in the 45° and vertical positions, N(45°)/N(0°), has been calculated after the method of Greisen[4] for various assumed values of the exponent, $0\leqq n\leqq 2$, from the expression for the directional counting rate given in terms of the directional flux, the solid angle and the area of the telescope

$$N(\theta)=\eta\int_\sigma\int_\Omega J(\theta)d\Omega d\sigma \text{ sec.}^{-1},$$
$$J(\theta)=J(0)\cos^n\theta, \quad 0\leqq\theta\leqq\pi/2,$$
$$J(\theta)=0, \quad \pi/2<\theta\leqq\pi,$$

where η is the over-all efficiency of the system. In making this calculation, proper account has been taken of the spread of zenith angles within the acceptance angle of the composite telescopes *ABC* and *BCD*.

The values of n which gave a calculated ratio, N(45°)/N(0°), equal to the experimental one at each atmospheric pressure are plotted as a function of atmospheric pressure in Fig. 2. These values of the exponent are independent of the experimental arrangement. Again the points from the Explorer Balloon Flight

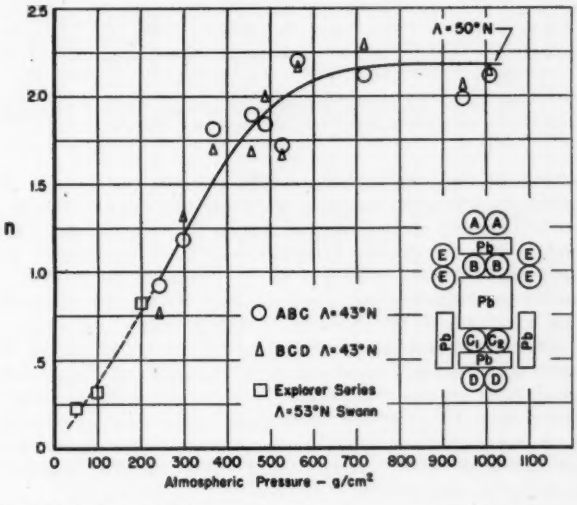

FIG. 2. Variation of n with atmospheric pressure assuming $J(\theta)=J(0)\cos^n\theta$.

Series are included and are seen to follow the same trend, even though they correspond to the total rather than the hard component of the flux.

* This work was supported by the Navy Bureau of Ordnance under Contract NOrd 7386.

[1] M. Schein and V. C. Wilson, Rev. Mod. Phys. **11**, 292 (1939).

** In particular:

$$ABC_{\text{net}}=[ABC-ABC_1C_2-ABCE+ABC_1C_2E],$$
$$BCD_{\text{net}}=[BCD-BC_1C_2D-BCDE+BC_1C_2DE].$$

[2] W. F. G. Swann, Rev. Mod. Phys. **11**, 242 (1939).

*** It is to be noted that the present experimental measurements have been made at only two zenith angles; therefore, they do not establish the form of the zenith angle law.

[3] K. I. Greisen, Phys. Rev. **61**, 212 (1942) and references therein.

Angular Correlation of Delayed Radiations

ARNE LUNDBY
Institute for Atomic Energy Studies and Norwegian Defence Research Establishment, Oslo, Norway

July 11, 1949

THE energy-lifetime relation of nuclear transitions and the internal conversion coefficient in the case of gamma-ray emission do not always lead to unique assignments of spin and relative parity values to excited energy levels of nuclei. It is therefore fortunate when two transitions follow each other in cascade, since, then, observation of the relative direction of emission of the two radiations frequently yields the necessary spectroscopic information. With coincidence circuits the method has been applied to transitions following each other in instantaneous succession.[1] The major experimental difficulties are in this case due to scattering effects and the presence of annihilation radiation.

We have extended the method of radiations which are delayed with respect to each other. Using delayed coincidence circuits, angular correlations can at present be measured when the lifetime of the intermediate state lies between about 10^{-8} and 10^{-2} sec. This state may be a metastable energy level or a short-lived alpha-

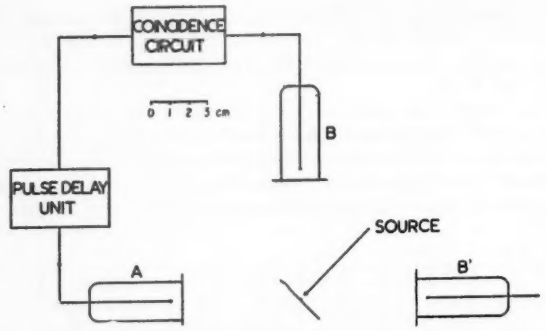

FIG. 1. Schematic diagram of experimental arrangement for measuring directional correlation of delayed radiations.

particle emitter. Since instantaneous coincidences are not recorded, the difficulties mentioned are ruled out. The major experimental difficulty is, in this case, due to the competition of the random with the genuine delayed coincidences. One should endeavor to make the efficiency of the detectors (Geiger-Müller counters) as large as possible and still keep the angular resolution high. Furthermore, the individual counting rates should be kept at a minimum, determined by the maximum practical time of the experiment. For half-lives shorter than about one μsec. the random coincidences are less troublesome. However, when the lifetime is shorter than 10^{-7} sec., the fluctuations in the time lag between the entrance of the ionizing radiation into the Geiger counter and the recording of the corresponding electrical pulse impose a limitation to the accuracy of the result.

With the experimental arrangement of Fig. 1 we have recorded delayed coincidences from a Hf^{181} source at angles 90° and 180° between the counters. The delay introduced in channel A was 2 μsec., while the sum of the effective pulse lengths in the two channels was 1.9 μsec. The Geiger counters in the A and B channels had mica windows of 3 and 1.6 mg/cm², respectively. The angular resolution was about ±9°.

It has been shown that the β^--decay of Hf^{181} leads directly to a 20-μsec. metastable state in Ta^{181}.[2] The β-transition is once-forbidden,[2] and the maximum energy is 0.405 Mev.[3] The Σ-radiation emitted in the decay of the metastable state has an energy of 0.130 Mev and is highly internally converted. It is probably a mixed electric octopole and magnetic quadrupole radiation.[3] Further internally converted γ-rays follow the 0.130-Mev transition, but they are probably of less importance in this experiment.

It is apparent that the observed delayed coincidences are mainly due to β-particles entering counter A and conversion electrons (chiefly from the 0.130-Mev transition) entering counter B. The genuine delayed coincidence rates were found to be 0.018±0.0017 (p.e.) min.$^{-1}$ and 0.02±0.0029 min.$^{-1}$ in the 90° and 180° positions, respectively, before the experiment had to be discontinued for some months. The random coincidence rate amounted to one-fourth of the genuine coincidence rate. A possible deviation from isotropic distribution must therefore certainly be less than 15 percent. It is, of course, quite probable that the distribution actually should be symmetrical owing to the following reason: In our delayed coincidence experiment we have selected the transitions in which the nuclei, decaying by β-emission to the metastable state, remain in this state for between two and four μsec. During this time an originally existing anisotropy could have been removed by external fields which may be acting on the magnetic moment of of the nucleus. The most likely effects would be the coupling between the nucleus and the atomic electrons, or the influence of other fields existing within the crystals or molecules in the source material.[4] On the other hand, if any appreciable alignment of the nuclear magnetic moments with respect to these fields occur, the relaxation time for the process may be rather long. It is therefore our purpose presently to measure angular correlations of the radiations preceding a short-lived state (e.g., Ta^{181*}, Te^{121*}, $Tm^{169*\text{ or }171*}$, Re^{187*}, Po^{213*}, RaC'*, ThC'*, etc.) and the radiations emitted from this state after the lapse of different time intervals. This can easily be achieved by introducing a variable delay in channel A (Fig. 1). It should then be possible to get an indication of the relaxation time for the alignment process, which further may give us some information about the fields acting on the nucleus.

By applying a magnetic field to the sample under low temperature it may even be possible to influence the angular distribution by external means. The corresponding relaxation times may then be studied.

[1] Kikuchi, Watase, and Itoh, Zeits. f. Physik **119**, 185 (1942); R. Beringer, Phys. Rev. **63**, 23 (1943); W. M. Good, Phys. Rev. **70**, 978 (1946); E. L. Brady and M. Deutsch, Phys. Rev. **72**, 870 (1947); A. H. Ward and D. Walker, Nature **163**, 168 (1949).
[2] A. Lundby, Phys. Rev. (to be published). See also S. DeBenedetti and F. K. McGowan, Phys. Rev. **74**, 728 (1948); Bunyan, Lundby, Ward, and Walker, Proc. Phys. Soc. **61**, 300 (1948).
[3] K. Y. Chu and M. L. Wiedenbeck, Phys. Rev. **75**, 226 (1949).
[4] G. Goertzel, Phys. Rev. **70**, 897 (1946).

On the Polarization of Slow Neutrons

J. STEINBERGER AND G. C. WICK
Radiation Laboratory, University of California, Berkeley, California
August 15, 1949

RECENT measurements[1] of Bloch's polarization cross section, p, for thermal neutrons in cold-rolled iron yield a value $p=3.1$ barns, about a factor of 3 larger than the latest previous theoretical value,[2] and one might think that there is a serious disagreement here, requiring some drastic correction in the magnetic interaction law. It has been pointed out, however,[3] that a critical revision of some factors entering the theory leads to a different conclusion. It is the purpose of this note to give a more detailed account of this work.

We are concerned here with an analysis of the "single transmission experiment." A beam of slow neutrons is detected after passing through a slab of iron. The experiment is performed alternately with the iron unmagnetized, and magnetized in a direction perpendicular to the neutron beam. For unmagnetized iron the scattering cross section for both spin orientations of the neutrons is the same. However, when the iron is magnetized, there is an additional contribution from the scattering of the neutrons on the magnetically active d electrons, which is of opposite sign for the two spin orientations: $\sigma_+=\sigma+p$; $\sigma_-=\sigma-p$. If a neutron beam of intensity I_0 passes through a slab of unmagnetized iron d cm thick, with N atoms per cubic cm, it will emerge with intensity $I_u=I_0e^{-Nd\sigma}$. When the iron is then magnetized, the transmitted intensity increases:

$$I_m=I_0/2[e^{-Nd\sigma_+}+e^{-Nd\sigma_-}]=(I_0/2)e^{-Nd\sigma}[e^{+Ndp}+e^{-Ndp}],$$
$$I_m/I_u=\cosh Ndp.$$

The experiment therefore measures p.

The theoretical determination of p, which is somewhat complicated by crystal effects, has been carried out by Halpern, Hamermesh, and Johnson.[4]

For saturated iron:

$$p=\left(\frac{\sigma_{\text{coh}}}{4\pi}\right)^{\frac{1}{2}}\frac{e^2}{mc^2}\mu_n\mu_e\left(\frac{\lambda}{2a}\right)^2\sum_{l<2a/\lambda}\frac{N(l)}{l}\left(1+\frac{l^2\lambda^2}{4a^2}\right)F(l), \qquad (1)$$

where

σ_{coh} = coherent scattering cross section of the iron nucleus,
μ_n = neutron magnetic moment in nuclear magnetons,
μ_e = magnetic moment of all unpaired electrons, in electronic magnetons,
= 2.18 for iron,
λ = de Broglie wave-length of the neutrons,
a = lattice constant of the iron = 2.86×10^{-8} cm,

$$F(l)=(a/2\pi l)\int_0^\infty \sin(2\pi lr/a)\varphi^2 r\,dr \Big/ \int_0^\infty \varphi^2 r^2\,dr,$$

φ = wave function of d electrons (electrons with unpaired spin).

The summation is extended over all positive numbers l, such that $l^2=2n$, $n=1, 2, 3\cdots$.

$N(l)$ is a weight factor for the Debye ring l and is equal to twice the number of ways in which three integers (positive, negative, or zero) can be chosen such that the sum of their squares is equal to l^2. Actually formula (1) is somewhat simpler than the one derived in reference 2. In (1) the reduction in the elastic scattering due to the thermal motion of the lattice points has been neglected. This is done for the following reason. The scattering p is due to the interference between the nuclear scattered wave and the magnetic wave. This interference is preserved in the inelastic scattering. Now whenever the elastic scattering is diminished by the thermal motions, the inelastic scattering is increased by *approximately* the same amount. It is, therefore, a good approximation to say that that which disappears from the elastic scattering reappears in the inelastic scattering. Both effects are, therefore, neglected. Previously only the reduction in elastic scattering had been taken into account, resulting in too low a value for p.

TABLE I. Form factors $F(l)$ as calculated with different wave functions.

l^2	Free atom (Hamermesh[2])	Atom in solid, exchange taken into account, $\varphi=0$ at atomic radius	Atom in solid, exchange taken into account, $\partial\varphi/\partial r=0$ at atomic radius
2	0.48	0.605	0.572
4	0.28	0.453	0.381
6	0.19	0.315	0.269
8	0.12	0.223	0.192
10	0.08	0.157	0.135
12	0.053	0.123	0.104
14	0.035	0.082	0.067

The greatest difficulty in evaluating p comes from the uncertainty in the d electron wave functions which occur in the form factors $F(l)$. Hamermesh[2] has used the Hartree wave functions for free iron atoms. If one tries to improve this slightly by recalculating the wave functions with a Wigner-Seitz boundary condition, one gets hopelessly large positive energies for the d electron states. Evidently the Hartree approximation is insufficient, and it is necessary to take the exchange interaction into account. This has been done roughly in the following way. The d electrons are supposed to move in the potential of the nucleus which is shielded by the inner shells and by 7 $3d$ electrons. The shielding potentials are those of the Hartree calculation for the free atom. To this are added the Fock exchange integrals of a $3d$ electron with all other shells and with its own. In this potential 2 new wave functions are calculated, one zero, and the other with zero derivative at the atomic radius. The first corresponds to the top, the last to the bottom of the d band. There is some reason to believe[5] that the magnetic d electrons are near the top of the band and that the first wave function should be used. However, p has been computed for both. The wave functions are shown in Fig. 1 and the form factors in Table I.

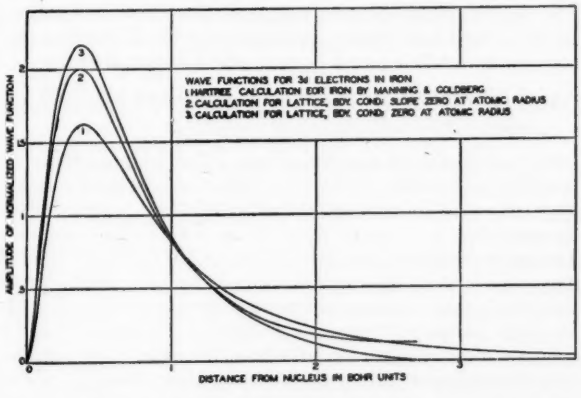
WAVE FUNCTIONS FOR 3d ELECTRONS IN IRON
1 HARTREE CALCULATION FOR IRON BY MANNING & GOLDBERG
2 CALCULATION FOR LATTICE, BDY. COND: SLOPE ZERO AT ATOMIC RADIUS
3 CALCULATION FOR LATTICE, BDY. COND: ZERO AT ATOMIC RADIUS
AMPLITUDE OF NORMALIZED WAVE FUNCTION
DISTANCE FROM NUCLEUS IN BOHR UNITS

FIG. 1. Wave functions for the $3d$ electrons in iron. 1. Hartree wave function for a free iron atom. Exchange not taken into account. 2. Wave function with zero slope at the atomic radius and exchange taken into account. 3. Wave function zero at the atomic radius and exchange taken into account.

The third and only other change which has been made is in the value of σ_{coh}, the cohrerent scattering cross section of the iron nucleus.[6] Transmission measurements on fast epithermal neutrons give for the scattering cross section of an iron nucleus a value $\sigma=11.0$ b.[7] In order to obtain σ_{coh} one must subtract from σ the incoherent part σ_{inc} associated with isotopic disorder and random orientation of the nuclear spins. The main difficulty in the past has been in estimating this incoherent cross section. Recent work indicates that it is quite small.[8,9] We assume a tentative value $\sigma_{inc}=1$ b, then

$$\sigma_{coh}=(11.0-1.0)\text{b}=10\text{ b}$$

which is considerably higher than the value 6.75 b which was apparently used by Halpern and co-workers.[2,4]

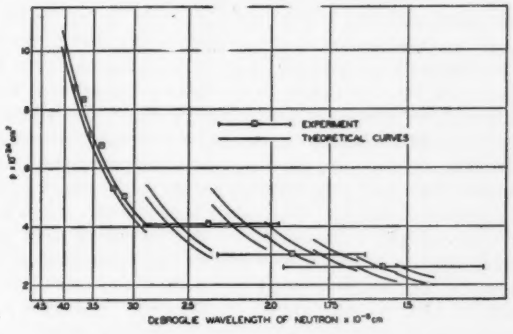

FIG. 2. Observed and calculated values of the magnetic scattering cross section as a function of the neutron wave-length. The experimental points are those of Hughes.

The result of the three improvements described is to bring the theoretically calculated value of p into quite close agreement with the experimental results. Both have been plotted as a function of the velocity of the neutrons in Fig. 2. The agreement is closer than can be justified by the inadequate knowledge of the $3d$ wave functions.

The chief pleasure in this work cam from illuminating discussions with Drs. Fermi, Hughes, Placzek, and Teller.

[1] Hughes, Wallace, and Holtzman, Phys. Rev. **73**, 1277 (1948); experimental values $p\sim2$ b and $p\sim2.2$ b, lower than the recent value of Hughes *et al.*, but definitely higher than the old theoretical value, had already been reported previously by the Stanford group, see Bloch, Condit, and Staub, Phys. Rev. **70**, 972 (1946).

[2] M. Hamermesh, Phys. Rev. **61**, 17 (1942).

[3] J. Steinberger and G. C. Wick, Phys. Rev. **74**, 1207 (1948).

[4] Halpern, Hamermesh, and Johnson, Phys. Rev. **59**, 986 (1941).

[5] See for instance J. C. Slater, Phys. Rev. **52**, 198 (1937).

[6] Independently of our communication (see reference 3) the need for a revision of σ_{coh} in connection with neutron polarization has been pointed out by J. M. Cassels, Phys. Rev. **74**, 111 (1948).

[7] W. W. Havens, Jr. and L. J. Rainwater, Phys. Rev. **75**, 1296 (1949). See also Havens, Rainwater, Wu, and Dunning, Phys. Rev. **73**, 963 (1948), as well as the high velocity part of Fig. 2 in the paper of Hughes *et al.* (reference 1).

[8] Measurements below the crystal cut-off of Hughes *et al.* (reference 1, see especially p. 1281) give a value ~1.5 b for the sum of the incoherent cross section σ_{inc} and the thermal inelastic scattering cross section, which is of the order of 0.5 b. Hence a (very crude) estimate of $\sigma_{inc}=1$ b. A direct measurement of the incoherent cross section as being 0.8 b is mentioned by J. M. Cassels and R. Latham, Phys. Rev. **74**, 103 (1948). Moreover, Burghy, Hughes, and Woolf, Phys. Rev. **76**, 188 (1949) from measurements on single crystals arrive at the conclusion that σ_{inc} is much smaller than the thermal inelastic scattering cross section.

[9] H. Staub has kindly informed us of transmission measurements on a single crystal which also lead to our estimate $\sigma_{inc}=1$ b. We are very indebted to Dr. Staub for communicating these and other results on neutron polarization to us before publication.

A New Molecular Beam Resonance Method*

NORMAN F. RAMSEY
Harvard University, Cambridge, Massachusetts
August 22, 1949

IN past molecular beam resonance experiments,[1-3] the oscillating magnetic or electric field has been extended approximately uniformly throughout the region in which the molecular states were investigated. It is the purpose of this letter to point out that resonance curves of a different and often more useful character can be obtained by suitably varying the amplitude and phase of the oscillating field along the path of the beam.

A particular case that has been investigated in detail theoretically is that in which the oscillating field is applied in two limited regions at the entrance and exit from the space in which the states are investigated. In this case the formula for the transition probability induced by the oscillating field has been derived exactly and has been numerically averaged over the velocity distribution of the molecules in the beam. For the case of a magnetic moment of spin ½, the mean transition probability induced by an oscillating magnetic field, of such a strength as to make the transition probability at exact resonance a maximum, is shown in Fig. 1 in the immediate neighborhood of resonance. The curve[4] corresponding to past methods with an oscillating field strength to produce the same transition probability at resonance is also shown for comparison purposes on the same figure. It can be seen that the new technique produces a curve whose width is 0.6 that of the corresponding standard method. By reducing the value of the oscillating field below that to give maximum transition probability at resonance, the sharpness of the curve can be further increased both with this technique as shown in Fig. 1 and with the standard technique.[5] If a complete curve were taken so that the effect of the finite length of the oscillating field regions affected the result, the curve should be similar to that of Fig. 2.

There are several advantages to the use of separated oscillating fields: (1) The resonance curves are theoretically sharper making possible higher precision measurements with the same length of oscillating field. (2) The resonances are not broadened by irregularities in the homogeneous constant fields since the space average value of the field over the path of the molecule determines the resonance position. This advantage is of great practical importance and in many cases should increase the measurement precision by factors of ten or more. Since the averaging is only along the path of the molecule, considerable uniformity must still be preserved over the beam height. (3) This technique is more easily adapted to very short wave-length radiation where the wave-length of the radiation is less than the length of the homogeneous field region. (4) The technique is adaptable to experiments where the oscillating field cannot be made to penetrate the region where the measurement is desired, as in an experiment now being started on the Larmor precession frequency of neutrons in iron. (5) By introducing a 90° relative phase shift between the two oscillatory fields the resonance curve can be altered to a dispersion type curve which is particularly suited for a precision measure of the position of exact resonance.

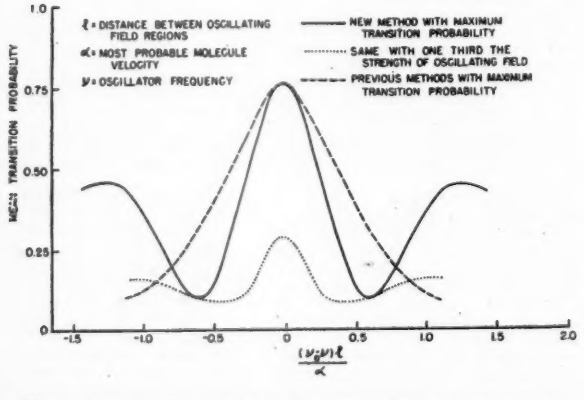

FIG. 1. Transition probability in immediate vicinity of resonance.

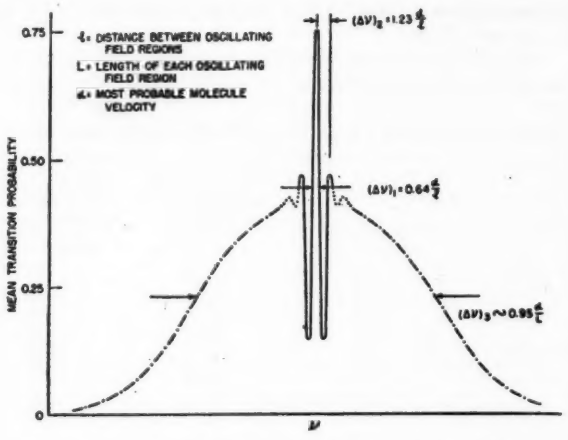

FIG. 2. Transition probability showing effect of finite length of oscillating field regions.

* This work was assisted by the Joint Program of the ONR and the AEC.
[1] Rabi, Millman, Kusch, and Zacharias, Phys. Rev. **55**, 526 (1939).
[2] Kellogg, Rabi, Ramsey, and Zacharias, Phys. Rev. **56**, 728 (1939).
[3] Kusch, Millman, and Rabi, Phys. Rev. **57**, 765 (1940).
[4] H. C. Torrey, Phys. Rev. **59**, 293 (1941).
[5] Bloch, Nicodemus, and Staub, Phys. Rev. **74**, 1025 (1948).

A Suggestion Regarding Emission Phenomena in (Ba−Sr)O Cathodes

E. S. RITTNER, F. K. DU PRÉ, AND R. A. HUTNER
Philips Laboratories, Inc., Irvington-on-Hudson, New York
August 10, 1949

THE model generally used to explain thermionic emission, i, and electrical conductivity, σ, of (Ba−Sr)O cathodes consists of a donor level widely separated from the conduction band ($\Delta\epsilon\sim 1.4$ ev).[1,2] This model leads to the following formulas:

$$i=[n_b^{\frac{1}{2}}(8\pi m)^{\frac{1}{2}}e(kT)^{5/4}/h^3](1-r)\exp[-(\chi+\tfrac{1}{2}\Delta\epsilon)/kT], \quad (1)^3$$

$$\sigma=\sigma_0\exp(-\Delta\epsilon/2kT), \quad (2)$$

where n_b is the density of donors and χ the electron affinity. The temperature dependence of i and σ for a well-activated cathode is thus satisfactorily accounted for using the above $\Delta\epsilon$ and $\chi\sim 0.3$ ev, corresponding to a work function of ~ 1 ev. However, there remains the difficulty that, taking n_b as $3\times 10^{17}/\text{cm}^3$, the chemically determined value;[4] the work function as 1.01 ev, based on recent data by Wright;[5] and assuming the reflection coefficient, r, to be zero, the calculated value of i at 740°C is 51 amp/cm² as compared to experimental d.c. values[5] of the order of 0.5 amp/cm².

Many attempts have been made to explain this difficulty. We think, however, that the situation has been completely changed by the recent work of Vink,[6] who has extensively investigated the conductivity of (Ba−Sr)O cathodes over a much wider temperature range than that employed previously. This work reveals a region of lower activation energy in temperature range *I* (600–800°K) than that in range *II* (800−1000°K).[7] The value of the slope in range *I* decreases with activation and in an active cathode can be as low as 0.1–0.2 ev. Vink has concluded that there are two parallel conduction mechanisms in the cathode. One is the electron conduction through adjoining particles of the coating, which dominates below 800°K. The other is the conduction by the electron gas in the pores between the particles, which dominates above 800°K. The latter conclusion is supported by his calculations of the coating resistance based upon the electron gas

hypothesis. Moreover, the activation energy in range *II*, after correcting for the slope in range *I*, is substantially equal to the work function, thus confirming his picture. If Vink's conclusions are accepted, then the previous assumption of a donor level about 1.4 ev below the conduction band appears unwarranted. In fact, Vink's slope in range *I* would lead one to expect a smaller value of $\Delta\epsilon$, which might be as low as 0.1–0.4 ev in an active cathode.

What we want especially to point out here is that donors this close to the conduction band are highly, if not completely, ionized above 800°K for $n_b=3\times10^{17}/\text{cm}^3$. If one assumes completely ionized donors and a negligible contribution from the full band,[8] then the emission equation becomes[3]

$$i=n_b e(2\pi m)^{-\frac{1}{2}}(kT)^{\frac{1}{2}}(1-r)\exp(-\chi/kT). \quad (3)$$

Note that the work function in this case is equal to χ and should be determined from an $i/T^{\frac{1}{2}}$ plot; using Wright's data,[5] we obtain $\chi=1.08$ ev. If n_b is again taken as $3\times10^{17}/\text{cm}^3$ and $r=0$, Eq. (3) predicts an emission density at 740°C of 1.0 amp/cm², compared to the experimental d.c. values of the order of 0.5 amp/cm². For the case of strongly, but not completely, ionized donors, the calculated value is somewhat lower than 1.0 amp/cm². Hence, the concept of highly ionized donors greatly improves the agreement with experiment for well-activated (Ba−Sr)O cathodes.

We are indebted to Professor G. E. Uhlenbeck for the final form of this letter and to Dr. O. S. Duffendack for his encouragement and support.

[1] A. S. Eisenstein, *Advances in Electronics. 1. Oxide Coated Cathodes* (Academy Press, Inc., New York, 1948).
[2] E. Nishibori and H. Kawamura, Proc. Phys. Math. Soc. Japan **22**, 378 (1940).
[3] R. H. Fowler, *Statistical Mechanics* (Cambridge University Press, London, 1936), p. 402.
[4] R. O. Jenkins and R. H. S. Newton, Nature **163**, 572 (1949).
[5] D. A. Wright, Proc. Phys. Soc. **B62**, 188 (1949). Wright represents his data by an equivalent Richardson formula which we replotted in the $i/T^{5/4}$ form.
[6] H. J. Vink, Thesis, Leiden, 1948 (in Dutch with English summary). Limited copies available at Philips Research Laboratories, Eindhoven, Netherlands. See forthcoming paper by Loosjes and Vink in Philips Research Reports.
[7] Vink also reports a third region of still different shope above 1000°K which does not concern us here.
[8] With a thermal band separation as small as 2 ev, the full band contribution at 1200°K is negligible.

The Detection of Heavy Particles in the Primary Cosmic Radiation*

MARTIN A. POMERANTZ AND FRANK L. HEREFORD
Bartol Research Foundation of The Franklin Institute, Swarthmore, Pennsylvania
July 14, 1949

UTILIZING a new technique which has rendered feasible the selective detection of the charged components of cosmic radiation, the composition of the primaries has been established and heavy particles have been discovered. The results, originally described only in Navy reports[1] have subsequently been confirmed by investigations involving photographic plates and cloud chambers.[2] Although it had heretofore been our intention to withhold publication pending the completion of an elaborate series of experiments of the type to be described, preoccupation with other matters has repeatedly introduced delays to such an extent that it now seems expedient to report briefly upon the results obtained thus far.

The method utilizes G-M counters filled under conditions exploiting the dependence of the probability of discharge upon specific ionization. The combination of such counters into a coincidence train, and the establishment of a minimum range through interposed absorber, result in a device capable of discriminating violently among different types of particles.

It is well known that the probability of discharge E (the so-called "efficiency") of a G-M counter is determined by the probability that a particle will produce at least one ion pair during its traversal of the sensitive volume of the counter.

E is given by the expression:[3]

$$E=1-e^{-\bar{l}sp}, \quad (1)$$

where s=number of ion pairs per cm produced at standard pressure in the gas with which counter is filled, $\bar{l}$=average path length through the counter, p=pressure in counter (fraction of an atmosphere). In the case of a coincidence train, the probability of registering an event is determined by the product of the probabilities of discharge of the individual components. Hence, for identical counters, this is given by:

$$E_n=E^n, \quad (2)$$

where E_n is the probability of an n-fold coincidence.

Table I indicates the degree of discrimination which it is possible to realize by means of a suitable combination of G-M counters filled at very low pressure. The notation employed in this table is self-explanatory. It is seen that heavily-ionizing particles may be detected under conditions precluding the triggering of an event by particles of minimum ionization. Table II summarizes the pertinent quantities characterizing a particular typical experiment. The final column labeled E^4 indicates the expected counting efficiency for various particles having sufficient energy to penetrate the terrestrial magnetic field. The experimentally-observed counting efficiency near the "top of the atmosphere" equal to 0.23 ± 0.03 should be compared with that of 0.02 expected for a primary radiation consisting entirely of protons.

TABLE I. Dependence of counting efficiency E upon specific ionization. $E=1-e^{-\bar{l}sp}$; coincidence counting efficiencies ${}_4E^n$, and discrimination obtainable for particles of various specific ionizations.

${}_1E^1$	n	${}_1E^n$	${}_4E^n$	${}_4E^n/{}_1E^n$
25%	4	0.4%	24%	60
18%	4	0.1%	9%	90
50%	8	0.3%	61%	203
37%	8	0.04%	25%	625

TABLE II. Typical flight, 4 counters (6 cm Hg of H_2) in coincidence.*

Particle	Relative prim. ion.	E^4
Electron	1	0.02
Mesotron	1	0.02
Proton	1	0.02
Helium	4	0.50
Lithium (and heavier)	≥10	≥0.96

* E^4=expected counting efficiency for various particles penetrating terrestrial magnetic field. Observed counting efficiency above 90,000 ft. $E_0^4=0.23\pm0.03$.

The method of analyzing the primary cosmic radiation on the basis of these experiments is exemplified by the following set of equations:

$$1=f_P+f_\alpha+f_H, \quad (3)$$

$$E^4=f_P E_P{}^4+f_\alpha E_\alpha{}^4+f_H E_H{}^4, \quad (4)$$

$$\bar{E}^4=f_P \bar{E}_P{}^4+f_\alpha \bar{E}_\alpha{}^4+f_H \bar{E}_H{}^4. \quad (5)$$

Here f_A represents the fraction of the total primary radiation comprised of particles of type A; $E_A{}^n$ is the efficiency of an n-fold coincidence train for particles of type A; E^n is the observed net counting efficiency; P, α, and H identify protons, helium nuclei, and heavier particles respectively. All quantities E are determined experimentally, and from a comparison among the data obtained in independent experiments where new values of E appear, the fractions f_A may be computed. It is seen that $(k-1)$ flights determine the relative intensities of k types of particles.

Flights embodying counters filled at different pressures, and containing different quantities of interposed absorber, are still in progress. Heavy particles were first detected during a free-balloon

ascent on July 11, 1947, in which events ascribable to primaries of $Z \geq 2$ were observed at altitudes exceeding 15 mm of Hg. It has since become possible, through analyses such as that described above, to ascertain that approximately one-third of the incoming cosmic rays are alpha-particles (the presence of helium atoms was originally predicted by Swann[4]), and the remainder predominantly protons, with a small percentage of particles having higher atomic numbers.

The possible influence of stars, bursts, air showers, etc., upon these experiments has been investigated by means of an arrangement whereby an out-of-line counter replaces an in-line counter in the quadruple coincidence train at predetermined altitudes during the course of a flight. The relative frequency of out-of-line events compared with that of events produced by single particles makes it improbable that spurious effects are responsible for the high efficiencies observed.

* Assisted by the Joint Program of the ONR and the AEC.
[1] Progress Report, Contract N6ori-144, Bartol Research Foundation, July 15, 1947; subsequent dates. Semi-Annual Report, Contract N6ori-144, Bartol Research Foundation, September 15, 1947; September 15, 1948; March 15, 1949. See also Phys. Rev. **75**, 1316 (1949).
[2] Freier, Lofgren, Ney, Oppenheimer, Bradt, and Peters, Phys. Rev. **74**, 213 (1948).
[3] W. E. Danforth and W. E. Ramsey, Phys. Rev. **49**, 854 (1936).
[4] W. F. G. Swann, J. Franklin Inst. **236**, 1 (1943).

Nuclear Quadrupole Moments and Shell Structure

R. D. HILL
Physics Department, University of Illinois, Urbana, Illinois
August 10, 1949

IT is generally accepted that positive quadrupole moments (Q) indicate nuclei which are elongated in the direction of the spin (I) axis, and *vice versa* for negative Q. In this note it is suggested that the spatial distortion of nuclei, and hence Q values, arise in the first order of approximation from incomplete proton and/or neutron sub-shells.

In Table I are tabulated the nuclei for which Q values are known.[1,2] On the basis of nuclear shell theory, level assignments of the nucleons in the incomplete shells are given in column 4 of this table. These assignments lead to conclusions as to the signs of the quadrupole moments, which are also given in column 4. In drawing these conclusions the following assumptions were made: (1) The shapes of nuclei are determined by the probability-density distributions $\psi\psi^*$ of the independent nucleons in the incomplete shells. (2) Completely closed shells or sub-shells (which are spherically symmetrical) do not contribute to Q. Likewise, since pairs of nucleons make no contribution to I, unfilled sub-shells with even numbers of nucleons to a first order of approximation make no contribution to Q. Accordingly, only incomplete shells with odd numbers of nucleons are listed in the table. (3) In an unfilled shell having an odd number of nucleons, the "unpaired" nucleon has an m_j value equal to I, and the other nucleons distribute themselves in pairs among the remaining values of m_j (m_j is the magnetic quantum number with respect to the I field). (4) A sub-shell with only one nucleon in the state $m_j = |I|$ endows the nucleus with a negative Q value. A sub-shell with an odd number of nucleons in states $m_j = |I|, \pm\frac{1}{2}, \pm\frac{3}{2}, \cdots$ generally will produce a nucleus of positive Q value, the magnitude being the greater the more the nucleons are concentrated in the states of lower values of m_j.

The order of the sub-shells follows closely that given by Mayer.[3] There is a certain amount of arbitrariness in selecting sub-shells for the higher Z and N nuclei, but for Z or $N \lesssim 20$ the latitude of selection is fairly narrow. The case of $_{19}K^{39}$ is of interest because the shell interpretation indicates a positive Q value and the tabulated negative value is as yet only an estimate.[2] Other particularly rigid selections are In^{113}, In^{115}, Sb^{121}, Hg^{201} and Bi^{209}, which occur in the regions of closed shells. The experimental values in these cases, and in all other cases with the possible exception of Xe^{131}, are in accord with the shell interpretation. It would appear also that apart from Q being dependent upon the distribution of nucleons among the m_j states, the magnitude of Q increases with increase of oscillator quantum number of the unfilled nucleon level.

TABLE I. Interpretation of quadrupole moments.

Nucleus	Q	I	Nucleon configuration of unfilled shells*
$_1H^2$	+0.0027	1	$1s_{1/2}$ proton, $1s_{1/2}$ neutron. Q = zero
$_3Li^6$	~0	1	$1p_{1/2}$ proton, $1p_{1/2}$ neutron. Q = zero
$_3Li^7$	−0.020	3/2	$1p_{3/2}$ proton, $m_j = \|3/2\|$ negative Q
$_5B^{10}$	+0.060	3	$3p_{3/2}$ protons, $m_j = \pm 1/2, \|3/2\|$ } positive Q $3p_{3/2}$ neutrons, $m_j = \pm 1/2, \|3/2\|$ }
$_5B^{11}$	+0.030	3/2	$3p_{3/2}$ protons, $m_j = \pm 1/2, \|3/2\|$ positive Q
$_7N^{14}$	+0.020	1	$1p_{1/2}$ proton, $1p_{1/2}$ neutron. Q = zero
$_{13}Al^{27}$	+0.156	5/2	$5d_{5/2}$ protons, $m_j = \pm 1/2, \pm 3/2, \|5/2\|$ positive Q
$_{16}S^{33}$	−0.050	3/2	$1d_{3/2}$ neutron, $m_j = \|3/2\|$ negative Q
$_{17}Cl^{35}$	−0.079	3/2	$1d_{3/2}$ proton, $m_j = \|3/2\|$ negative Q
$_{17}Cl^{37}$	−0.062	3/2	$1d_{3/2}$ proton, $m_j = \|3/2\|$ negative Q
$_{19}K^{39}$	−0.030	3/2	$3d_{3/2}$ protons, $m_j = \pm 1/2, \|3/2\|$ positive Q
$_{19}K^{41}$	−0.020	3/2	$3d_{3/2}$ protons, $m_j = \pm 1/2, \|3/2\|$ positive Q
$_{29}Cu^{63}$	−0.010	3/2	$1p_{3/2}$ proton, $m_j = \|3/2\|$ negative Q
$_{29}Cu^{65}$	−0.010	3/2	$1p_{3/2}$ proton, $m_j = \|3/2\|$ negative Q
$_{31}Ga^{69}$	+0.232	3/2	$3p_{3/2}$ protons, $m_j = \pm 1/2, \|3/2\|$ positive Q
$_{31}Ga^{71}$	+0.147	3/2	$3p_{3/2}$ protons, $m_j = \pm 1/2, \|3/2\|$ positive Q
$_{33}As^{75}$	+0.300	3/2	$3p_{3/2}$ protons, $m_j = \pm 1/2, \|3/2\|$ positive Q
$_{35}Br^{79}$	+0.280	3/2	$3p_{3/2}$ protons, $m_j = \pm 1/2, \|3/2\|$ positive Q
$_{35}Br^{81}$	+0.230	3/2	$3p_{3/2}$ protons, $m_j = \pm 1/2, \|3/2\|$ positive Q
$_{36}Kr^{83}$	+0.150	9/2	$7g_{9/2}$ neutrons, $m_j = \pm 3/2, \pm 5/2, \pm 7/2, \|9/2\|$ positive Q
$_{37}Rb^{87}$	+0.170	3/2	$3p_{3/2}$ protons, $m_j = \pm 1/2, \|3/2\|$ positive Q
$_{49}In^{113}$	+1.300	9/2	$9g_{9/2}$ protons, $m_j = \pm 1/2, \pm 3/2, \pm 5/2, \pm 7/2, \|9/2\|$ positive Q
$_{49}In^{115}$	+1.17	9/2	$9g_{9/2}$ protons, $m_j = \pm 1/2, \pm 3/2, \pm 5/2, \pm 7/2, \|9/2\|$ positive Q
$_{51}Sb^{121}$	−0.90	5/2	$1d_{5/2}$ proton, $m_j = \|5/2\|$ negative Q
$_{53}I^{127}$	−0.60	5/2	$1d_{5/2}$ proton, $m_j = \|5/2\|$ negative Q
$_{53}I^{129}$	−0.43	7/2	$1g_{7/2}$ proton, $m_j = \|7/2\|$ negative Q
$_{54}Xe^{131}$	~0	3/2	$1d_{3/2}$ neutron, $m_j = \|3/2\|$ negative Q. or $3d_{3/2}$ neutrons, $m_j = \pm 1/2, \|3/2\|$ positive Q
$_{57}La^{139}$	+0.20	7/2	$7g_{7/2}$ protons, $m_j = \pm 1/2, \pm 3/2, \pm 5/2, \|7/2\|$ positive Q
$_{63}Eu^{151}$	+1.20	5/2	$5d_{5/2}$ protons, $m_j = \pm 1/2, \pm 3/2, \|5/2\|$ positive Q
$_{63}Eu^{153}$	+2.50	5/2	$5d_{5/2}$ protons, $m_j = \pm 1/2, \pm 3/2, \|5/2\|$ positive Q
$_{70}Yb^{173}$	+3.9	5/2	$5f_{5/2}$ neutrons, $m_j = \pm 1/2, \pm 3/2, \|5/2\|$ positive Q
$_{71}Lu^{175}$	+5.9	7/2	$3g_{7/2}$ protons, $m_j = \pm 1/2, \|7/2\|$ positive Q
$_{71}Lu^{176}$	+7	$\geqslant 7$	$3g_{7/2}$ protons, $m_j = \pm 1/2, \|7/2\|$ $7f_{7/2}$ neutrons, $m_j = \pm 1/2, \pm 3/2, \pm 5/2, \|7/2\|$ } positive Q
$_{73}Ta^{181}$	+6.0	7/2	$5g_{7/2}$ protons, $m_j = \pm 1/2, \pm 3/2, \|7/2\|$ positive Q
$_{75}Re^{185}$	+2.8	5/2	$3d_{5/2}$ protons, $m_j = \pm 1/2, \|5/2\|$ positive Q
$_{75}Re^{187}$	+2.6	5/2	$3d_{5/2}$ protons, $m_j = \pm 1/2, \|5/2\|$ positive Q
$_{80}Hg^{201}$	+0.50	3/2	$3p_{3/2}$ neutrons, $m_j = \pm 1/2, \|3/2\|$ positive Q
$_{83}Bi^{209}$	−0.40	9/2	$1h_{9/2}$ proton, $m_j = \|9/2\|$ negative Q

* The number in front of the angular momentum value of the nucleon state denotes the number of nucleons in this state, not the principal quantum number.

[1] H. H. Goldsmith and D. R. Inglis, BNL-1-5 (October, 1948). B. T. Feld, Nuclear Science Series, Preliminary Report No. 2 (September, 1948).
[2] W. Gordy, Phys. Rev. **76**, 139 (1949).
[3] M. G. Mayer, Phys. Rev. **75**, 1969 (1949).

The Equation of State of Gaseous He^3

J. VAN KRANENDONK, K. COMPAAN, AND J. DE BOER*
Institute for Theoretical Physics, University of Amsterdam, Amsterdam, Netherlands
August 16, 1949

RECENT experiments[1,2] with pure He^3 show that it can be expected that in the near future measurements of the second virial coefficient $B(T)$ of the equation of state $PV = RT(1 + B/V + \cdots)$ will be available. In this connection it might be of interest to communicate briefly the results of a theoretical calculation of the second virial coefficient of He^3.

As the intermolecular forces, which are determined entirely by the electronic structure of the molecules, are the same in the cases He^3 and He^4, the second virial coefficients would be exactly equal in classical theory. In quantum theory, however, the second virial coefficients are not equal, because of the difference in de Broglie wave-length of He^3 and He^4 molecules to which must be added the influence of the fact that the wave functions in He^3 must be anti-symmetrical and those of He^4 symmetrical at permutation of the molecules.

TABLE I. Values of $BT^{3/2}$ in cm³ degree$^{3/2}$/mole.

T(°K)	He³	He⁴
0.51	− 44.7	−388
1.02	−177.5	−401
2.04	−333.1	−477
3.07	−422.5	−543
4.09	−484.7	−592
5.11	−524.8	−625
6.13	−555.0	−644
7.15	−575.7	−654

The general expression for the second virial coefficient in quantum theory is:[3,4]

$$B=-\frac{N}{2\pi^3}\left(\frac{h^2}{\pi m\kappa T}\right)^{3/2}\int_0^\infty\sum_l(2l+1)\eta_l(k)\exp\left(-\frac{h^2k^2}{m\kappa T}\right)kdk$$
$$+N\left(\frac{h^2}{\pi m\kappa T}\right)^{\frac{1}{2}}\sum_n\sum_l(2l+1)(e^{-E_{nl}/\kappa T}-1)+\frac{N}{16}\left(\frac{h^2}{\pi m\kappa T}\right)^{\frac{1}{2}}\cdots. \quad (1)$$

The first term corresponds to the states of relative motion with *positive energies* $E=h^2k^2/m$, k being the wave number, l the angular momentum quantum number and the phase $\eta_l(k)$ being connected with the asymptotic behavior of the eigenfunction $\psi_{k,l}(r)$ corresponding to the state l, k. The second term gives the contribution of the stationary states of *discrete negative energies*. The *influence of the statistics*, i.e. of the symmetry character of the wave functions, is reflected firstly in the last term which is positive for He³ (F. D. statistics) and negative for He⁴ (B. E. statistics), and secondly in the fact that the summations must be carried out only over odd values of l in the case of He³ and only over even values of l for He⁴.

The values for $\eta_l(k)$ have been calculated as functions of k for $l=1, 3, \cdots 21$, by numerical integration of the wave equation using the potential field $4\epsilon[(\sigma/r)^{12}-(\sigma/r)^6]$ with the values of ϵ and σ which fitted the second virial coefficient[5,6] and transport-phenomena[7] of He⁴ from high to very low temperatures. No stationary state of negative energy exists in the case of He³ (as in the case of He⁴, where a virtual level appeared at an energy just somewhat larger than zero), so that the second term in (1) disappears. The resulting values of $BT^{\frac{1}{2}}$ in cm³ degree$^{\frac{1}{2}}$/mole for He³ are compared with those of He⁴ in Table I. The difference between the two values becomes quite large for lower temperatures, which, however, will not easily be accessible for experimental work. The contribution of the last term of (1) to $BT^{\frac{1}{2}}$ is constant and equal to +91.0 cm³ degree$^{\frac{1}{2}}$/mole for He³. A detailed article will appear in *Physica*.

* Currently a visiting professor at the Ohio State University, Columbus, Ohio.

[1] Sydoriak, Grilly, and Hammel, Phys. Rev. **75**, 303 (1949).
[2] Grilly, Hammel, and Sydoriak, Phys. Rev. **75**, 1103 (1949).
[3] E. Beth and G. E. Uhlenbeck, Physica **4**, 915 (1937).
[4] H. S. W. Massey and R. A. Buckingham, Proc. Roy. Soc. **A168**, 378 (1938).
[5] J. de Boer and A. Michels, Physica **5**, 945 (1938).
[6] J. de Boer and A. Michels, Physica **6**, 409 (1939).
[7] J. de Boer, Physica **10**, 348 (1943).

On the Hot-Wire Length Correction

F. N. FRENKIEL
Naval Ordnance Laboratory, White Oak, Silver Spring, Maryland
August 22, 1949

THE following remarks should be made concerning two of the conclusions reached in my preceding Letter to the Editor[1] and to which S. Corrsin and L. S. G. Kovasznay refer.[2]

(1) In this last reference it is said that, contrary to my conclusion, the longitudinal turbulent energy measured with a wire of non-negligible length does not approach zero when $l\to\infty$. It seems desirable to add the following additional explanation: When the length of the wire l is very small compared to the scale of turbulence and the variation of the instantaneous turbulent velocity u' along the wire is neglected, then the mean square voltage is equal to $\langle e^2\rangle_{Av}=k^2l^2\langle u'^2\rangle_{Av}$. The factor kl can be found from the calibration of the wire. The *longitudinal turbulent energy* is then given by $\langle u'^2\rangle_{Av}=\langle e^2\rangle_{Av}/k^2l^2$.

If now the length l cannot be neglected then the measured square voltage is equal to $\langle e_b^2\rangle_{Av}=2k^2\langle u'^2\rangle_{Av}\int_0^l(l-s)R_v(s)ds$. The *measured longitudinal turbulent energy* will be given by $\langle u_b'^2\rangle_{Av}=\langle e_b^2\rangle_{Av}/k^2l^2$. When $l\to\infty$, $\langle e_b^2\rangle_{Av}$ becomes proportional to l. It results therefore that the *measured longitudinal turbulent energy* $\langle u_b'^2\rangle_{Av}$ is proportional to $1/l$ and approaches zero when $l\to\infty$.

(2) An error appeared indeed in the transcription of the value of I_b for the Gaussian longitudinal correlation function. The correct value which was given in the paper[3] referred to in my first Letter to the Editor is the one which Corrsin and Kovasznay recalculate in their comments.

[1] F. N. Frenkiel, Phys. Rev. **75**, 1263 (1949).
[2] S. Corrsin and L. S. G. Kovasznay, Phys. Rev. **75**, 1954 (1949).
[3] F. N. Frenkiel, NOLM 9658 and 9723.

Equation of the Magnetic Threshold Curve of a Superconductor

G. PRESTON BURNS
Physics Department, Mary Washington College of the University of Virginia, Fredericksburg, Virginia
August 9, 1949

A PARABOLIC relationship between magnetic threshold fields and temperature of superconductors has been assumed by various authors,[1] empirical formulas[2] of the type

$$H=A+CT^2+DT^3+ET^4+\cdots$$

have been made to fit experimental data and a three-halves power relationship has been suggested.[3]

On the basis of the Gorter-Casimir expression[4] for the jump in atomic heat of a superconductor at its transition temperature and the assumption that the electron contribution to the specific heat of a body in the superconducting state is proportional to the cube of the absolute temperature, an equation has been derived for the magnetic threshold curve of a superconductor.

The jump in specific heat of a superconductor at its transition temperature is defined by

$$\Delta C=C_S-C_N=\frac{VT}{8\pi}\left[\frac{d^2(H^2)}{dT^2}\right], \quad (1)$$

where C_N and C_S are the atomic heats of the body in the normal and superconducting states, respectively, H is the magnetic threshold field at temperature T and V is the atomic volume.

It is assumed that

$$C_N=D_NT^3+\gamma_NT \quad (2)$$

and

$$C_S=D_ST^3+\gamma_ST, \quad (3)$$

where

$$\gamma_S=KT^2. \quad (4)$$

The T^3 term in Eqs. (2) and (3) is due to lattice vibrations and the linear term is the electron contribution to the atomic heat of the body.

Assuming that $D_S=D_N$, substitution of Eqs. (2), (3) and (4) into Eq. (1) gives

$$KT^2-\gamma_N=\frac{V}{8\pi}\left[\frac{d^2(H^2)}{dT^2}\right]. \quad (5)$$

Using the boundary conditions $dH/dT=0$ at $T=0$, $T=T_c$ when $H=0$ and $H=H_0$ when $T=0$ the solution of Eq. (5) is

$$H^2=H_0^2-\frac{4\pi\gamma_N}{V}T^2+\frac{2\pi K}{3V}T^4, \quad (6)$$

where

$$H_0^2=\frac{4\pi\gamma_N}{V}T_c^2-\frac{2\pi K}{3V}T_c^4. \quad (7)$$

Examination of Eq. (6) shows that, if

$$T_c^2<3\gamma_N/K, \tag{8}$$

then the curve does not cross the T-axis. If

$$T_c^2>3\gamma_N/K, \tag{9}$$

the curve crosses the T-axis at two points given by

$$T_c^2=\frac{b\pm(b^2-4CH_0^2)^{\frac{1}{2}}}{2C}, \tag{10}$$

where

$$b=(4\pi\gamma_N/V) \quad \text{and} \quad C=(2\pi K/3V). \tag{11}$$

The slope of this curve at $T=T_c$ is infinite. If

$$T_c^2=3\gamma_N/K, \tag{12}$$

then Eq. (6) becomes

$$H=\pm H_0(1-T^2/T_c^2), \tag{13}$$

where

$$H_0=\pm 3\gamma_N/K(2\pi K/3V)^{\frac{1}{2}}. \tag{14}$$

This curve is a parabola whose slope at $T=T_c$ is finite and equal to $\pm 2H_0/T_c$.

The first case, Eq. (8), is eliminated because the curve does not cross the T-axis and the second case, Eq. (9), is eliminated because under this condition the threshold curve is perpendicular to the T-axis at $T=T_c$. There remains only the possibility of the third case, Eq. (12).

It is concluded, therefore, that for those elements whose electronic specific heats obey the T law the threshold curve is a parabola.

[1] J. A. Kok, Physica 1, 1103 (1934); J. de Launay and M. C. Steele, Phys. Rev. 73, 1450 (1948).
[2] J. A. Kok, Dissertation, Leiden (1935); A. D. Missner, Proc. Roy. Soc. 174, 266 (1940).
[3] M. J. Sienko and R. A. Ogg, Phys. Rev. 71, 319 (1947).
[4] C. J. Gorter and H. Casimir, Physica 1, 306 (1934).

The Decay Probability of Be^7 as a Function of the Ionization of the Atom

P. Benoist, R. Bouchez, P. Daudel, and R. Daudel
Institut du Radium, Laboratoire Curie, Paris, France
and
A. Rogozinski
Laboratoire de Physique Cosmique, Paris, France
August 16, 1949

THE decay probability of a nucleus as a result of the capture of its orbital electrons is proportional to the electron density $|\Psi_0|^2$ within the nuclear field. This density is equal to the sum of the partial densities $|\Psi_0|_K^2$ and $|\Psi_0|_L^2\cdots$ due, respectively, to K and L electrons of the atom in question, and also to the electron density arising from electrons belonging to neighboring atoms. Therefore, the total density is different for an atom existing (a) in an isolated state, (b) in a rarefied or in a dense medium (density effect), or (c) in a compound. However, the theoretical evaluation of the capture probability is very difficult, since it closely depends on data, which are unfortunately not well known, concerning electron density functions within the nuclear field of the atom.[1-3] (Compare also the letter of Professor Seitz, quoted by Segrè and Wiegand.[4]) It can be shown that the ratio of densities of electrons $2s$, $|\Psi_0|_{L_I}^2$, and $1s$, $|\Psi_0|_K^2$, for a single atom of Be^7 in free space amounts to about 0.018 or 0.033, according to whether one applies the method of Slater[5] or the method of Hartree with exchange.[6] However, it is still necessary to take into account (a) that the departure of L_I electrons produces an increase of about 6.5×10^{-3} in $|\Psi_0|_K^2$,[1] which becomes, say, $|\Psi_0'|_K^2$; (b) that, in the metal, the L electrons consist of a mixture of 50 percent s- and 50 percent p-states;[7] and (c) that, when present as fluoride, for example, Be is only partially ionized,[8] the ionization being, in this case, 87 percent.

Thus, in Paris experiments, where Be metal was compared with BeF_2, it can be shown that:

$$\frac{T_{(BeF_2)}-T_{(Be)}}{T_{(Be)}}\simeq 1-\frac{|\Psi_0'|_K^2}{|\Psi_0|_K^2+|\Psi_0|_{L_I}^2}\simeq 0.011,$$

T standing for the decay constant. No account was taken in this estimation of the effect of electron density produced by the element which is combined with Be, nor by neighboring atoms other than fluorine (density effect, impurity effect).

In brief, one can state that the decay probability of a compound BeX (F_2Be, Cl_2Be, OBe) is lower the more electro-negative the X atom (hence the choice of BeF_2 as the compound for comparison in the present experiments), and is lower also the less dense the compound (hence the second reason for the choice of BeF_2 in preference to BeO which is denser).

Several experiments were carried out in order to demonstrate the existence of a possible effect of the ionization of the atom on the decay constant of Be^7.

The possibility of such an effect was pointed out independently by E. Segrè[9] and by R. Daudel.[10] A first experiment was carried out at the Collège de France, Paris;[2] a comparison was made between metallic Be and an aqueous solution of $BeCl_2$. A block of five G-M counters, connected in parallel and feeding a scale-of-1000, was used as the detecting apparatus. Its stability was such that a variation of γ-activity of the order of 3×10^{-3} could be detected. These measurements gave

$$\frac{T_{(BeCl_2)}-T_{(Be)}}{T_{(Be)}}\simeq 5\times10^{-3}.$$

This result, only about equal to the standard deviation of the measurement, did not yield a definite proof of the existence of the phenomenon.

Further measurements were carried out in France[3,11] and in the U.S.A. using a more sensitive method, by means of which small differences in activity between two very active samples could be measured. The French apparatus consisted essentially of two differential ionization chambers filled with air at atmospheric pressure. The small differential ionization current given by the chambers was measured by means of a $VX32$ electrometer triode, fed by a very stable balanced circuit;[12] in fact, the drift observed during the four months duration of the experiment was about 20 mm scale divisions, equivalent to a shift of about 15 mv on the grid. The grid was kept floating and the sensibility was limited only by fluctuations in the currents through the chambers, which were of the order of 10^{-7} e.s.u. The entire apparatus was located inside an almost spherically shaped chamber surrounded by a layer of distilled water, one meter thick. The ionization background observed within the chamber was due only to the penetrating component of the cosmic radiation, as measured by high pressure ionization chambers and G-M counters.[13]

One of the sources consisted of metallic Be^7 and the other of anhydrous non-crystallized Be^7F_2 each of which was initially equivalent to about 40 μg Ra. The former Be^7 source, however, contained a small amount of Na, which tends to augment the effect investigated. With the Be^7 source available, it was possible to distinguish relative differences in their activities of less than 5×10^{-4}. The results obtained yielded the following value:

$$\frac{T_{(BeF_2)}-T_{(Be)}}{T_{(Be)}}=(0.01\pm0.003)$$

which provides evidence of the existence of an effect of the orbital electrons on the decay constant of Be^7.

Experiments using a similar method, carried out in the U.S.A.

by E. Segrè and C. E. Wiegand[4] on metallic Be and BeO, gave

$$\frac{T_{(BeO)}-T_{(Be)}}{T_{(Be)}}=(3.0\pm1.8)10^{-4},$$

a value which is of the order of the experimental errors.

The results obtained seem to be in agreement qualitatively with the above theoretical considerations: In the series BeF_2, $BeCl_2$, and OBe, the compound BeF_2 which contains the most electro-negative element should thus display the longer period.

This work was performed at Université de Paris, Laboratoire Curie, under the direction of Professor I. Curie.

Note: This letter had already been written, when we received from Professor E. Segrè a copy of his new paper (Leininger, Segrè, and Wiegand, Phys. Rev. **76**, 897 (1949)) for which we are very grateful to the authors. Their latest results concern metallic Be and crystallized BeF_2 and they find:

$$\frac{T_{(BeF_2)}-T_{(Be)}}{T_{(Be)}}=(1.675\pm0.19)10^{-3}.$$

This value is still several times smaller than ours, obtained with almost similar samples of about $\frac{1}{10}$th the activity. However, the essential feature of all the results is that the experimental evidence of the effect investigated, in Paris as in Berkeley, is established; and that for the first time it has been possible to influence the decay constant of a radioactive element.

[1] P. Benoist, Comptes Rendus **228**, 309 (1949).
[2] Bouchez, Daudel, Daudel, and Muxart, J. de phys. et rad. **XI**, 336 (1947).
[3] Bouchez, Daudel, Daudel, Muxart, and Rogozinski, J. de phys. et rad, June, 1949.
[4] E. Segrè and C. E. Wiegand, Phys. Rev. **75**, 39 (1949).
[5] J. C. Slater, Phys. Rev. **36**, 57 (1930).
[6] Hartree, Proc. Roy. Soc. London **149**, 210 (1935); **150**, 9 (1935).
[7] Pauling, Conferences, Oxford, 1948.
[8] D'après les électronégativités et les courbes de Pauling.
[9] E. Segrè, Phys. Rev. **71**, 274 (1947).
[10] R. Daudel, La Revue Scientifique (Paris) **85**, 162 (1947).
[11] Bouchez, Daudel, Daudel, and Muxart, Comptes Rendus **227**, 525 (1948).
[12] A. Rogozinski, Comptes Rendus **208**, 427 (1939).
[13] A. Rogozinski and M. Lesage, Comptes Rendus **226**, 1131 (1948).

Statistics of the Three-Dimensional Ferromagnet

TAKEHIKO OGUCHI
Tokyo Institute of Technology, Oh-okayama, Tokyo, Japan
August 11, 1949

THE three-dimensional Ising problem (the simple cubic lattice) is formulated through a turned-over V-shaped matrix by extending the screw method of Kramers and Wannier.[1] A largest eigenvalue of this matrix is solved by the perturbation procedure of Ashkin and Lamb,[2] and the partition function f and the total magnetization M are obtained in the form of the low temperature power series. The results are the following:

$$\left.\begin{aligned} f^{1/N}&=\beta^{-\frac{1}{2}}(1+\beta^6+3\beta^{10}-3\beta^{12}+15\beta^{14}-30\beta^{16}\cdots)\\ M/Nm&=1-2\beta^6-12\beta^{10}+14\beta^{12}-90\beta^{14}+192\beta^{16}\cdots\end{aligned}\right\}, \tag{1}$$

$$\beta=\exp(-J/kT), \tag{2}$$

where N is the total number of the spins, m denotes the magnetic moment of each spin, and J is the energy gained if two neighbors change from an anti-parallel to a parallel position. These results completely agree with those given by van der Waerden.[3]

An approximational treatment of ferromagnetism is the one developed by Bethe.[4] Afterwards, Takagi[5] obtained the same results by a more elementary treatment of the combinatorial problem. Further, by the tedious calculations from Takagi's formulas, the partition function and the total magnetization can be expressed in a form explicitly including only the temperature;

$$\left.\begin{aligned} f^{1/N}&=\frac{(1-\beta^2)^3(1+(1+4\beta^2)^{\frac{1}{2}})^3}{4\beta^{\frac{3}{2}}\{1-6\beta^4+8\beta^6+(1-2\beta^2)(1+4\beta^2)^{\frac{1}{2}}\}}\\ \frac{M}{Nm}&=\frac{\sqrt{2}\{1-6\beta^4+(1-2\beta^2)(1+4\beta^2)^{\frac{1}{2}}\}^{\frac{1}{2}}}{1+(1-2\beta^2)(1+4\beta^2)^{\frac{1}{2}}}\end{aligned}\right\}. \tag{3}$$

These may be expanded in power series of β as follows:

$$\left.\begin{aligned} f^{1/N}&=\beta^{-\frac{1}{2}}(1+\beta^6+3\beta^{10}-3\beta^{12}+15\beta^{14}-33\beta^{16}\cdots)\\ M/Nm&=1-2\beta^6-12\beta^{10}+14\beta^{12}-90\beta^{14}+216\beta^{16}\cdots\end{aligned}\right\}. \tag{4}$$

Thus the Bethe-Takagi approximation deviates from a rigorous series at β^{16}.

The partition function and the total magnetization of the two-dimensional hexagonal lattice, which has the same number of nearest neighbors as that of the simple cubic lattice, are obtained by the screw method with the results

$$\left.\begin{aligned} f^{1/N}&=\beta^{-\frac{1}{2}}(1+\beta^6+3\beta^{10}-\beta^{12}\cdots)\\ M/Nm&=1-2\beta^6-12\beta^{10}+2\beta^{12}\cdots\end{aligned}\right\}. \tag{5}$$

The comparison with (1), (4), and (5) shows that the Bethe-Takagi approximation, when the number of nearest neighbors is 6, is better for the simple cubic lattice than it is for the two-dimensional hexagonal lattice.

A detailed account will be published in Journal of the Physical Society of Japan.

The author desires to express his sincere thanks to Professor Y. Takagi for kind guidance and interest in the course of this work.

[1] H. A. Kramers and G. H. Wannier, Phys. Rev. **60**, 252 (1941).
[2] J. Ashkin and W. E. Lamb, Phys. Rev. **64**, 159 (1943).
[3] v. d. Waerden, Zeits. f. Physik **118**, 473 (1941).
[4] H. A. Bethe, Proc. Roy. Soc. **150A**, 552 (1935).
[5] Y. Takagi, Proc. Phys. Math. Soc. Japan **23**, 44, 553 (1941).

The Phenomenological Theory of Superconductors

A. R. MILLER
Royal Society Mond Laboratory, Cambridge University, Cambridge, England
August 16, 1949

IT is well known that if the acceleration equation for *perfect conductivity* be used with the Maxwell equations, the resulting equation can be integrated with respect to the time variable and gives an equation which contains a constant of integration equal to the external magnetic field when perfect conductivity was established. In formulating their description of the electrodynamical behavior of a *superconductor*, F. and H. London[1] assumed a more restricted equation to describe the magnetic behavior, based on the empirical fact (the Meissner effect) that the magnetic induction inside a superconductor always vanishes, irrespective of the external magnetic field at the onset of superconductivity. The important theoretical point, established by the Meissner-Ochsenfeld experiment, is the *thermodynamic reversibility* of the superconducting transition in a magnetic field. The magnetic induction in a superconducting medium is independent of the path by which the superconducting state is reached; that is, it is a single-valued function of the parameters which specify the state of the system.

A gauge invariant formulation of classical electrodynamics has been given by Eckart[2] and his method has been used by Cook[3] to derive equations for a superconducting medium. He deduced the Euler equations of motion of the system from the Lagrangian by varying the *velocities*, and obtained

$$\Lambda c\,\mathrm{curl}\mathbf{J}+\mathbf{H}=0 \tag{1}$$

immediately, apparently without having to make an assumption equivalent to the vanishing of an integration constant. In the

course of a paper on the hydrodynamical equations of a non-viscous electronic fluid, Sorokin[4] has also discussed the use of the variational principle. He advances reasons for supposing that in applying the method to a "superfluid," it is necessary to vary the velocities and not the positional coordinates of the particles, since the description of the "superfluid" depends on the former rather than the latter. He also deduces Eq. (1) from the Lagrangian. Both authors point out that this equation depends on more than simply vanishing viscosity, but neither indicates where the more stringent conditions is introduced in using the variational method.

The use of the Lagrangian implies that for every thermodynamical state of the system there is only one possible value of the magnetic induction, since there is a one-one correspondence between the values of the Lagrangian and of the parameters which specify the state of the system. As has been pointed out above, this is the theoretical implication of the Meissner effect. Thus, to formulate the Lagrangian of the system and to use the variational method automatically ensures that this experimental fact is included in the formulation. It is therefore hardly a matter for surprise that an analysis, which assumes implicitly the single-valued property of the parameters which is the essence of the thermodynamic reversibility demonstrated by the Meissner-Ochsenfeld experiment, should lead to Eq. (1) without any arbitrary constant.

[1] F. and H. London, Proc. Roy. Soc. **A149**, 71 (1935); F. London, *Une Conception Nouvelle de la Supraconductivilité* (Hermann et Cie, Paris, 1937).
[2] C. Eckart, Phys. Rev. **54**, 920 (1938).
[3] E. Cook, Phys. Rev. **58**, 357 (1940).
[4] V. S. Sorokin, J. Exper. Theor. Phys. U.S.S.R. **19**, 553 (1949).

Erratum: Excitation Functions for (α,n), $(\alpha,2n)$ and $(\alpha,3n)$ Reactions on Indium

[Phys. Rev. **76**, 424 (1949)]

GEORGES M. TEMMER
Department of Physics, University of California, Berkeley, California

THE following typographical errors have been noted in the above paper:

Caption of Fig. 2, page 425, second line, should read: Circles indicate $In^{115}(\alpha,n)Sb^{118}$, triangles indicate $In^{115}(\alpha,2n)Sb^{117}$, squares indicate $In^{115}(\alpha,3n)Sb^{116}$ cross sections; arrows A and B indicate the Coulomb barrier heights for $r_0=1.5$ and $r_0=1.3$, etc.

Page 425, column 1, sixteen lines from the bottom instead of: ". . . upon quarter-mil foil." read: ". . . upon quarter-mil aluminum foil."

Nuclear Spin $\frac{1}{2}$ for Te^{123} and Isotope Shift in the Tellurium Spectrum

J. E. MACK AND O. H. ARROE
University of Wisconsin, Madison, Wisconsin*
August 11, 1949

FROM the hollow-cathode discharge spectrum** of 123-enriched tellurium*** we have found that the spin of the Te^{123} nucleus is $\frac{1}{2}$ unit. Unfortunately the electron structure of tellurium is not sufficiently well known at present to allow the determination of the nuclear magnetic moment, μ_{123}. However, in verifying Fowles' discovery[1] of spin $\frac{1}{2}$ for Te^{125}, we find the splitting of the lines in the spectra of the two isotopes to be identical except for a scale factor, which yields the tentative value $\mu_{125}/\mu_{123}=1.208$ (greatest deviation found, 5 percent) for the ratio of the moments.

An isotope shift of the order of hundredths of a wave number unit is evident in several of the lines.

Earlier tellurium hollow-cathode spectra in this laboratory were obtained by Mr. J. S. Ross; further investigations, including especially that of the isotope shift, are under way in this laboratory.

* Work done on Navy contract N7onr-285TO#1, NR 019 107.
** With auxiliary dispersion produced by a special Hilger spectrograph bought with funds granted by the University Research Committee.
*** Produced by the Y-12 plant, Carbide and Carbon Chemicals Corporation, and obtained by allocation from the United States Atomic Energy Commission.
[1] G. R. Fowles, Phys. Rev. **76**, 571 (1949); kindly communicated to us in advance by Professor Jenkins.

Three-Body Scattering with Central and Tensor Forces

ROY THOMAS
Department of Physics, University of New Mexico, Albuquerque, New Mexico
June 29, 1949

THE scattering of neutrons and deuterons (or protons and deuterons) has been calculated using a combination of central and tensor type interaction. The interaction between any two elementary particles is taken to be of the following form.

$$U(r)=G_{ij}(1+\gamma S_{ij})J(r).$$

γ is taken to equal 0.775. The function $J(r)$ which represents the range and depth of the nuclear interaction equals $V\exp(-4\alpha r^2)$. V represents the depth of the interaction and $1/2(\alpha)^{\frac{1}{2}}$ represents the range of the nuclear forces. S_{ij} represents the tensor operator $3(\boldsymbol{\sigma}_i\cdot\mathbf{r})(\boldsymbol{\sigma}_j\cdot\mathbf{r})/r^2-(\boldsymbol{\sigma}_i\cdot\boldsymbol{\sigma}_j)$. The exchange character of interaction is represented by G_{ij}, five forms of which are used.

1. Ordinary	$G_{ij}=1$
2. Majorana	$G_{ij}=P_{ij}$
3. Heisenberg	$G_{ij}=P_{ij}Q_{ij}$
4. Charge symmetric	$G_{ij}=-\frac{1}{2}(\boldsymbol{\tau}_i\cdot\boldsymbol{\tau}_j)$
5. Charge and spin symmetric	$G_{ij}=-\frac{1}{2}(\boldsymbol{\tau}_i\cdot\boldsymbol{\tau}_j)(\boldsymbol{\sigma}_i\cdot\boldsymbol{\sigma}_j)$.

P_{ij} and Q_{ij} represent operators which interchange the space coordinates and the spin coordinates of the nuclear particles, i and j, respectively. The operators τ and σ represent the isotopic spin and ordinary spin of a nuclear particle. The deuteron wave function is represented by

$$\psi_D(\rho)=(2\alpha/\pi)^{3/4}\exp\{-\alpha\rho^2\}.$$

The Born approximation is used in calculating the cross section for scattering. The use of the Born approximation is questionable in view of the fact that the kinetic energy is of the same order as the interaction energy. The evaluation of the spin sums is completed by means of spur theory with annihilation operators; the spin wave function therefore need not explicitly be written down. The spin sums were first evaluated and then the space integrals completed. Since the spur of the tensor operator is zero, the total cross section for the scattering process is just the algebraic sum of the cross section for the central forces and the cross section for the tensor forces.

In making these calculations, the Coulomb repulsion between the two protons is neglected. This is not a serious defect, since at high energies the Coulomb terms contribute only at very small angles. Under these conditions, the scattering of neutrons and deuterons is identical with the scattering of protons and deuterons. The scattered wave function is also anti-symmetrized with respect to the two neutrons or the two protons in the scattering process in order to satisfy the Pauli principle. The partial cross section is $\sigma(\theta)d\omega$ where $\sigma(\theta)=C(\sigma_C+\sigma_T)$. ($\sigma_C$—central interaction contribution; σ_T—tensor interaction contribution.) The constant C

equals $(\mu/2\pi\hbar^2)^2(\pi^2V^2/100\alpha^2)$. θ is the scattering angle in the center of gravity system. μ and k are the reduced mass and the propagation vector in the relative coordinates. We now define the following functions.

$$\begin{aligned}
i&=2.53\exp\{-\tfrac{3}{10}(k^2/\alpha)(1.25+\cos\theta)\},\\
g&=1.25\exp\{-\tfrac{3}{16}(k^2/\alpha)(1-\cos\theta)\},\\
b&=1.05\exp\{-\tfrac{1}{4}(k^2/\alpha)\},\\
A&=\exp\{-\tfrac{1}{16}(k^2/\alpha)(1-\cos\theta)\},\\
B&=\exp\{-\tfrac{1}{4}(k^2/\alpha)(1.25+\cos\theta)\},\\
x&=I\{[k/2(\alpha)^{\frac{1}{2}}]\sin(\theta/2)\}\\
y&=I\{[k/2(2\alpha)^{\frac{1}{2}}]\cos(\theta/2)\},\\
z&=I\{[k/2(5\alpha)^{\frac{1}{2}}][1.25+\cos\theta]^{\frac{1}{2}}\},\\
I(\Delta)&=1/\Delta^3\{[3(\pi)^{\frac{1}{2}}/2]P(\Delta)-(2\Delta^3+3\Delta)\exp(-\Delta^2)\}.
\end{aligned}$$

Here $P(\Delta)$ is the probability function which is normalized such that

$$P(0)=0,\quad P(\infty)=1.$$

The cross sections calculated for these five exchange operators are tabulated below.

1. Ordinary $\sigma_C=[2g-\frac{1}{2}(b+i)]^2+\frac{1}{2}(b+i)^2$
   $\sigma_T=[A(1.94x-0.81y)-0.98Bz]^2+4.8B^2z^2$
2. Majorana $\sigma_C=[2b-\frac{1}{2}(g+i)]^2+\frac{1}{2}(g+i)^2$
   $\sigma_T=[A(0.97x-1.62y)+0.98Bz]^2+4.8B^2z^2$
3. Heisenberg $\sigma_C=[g+\frac{1}{2}(i-2b)]^2+\frac{1}{2}(i-2b)^2$
   $\sigma_T=[A(0.97x-1.62y)+0.98Bz]^2+4.8B^2z^2$
4. Charge symmetric $\sigma_C=\frac{3}{2}(b-i)^2$
   $\sigma_T=[0.81Ay-0.98Bz]^2+4.8B^2z^2$
5. Charge and spin symmetric $\sigma_C=\frac{1}{2}[i-(b/3)]^2+(8/3)b^2$
   $\sigma_T=[0.81Ay-0.98Bz]^2+4.8B^2z^2$.

In the above formulas the first line representing the cross section is obtained from the central forces. The second line is a contribution from the tensor interactions. We see that exchange operators two and three give the same tensor contribution to the scattering, and furthermore, the tensor contribution of 4 and 5 are equal to one another.

For relative energies, less than 10 Mev, the tensor contribution may be disregarded compared to the magnitude of the cross section from the central interactions only. For relative energies of the order of 20 Mev, the tensor terms make an appreciable contribution to the cross section. This contribution changes the angular behavior of the cross sections in a marked manner for the symmetric exchange of cases 4 and 5.

Experimental data on a three-body scattering with relative energies between 10 and 30 Mev would be very useful on deciding upon one of these five types of exchange interactions; and also, whether tensor forces actually exist in nature.